Université de Sherbrooke

Exploring Flavivirus interactions to uncover new potential drug targets

By
Carolin Brand
Biochemistry Program

Thesis presented at the Faculty of Medicine and Health Sciences
for the fulfillment of the doctoral degree diploma *philosophiae doctor* (Ph.D.)
in Biochemistry

Sherbrooke, Québec, Canada
September 2023

Members of the evaluation committee:
Prof. Martin Bisaillon, Département de biochimie et génomique fonctionnelle, Université de Sherbrooke
Prof. Brian Geiss, Department of Microbiology, Immunology, and Pathology, Colorado State University
Prof. Benoit Laurent, Département de biochimie et génomique fonctionnelle, Université de Sherbrooke
Prof. Nancy Dumais, Département de biologie, Université de Sherbrooke
Prof. Amélie Fradet-Turcotte, Dép. de biologie moléculaire, biochimie médicale et pathologie, Université Laval

RÉSUMÉ

Investigation des interactions chez les Flavivirus dans le but de découvrir des nouvelles cibles thérapeutiques

Par
Carolin Brand
Programme de Biochimie

Thèse présentée à la Faculté de médecine et des sciences de la santé en vue de l'obtention du diplôme de *philosophiae doctor* (Ph.D.) en Biochimie, Faculté de médecine et des sciences de la santé, Université de Sherbrooke, Sherbrooke, Québec, Canada, J1H 5N4

Les flavivirus comprennent d'importants agents pathogènes humains tels que le virus Zika, le virus de la fièvre jaune et le virus du Nil occidental. Bien que la majorité des infections soient asymptomatiques et la plupart des cas symptomatiques soient associés à une maladie pseudo-grippale, un faible pourcentage des infections par les flavivirus peut entraîner des maladies graves qui peuvent être mortelles. Malgré plusieurs décennies d'efforts de recherche, aucun médicament antiviral n'est actuellement disponible pour traiter ces infections. Par conséquent, de nouvelles cibles potentielles pour la découverte et/ou la conception de thérapies antivirales sont nécessaires.

L'identification et la compréhension des interactions virus-hôte ont été proposées comme une voie prometteuse pour le développement de nouvelles stratégies pour traiter ou prévenir les infections. Ici, les interactions entre trois flavivirus (Kunjin, Zika, fièvre jaune) et leurs cellules hôtes ont été étudiées à l'aide du séquençage de l'ARN ainsi que de la protéomique quantitative (SILAC). Plusieurs centaines de gènes et protéines se sont avérés être exprimés de manière différentielle lors de ces infections, et environ 600 à 900 modulations dans l'épissage alternatif des transcrits cellulaires ont été identifiées. Plusieurs de ces gènes/protéines seraient des candidats intéressants à étudier davantage pour leurs rôles dans les infections virales et leur potentiel à être ciblés pour supprimer la réplication virale.

Une autre approche intéressante pour le développement de composés thérapeutiques est de cibler les interactions protéine-protéine. Ici, l'interaction entre les protéines NS3 et NS5 du virus du Nil occidental, qui est essentielle pour la réplication virale, a été caractérisée. Sept résidus à la surface de la protéine NS3, regroupés en deux petites régions, se sont révélés critiques pour la réplication virale, possiblement en médiant l'interaction NS3:NS5. Ces deux petites régions pourraient être des cibles intéressantes pour le développement futur de médicaments contre les flavivirus.

En conclusion, les travaux présentés dans cette thèse ont mis en évidence plusieurs gènes/protéines humains ainsi que deux régions à la surface de la protéine virale NS3 qui mériteraient d'être étudiés davantage afin de déterminer leur potentiel à être ciblés pour le développement de thérapies antivirales.

Mots clés : Flavivirus, virus du Nil occidental, virus Zika, virus de la fièvre jaune, interaction protéine-protéine, interaction virus-hôte, séquençage d'ARN, SILAC

SUMMARY

Exploring Flavivirus interactions to uncover new potential drug targets

By
Carolin Brand
Biochemistry Program

Thesis presented at the Faculty of medicine and health sciences for the fulfillment of the Doctor degree diploma *philosophiae doctor* (Ph.D.) in Biochemistry, Faculty of medicine and health sciences, Université de Sherbrooke, Sherbrooke, Québec, Canada, J1H 5N4

Mosquito-borne Flaviviruses include important human pathogens such as dengue virus, Zika virus, Yellow Fever virus, and West Nile virus. Although most infections are asymptomatic and most symptomatic cases are associated with a flu-like illness, a small fraction of Flavivirus infections can lead to severe illness, including encephalitis and hemorrhagic fever which may be fatal. Despite several decades of research efforts, no specific antiviral drugs are currently available to treat Flavivirus infections. Therefore, new potential targets for the discovery and/or design of antiviral therapies are needed.

Identifying and understanding virus-host interactions has been proposed to be a promising avenue for the development of novel strategies to treat or prevent infections. Here, Flavivirus-host interactions were investigated using RNA sequencing as well as SILAC/MS, and the coding transcriptomes and proteomes of cells infected with three different Flaviviruses, namely Kunjin virus, Zika virus and Yellow Fever virus, was compared to those of mock-infected cells. Approximately 300-500 genes and 550-700 proteins were found to be differentially expressed during Flavivirus infections, and roughly 600-900 modulations in alternative splicing of host transcripts were identified. Moreover, 51 genes, 39 alternative splicing events and 57 proteins were found to be affected in all three Flavivirus infections. Several of these genes/proteins would be interesting candidates to study further for their roles in viral infections and their potential to be targeted to suppress viral replication.

Another attractive target for the development of therapeutic compounds are protein-protein interactions. Here, the West Nile virus NS3:NS5 interaction, which is essential for viral replication, has been characterized using site-directed mutagenesis based on an interaction model that was developed *in silico*. Seven residues on the surface of the NS3 protein, clustered in two 'hotspots', were found to be critical for viral replication, possibly by mediating the NS3:NS5 interaction. These two 'hotspots' could be interesting targets for future anti-flaviviral drug development.

In conclusion, the work presented in this thesis has highlighted several human genes/proteins as well as two regions on the surface of the viral protein NS3 that deserve further study to determine their potential to be targeted for the development of antiviral therapies.

Keywords : Flavivirus, West Nile virus, Zika virus, Yellow Fever virus, protein-protein interaction, virus-host interaction, RNA sequencing, SILAC

TABLE OF CONTENTS

LIST OF FIGURES

Introduction

Article 1

Article 2

Discussion

Appendix

LIST OF TABLES

Introduction

Appendix

LIST OF ABBREVIATIONS

2-5A	2’,5’-linked oligoadenylate
2D DIGE	two-dimensional differential gel electrophoresis
2D PAGE	two-dimensional polyacrylamide gel electrophoresis
2K	2K peptide
4EBP	eIF4E-binding proteins
A	adenosine
Å	Ångström, 1Å = 0.1 nanometer
AIDS	acquired immuno-deficiency syndrome
AS	alternative splicing
ASE	alternative splicing event
ATP	adenosine triphosphate
B.C.	before Christ
C	capsid (structural protein)
C	cytosine
cDNA-AFLP	complementary deoxyribonucleic acid - amplified fragment length polymorphism
cGAS	cyclic GMP-AMP synthase
co-IP	co-immunoprecipitation
COVID-19	coronavirus disease 2019
CPA	cleavage and polyadenylation
CTD	carboxy-terminal domain
C-terminal	carboxy-terminal
DB	dumb bell
DD-RT-PCR	differential display reverse transcription polymerase chain reaction
de novo	latin, meaning "from the beginning"
DEET	N,N-diethyl-meta-toluamide
DENV	dengue virus

DF	dengue fever
DHF	dengue hemorrhagic fever
DISC	death-inducing signaling complex
DNA	deoxyribonucleic acid
dsDNA	double-stranded deoxyribonucleic acid
dsDNA-RT	double-stranded deoxyribonucleic acid reverse-transcribing
dsRNA	double-stranded ribonucleic acid
DSS	dengue shock syndrome
E	envelope (structural protein)
e.g.	exempli gratia (latin, meaning “for example”)
eEF	eukaryotic elongation factor
eIF	eukaryotic initiation factor
ER	endoplasmic reticulum
ERAD	endoplasmic reticulum-associated degradation
eRF	eukaryotic release factor
ESE	exonic splicing enhancer
et al.	*et alia* (latin, meaning “and others”)
G	guanine
GDP	guanosine diphosphate
GMP	guanosine monophosphate
GO	gene ontology
GTase	guanylyltransferase
GTP	guanosine triphosphate
h	hour
HIV	human immunodeficiency virus
i.e.	*id est* (latin, meaning “that is”)
ICTV	International Committee on Taxonomy of Viruses
IFIT	interferon induced protein with tetratricopeptide repeats
IFITM	interferon induced transmembrane protein
IFN	interferon
IFNAR	interferon alpha receptor

IFNGR	interferon Gamma Receptor
IFNLR	interferon Lambda Receptor
IL	interleukin
in silico	pseudo-latin, meaning "performed on computer or via computer simulation"
in vitro	latin, meaning "in glass"
in vivo	latin, meaning "within the living"
IR3535	ethyl butylacetylaminopropionate
IRE1	inositol requiring kinase 1
IRES	internal ribosome entry site
IRF	interferon regulatory transcription factor
ISG	interferon-stimulated gene
ISGF3	interferon-stimulated gene factor 3
ISRE	interferon-stimulated response element
ITC	isothermal titration calorimetry
JAK	Janus kinase
JEV	Japanese encephalitis virus
KUNV	Kunjin virus
M	membrane (structural protein)
MAPK	mitogen-activated protein kinase
MAVS	mitochondrial antiviral-signaling protein
MD	molecular dynamics
Met-tRNAi	initiating methionyl transfer ribonucleic acid
Mg	magnesium
microRNA	micro ribonucleic acid
MOI	multiplicity of infection
mRNA	messenger
MS	mass spectrometry
MTase	methyltransferase
n/a	not available
NI	nucleoside inhibitor

NLR	NOD-like receptor
NNI	non-nucleoside inhibitor
NRG1	neuregulin 1
NS	non-structural protein
nt	nucleotide
N-terminal	amino-terminal
NTP	ribonucleoside triphosphate
NTPase	nucleoside triphosphatase
OAS	2'-5'-oligoadenylate synthetase
ORF	open reading frame
PABP	polyA binding protein
PAC-Seq	polyadenosine click sequencing
PAMP	pathogen-associated molecular pattern
PAP	polyA polymerase
PAS	polyadenylation signal
P-bodies	processing bodies
PERK	protein kinase R-like endoplasmic reticulum kinase
PI3K	phosphoinositide 3-kinase
PIC	preinitiation complex
PK	pseudoknot
PKA	protein kinase A
PKR	protein kinase R
Pol	ribonucleic acid polymerase
polyA	polyadenosine
post-TC	post-termination complex
PPI	protein-protein interaction
ppRNA	5' diphosphorylated ribonucleic acid
pre-mRNA	pre-messenger ribonucleic acid
prM	precursor membrane protein
PRR	pattern recognition receptor
RBP	ribonucleic acid-binding protein

RdRp	ribonucleic acid-dependent ribonucleic acid polymerase
RIDD	regulated inositol requiring kinase 1-dependent decay
RIG-I	retinoic acid-inducible gene I
RLR	retinoic acid-inducible gene I-like receptor
RNA	ribonucleic acid
RNase	ribonuclease
RNA-Seq	next generation ribonucleic acid sequencing
rRNA	ribosomal ribonucleic acid
RTPase	ribonucleic acid triphosphatase
SAH	S-adenosyl-L-homocysteine
SAM	S-adenosyl methionine
SARS-CoV-2	Severe acute respiratory syndrome coronavirus 2
scRNA-Seq	single cell ribonucleic acid sequencing
SDS-PAGE	sodium dodecyl sulfate polyacrylamide gel electrophoresis
sfRNA	subgenomic flavivirus RNA
SG	stress granule
shHP	short hairpin
SILAC	stable isotope labeling by amino acids in cell culture
SL	stem loop
snoRNA	small nucleolar ribonucleic acid
snRNA	small nuclear ribonucleic acid
snRNP	small nuclear ribonucleoprotein
spp	species (plural form)
SPR	surface plasmon resonance
ssDNA	single-stranded deoxyribonucleic acid
ssRNA	single-stranded ribonucleic acid
ssRNA-RT	single-stranded ribonucleic acid reverse-transcribing
STAT	signal transducer and activator of transcription
STING	stimulator of interferon genes
T	thymine
TAM	Tyro3, Axl, Mer

TBK1	TANK Binding Kinase 1
TBP	TATA-binding protein
TC	ternary complex
TCA cycle	tricarboxylic acid cycle
TF	transcription factor
TLR	Toll-like receptor
tRNA	transfer ribonucleic acid
TYK2	tyrosine kinase 2
U	uracil
UBL	ubiquitin-like
uORF	upstream open reading frame
UPR	unfolded protein response
UTR	untranslated region
WB	western blot
WNV	West Nile virus
XBP1	X-Box Binding Protein 1
XRN1	5'-3' exoribonuclease 1
YFV	yellow fever virus
ZIKV	Zika virus

1 INTRODUCTION

1.1 Infectious diseases

An infectious disease, also referred to as transmissible or communicable disease, is the illness that an organism develops when a pathogen invades its body. There is a wide variety of microorganisms, such as viruses, bacteria, fungi, and protozoans, that can cause infections. These infectious agents can enter the host body through different ways, for instance inhalation of airborne microbes, ingestion of contaminated food or water, skin contact, bites from vectors (e.g. ticks or mosquitoes), sexual contact, and maternal-fetal transmission via the placenta and birth canal. Some infections (e.g. measles, malaria) affect the entire body, whereas others (e.g. common cold) affect only one organ or system of the body. Moreover, some infections cause mild symptoms, whereas others are deadly (Baylor College of Medecine, 2022; Infectious Diseases Society of America, 2022).

Infectious diseases have caused many epidemics and pandemics over the course of human history, resulting in a great number of deaths. The earliest documented epidemic, which is suspected to have been typhoid fever or Ebola, occurred in 430 B.C., killing as much as two thirds of the population of Athens (History.com, 2021; Jarus, 2021). Major epidemics and pandemics in human history that have caused several million deaths are displayed in Table 1.

In recent human history, significant advances in prevention and treatment of infections have been made, including vaccines, antibiotics and other antimicrobials, adequate sewage treatment and access to clean water, sanitary handling of food, and surveillance of communicable diseases. Yet, infectious diseases still claim millions of lives every year, especially in low-income countries. Growing populations as well as frequent and long-distance travel facilitate the spread of infections. Moreover, new and potentially dangerous pathogens emerge every year, and already known pathogens may develop a resistance to available treatments (Baylor College of Medecine, 2022; Infectious Diseases Society of America, 2022).

Table 1. Major epidemics and pandemics in human history. Data was obtained from (History.com, 2021; Jarus, 2021).

Name	Years	Estimated number of deaths	Disease	Geographical distribution
Antonine plague	165-180	5 million	Smallpox or measles?	Roman Empire
Plague of Justinian	541-542	25 million	Bubonic plague	Byzantine Empire
Black Death	1346-1353	75-200 million	Bubonic plague	Europe, North Africa, Asia
Cocoliztli epidemic	1545-1548	15 million	Salmonella?	Mexico & central America
American plagues	16th century	90% of indigenous population	Smallpox (amongst others)	Western hemisphere
Spanish flu	1918-1920	20-50 million	Influenza	Worldwide
HIV/AIDS	1981-present	36 million	Acquired immuno-deficiency syndrome	Worldwide
COVID-19	2019-present	6 million	Coronavirus disease 2019	Worldwide

1.1.1 Zoonotic diseases

60-75% of existing and newly identified infectious diseases are zoonoses. A zoonosis is a disease or infection that has spread from a vertebrate animal to humans. The transmission of an infection from an animal to a human is called a spillover event (World Health Organization, 2020; reviewed in Ellwanger and Chies, 2021). It can occur through any contact with a domestic, agricultural, or wild animal, including direct contact with an animal or its body fluids, contact with areas where animals live or objects that have been contaminated, a bite from a vector, and ingestion of contaminated food or water. A given microorganism may cause different symptoms in animals and humans, and an animal may appear to be healthy, despite carrying a pathogen that is dangerous for humans (Centers for Disease Control and Prevention, 2022a; World Health Organization, 2020). Once a first human is infected in a spillover event, the pathogen may or may not spread in the human population. In some cases, the conditions are not favorable for its dissemination, the pathogen does not spread, and the animal-to-human transmission is a dead-end spillover without impact on the human population (reviewed in Ellwanger and Chies, 2021). In other cases

(e.g. Ebola, COVID-19), the pathogen may spread in the population though human-to-human transmission, leading to an epidemic or a pandemic (World Health Organization, 2021, 2020). Some diseases that started as zoonoses may even evolve into human-only strains, like HIV (World Health Organization, 2020).

1.2 Viruses

Viruses are small biological entities at the edge of living and non-living. They are composed of genomic material, which can be DNA or RNA, as well as a protein capsid, and sometimes a lipid envelope containing one or more receptor proteins. Their replication is dependent on their host cell, which makes them obligate intracellular parasites. A viral replication cycle includes attachment and entry of the virus into the host cell, decoding of viral genomic information, viral genome replication, and assembly and release of new virions containing the viral genome from the host cell (reviewed in Flint et al., 2015).

1.2.1 Virus classification and nomenclature

Regarding viral nomenclature, there is no consistent system for naming new viral isolates. For example, some viruses were named for the scientists who discovered them (e.g. Epstein-Barr virus) or for the geographic region where they were discovered (e.g. Sendai virus). Other virus names are associated with the disease that they cause, or the area of the body that they affect (e.g. poliovirus and rhinovirus, respectively). Other origins of designations as well as combinations of the above-mentioned examples of nomenclature (e.g. Rous sarcoma virus) are also used (reviewed in Flint et al., 2015).

1.2.1.1 Baltimore classification

In 1971, David Baltimore proposed a viral classification system based on their genome types and how viral mRNA is produced from the viral genome. The Baltimore classification includes 7 groups: double-stranded DNA (dsDNA) viruses, single-stranded DNA (ssDNA) viruses, double-stranded RNA (dsRNA) viruses, single-stranded positive-sense RNA ((+)ssRNA) viruses, single-stranded negative-sense ((-)ssRNA) viruses, single-stranded

RNA reverse-transcribing (ssRNA-RT) viruses, and double-stranded DNA reverse-transcribing (dsDNA-RT) viruses (Figure 1) (reviewed in Baltimore, 1971; Flint et al., 2015).

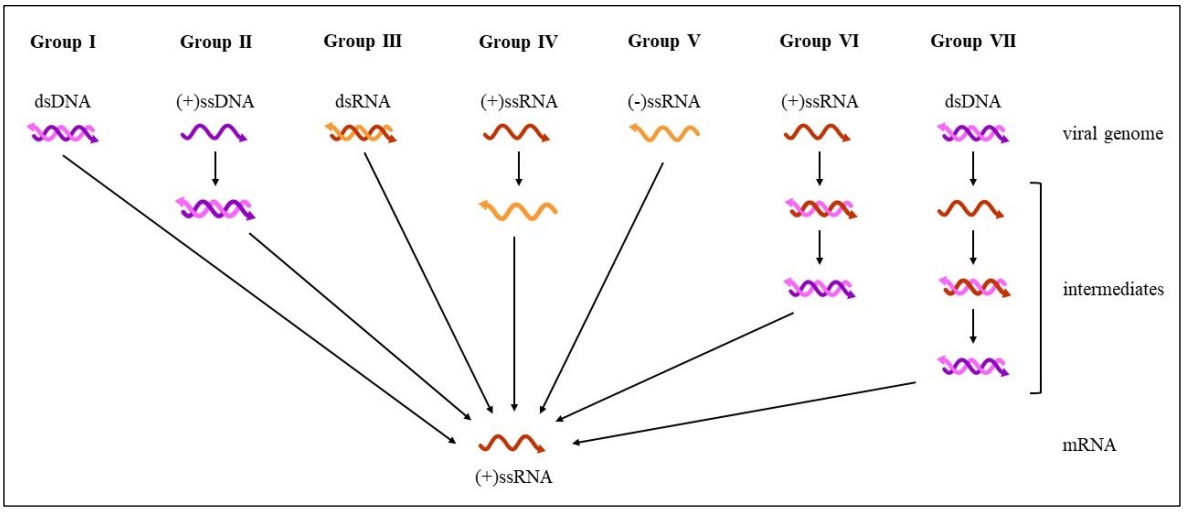

Figure 1. Baltimore classification of viruses. The Baltimore classification system is based on the nature of the viral genome and the way to produce viral mRNA from the genome. It includes 7 groups. Figure adapted from (Flint et al., 2015).

1.2.1.2 International Committee on Taxonomy of Viruses (ICTV)

Since 1971, the International Committee on Taxonomy of Viruses (ICTV) has been publishing reports on virus classification about twice a decade. The system is made of a fifteen-rank structure: realm, subrealm, kingdom, subkingdom, phylum, subphylum, class, subclass, order, suborder, family, subfamily, genus, subgenus, and species (ICTV Executive Committee, 2020). The species concept has been controversial among virologists for a long time for multiple reasons, one of them being the lack of a clear definition of a virus species, although various definitions had been proposed. In 1991, the ICTV defined a virus species as "a polythetic class of viruses that constitute a replicating lineage and occupy a particular ecological niche" (reviewed in Van Regenmortel, 2011). In 2013, the definition was changed to "a monophyletic group of viruses whose properties can be distinguished from those of other species by multiple criteria". Moreover, it has been established that the ICTV is not responsible for classifying and naming virus taxa below the rank of species, such as serotypes, genotypes, strains, variants, and isolates (Adams et al., 2013).

1.3 Flaviviruses

According to the ICTV virus taxonomy 2019 release, the genus *Flavivirus* includes 53 species, amongst others the important human pathogens dengue virus, yellow fever virus, Zika virus, West Nile virus, and Japanese encephalitis virus. It is part of the family *Flaviviridae*, the order *Amarillovirales*, the class *Flasuviricetes*, the phylum *Kitrinoviricota*, the kingdom *Orthornavirae* and the realm *Riboviria*. The type species of the genus *Flavivirus* is yellow fever virus (International Committee on Taxonomy of Viruses, 2019). According to the Baltimore classification, Flaviviruses are part of group IV (+)ssRNA viruses.

1.3.1 Antigenic and phylogenetic classification of Flaviviruses

The majority of Flaviviruses can be divided into eight serocomplexes: tick-borne encephalitis, Rio Bravo, Japanese encephalitis, Tyuleniy, Ntaya, Uganda S, dengue, and Modoc. Viruses that induce antibodies which are able to cross-neutralize each other belong to the same serocomplex. In addition to being antigenically alike, viruses in each serocomplex also have similar geographical distribution or share the same transmission vectors. However, some Flaviviruses failed to cross-react significantly with other Flaviviruses, and could not be assigned to any serocomplex (Calisher et al., 1989).

Flaviviruses can also be classified based on phylogenetic analyses using nucleotide or amino acid sequences of individual proteins (Gaunt et al., 2001; Kuno et al., 1998), the full-length polyprotein (reviewed in Rathore and St. John, 2020), or the entire genome (Cook and Holmes, 2006). These analyses identified three clusters of flaviviruses, namely mosquito-borne, tick-borne, and no-known-vector viruses, which can be further divided into clades (Figure 2). Clades were found to correlate well with previously established antigenic complexes (Kuno et al., 1998) as well as with vector species, vertebrate hosts, and associated disease (Gaunt et al., 2001). The exact phylogenetic tree topology depends on the nucleotide or amino acid sequences that are aligned, and the ancestral mode of transmission, as well as the chronological order in which different traits were derived are still debated.

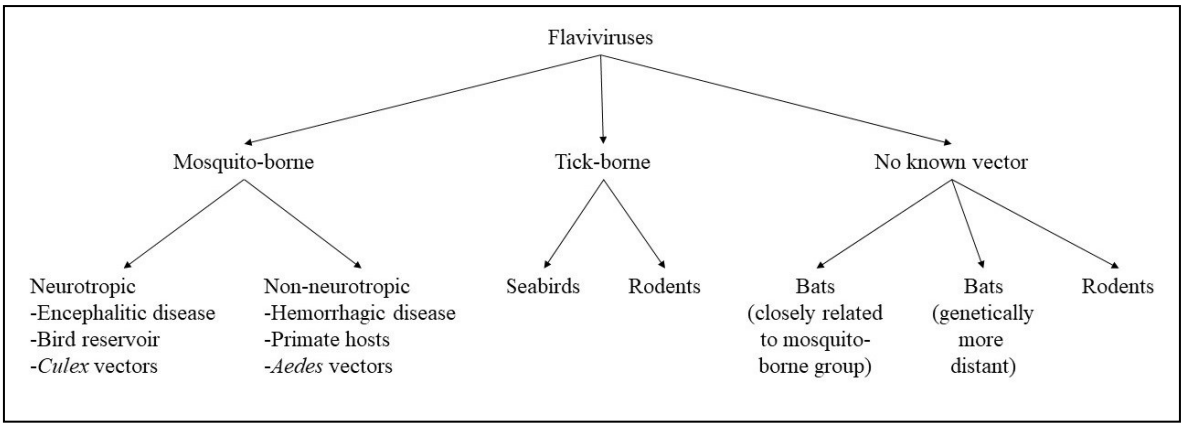

Figure 2. Classification of flaviviruses based on phylogenetic analyses. Flaviviruses can be divided into three clusters, namely mosquito-borne, tick-borne, and no-known-vector viruses. They can be further divided into clades which correlate well with vector species, vertebrate hosts, and associated disease. Figure adapted from (Gaunt et al., 2001).

1.3.2 Mosquito-borne Flaviviruses and human health

Several mosquito-borne Flaviviruses, such as dengue virus (DENV), West Nile virus (WNV), yellow fever virus (YFV), Zika virus (ZIKV) and Japanese encephalitis virus (JEV), are important human pathogens. They are found mostly in tropical and subtropical areas, and more than half of the world's population lives at risk of exposure to at least one pathogenic Flavivirus (Table 2).

1.3.2.1 Transmission of mosquito-borne Flaviviruses

Mosquito-borne Flaviviruses are transmitted to vertebrate hosts through mosquito bites. In infected mosquitos, virus accumulates in the salivary gland, leading to high viremia in the saliva. While taking a blood meal, mosquitoes inject their saliva in the dermal layer of the skin to release at least one vasodilator, one coagulation inhibitor and one platelet inhibitor for a more efficient feeding (reviewed in Colpitts et al., 2012). If they are a Flavivirus carrier, a high dose of virus is thus injected extravascularly into the skin. In addition, a low dose of virus has been shown to be inoculated intravascularly during feeding (Styer et al., 2007). Upon injection into the skin, Flaviviruses infect dendritic cells of the epidermis and dermis, which then infiltrate the lymphatic system to disseminate the virus throughout the human body (reviewed in Burrell et al., 2017; Daep et al., 2014). Depending on the species of Flavivirus, preferred host cells may be endothelial cells (DENV), hepatocytes (YFV), or

neurons and other brain cells (WNV, ZIKV, JEV) (reviewed in Guarner and Hale, 2019). In addition, Flaviviruses have been found to infect natural killer cells, monocytes, macrophages, lymphoid (T and B) cells (reviewed in Daep et al., 2014).

Table 2. Recent statistics of Flavivirus impact on human health. The number of people at risk of infection, countries affected, clinical cases and deaths per year associated with dengue virus (World Health Organization, 2022), Japanese encephalitis virus (World Health Organization, 2019a), yellow fever virus (World Health Organization, 2019b) and Zika virus (Xu et al., 2022) are shown.

Virus	Population at risk	Number of countries affected	Estimated number of clinical cases per year	Estimated number of deaths per year
DENV	3.9 billion	129 (worldwide)	96 million (any severity)	n/a
JEV	>3 billion	24 (South-East Asia, Western Pacific)	68,000	14,000-20,000
YFV	n/a	47 (Africa, Central & South America)	84,000-170,000 (severe cases)	29,000-60,000
ZIKV	6.22 billion	86 (South Asia, Central Africa, Americas)	n/a	n/a

Mosquito-borne Flaviviruses are mainly transmitted horizontally in transmission cycles between mosquito vectors, either *Culex* or *Aedes* spp, and mammalian or avian hosts (Figure 3). *Culex* mosquitoes are nighttime biters and prefer a habitat with trees and vegetation in temperate regions. Flaviviruses transmitted by *Culex* spp, such as WNV and JEV, are maintained in a transmission cycle between several species of *Culex* mosquito vectors and >250 species of birds (WNV) or pigs and wading birds (JEV) which develop high viremia and thus serve as amplifying hosts. Humans can be infected, but since viral titers in their bloodstream are too low to infect subsequent biting mosquitoes, they are incidental dead-end hosts (Centers for Disease Control and Prevention, 2022b; reviewed in Hale, 2023). Daytime feeding *Aedes* mosquitoes prefer tropical and subtropical climates, but given their invasive nature, they are increasingly found in more temperate regions. They transmit Flaviviruses, including DENV, ZIKV and YFV, in two distinct transmission cycles,

namely a sylvatic cycle and an urban cycle. In the enzootic, sylvatic cycle, Flaviviruses circulate between non-human primate hosts and arboreal *Aedes* spp vectors. In the urban cycle, they circulate between human hosts and domesticated *Aedes* spp mosquitoes, mostly *Ae. aegypti*. These two transmission cycles are connected by bridge vectors, i.e. some *Aedes* species that feed on both non-human primates and humans, and humans who enter the forest and then return to villages, rural towns and cities, such as forestry workers and travelers (reviewed in Hale, 2023; Vasilakis and Weaver, 2016).

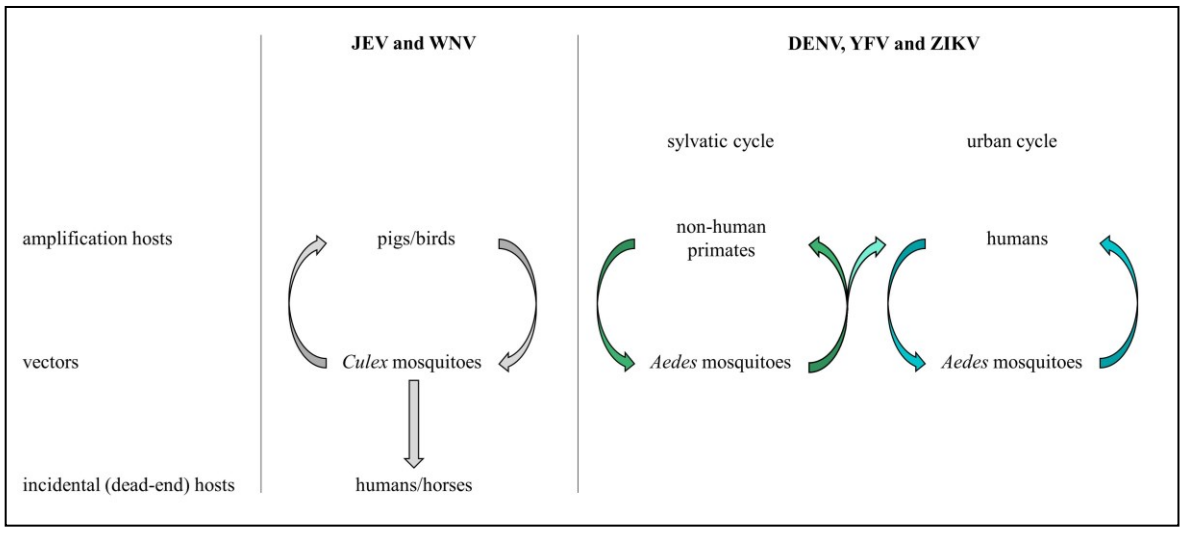

Figure 3. Mosquito-borne Flavivirus transmission cycles. Flaviviruses transmitted by *Culex* spp mosquitoes rely on pigs (JEV) and birds (JEV, WNV) as amplification hosts, whereas humans are incidental dead-end hosts. Flaviviruses transmitted by *Aedes* spp mosquitoes (DENV, YFV, ZIKV) have two distinct transmission cycles involving non-human primates and humans as amplification hosts, respectively. Figure created with information from (Centers for Disease Control and Prevention, 2022b; Hale, 2023; Vasilakis and Weaver, 2016).

Vertical transmission of Flaviviruses, i.e. transmission from a mother to her offspring, has also been observed. In mosquitoes, transgenerational transmission of DENV (Rosen, 1987), JEV (Rosen, 1988), YFV (reviewed in Monath, 2001), WNV (Nelms et al., 2013) and ZIKV (Lai et al., 2020) has been documented. In humans, ZIKV can be transmitted from mother to fetus during pregnancy (World Health Organization, 2018), and there is evidence that it can be transmitted through breastfeeding (Blohm et al., 2018).

1.3.2.2 Symptoms of Flavivirus infections

Most Flavivirus cases (approximately 80%) are asymptomatic, and for people who show symptoms, the most common are fever, headache, muscle and joint pain, rash, nausea and vomiting (World Health Organization, 2022, 2019a, 2019b, 2018). However, in a small fraction of cases, Flaviviruses can cause severe illness that may be fatal.

Symptomatic dengue used to be classified into dengue fever (DF), dengue hemorrhagic fever (DHF) and dengue shock syndrome (DSS), but following a revision in 2009, it is now classified into non-severe dengue with or without warning signs and severe dengue (Horstick et al., 2015). Severe dengue may manifest in dengue patients when fever drops below 38°C after approximately 3-7 days. It is associated with fluid accumulation, plasma leaking, severe bleeding, respiratory distress and organ impairment (World Health Organization, 2022). The risk of developing severe dengue depends on the serotype, and secondary infection with a different serotype is more likely to result in severe dengue than primary infection (Soo et al., 2016).

Approximately 1 in 250 JEV infections is associated with severe symptoms including disorientation, seizures, spastic paralysis, and coma. Up to 30% of those who show disease symptoms die from the infection, and 20-30% of those who survive suffer permanent sequelae such as paralysis, recurrent seizures or inability to speak (World Health Organization, 2019a).

Approximately 15% of symptomatic yellow fever patients enter a second, more severe phase shortly after recovering from initial symptoms. In this phase, patients experience high fever, jaundice, abdominal pain, and vomiting. Moreover, bleeding from mouth, nose, eyes, and stomach may occur. Approximately half of the patients who enter the more severe phase die within 7-10 days (Pan American Health Organization, 2023; World Health Organization, 2019b).

ZIKV infection has different effects depending on the age of the patient. In adults and older children, it may cause neuropathy, myelitis, or Guillain-Barré syndrome. When

infection occurs during pregnancy, ZIKV may cause pregnancy complications such as fetal loss, preterm birth or stillbirth, and the fetus may develop microcephaly or other congenital abnormalities (World Health Organization, 2018).

1.3.2.3 Treatment and prevention of Flavivirus infections

There are currently no specific antiviral drugs to treat Flavivirus infections. Patients should rest and stay hydrated. Supportive care, including certain types of pain killers and fever reducers, are used to relieve symptoms. For patients with yellow fever, specific care to treat liver and kidney failure has been shown to improve outcomes (Mayo Clinic, 2022; World Health Organization, 2022, 2019b, 2019a).

Prevention of mosquito-borne Flavivirus infections relies mainly on immunization, protection from mosquito bites, and vector control.

1.3.2.3.1 Vaccination

The first vaccines to prevent a Flavivirus infection (YFV) were developed in 1928 (Hindle, 1928). The live attenuated yellow fever 17D vaccine, of which three substrains are still produced and used internationally for vaccination campaigns today, was developed in the 1930s by passage of the wild-type strain Asibi in chicken and mouse tissue. One dose confers protection in >95% of recipients within 30 days following administration, and it is considered to give lifelong protection in most populations. In fact, neutralizing antibodies have been detected up to 60 years after vaccination (reviewed in Collins and Barrett, 2017). For many years, the yellow fever 17D vaccine was considered to be one of the safest vaccines available. However, rare serious adverse events with high lethality have been reported since 2001. One study during a vaccination campaign in Argentina reported 0.05 confirmed cases of vaccine-associated viscerotropic disease per 100,000 doses administered. Another study found 1.03 cases of vaccine-associated neurotropic disease per 100,000 doses during a campaign in Brazil. Despite these serious adverse events, vaccination remains the best strategy to prevent yellow fever (reviewed in de Menezes Martins et al., 2015).

The first licenced vaccine against JEV was developed in 1935 by inactivation of virus extracted from brain homogenates of mice infected with the Nakayama strain. It was the only available vaccine against JEV for several decades, but ultimately its production was halted in 2006 for multiple reasons, including the need for 2-3 primary doses plus boosters. Currently, a live-attenuated cell culture-derived vaccine based on the SA_{14}-14-2 strain, first licenced in 1988 in China, is the most widely used vaccine in endemic areas (reviewed in Yun and Lee, 2014). The protective efficacy of a single dose of this vaccine was found to be 94.5% to 99.3% (Bista et al., 2001; Kumar et al., 2009; Ohrr et al., 2005). Moreover, there are several cell culture-derived killed-inactivated vaccines that were developed from different JEV strains and that are produced in different cell lines: the Beijing-3 strain has been produced in PHK (primary hamster kidney) or Vero (African green monkey kidney) cells, and the Beijing-1 strain as well as the SA_{14}-14-2 strain are produced in Vero cells. Finally, a recombinant live-attenuated chimeric YF-JEV has been genetically engineered and produced in Vero cells. In this chimeric virus, the structural proteins prM and E from the JEV SA_{14}-14-2 strain are expressed in the context of the YFV 17D strain (reviewed in Yun and Lee, 2014).

The first licenced DENV vaccine (Dengvaxia / CYD-TDV) received FDA approval in 2015 and is now available in more than 20 countries (reviewed in Norshidah et al., 2021). This tetravalent vaccine is composed of four recombinant, live-attenuated dengue viruses. Each of the chimeric viruses expresses the wild-type prM and E proteins of one of the four dengue virus serotypes on the YFV 17D backbone (reviewed in Guy et al., 2011). The vaccine has been shown to be highly effective in preventing dengue disease caused by any of the four serotypes. However, retrospective analyses of the long-term safety data have shown an increased risk of development of severe dengue in people who were seronegative at the time of immunization and who had a spontaneous dengue infection approximately 3 years after receiving the vaccine. Therefore, vaccination is only recommended for those who are seropositive to prevent severe secondary dengue infection (reviewed in Norshidah et al., 2021; Wilder-Smith, 2020). In 2022, a second tetravalent, live-attenuated DENV vaccine (Qdenga / Denvax / TAK003) was approved in Indonesia and Europe. This vaccine can be administered to adults and children aged 4 years and older, regardless of previous dengue

exposure (European Medicines Agency, 2023; Takeda, 2022a, 2022b). It consists of four recombinant live-attenuated viruses, namely an attenuated DENV2 strain, as well as chimeric viruses for DENV1, DENV3 and DENV4 which express the corresponding prM and E proteins on the DENV2 backbone (Huang et al., 2013). Currently, several other dengue vaccine candidates are under development, amongst others two live-attenuated dengue vaccines that are in phase III clinical trials (reviewed in Kariyawasam et al., 2023; Norshidah et al., 2021; Wilder-Smith, 2020).

1.3.2.3.2 Protection from mosquito bites

If vaccination is not an option (e.g. no licenced vaccine available, contraindications for certain populations, limited access in remote areas), Flavivirus infections can be prevented by protection from mosquito bites. It is recommended to wear light-colored, long-sleeved clothing, to apply insect repellent containing DEET, IR3535 or icaridin, to install window screens, and to sleep under a mosquito net (World Health Organization, 2022, 2018).

1.3.2.3.3 Vector surveillance and control

Control of vector populations remains an important aspect in the prevention of Flavivirus transmission. Although the use of persistent insecticides has been successful in the past, their highly toxic nature makes them environmentally unacceptable nowadays (reviewed in Vasilakis and Weaver, 2016). Instead, efforts are focused on eliminating mosquito breeding sites or preventing mosquitoes from accessing them by removing standing water from flowerpots, cleaning up and properly disposing of used tires and other solid waste, as well as covering and regularly emptying and cleaning water storage containers (World Health Organization, 2022, 2018). Mosquito populations can also be reduced by using lethal traps, and by releasing mosquitoes harboring the *Wolbachia* bacteria or genetically modified mosquitoes. The *Wolbachia* bacteria interferes with viral replication in the mosquito and thus suppresses viral transmission, whereas the genetically modified mosquitoes carry a dominant lethal gene that kills all offspring from mating with wild female mosquitoes (reviewed in Vasilakis and Weaver, 2016). The effectiveness of control measures can be assessed through active monitoring and surveillance of mosquito vector abundance and species composition

(World Health Organization, 2022). A study from Mexico compared three strategies of vector control, namely an intervention to promote community participation in vector breeding site elimination, ultra-low volume spraying of insecticides, and both. Dengue incidence was found to be reduced approximately two-fold in each study group (17.4%, 14.3% and 14.4%, respectively) compared to the control group (30.2%), with ultra-low volume spraying of insecticides being slightly more efficient but less cost-effective than community participation (Mendoza-Cano et al., 2017).

1.3.3 Flavivirus replication cycle

Binding of the envelope (E) protein to receptors and attachment factors on the host cell surface triggers receptor-mediated endocytosis. Glycosaminoglycans are thought to attach and concentrate virus particles on the cell surface, whereas calcium-dependent lectin receptors, $\alpha_v\beta_3$ integrin, as well as phosphatidylserine, TIM and TAM receptors have been proposed as candidate receptors for Flavivirus entry in different cell types (reviewed in Kaufmann and Rossmann, 2011; Perera-Lecoin et al., 2013). The E protein undergoes a conformational change and trimerizes as a result of the acidic environment in the late endosome, which causes the viral and endocytic membranes to fuse and results in the release of the viral nucleocapsid core into the cytoplasm (reviewed in Kaufmann and Rossmann, 2011; Stiasny et al., 2011). Viral RNA then dissociates from the capsid (C) protein and the viral genome is translated into the viral polyprotein by ribosomes on the rough ER (Stohlman et al., 1975). Three viral proteins, namely prM, E and NS1, contain signal sequences which cause their translocation into the ER lumen (reviewed in Perera and Kuhn, 2008). Moreover, the transmembrane domains of NS2A, NS2B, NS4A, 2K and NS4B are inserted into the ER membrane, and only C, NS3 and NS5 stay in the cytoplasm (reviewed in Lindenbach et al., 2007; Perera and Kuhn, 2008). The polyprotein is cleaved into individual viral proteins by host signalases in the ER lumen and the viral NS2B-NS3 protease in the cytoplasm (reviewed in Perera and Kuhn, 2008). Polyprotein translocation and processing has been shown to occur co- and post-translationally (reviewed in Lindenbach et al., 2007). Once synthesized and processed, the individual viral proteins assume their respective functions, and replication of the viral genome is initiated. ER membrane curvature is induced to form replication organelles that are connected to the cytoplasm only though a small pore (Gillespie et al.,

2010; Miller et al., 2007, 2006; Uchil and Satchidanandam, 2003; Welsch et al., 2009; reviewed in Paul and Bartenschlager, 2013). Viral replication takes place in these vesicles where viral proteins and RNA are protected from host proteases and nucleases (Uchil and Satchidanandam, 2003; reviewed in Paul and Bartenschlager, 2013) as well as interferon-stimulated proteins with antiviral activity, such as PKR, OAS and MxA (Hoenen et al., 2007). Furthermore, all components necessary for viral replication are concentrated in these compartments, thus ensuring highly efficient replication (reviewed in Paul and Bartenschlager, 2013). First, the single-stranded positive sense genomic RNA is transcribed into a negative strand, thus forming double-stranded RNA (dsRNA), also known as replicative form or replication intermediate. This step of viral replication relies mostly on the NS5 RdRp, and NS3 does not seem to be strictly necessary. The dsRNA then serves as template for the synthesis of a large number of capped (+)ssRNA viral genomes. This step is

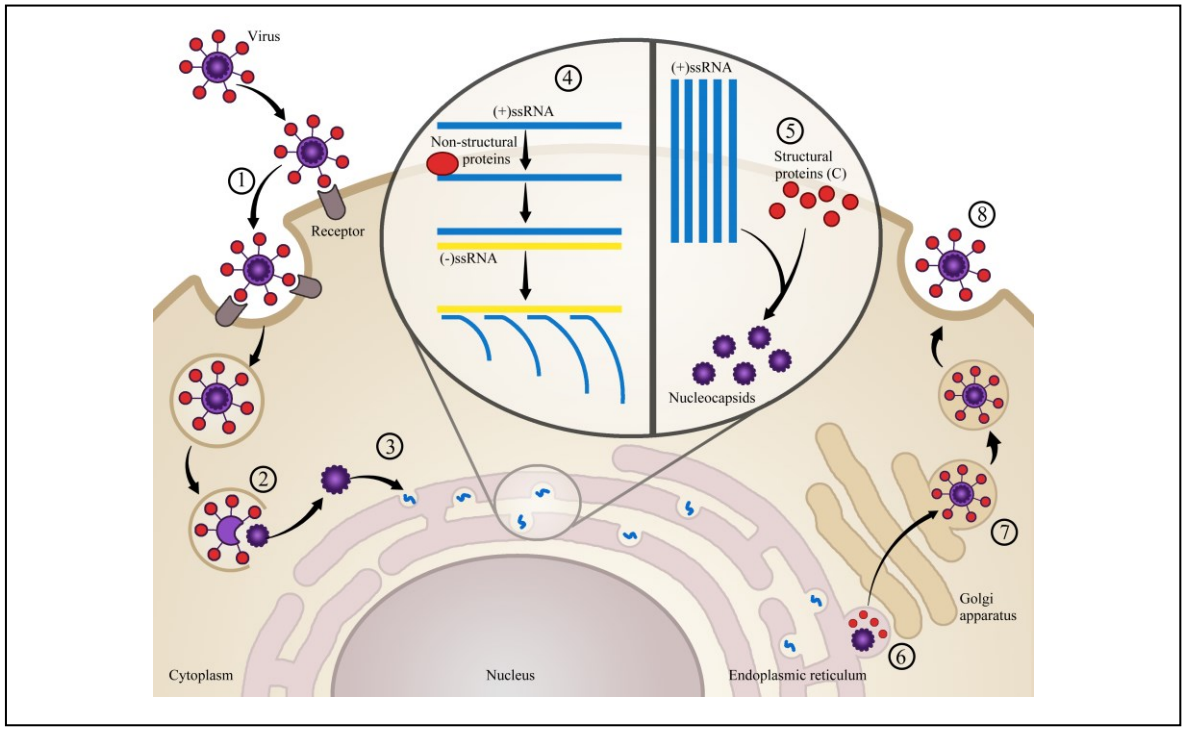

Figure 4. Flavivirus replication cycle. The virus enters the host cell through receptor-mediated endocytosis (1) which is followed by release of the viral genome into the cytoplasm (2). Viral RNA is translated into viral proteins at the rough ER (3). The non-structural proteins form the replication complex that produces many new viral genomes (4). These genomes are associated with capsid proteins to form nucleocapsids (5) that bud into the ER containing the other two structural proteins (6). The nascent virions mature in the trans-Golgi network (7) and are released from the host cell through exocytosis (8). Figure adapted from (Suthar et al., 2013).

much more complex, given that it requires dsRNA unwinding. Moreover, it is coupled to positive strand capping, and therefore involves the replicase complex formed of the NS3 helicase domain and both domains of NS5 (reviewed in Saeedi and Geiss, 2013). Once released from the replication compartments, the newly generated viral genomes are used for multiple purposes (Miorin et al., 2013; reviewed in Saeedi and Geiss, 2013). Some of them are translocated to the rough ER for further viral protein synthesis. Others are directed toward P-bodies for the generation of sfRNA (Funk et al., 2010; Pijlman et al., 2008). Finally, some of the nascent viral genomes bind C proteins to form nucleocapsids and then bud into the ER lumen through the ER membrane containing prM and E glycoproteins, resulting in the formation of immature virus particles (reviewed in Lindenbach et al., 2007). Budding has been shown to take place close to the neck of replication organelles to limit the exposure of viral RNA to host cell nucleases and sensors of the innate immune response (Welsch et al., 2009). While the immature virus particles travel through the trans-Golgi network, the prM protein is cleaved into the mature M protein, and the E protein undergoes conformational changes (reviewed in Perera and Kuhn, 2008). Mature, infectious virus particles are finally released by exocytosis (reviewed in Lindenbach et al., 2007; Suthar et al., 2013). In addition to infectious virions, non-infectious subviral particles are also assembled in the ER and released from infected cells. They only contain a lipid envelop and the two viral glycoproteins, but no nucleocapsid (Schalich et al., 1996; reviewed in Mukhopadhyay et al., 2005). They are also called defective interfering particles, since they possess hemagglutination activity and have been proposed to act as decoys to confuse the immune system (reviewed in Heinz and Allison, 2000). The Flavivirus replication cycle is illustrated in Figure 4.

1.3.4 Flavivirus genome and proteins

Flaviviruses have a positive-sense, single-stranded RNA ((+)ssRNA) genome of approximately 11kb. Their genome possesses a 5’ cap structure but no 3’ poly-A tail. It also contains 5’ and 3’ untranslated regions (UTRs) as well as one open reading frame (ORF) that encodes the viral polyprotein (Figure 5). The viral genome also functions as the viral mRNA. The polyprotein is cleaved by viral and host proteases into three structural (capsid (C), membrane (M), envelope (E)) and seven or eight non-structural proteins (NS1, NS2A, NS2B,

NS3, NS4A, (2K), NS4B, NS5), depending on whether the 2K peptide is considered to be an individual protein or part of the NS4B protein. Of these viral proteins, only two exhibit enzymatic activities, namely NS3 and NS5 (reviewed in Chambers et al., 1990a; Lindenbach et al., 2007).

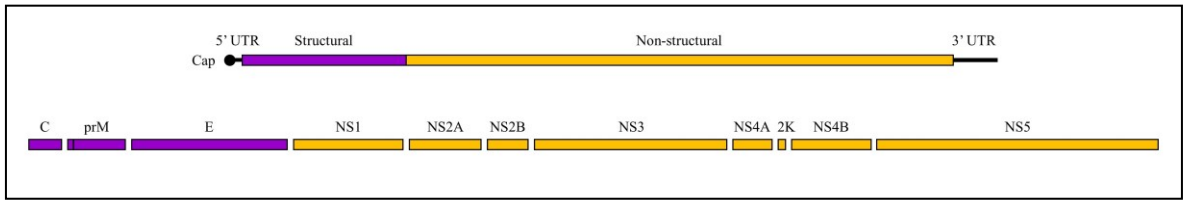

Figure 5. Flavivirus genome and proteins. Schematic linear representation of the Flavivirus genome with its 5' cap structure, 5' and 3' UTRs, and ORF encoding three structural (purple) and eight non-structural (yellow) proteins. Figure adapted from (Sampath and Padmanabhan, 2009).

1.3.4.1 Subgenomic Flavivirus RNA

Non-coding subgenomic Flavivirus RNA (sfRNA) is derived from the 3' UTR of the Flavivirus genome (Lin et al., 2004; Pijlman et al., 2008). It is highly structured, and it is produced by incomplete degradation of the viral genome by the cellular 5'-3' ribonuclease XRN1 (Pijlman et al., 2008). In fact, stem loop (SL) and pseudoknot (PK) interactions form rigid secondary structures which stall XRN1, thus protecting the RNA from complete degradation (Funk et al., 2010; Silva et al., 2010). Up to four sfRNAs have been shown to be produced (Figure 6) (Filomatori et al., 2017; Silva et al., 2010). These sfRNAs dysregulate post-transcriptional processes, such as host mRNA decay through binding and inactivating XRN1 (Moon et al., 2012), as well as RNA splicing via interaction with RNA-binding proteins (Michalski et al., 2019). They also promote virus replication, cytopathicity and pathogenicity ((Funk et al., 2010; Pijlman et al., 2008)).

1.3.4.2 Structural proteins

The three structural proteins, together with the (+)ssRNA genome, make up virus particles. The capsid (C) protein encloses the viral RNA genome, whereas the envelope (E) and membrane (M) glycoproteins are inserted into the lipid envelope of mature viruses. Collectively, the structural proteins mediate virus entry into host cells, and they are involved

in the assembly and release of new virions (reviewed in Kaufmann and Rossmann, 2011; Lindenbach et al., 2007; Mukhopadhyay et al., 2005).

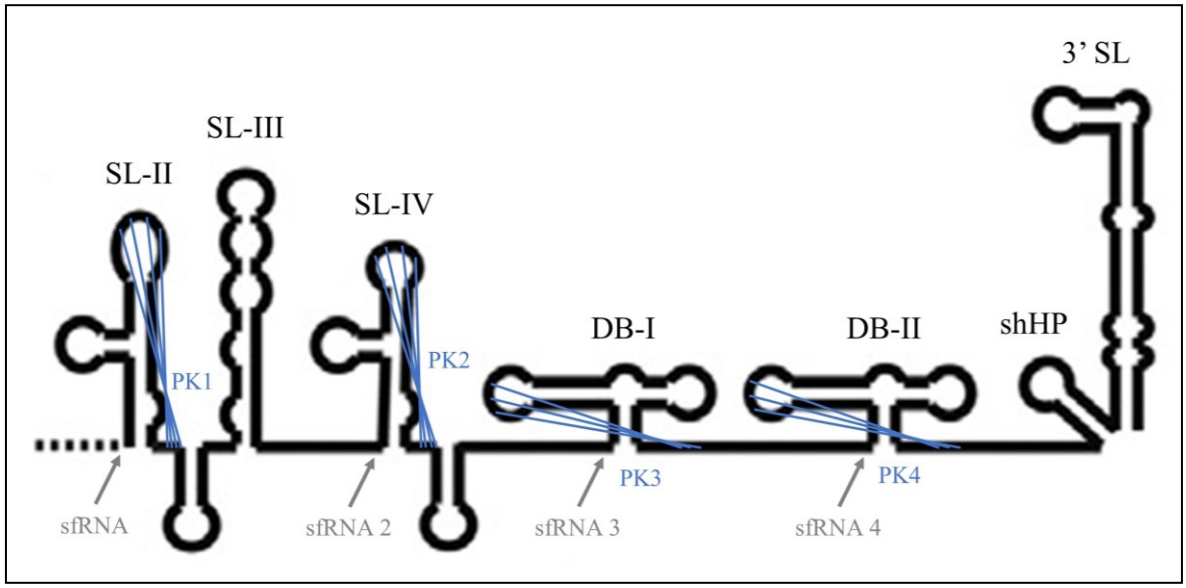

Figure 6. Structure of the Flavivirus genome 3' UTR. Secondary structures of the Flavivirus genome 3' UTR, as well as XRN1 stalling sites for the formation of sfRNAs are shown. SL = stem loop, DB = dumb bell, PK = pseudoknot, shHP = short hairpin. Figure adapted from (Clarke et al., 2015; Slonchak and Khromykh, 2018).

1.3.4.3 Non-structural proteins

Among the non-structural proteins, only two are known to possess enzymatic activities, namely NS3 and NS5 (reviewed in Lindenbach et al., 2007). In addition to their enzymatic functions, NS3 plays a role in virus assembly (Kümmerer and Rice, 2002; Patkar and Kuhn, 2008), and NS5 blocks interferon signaling to evade the cellular immune response (Ashour et al., 2009; Laurent-Rolle et al., 2010).

The other non-structural proteins support viral replication in various ways. The function of NS1 depends on its cellular localization and oligomerization state. The intracellular NS1 dimer most likely stabilizes the association between the viral replication complex and membranes, thus promoting viral genome replication (Mackenzie et al., 1996; Muylaert et al., 1996; reviewed in Muller and Young, 2013). The secreted NS1 hexamer elicits both a protective and pathogenic immune response by interacting with a wide range

of host cell components involved in innate and adaptive immunity (reviewed in Muller and Young, 2013).

The rest of the non-structural proteins, namely NS2A, NS2B, NS4A, 2K, and NS4B, are small proteins with multiple transmembrane domains (Li et al., 2015; Miller et al., 2007, 2006; Nemésio et al., 2012; Xie et al., 2013). They are components of the viral replication complex which is located in ER-membrane derived replication compartments (Mackenzie et al., 1998; Welsch et al., 2009). NS2A induces membrane rearrangements (Leung et al., 2008), participates in the production of infectious virus particles (Kümmerer and Rice, 2002; Liu et al., 2003; Xie et al., 2013), and inhibits interferon signaling to evade the cellular antiviral response (Liu et al., 2004; Muñoz-Jordán et al., 2003; Tu et al., 2012). NS2B is an essential cofactor for the NS3 protease (Chambers et al., 1991; Falgout et al., 1991). NS4A acts as a cofactor for the NS3 helicase (Shiryaev et al., 2009). It also participates in the formation of viral replication compartments via induction of ER membrane rearrangements (Miller et al., 2007; Roosendaal et al., 2006), and it is involved in immune evasion though inhibition of interferon signaling (Muñoz-Jordán et al., 2003). The 2K peptide, which is located between NS4A and NS4B in the viral polyprotein, is sometimes considered to be part of the NS4A protein (Roosendaal et al., 2006), whereas others have shown its role as signal peptide for the translocation and insertion of NS4B into the ER membrane (Lin et al., 1993; Muñoz-Jordán et al., 2005). Moreover, complete cleavage of the viral polyprotein generates a free 2K peptide which is not part of NS4A or NS4B. This peptide has been proposed to be involved in evasion of the immune response, as well as membrane rearrangements for efficient viral replication (Zou et al., 2009). Finally, NS4B serves as cofactor for the NS3 helicase (Umareddy et al., 2006). It has also been proposed to mediate cell death (Evans and Seeger, 2007), and it has been shown to inhibit interferon signaling (Muñoz-Jordán et al., 2003).

1.3.4.3.1 Non-structural protein 3

Non-structural protein 3 (NS3) is the second largest and the second most conserved Flavivirus protein. It contains two domains, namely an N-terminal protease domain and a C-terminal helicase domain, which are coupled via a short flexible linker (Figure 7) (Luo et al.,

2008a). Various conformations with different relative orientations of the two domains have been reported (Luo et al., 2010, 2008a), suggesting that different conformational states could exist *in vivo*. Moreover, RNA binding has been suggested to induce structural changes in NS3 (Benzaghou et al., 2006; Luo et al., 2008b). Although some studies have found that the two domains function independently from one another (Assenberg et al., 2009; Gebhard et al., 2012), most studies demonstrate a functional coupling between the two domains (Luo et al., 2010, 2008a; Mastrangelo et al., 2007; Xu et al., 2006, 2005). The NS3 protein possesses multiple enzymatic activities, namely serine protease (Chambers et al., 1990b; Preugschat et al., 1990; Wengler et al., 1991), RNA helicase (Li et al., 1999; Utama et al., 2000), nucleoside triphosphatase (NTPase) (Takegami et al., 1995; Warrener et al., 1993; Wengler and Wengler, 1991), and RNA triphosphatase (RTPase) (Bartelma and Padmanabhan, 2002; Wengler and Wengler, 1993).

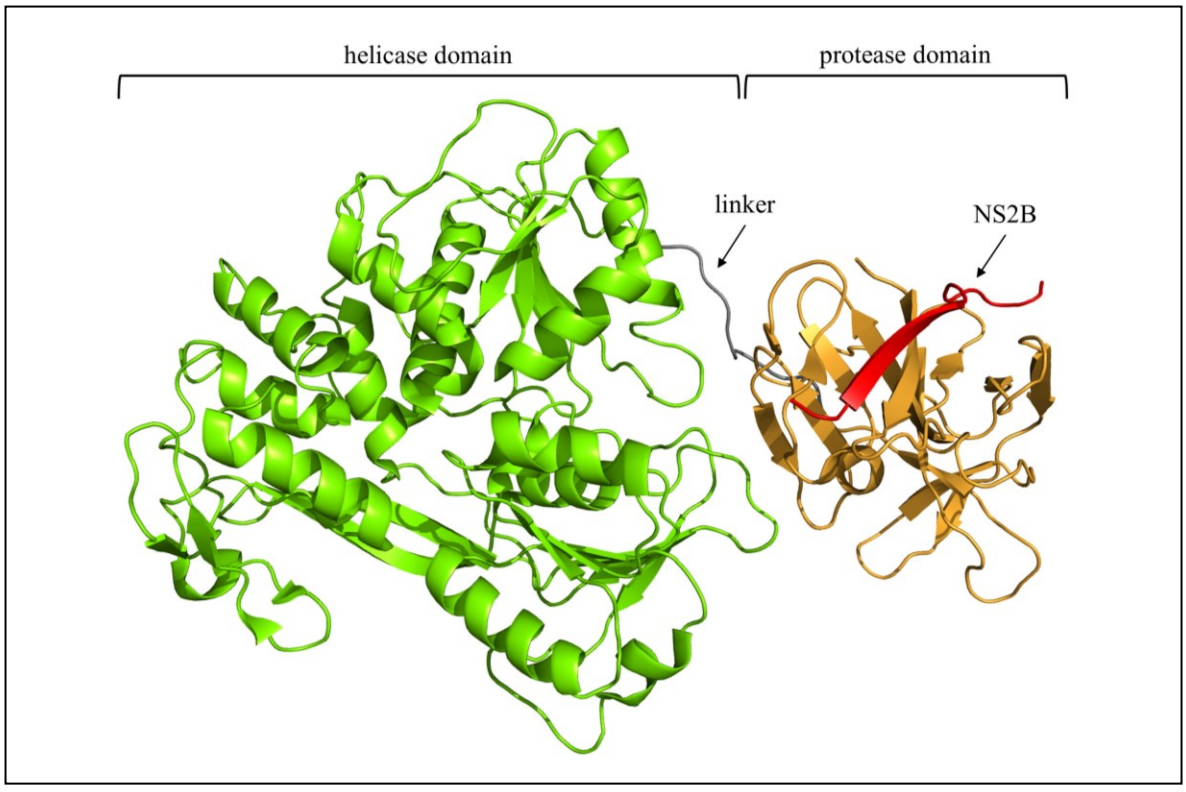

Figure 7. NS3 structure. The crystal structure of full-length NS3 from DENV, pdb 2VBC (Luo et al., 2008a), was visualized using PyMOL. The protease domain (residues 19-168) is colored in orange, NS2B (residues 49-63) in red, the inter-domain linker (169-179) in gray, and the helicase domain (180-618) in green.

The N-terminal third of NS3 constitutes the protease domain (Figure 8) (Chambers et al., 1990b; Preugschat et al., 1990; Wengler et al., 1991). It contains four regions of homology with serine proteases. The catalytic triad comprises residues H51-D75-S135 (DENV and ZIKV numbering) (Bazan and Fletterick, 1989; Gorbalenya et al., 1989). It is located in a cleft between two β-barrels, and it is strictly conserved among Flaviviruses (Erbel et al., 2006). The substrate binding pocket includes residues D129, F130, Y150, N152, and G153 (DENV numbering, correspond to ZIKV D129, Y130, Y150, N152, and G153) (Bazan and Fletterick, 1989; Valle and Falgout, 1998). Substrate cleavage sites generally contain two basic residues followed by a residue with a small side chain, such as Gly-(Ala)-Arg-Arg↓Ser (reviewed in Chambers et al., 1990a), although the exact sequence varies within the viral polyprotein and between different Flaviviruses (Yotmanee et al., 2015). NS3 protease cleavage sites in the viral polyprotein are located at the C/prM, NS2A/NS2B, NS2B/NS3, NS3/NS4A, NS4A/2K and NS4B/NS5 junctions (Chambers et al., 1991; Lin et al., 1993; Lobigs, 1993).

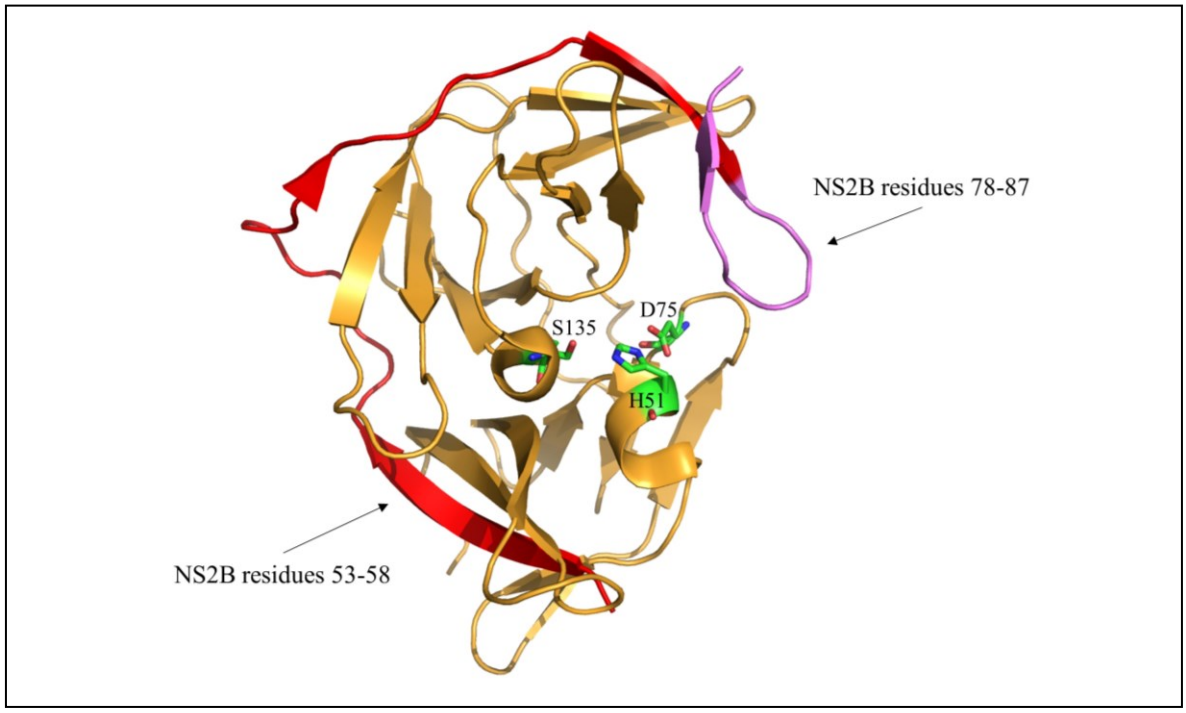

Figure 8. NS2B-NS3 protease structure. The crystal structure of unlinked NS2B-NS3 protease from ZIKV, pdb 5H4I (Zhang et al., 2016), was visualized using PyMOL. The NS3 protease (residues 17-171) is colored in orange, NS2B residues 50-80 in red, and NS2B residues 81-87 that form part of the active protease site in violet. Residues of the catalytic triad are shown as sticks and labeled.

For the formation of an active NS3 protease, the cytoplasmic portion of the NS2B protein is required (Chambers et al., 1993). NS2B residues 53-58 (WNV numbering, correspond to ZIKV 52-57) form a β-strand which folds into the N-terminal β-barrel of NS3, thus stabilizing the protease structure (Erbel et al., 2006). Residues 64-96 (WNV numbering, correspond to ZIKV 63-95) wrap around the NS3 protease domain, and residues 78-87 (WNV numbering, correspond to ZIKV 77-86) undergo a conformational change upon substrate binding to form β-hairpin that becomes part of the protease active site and stabilizes it (Aleshin et al., 2007; Erbel et al., 2006).

The larger, C-terminal domain of NS3 is the helicase domain, and it can be further divided into three subdomains (Figure 9). Subdomains 1 and 2 contain seven conserved helicase motifs characteristic of superfamily 2 helicases, including Walker A and Walker B motifs (Mastrangelo et al., 2007; Wu et al., 2005; Xu et al., 2005). The ssRNA binding tunnel is located between subdomains 1 and 2 on one side and subdomain 3 on the other side (Luo et al., 2008b). The helical gate is formed by α-helix 2 of subdomain 2, α-helix 6 of subdomain 3, and a β-hairpin protruding from subdomain 2 toward subdomain 3 (Mastrangelo et al., 2012). The β-hairpin disrupts base stacking between the two RNA strands to open the dsRNA helix, such that the 3’ end of the negative strand enters the RNA binding tunnel, and the 5’ end of the positive strand moves along the protein’s surface (Luo et al., 2008b; reviewed in Luo et al., 2015). A basic pocket near the interface between the helicase and protease domains constitutes the NTPase/RTPase active site (Luo et al., 2008a). Walker A and Walker B motifs mediate substrate binding and coordination of a magnesium ion, respectively (Assenberg et al., 2009; Benarroch et al., 2004; Mastrangelo et al., 2007). Residues R457, R458, R460 and R463 (DENV numbering), which are located in proximity to the catalytic site, have been shown to be crucial for both activities (Sampath et al., 2006). Residues P195, A316, T317, P326, A455 and Q456 (DENV numbering) form the exit channel for the phosphate product generated during NTPase and RTPase reactions (Luo et al., 2008b). The RNA unwinding site and the NTPase catalytic site are at a distance of approximately 30Å from one another (Mastrangelo et al., 2012), and the mechanism by which RNA unwinding and ATP hydrolysis are coupled remains elusive (Du Pont et al., 2020; reviewed in Li et al., 2014; Luo et al., 2015).

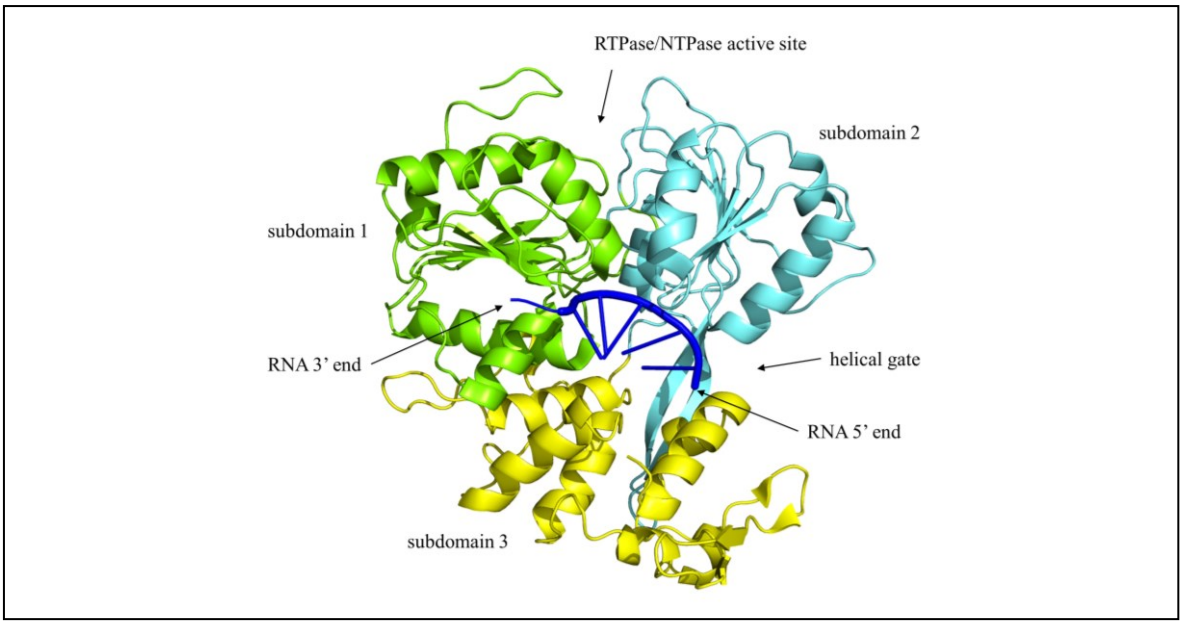

Figure 9. NS3 helicase structure. The crystal structure of the NS3 helicase domain from DENV bound to ssRNA, pdb 2JLU (Luo et al., 2008b), was visualized using PyMOL. Subdomains 1 (residues 168-326), 2 (residues 327-481) and 3 (residues 482-618) are colored in green, blue, and yellow, respectively. The RTPase/NTPase active site, the helical gate as well as the 5' and 3' ends of the ssRNA are labeled.

As already mentioned, the NS3 helicase domain possesses helicase, NTPase and RTPase activities (Li et al., 1999; Wengler and Wengler, 1993, 1991). The NTPase and RTPase reactions share the same catalytic site (Bartelma and Padmanabhan, 2002; Benarroch et al., 2004; Sampath et al., 2006). However, although dsRNA unwinding is driven by the energy released from NTP hydrolysis, especially ATP and GTP, it takes place at a distinct site called helical gate (Li et al., 1999; Mastrangelo et al., 2012; reviewed in Luo et al., 2015). The NS3 helicase disrupts secondary structures in the viral RNA, which are found especially in the 5' and 3' UTRs, to allow for the assembly of the replicase complex at the 3' end, as well as an efficient RTPase reaction at the 5' end (Wang et al., 2009). It also unwinds the dsRNA replication intermediate to release the positive strand for translation of viral proteins or packaging into virions, and to make the negative strand available as template for further genome replication (reviewed in Li et al., 2014; Luo et al., 2015). The NS3 RTPase catalyzes the removal of the γ-phosphate from the 5' end of the newly synthesized positive-strand RNA to form a diphosphorylated 5' end, which represents the first step in the synthesis of the 5' cap structure (Wengler and Wengler, 1993).

The enzymatic activities of the NS3 helicase domain are enhanced through its interaction with other macromolecules. NTPase activity is stimulated by ssRNA binding to residues R184, K185, R186, and K187 (DENV numbering) (Li et al., 1999; Warrener et al., 1993; Yon et al., 2005). Moreover, the presence of NS5 has been shown to increase both NTPase and RTPase activities (Cui et al., 1998; Yon et al., 2005). Finally, NS4A and NS4B are cofactors for the NS3 helicase activity. NS4A binds to the helicase domain and reduces the amount of ATP required for the unwinding of dsRNA (Shiryaev et al., 2009), whereas NS4B facilitates dissociation of NS3 from ssRNA (Umareddy et al., 2006) by interacting with subdomains 2 and 3 (Zou et al., 2015).

1.3.4.3.2 Non-structural protein 5

NS5 is the largest and the most conserved Flavivirus protein. It contains two domains, namely an N-terminal capping enzyme and a C-terminal RNA-dependent RNA polymerase (RdRp), which are coupled via a short linker (Figure 10) (Lu and Gong, 2013). Different relative orientations of the two domains, as well as rather compact and more extended overall structures have been observed, suggesting the possibility of different conformational states for NS5 (Bussetta and Choi, 2012; Lu and Gong, 2013; Zhao et al., 2015). The NS5 protein possesses multiple enzymatic activities, namely methyltransferase (MTase) (Egloff et al., 2002; Ray et al., 2006), guanylyltransferase (GTase) (Issur et al., 2009), and RNA-dependent RNA polymerase (RdRp) (Guyatt et al., 2001; Tan et al., 1996).

The N-terminal domain of NS5 constitutes the capping enzyme (Figure 11). It has two distinct substrate binding pockets. The GTP binding pocket includes residues K14, L17, N18, L20, F25, K29 and S150 (DENV numbering, correspond to YFV K13, L16, N17, L19, F24, K28 and S150) and is also the active site for the GTase reaction (Egloff et al., 2007, 2002). The SAM/SAH binding pocket includes residues S56, G86, W87, T104, K105, D131, V132, I147 and Y219 (DENV numbering, correspond to YFV S56, G86, W87, T104, L105, D131, V132, I147 and Y220) (Egloff et al., 2002) and is located close to the catalytic tetrad K61-D146-K181-E217 (DENV numbering, correspond to YFV K61-D146-K182-E218) for the MTase reactions (Ray et al., 2006). These two pockets are separated by a positively charged surface groove of 12-15Å, which is believed to bind viral RNA (Egloff et al., 2007,

2002; Geiss et al., 2009; Zhou et al., 2007). Moreover, residues F25, K30, R57, K181 and R212 (DENV numbering, correspond to YFV F24, R29, R57, K182 and R213), which are located at the base of helix A2, have been shown to bind 5' diphosphorylated RNA (ppRNA), further suggesting that the groove between helices A2 and A3 constitutes the entry site for RNA into the capping enzyme (Henderson et al., 2011).

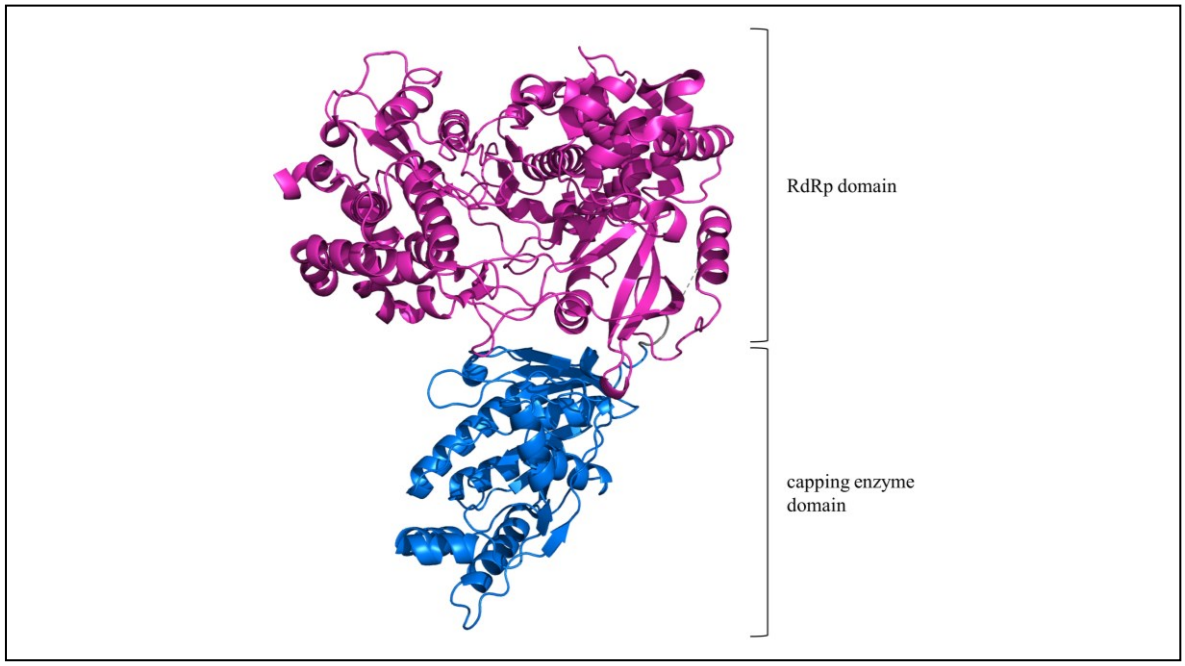

Figure 10. NS5 structure. The crystal structure of full-length NS5 from JEV, pdb 4K6M (Lu and Gong, 2013), was visualized using PyMOL. The capping enzyme domain (residues 1-266) is colored in blue, the inter-domain linker (residues 267-275) in gray, and the RdRp (residues 276-905) in magenta. Three residues from the linker region were unresolved in the crystal structure and are represented by a dashed line.

As already mentioned, the NS5 capping enzyme domain possesses GTase and MTase activities which contribute to capping the 5' end of the viral genome. In fact, the NS5 capping enzyme first transfers a GMP to the 5' diphosphate end of nascent viral RNA (Issur et al., 2009), and then it transfers methyl groups to the N7 position of the guanine as well as the 2'-*O* position of the first nucleotide's ribose (Egloff et al., 2002; Ray et al., 2006), using GTP and S-adenosyl-L-methionine (SAM) as donors, respectively. N7-methylation has been shown to precede 2'-*O*-methylation (Ray et al., 2006; Zhou et al., 2007).

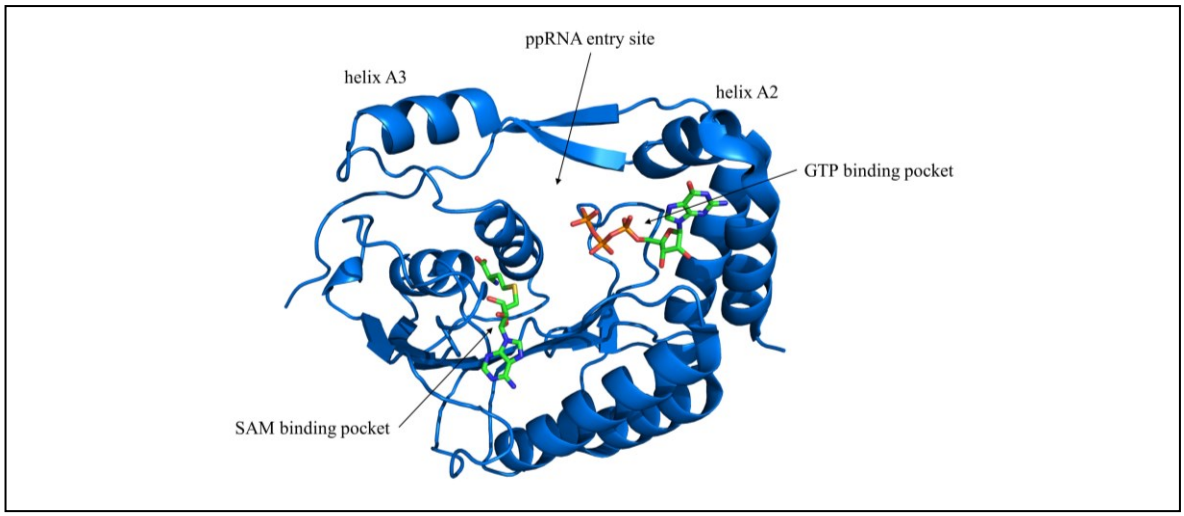

Figure 11. NS5 capping enzyme structure. The crystal structure of the NS5 capping enzyme domain from YFV bound to GTP and SAH, pdb 3EVD (Geiss et al., 2009), was visualized using PyMOL. The ppRNA entry site between helices A2 and A3 as well as the GTP and SAM binding pockets are labeled.

The C-terminal domain of NS5 constitutes the RNA-dependent RNA polymerase (RdRp). It adopts the canonical right-hand conformation with fingers, palm and thumb subdomains (Figure 12), and it contains seven catalytic motifs that are conserved among all viral RdRps. Motifs A through E are located in the palm subdomain, whereas motifs F and G are located in the fingers subdomain. Moreover, the catalytic active site is situated within the palm subdomain near the interface with the thumb and fingers subdomains (Malet et al., 2007; Yap et al., 2007). The NS5 RdRp contains two RNA binding tunnels that connect to the active site. The RNA template tunnel is between the fingertips and the thumb subdomain (Yap et al., 2007). The second RNA binding tunnel, located between the fingers and palm subdomains, is approximately perpendicular to the first one and goes across the entire protein (Malet et al., 2007). The back of this channel serves as entry site for NTPs, and the dsRNA product would exit though the front of this RNA binding tunnel (reviewed in Choi and Rossmann, 2009).

As its name suggests, the RdRp domain replicates the viral RNA genome (Selisko et al., 2006; Tan et al., 1996). Moreover, RNA synthesis has been demonstrated to be performed *de novo* (Ackermann and Padmanabhan, 2001). Two conserved residues, namely W795 and

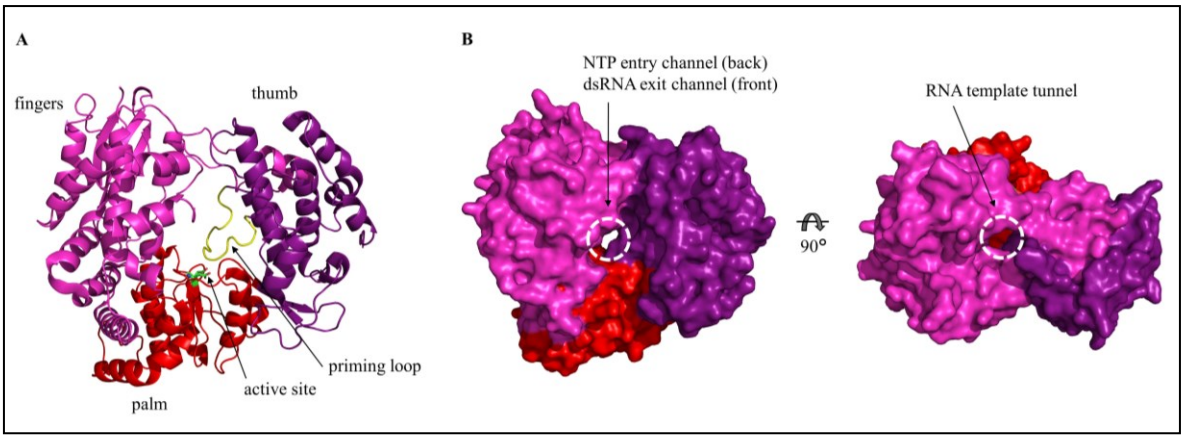

Figure 12. NS5 RdRp structure. The crystal structure of the NS5 RdRp domain from WNV, pdb 2HFZ (Malet et al., 2007), was visualized using PyMOL. The fingers subdomain (residues 274-498 and 542-609) is colored in pink, the palm subdomain (residues 499-541 and 610-717) in red, and the thumb subdomain (residues 718-905) in purple. [A] Cartoon representation. The priming loop (residues 796-809) is colored in yellow, and aspartic acid residues 536 and 669 that coordinate the catalytic magnesium ions are shown as sticks. [B] Surface representation. The RNA template channel is between the fingers and thumb subdomains. NTPs enter the active site through a second channel from the back of the RdRp domain.

H798 (DENV numbering, correspond to WNV W800 and H803) from the priming loop which protrudes from the thumb subdomain toward the active site in the palm subdomain, form stacking interactions with nucleotides and thus provide an initiation platform (Selisko et al., 2012; Yap et al., 2007). Residue W795 stabilizes a GTP molecule at the i-1 position, which is 6-7 Å from the catalytic motif G662-D663-D664 (DENV numbering, correspond to WNV G667-D668-D669) (reviewed in Choi and Rossmann, 2009; Noble and Shi, 2012). This GTP is crucial for initiation, regardless of the nucleotide sequence at the 3' end of the template RNA (Nomaguchi et al., 2003). It is thought to stabilize the initiating ATP at the i position and to contribute to the proper positioning of the ATP's 3' hydroxyl group for the formation of a phosphodiester bond with the second nucleotide at the i+1 position (reviewed in Choi and Rossmann, 2009). The initiating ATP at the i position is stacked against H798 (Selisko et al., 2012), and the incoming nucleotide is held in place at the i+1 position by two Mg^{2+} ions which are coordinated by D533 and D664 (DENV numbering, correspond to WNV D536 and D669) (Yap et al., 2007; reviewed in Choi and Rossmann, 2009). Once a covalent bond is formed between the first two nucleotides, the GTP molecule is released from the i-1 position. To allow elongation of the nascent dsRNA, the RdRp switches to an open

conformation (reviewed in Choi and Rossmann, 2009). Motif G of the fingertip region has been proposed to play a role in translocation of the template RNA, but the exact mechanism remains elusive (reviewed in Choi and Rossmann, 2009; Wu et al., 2015).

1.3.5 Flavivirus replicase complex

The core of the Flavivirus replicase complex is formed by the two viral enzymes NS3 and NS5 (Figure 13). The other non-structural proteins are also part of the replicase complex, and they have different functions to support viral replication (reviewed in Klema et al., 2015; van den Elsen et al., 2021). NS2B is an essential cofactor for the NS3 protease (Aleshin et al., 2007; Erbel et al., 2006). In addition, NS4A and NS4B are cofactors for the NS3 helicase (Shiryaev et al., 2009; Umareddy et al., 2006; Zou et al., 2015). NS2B, NS4A and NS4B anchor the replicase to the ER membrane via their transmembrane regions (Li et al., 2015; Miller et al., 2007, 2006). NS4B has also been shown to recruit NS1 to the replicase complex

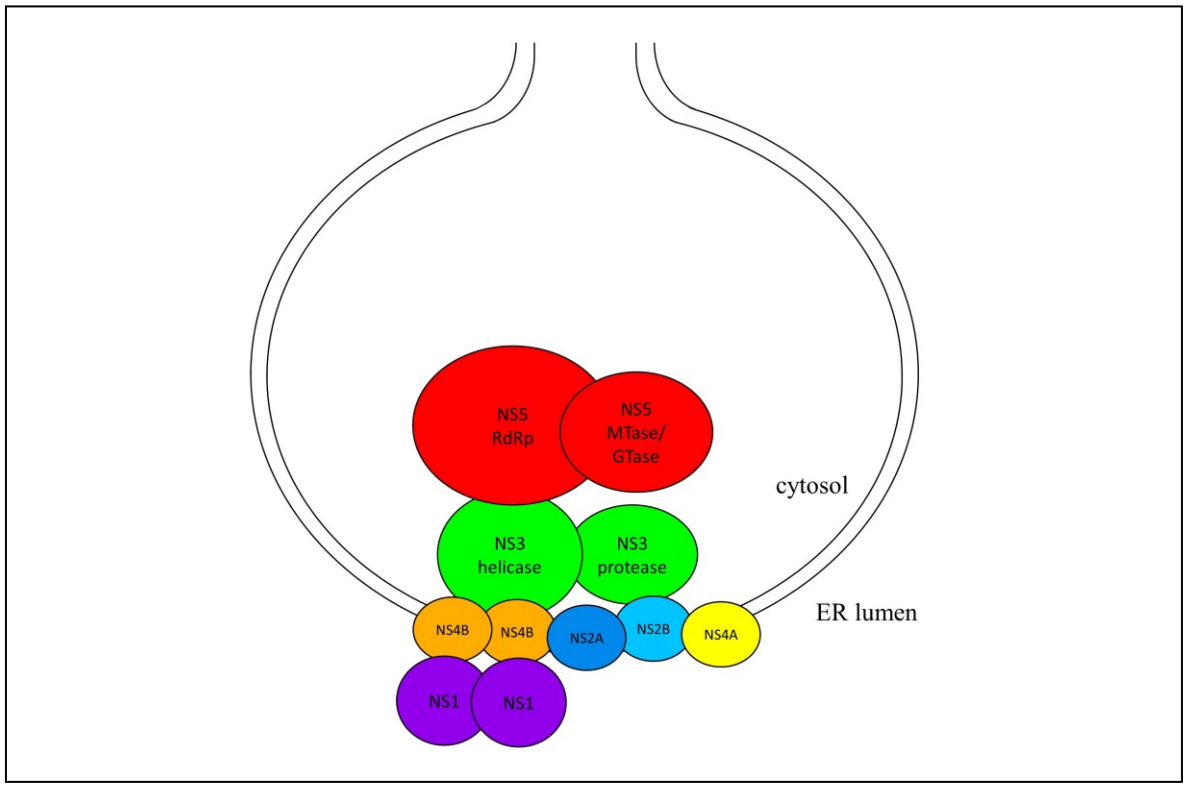

Figure 13. Schematic representation of the Flavivirus replicase complex. Viral proteins that form the replicase complex located in the ER-derived replication organelle are shown. Figure adapted from (Klema et al., 2015; van den Elsen et al., 2021).

(Chatel-Chaix et al., 2015). NS5 does not interact with any of the small transmembrane non-structural proteins, and it is recruited to the replicase complex only via direct interaction with NS3 (Kapoor et al., 1995; reviewed in Klema et al., 2015). The NS3:NS5 interaction is mostly thought to be mediated by the NS5 RdRp domain (Brooks et al., 2002; Johansson et al., 2001; Moreland et al., 2012; Tay et al., 2015; Vasudevan et al., 2001) and the NS3 helicase domain (Johansson et al., 2001; Moreland et al., 2012), although there is some evidence for a contribution of the NS3 protease domain (Takahashi et al., 2012; Zou et al., 2011).

1.3.6 Flavivirus drug development

Many compounds have been studied for their potential antiviral activity, and most studies have identified inhibitors of any of the viral enzymes (NS2B-NS3 protease, NS3 helicase, NS5 capping enzyme, NS5 RdRp) since they play essential roles in viral replication and have been well characterized. These potential antiviral compounds bind either the active site to directly inhibit enzymatic activity (competitive inhibitors), or an allosteric site to induce a conformational change in the protein which negatively affects its enzymatic activity (non-competitive inhibitors) (reviewed in Lim et al., 2015; Luo et al., 2015; Qian and Qi, 2022).

Inhibition of the viral protease activity has been shown to suppress viral replication, thus making the NS2B-NS3 protease an interesting drug target. Small molecule compounds as well as peptide-based compounds have been investigated for their ability to inhibit the protease activity. Given that peptides are mostly non-permeable to diffuse through cell membranes, and are generally unstable *in vivo*, the development of small molecule inhibitors appears more attractive. In general, competitive inhibitors show less efficacy *in vivo* than non-competitive inhibitors. This may be due to the shallow active site, which causes most compounds to bind only weakly, thus making it challenging to develop highly potent inhibitors. Moreover, since the NS2B-NS3 protease is a serine protease and humans also have serine proteases, there is a high risk for adverse effects (reviewed in Qian and Qi, 2022; Samrat et al., 2022). Another interesting target for potential protease inhibitors is the NS2B-NS3 interaction, since NS2B acts as essential cofactor for the NS3 protease. In fact, several

compounds that interfere with the NS2B-NS3 interaction have been identified, and for two of them, antiviral efficacy has been demonstrated in an animal model (Li et al., 2017; Yao et al., 2019).

The NS3 helicase domain is considered less attractive as a potential antiviral drug target because of its dynamic nature which involves RNA binding, translocation, and unwinding (reviewed in van den Elsen et al., 2023). Moreover, given that it lacks specific pockets at the RNA and NTP binding sites, compounds targeting these sites are likely to cause toxicity by binding similar sites on human helicases (reviewed in Luo et al., 2015). Nevertheless, some inhibitory compounds have been identified in enzyme-based assays, but their antiviral efficacy was limited in cell-based assays (reviewed in Qian and Qi, 2022).

The NS5 capping enzyme is an attractive target for antiviral drug design, given that its catalytic cavity is different from that of the human cap methyltransferase RNMT (reviewed in Delgado-Maldonado et al., 2023). Several compounds, mostly SAM analogs and SAH derivatives, have been shown to inhibit NS5 MTase activity, but were not further developed due to poor cell permeability. Fleximers, which are nucleoside analogs with a split purine base, have shown favorable activity against Flaviviruses in cell-based assays (reviewed in Qian and Qi, 2022). Furthermore, GTP analogs have been shown to inhibit GTase activity *in vitro* and suppress viral replication in cell culture, but were reported to have low *in vivo* efficacy (Bullard et al., 2015; Geiss et al., 2011; Stahla-Beek et al., 2012).

Given that replication and transcription of human genes does not rely on an RNA-dependent RNA polymerase (RdRp), the NS5 RdRp is the most promising target for antiviral drug development with favorable safety. RdRp inhibitors can be divided into two categories, namely nucleoside analog inhibitors (NIs) which target the catalytic site and terminate viral RNA synthesis, and non-nucleoside analog inhibitors (NNIs) which bind surface cavities or allosteric pockets and induce conformational changes in the RdRp to inhibit its enzymatic activity. Several NNIs targeting the N pocket of the NS5 RdRp have been developed. Other NNIs have been shown to lock the polymerase in a closed conformation by binding the RNA template tunnel and thus suppressing RdRp activity. Nonetheless, NIs are considered to be

the most attractive compounds, considering their success with other viral polymerases (reviewed in Qian and Qi, 2022; van den Elsen et al., 2023). In fact, three NIs have been authorized for phase I clinical trials, namely Balapiravir (ClinicalTrials.gov, 2016a), Galidesivir/BCX4430 (ClinicalTrials.gov, 2016b; reviewed in Julander et al., 2021), and AT-752 (ClinicalTrials.gov, 2022; Good et al., 2021).

In addition to NS3 and NS5 catalytic sites, other viral components as well as host factors have been targeted for antiviral drug development. Compounds targeting the E protein to inhibit viral cell entry by inactivating virions or interfering with membrane fusion have been investigated (reviewed in Qian and Qi, 2022). Celgosivir has been shown to cause misfolding and accumulation of NS1 in the ER via inhibition of α-glucosidase, resulting in inhibition of DENV replication (Rathore et al., 2011). This compound has been approved for a phase II clinical trial (Watanabe et al., 2016), but the trial has been withdrawn due to lack of funding (ClinicalTrials.gov, 2020). Compound SBI-0090799 has been found to inhibit ZIKV replication by targeting NS4A and preventing the formation of replication compartments (Riva et al., 2021). Compounds targeting NS4B to inhibit DENV and YFV replication have been identified, yet their mechanisms of action are still unclear (Guo et al., 2016; Moquin et al., 2021). Moreover, host factors involved in nucleotide synthesis and lipid metabolism have been targeted to inhibit Flavivirus replication (reviewed in Qian and Qi, 2022).

Finally, protein-protein interactions within the replication complex have been studied as potential antiviral drug targets, particularly the interaction of the NS3 protein with its cofactors NS2B and NS4B, as well as with the only other viral protein with enzymatic activities, NS5. As previously stated, several inhibitors of the NS2B-NS3 interaction have been identified, and two of them have shown antiviral efficacy in animal models (Li et al., 2017; Yao et al., 2019). Compounds interfering with the NS3-NS4B interaction have also been described. JNJ-A07 targets NS4B and blocks *de novo* complex formation with NS3. Its strong anti-DENV activity has been demonstrated in a cell-based assay and in mice (Kaptein et al., 2021). JNJ-1802, which is another inhibitor of the NS3-NS4B interaction from the same chemical series as JNJ-A07, has shown efficacy against DENV in non-human primates

(Goethals et al., 2023), and is currently studied in a phase II clinical trial (ClinicalTrials.gov, 2023). Lastly, the interaction between the two viral enzymes NS3 and NS5 has been suggested to be an attractive target for antiviral drug development (Takahashi et al., 2012; Zou et al., 2011). Recently, repurposed drugs I-OMe tyrophostin AG538 and suramin hexasodium have been shown to inhibit the NS3:NS5 interaction via direct binding to NS5, leading to strong antiviral activity against DENV, ZIKV and WNV in a cell-based assay (Yang et al., 2022). Earlier this year, two other compounds named C-9 and C-30 have been reported to block the NS3:NS5 interaction. Their inhibitory effect on DENV, ZIKV and WNV replication has been demonstrated in infected cells, and the antiviral activity of C-30 against DENV has been confirmed in a mouse model (Celegato et al., 2023).

1.4 Human host cells

As stated previously, humans are among the host species that can be infected by mosquito-borne Flaviviruses (reviewed in Hale, 2023). A good knowledge of human biology is essential to understand Flavivirus pathogenesis. It is also crucial for the development of successful antiviral therapies, for example to prevent severe side effects (reviewed in Tatonetti et al., 2009).

The human organism has many levels of organization. It comprises eleven organ systems, each of which is composed of multiple organs working together to perform a common function. Each organ consists of at least two types of tissues, which are made of cells. Cells are the fundamental structural and functional units of life, considering that they are the lowest level of organization capable of performing all the activities necessary for life. Cells can be subdivided into smaller structures that perform a specific function, called organelles, which in turn are made of molecules (reviewed in Campbell and Reece, 2007; Tortora and Derrickson, 2007).

One of the key molecules that is found in all living cellular organisms is DNA (Hiyoshi et al., 2011). It contains all the information needed for cells to function and for the organism to develop (reviewed in Snustad and Simmons, 2012). In human cells, most of the DNA is located in the nucleus, and a small amount is in the mitochondria. Mitochondrial DNA

molecules are circular, whereas nuclear DNA molecules are linear and form chromosomes. Each DNA molecule can be divided into segments called genes, and all the genes in a cell make up its genome (reviewed in Karp, 2010; Snustad and Simmons, 2012).

1.4.1 Gene expression

For the information contained in the cell's genome to give rise to the molecules and organelles that make up the cell, genes need to be expressed. Gene expression is a complex process involving multiple highly regulated steps, including transcription, mRNA processing, and translation (reviewed in Buccitelli and Selbach, 2020; Karp, 2010; Watson et al., 2012).

1.4.1.1 Transcription

Transcription is the process of copying a gene made of DNA into an RNA molecule by an enzyme called DNA-dependent RNA polymerase. Eukaryotic cells have three RNA polymerases that copy DNA into RNA, namely Pol I, Pol II and Pol III. Pol II is responsible for transcribing essentially all protein-coding genes into messenger RNAs (mRNAs), most small nuclear RNAs (snRNAs and snoRNAs), most microRNAs, and telomerase RNA, whereas Pol I transcribes larger ribosomal RNAs (rRNAs), and Pol III transcribes transfer RNAs (tRNAs), some small nuclear RNAs (snRNAs) and rRNA 5S. The process of transcription involves many steps which can be grouped into three phases, i.e. initiation, elongation, and termination (reviewed in Karp, 2010; Watson et al., 2012).

1.4.1.1.1 Transcription initiation

For an efficient initiation of transcription at a gene's promoter, multiple initiation factors are required. These general transcription factors help the RNA polymerase recognize the promoter and provide a binding site for the enzyme. In addition, the promoter indicates which DNA strand is transcribed, and at what position transcription begins. The minimal promoter recognized by Pol II is about 40-60 nt in length and contains multiple sequence elements that are recognized and bound by general transcription factors. It can be located upstream or downstream of the transcription initiation site. Moreover, there are other

regulatory sequences, usually upstream of the minimal promoter, that are required for an efficient transcription *in vivo*, including promoter-proximal elements, upstream activation sequences, enhancers, silencers, boundary elements, and insulators. These sequence elements bind regulatory proteins and can be up to hundreds of kilobases away from the minimal promoter (reviewed in Karp, 2010; Watson et al., 2012).

The formation of the preinitiation complex starts with the binding of the general transcription factor TFIID, more precisely its subunit TBP (TATA-binding protein), to the TATA box in the minimal promoter. Other TFIID subunits, called TAF (TBP-associated factors), recognize other sequence elements of the minimal promoter. The DNA-bound TBP deforms the TATA sequence of the promoter, and the following components progressively complete the assembly of the preinitiation complex in this order: TFIIA, TFIIB, TFIIF attached to the RNA polymerase, TFIIE, and finally TFIIH (reviewed in Karp, 2010; Watson et al., 2012). The helicase activity of the TFIIH subunit XBP then starts to unwind the DNA (reviewed in Cramer, 2019).

Given that the DNA in human cells is highly condensed in the form of chromatin, thus restricting access to the promoter region and complicating the assembly of the preinitiation complex, transcriptional activators are required to achieve high levels of transcription. On the one hand, activators bind the DNA near the gene, and on the other hand, they bind proteins such as the Mediator complex and chromatin remodeling factors (reviewed in Karp, 2010; Watson et al., 2012).

Once the preinitiation complex is assembled at the promoter and up to 14 nucleotides of the template DNA are unwound, *de novo* RNA synthesis is initiated. The first two ribonucleoside triphosphate substrates (NTPs), which are complementary to the DNA strand that is transcribed, enter the active site of the RNA polymerase and are covalently linked to each other. The following nucleotides are then attached to the 3’ end of the nascent RNA in the same way. The newly synthesized RNA thus grows from its 5’ terminus in a 3’ direction, while the polymerase moves along the template DNA strand in a 3’ → 5’ direction (reviewed in Karp, 2010; Watson et al., 2012).

For the Pol II polymerase to escape from the preinitiation complex and transition into the elongation phase, the carboxyl-terminal domain (CTD) of its largest subunit needs to be phosphorylated. The CTD is made of 52 repeats of a Tyr-Ser-Pro-Thr-Ser-Pro-Ser polypeptide, and the CDK7 subunit of TFIIH phosphorylates the serine residue at the fifth position in these repeats (reviewed in Cramer, 2019; Karp, 2010; Watson et al., 2012).

1.4.1.1.2 Transcription elongation

When the nascent RNA reaches a length of approximately 10 nucleotides, the RNA polymerase escapes the promoter and transitions from initiation to elongation. Most initiation factors, including general transcription factors and the Mediator complex, are detached from the polymerase. Some of these factors remain at the promoter, whereas others are released. During elongation, new factors are recruited to the polymerase, namely elongation factors and factors involved in RNA processing (reviewed in Karp, 2010; Watson et al., 2012).

Throughout the elongation phase, the DNA helix in front of the polymerase is opened, the template DNA strand is transcribed into a complementary RNA strand, potential errors in the newly synthesized RNA are fixed, the nascent RNA strand is dissociated from the template DNA, and the two DNA strands are put back together. Multiple elongation factors work in concert with Pol II to accomplish this complex process. The FACT heterodimer composed of Spt16 and SSRP1 proteins dismantles nucleosomes downstream of the polymerase and reassembles them upstream of the polymerase once the DNA has been transcribed. Moreover, TFIIS helps the polymerase overcome pause sites and improves its proofreading by stimulating the cleavage of mismatched nucleotides (reviewed in Cramer, 2019; Watson et al., 2012).

To recruit factors involved in mRNA processing, the CTD of Pol II needs to be phosphorylated. In addition to the above-mentioned phosphorylation of the serine at position 5 in the CTD heptapeptide repeats during the initiation-elongation transition, the serine residue at position 2 is phosphorylated by the CDK9 subunit of P-TEFb during elongation (reviewed in Cramer, 2019; Karp, 2010; Watson et al., 2012).

1.4.1.1.3 Transcription termination

Near the end of a protein-coding gene, there is a specific sequence called polyadenylation signal (PAS). Once this sequence is transcribed by Pol II, cleavage and polyadenylation (CPA) factors are recruited to the CTD of the elongation complex and slow it down. They then bind the polyadenylation signal on the newly synthesized RNA and recruit other proteins, leading to the cleavage of the RNA and its polyadenylation (reviewed in Proudfoot, 2016; Watson et al., 2012).

Two models have been proposed for PAS-dependent termination, namely the allosteric model and the torpedo model. In the allosteric model, the elongating polymerase undergoes a conformational change leading to its dissociation from the template DNA upon transcribing the PAS, possibly caused by the recruitment of the large CPA complex. In the torpedo model, the polymerase continues to transcribe the template DNA after the cleavage of the newly synthesized RNA at the PAS. The 5'→3' exonuclease XRN2 then degrades the transcript downstream of the PAS until it catches up with the polymerase, triggering its dissociation from the template DNA (reviewed in Eaton and West, 2020; Proudfoot, 2016; Watson et al., 2012).

1.4.1.2 Pre-mRNA processing

Precursor messenger RNA processing is a multi-step process which occurs co-transcriptionally. It involves the addition of a cap structure and a polyA-tail at the 5' end and the 3' end of the nascent RNA, respectively, as well as the removal of non-coding introns (reviewed in Proudfoot, 2016; Watson et al., 2012).

1.4.1.2.1 Messenger RNA capping

The first step in pre-mRNA processing is the addition of a cap structure at its 5' end. The nascent RNA is capped in a three-step process during the initiation-elongation transition. First, one phosphate group is removed from the 5' triphosphate end of the newly synthesized RNA. Then, a GMP nucleotide is added to the diphosphate end in an inverted orientation, creating a 5'-5' triphosphate bridge. Finally, the inverted GMP nucleotide is methylated at

the 7 position of its guanine base and at the 2' position of its ribose. This methylguanosine cap protects the RNA from exonucleases and plays an important role in mRNA translation (reviewed in Karp, 2010; Watson et al., 2012). Furthermore, it also plays a role in marking mRNAs as self, compared to pathogen RNAs (reviewed in Schlee and Hartmann, 2016).

1.4.1.2.2 Splicing

Pre-mRNAs, like genes, are discontinuous, meaning that the sequence sections that eventually serve as template for protein synthesis are interrupted by intervening sequences. These intervening sequences are removed from the primary transcript during pre-mRNA processing via RNA splicing, and they are absent from the mature mRNA that is translated into a protein. Sequence segments that are eliminated during splicing are called introns, and the segments that contribute to the mature mRNA are called exons. However, not all exons are protein-coding, considering that some of them include the untranslated regions upstream of the start codon and downstream of the stop codon (reviewed in Karp, 2010; Lee and Rio, 2015; Watson et al., 2012).

Splicing is mediated by a large ribonucleoprotein (RNP) complex called spliceosome. The spliceosome is composed of five small nuclear ribonucleoprotein (snRNP) complexes, namely U1, U2, U4, U5, and U6, as well as other proteins. It recognizes introns through specific nucleotide sequences at their 5' and 3' ends (G/GU and AG/G, respectively), termed splice sites. In addition, a CU-rich sequence, called polypyrimidine track, near the 3' end of the intron as well as exonic splicing enhancers (ESEs) promote assembly of the spliceosome. ESEs are binding sites for SR proteins which are involved in recruitment of spliceosome components to the splice sites (reviewed in Karp, 2010; Lee and Rio, 2015; Watson et al., 2012).

Assembly of the spliceosome begins with the binding of the U1 snRNPs at the 5' splice site via its complementary nucleotide sequence. Next, U2AF binds the polypyrimidine tract and recruits the U2 snRNP near the 3' splice site, thus forming the pre-spliceosome (complex A). Base-pairing of the U2 snRNA creates a specific adenosine bulge. The U4/U6 and U5 snRNPs are then recruited to the pre-mRNA, establishing the precatalytic

spliceosome (complex B). A series of dynamic interactions between the pre-mRNA and the snRNPs, as well as among the snRNPs, leads to the release of U1 and U4 and the formation of an activated complex B (B^{act}). The first catalytic reaction is the cleavage of the 5' splice site. The free 5' exon is held in place by U5, whereas the 5' end of the intron binds the adenosine bulge near the 3' splice site, thus creating a lariat intron which is still attached to the 3' exon (complex C). The second catalytic reaction is the cleavage at the 3' splice site, leading to the release of the lariat intron and the simultaneous joining of the two exons. The postspliceosomal complex is then disassembled, and the lariat intron is rapidly degraded (reviewed in Karp, 2010; Lee and Rio, 2015; Watson et al., 2012).

Nearly all human genes undergo alternative splicing, a process in which different combinations of exons or varying lengths of exon fragments from the same gene are joined together via the use of different splice sites on the pre-mRNA, thus generating different mature mRNAs called isoforms. There are five main types of alternative splicing patterns, namely exon skipping, mutually exclusive exons, alternative 5' and 3' splice sites, and intron retention (Figure 14) (reviewed in Lee and Rio, 2015; Liu et al., 2022; Ule and Blencowe, 2019; Wright et al., 2022). Exon skipping is the most common type of alternative splicing with a proportion of approximately 46%. Intron retention, alternative 5' (donor) splice sites and alternative 3' (acceptor) splice sites account for roughly 4%, 5% and 10% of all alternative splicing events, respectively, whereas the remaining 35% represent other more complex events (Sammeth et al., 2008).

Alternative splicing can have multiple functional consequences. It can affect mRNA stability and/or localization, possibly preventing the transcript from being translated into a protein. Nonetheless, approximately 37% of human protein-coding genes have been found to generate multiple protein isoforms (reviewed in Baralle and Giudice, 2017). These isoforms can differ in their structure, activity, function, stability, cellular localization, and interaction partners (reviewed in Gunning, 2006; Sulakhe et al., 2019). For example, skipping of exon 6 in the transcript of the Fas receptor causes the loss of its transmembrane domain, resulting in a soluble Fas isoform. In contrast to full-length Fas, the isoform lacking the transmembrane domain is not located at the cell surface and therefore cannot interact with its ligand to induce

apoptosis (reviewed in Yabas et al., 2015). Overall, alternative splicing has been shown to diversify the proteome and to be involved in many biological processes, such as cellular differentiation and growth, neuronal development, aging, response to environmental change at all life stages, and various diseases (e.g. cancer, spinal muscular atrophy) (reviewed in Marasco and Kornblihtt, 2023; Wright et al., 2022).

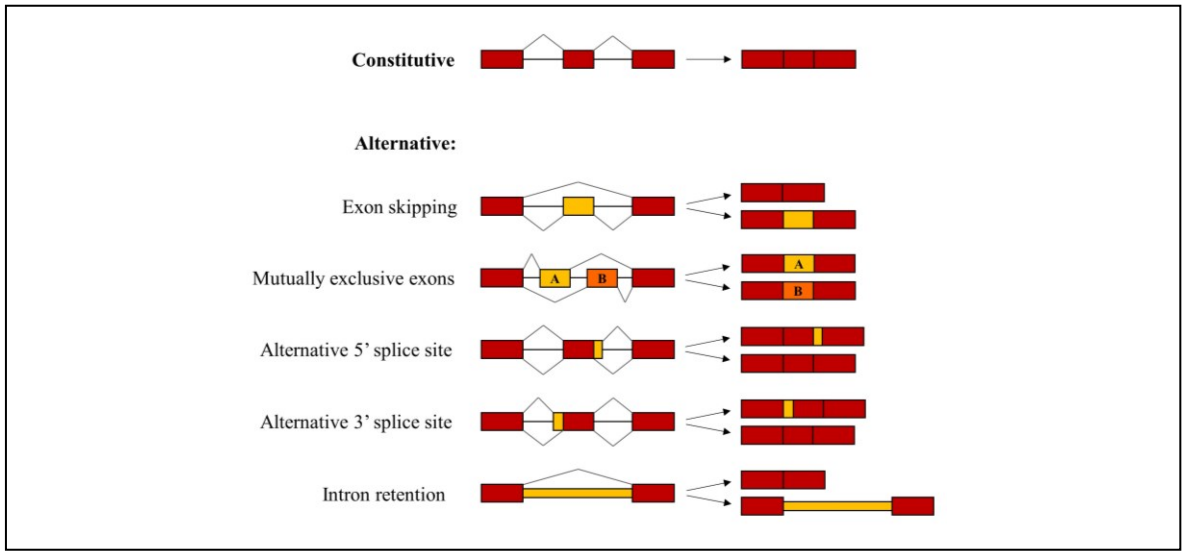

Figure 14. Types of alternative splicing events. The five different types of ASEs are shown. Figure adapted from (Liu et al., 2022).

1.4.1.2.3 Polyadenylation

The final step of pre-mRNA processing is the addition of a polyA tail at its 3' end, which occurs during the elongation-termination transition. Once the polyadenylation signal (PAS) is transcribed, cleavage and polyadenylation (CPA) factors bind the newly synthesized RNA and recruit other proteins, including polyA polymerase (PAP). An endonuclease cleaves the pre-mRNA downstream of the PAS, and PAP adds up to 250 adenosine residues to the 3' end without needing a DNA template. This polyA tail protects the mRNA from degradation by exonucleases (reviewed in Karp, 2010; Watson et al., 2012).

1.4.1.3 Translation

Once the mRNA is processed, it is transported from the nucleus to the cytoplasm to be translated into a protein. During translation, the information encoded in the mRNA in the

form of a combination of four different nucleotides is converted into a sequence of up to 20 different amino acids. To do so, the mRNA is divided into units made of three nucleotides, called codons. Each codon corresponds to a specific amino acid, except for the stop codons UAA, UAG and UGA. Given the lack of affinity between nucleotides and amino acids, transfer RNAs (tRNAs) are required as intermediates that bind each codon and its corresponding amino acid during translation. Finally, peptide bond formation between the amino acids is catalyzed by the ribosome, which is a large complex made of multiple proteins and RNAs. Given the large number of elements involved in translation, it is one of the cell's most complex processes. However, it can be divided into three distinct phases, namely initiation, elongation, and termination (reviewed in Karp, 2010; Watson et al., 2012).

1.4.1.3.1 Translation initiation

During translation initiation, a complex of an 80S ribosome and the first tRNA on the initiation codon (typically AUG) of the mRNA is formed. Multiple eukaryotic initiation factors (eIFs) are involved in the translation initiation pathway. First, eIF2 binds GTP and the initiating methionyl-tRNA (Met-tRNA$_i$) to form the ternary complex (TC). The TC, along with initiation factors eIF5, eIF3, eIF1 and eIF1A, then binds the small (40S) ribosomal subunit to form the 43S preinitiation complex (PIC). In parallel, the eIF4F complex binds the 5' cap structure on the mRNA, and polyA binding protein (PABP) binds its 3' polyA tail. The eIF4G subunit of eIF4F binds PABP, thus forming a circularized complex of the mRNA and RNA-binding proteins (RBPs). The eIF4A subunit of eIF4F, which is a helicase, then unwinds the mRNA secondary structure, allowing recruitment of the 43S PIC at the 5' cap structure to form the 48S initiation complex. The 48S complex then moves along the mRNA, from the 5' cap towards the 3' end, searching for the AUG initiation codon. Once the initiation codon is recognized via base-pairing with the anticodon of the Met-tRNA$_i$, the initiation complex stops scanning and is reorganized. Initiation factors eIF1, eIF2, eIF3 and eIF5 are released from the complex, whereas GTP-bound eIF5B is recruited before the large 60S ribosomal subunit joins the complex. Finally, eIF5B and eIF1A are dissociated, thus forming the 80S ribosome with the Met-tRNA$_i$ bound to the initiation codon of the mRNA, ready for the elongation phase (reviewed in Brito Querido et al., 2020; Karp, 2010; Merrick and Pavitt, 2018; Watson et al., 2012).

Although most mRNAs are subject to cap-dependent translation initiation, there are alternative initiation mechanisms. These prevail in stress conditions and viral infection when cap-dependent translation is downregulated. One of these alternative mechanisms is the internal ribosome entry site (IRES) promoted initiation, which relies on an alternative strategy to recruit the 40S ribosomal subunit that does not need a 5' cap or a free 5' end (reviewed in Kwan and Thompson, 2019; Merrick and Pavitt, 2018). Even though approximately 10% of cellular mRNAs are estimated to have IRESs, this mechanism is not very well understood, given that many of these mRNAs are translated cap-dependently under normal conditions and undergo IRES-mediated initiation only under cellular stress (reviewed in Kwan and Thompson, 2019).

1.4.1.3.2 Translation elongation

The ribosome has three sites that can accommodate tRNAs, namely A, P and E. At the end of the translation initiation phase, the Met-tRNA$_i$ is located in the P site. At the beginning of the elongation phase, the second aminoacyl-tRNA, with the help of elongation factor eEF1A, enters the A site of the ribosome. A peptide bond is formed between the tRNA-bound amino acids in the P and A sites by peptidyl transferase, which is part of the large ribosomal subunit, thus transferring the nascent peptide onto the tRNA in the A site. Conformational changes in elongation factor eEF2 then promote the translocation of the ribosome along the mRNA in a 5'→3' direction to the next codon, along with the passage of the deacylated tRNA and the newly formed peptidyl-tRNA from the P and A sites into the E and P sites, respectively. The deacylated tRNA is released from the E site, and the next aminoacyl-tRNA enters the A site, starting the next cycle of elongation (reviewed in Dever et al., 2018; Karp, 2010).

1.4.1.3.3 Translation termination

When the ribosome reaches one of the stop codons (UAA, UAG, UGA), there are no tRNAs with the complementary anticodon. Instead, release factor eRF1 recognizes any of the three stop codons and enters the A site of the ribosome. Together with eRF3, it stimulates

hydrolysis of the nascent polypeptide from the peptidyl-tRNA in the P site (reviewed in Hellen, 2018; Karp, 2010; Watson et al., 2012).

Once the newly synthesized protein is released, the post-termination complex (post-TC) is recycled to allow for a new round of translation. After dissociation of eRF3, ABCE1 splits the post-termination ribosome into four pieces, namely the large 60S ribosomal subunit, eRF1, ABCE1, and the small 40S ribosomal subunit still bound to mRNA and a deacylated tRNA in the P site. Release of these RNAs from the recycled 40S subunit can be mediated by initiation factors eIF1, eIF1A, eIF3, eIF3j, by eIF2D, or by MCT1 and DENR (reviewed in Hellen, 2018).

1.4.1.3.4 Translation reinitiation

Approximately half of mammalian genes have been found to contain one or more short upstream ORFs (uORFs, <30 bp) which are located upstream of the main protein coding ORF. These uORFs can also be translated in addition to the main ORF. After the dissociation of the ribosome at the uORF stop codon, some 40S subunits remain bound to the mRNA and resume scanning to reinitiate translation at the main ORF initiation codon. For a successful reinitiation, a new ternary complex composed of eIF2, GTP and Met-RNA$_i$ needs to be recruited (reviewed in Jackson et al., 2010).

1.4.2 Regulation of gene expression

Gene expression is regulated to express only a subset of genes in a given cell type under given circumstances, such as different developmental stages or environmental stimuli. Virtually any step of gene expression can be controlled, and control mechanisms can be grouped into multiple levels. Transcriptional control determines if, when, and how often a particular gene is transcribed. Processing control dictates how a pre-mRNA is processed into a mature mRNA. RNA transport and localization control regulates which mRNAs are exported from the nucleus to the cytoplasm, and where in the cytoplasm the mature mRNA is located. Translational control determines if, how often, and for how long a mRNA is translated. RNA degradation control governs which mRNAs are degraded, and when.

Finally, protein activity control mechanisms activate, inactivate, or degrade the protein product (reviewed in Alberts et al., 2002; Karp, 2010; Watson et al., 2012).

1.4.2.1 Transcription factors

Transcription factors are proteins that bind proximal or distal elements of promoters to regulate transcription. Their DNA binding domains recognize short (usually 6-12 nucleotides), specific sequences via high DNA-protein structural complementarity. Their protein-protein interaction domains recruit other proteins, such as RNA polymerase, cofactors that promote specific phases of transcription, or coactivators/corepressors that are involved in chromatin binding, nucleosome remodeling, or covalent modification of histones. Generally, to achieve specific DNA binding and effector function, transcription factors need to collaborate, e.g. through cooperative binding or synergistic regulation. Moreover, their effects are frequently context dependent and can vary depending on the local DNA sequence and availability of cofactors. The same transcription factor can function as an inhibitor in one situation and as an activator in different circumstances, so that the traditional classification of transcription factors as ‘activators’ and ‘repressors’ has been questioned (reviewed in Lambert et al., 2018; Mitsis et al., 2020; Ramírez-Clavijo and Montoya-Ortíz, 2013).

1.4.2.2 Epigenetic regulation of gene expression

Epigenetics is “the study of mitotically (and potentially meiotically) heritable alterations in gene expression that are not caused by changes in DNA sequence”. Epigenetic processes, such as DNA methylation and histone modification, regulate gene expression mainly at the level of transcription. Moreover, they are reversible, thus allowing the cell to change gene expression in response to stimuli (reviewed in Gibney and Nolan, 2010).

In humans, DNA methylation can occur on the 5’ position of cytosines preceding a guanosine. Covalent binding of a methyl group changes the biophysical characteristics of DNA, thus inhibiting or facilitating binding of specific proteins. DNA methylation is usually associated with gene silencing. More precisely, DNA methyl-binding proteins recognize methylated DNA and recruit corepressors and histone deacetylases, resulting in compaction

of DNA and chromatin remodeling (reviewed in Gibney and Nolan, 2010; Jaenisch and Bird, 2003).

To be packaged in the cell's nucleus, DNA wraps around histones and forms a condensed structure called chromatin. Histones can undergo various post-translational modifications, such as acetylation, methylation, and phosphorylation. These covalent modifications of histones can directly affect the structure of chromatin, or they can disrupt or promote binding of proteins to the chromatin to regulate transcription. For example, acetylation neutralizes the positively charged side chain of lysine residues, thus reducing the strength of interaction between histones and negatively charged DNA, which facilitates transcription (reviewed in Gibney and Nolan, 2010).

1.5 Virus-host interactions

As obligate intracellular parasites, viruses rely on multiple host cell functions for their replication, e.g. its protein synthesis machinery. Therefore, viruses hijack ribosomes to ensure translation of viral mRNAs. In turn, the host cell impairs the translation machinery, either selectively or globally, to restrict viral replication (reviewed in Stern-Ginossar et al., 2019). Moreover, the host cell activates the expression of genes involved in the antiviral response, such as interferons and interferon-stimulated genes, whereas viruses have strategies to limit or evade the cellular defense response (reviewed in Flint et al., 2015; Stern-Ginossar et al., 2019).

1.5.1 Antiviral response

Upon viral infection of host cells, intrinsic cellular defenses are triggered immediately. In addition, within minutes or hours after infection, the innate immune response is activated, whereas the activation of the adaptive immune response occurs several hours or days following exposure to the virus (reviewed in Flint et al., 2015).

The distinction of intrinsic and innate immunity is debated. Some scientists use both terms interchangeably. Others consider intrinsic defenses to be those that rely on components

that are constantly present in the host cell, although they can be further induced upon pathogen detection, and block viral replication directly, without inducing the synthesis of antiviral molecules (reviewed in Flint et al., 2015; Lee et al., 2021; Yan and Chen, 2012). According to this definition, the intrinsic defense response includes autophagy, formation of stress granules, and apoptosis. The innate immune response involves recruitment of antigen-presenting cells, natural killer cells and neutrophils to the site of infection, as well as the synthesis of interferons and the expression of interferon-stimulated genes (ISGs). The more specific adaptive immune response consists of activation, proliferation, and migration of T cells and B cells in order to resolve the infection (reviewed in Flint et al., 2015; Lee et al., 2021).

Innate immune sensors, also referred to as cellular pattern recognition receptors (PRRs), detect pathogen-associated molecular patterns (PAMPs), such as viral RNA, proteins, and carbohydrates. Binding of PAMPs to PRRs induces the expression of genes that encode antiviral and proinflammatory cytokines and chemokines via multiple signaling cascades, including NF-κB, interferon response, and inflammasome activation. The major PRRs that recognize Flaviviruses in human cells are RIG-I-like receptors (RLRs), Toll-like receptors (TLRs), NOD-like receptors (NLRs), and the cGAS-STING-dependent sensing pathway. RLRs are cytoplasmic proteins that detect viral RNA via RNA binding motifs, whereas TLR3 and TLR7/TLR8 are intracellular transmembrane glycoproteins that recognize viral dsRNA and ssRNA, respectively. These two classes of PRRs activate signaling cascades that results in the production of interferons as well as proinflammatory cytokines and chemokines. NLRs oligomerize and form inflammasomes upon binding PAMPs, ultimately leading to the production proinflammatory cytokines. cGAS was initially described as a sensor of viral DNA, yet there are studies that demonstrate activation of the cGAS-STING pathway in Flavivirus infections (reviewed in Gack and Diamond, 2016; Latanova et al., 2022; Lee et al., 2021).

1.5.1.1 Interferon response

The interferon system is a crucial part of the antiviral defense response. As previously mentioned, production of interferons is induced when PRRs detect PAMPs and activate

multiple signaling cascades. The newly synthesized interferons then activate the expression of interferon-stimulated genes (ISGs), and the proteins encoded by these ISGs establish an antiviral state and restrict viral replication (reviewed in Gack and Diamond, 2016; Lee et al., 2021).

There are three types of interferons. Type I interferons include IFN-α (13 subtypes), IFN-β, IFN-ε, and IFN-ω. IFN-γ is the only type II interferon, and type III interferons comprise IFN-λ1 (IL-29), IFN-λ2 (IL-28A), IFN-λ3 (IL-28B) and IFN-λ4 (reviewed in Flint et al., 2015; Mesev et al., 2019). Type I and type III IFNs can be secreted by almost all cell types in response to viral infections. Type II IFN secretion is specific for immune cells and controlled by cytokines, mainly IL-12 and IL-18 (reviewed in Schroder et al., 2004; Stanifer et al., 2019). To fulfill their function, interferons need to bind their cell surface receptors, whether they are on the cell that synthesized and secreted the interferon, or on a neighboring cell. All type I interferons bind IFNAR, whereas type II interferon binds IFNGR and type III interferons bind IFNLR (reviewed in Flint et al., 2015; Mesev et al., 2019). IFNAR and IFNGR are present on most cells, whereas IFNLR is restricted to epithelial cells and a specific subset of immune cells (reviewed in Mesev et al., 2019; Stanifer et al., 2019). Upon binding to their receptor, all IFNs can activate the JAK/STAT pathway to induce the expression of ISGs. Some ISGs are controlled by multiple IFNs, whereas others are selectively regulated by distinct IFNs (reviewed in Mesev et al., 2019; Platanias, 2005).

1.5.1.1.1 Type I interferon signaling

Canonical type I interferon signaling triggers the JAK/STAT pathway. Upon binding of IFNα/β to their receptor IFNAR, the receptor-associated kinases JAK1 and TYK2 phosphorylate STAT1 and STAT2, respectively. Phosphorylated STAT1 and STAT2 then dimerize and translocate to the nucleus, where they associate with IRF9 to form the trimolecular ISGF3 complex. This complex ultimately binds IFN-stimulated response elements (ISREs) in the promoters of ISGs to trigger their transcription. In this manner, several hundred ISGs are expressed, many of which are dedicated to establishing an antiviral state within the cell (reviewed in Ivashkiv and Donlin, 2014; McNab et al., 2015).

Besides the canonical pathway, type I interferons can signal through STAT1 homodimers which are generally involved in IFNγ signaling, as well as other STATs which are usually involved in other cytokine-mediated signaling pathways. IFNα/β may also activate the PI3K-mTOR and MAPK pathways. Through the activation of these various signaling cascades, type I IFNs induce the expression of a broad range of genes, including ones that encode cytokines, chemokines, pro-apoptotic and anti-apoptotic molecules, and molecules involved in metabolic processes (reviewed in McNab et al., 2015).

1.5.1.1.2 Interferon-stimulated genes (ISGs)

Well-known ISGs include PKR, OAS, IFITMs, IFITs, and members of the TRIM family (reviewed in McNab et al., 2015). PKR is one of relatively few IFN effector proteins and belongs to the family of kinases that phosphorylate eIF2α. The gene that encodes PKR is constitutively expressed at low levels, and IFN enhances its expression. PKR itself it is activated in the presence of dsRNA to phosphorylate the translation initiation factor eIF2α and inhibit protein synthesis (Samuel et al., 2006; reviewed in Pindel and Sadler, 2011). OAS proteins are also encoded by ISGs and function as PRRs that bind dsRNA. Once activated by dsRNA, OAS catalyzes the oligomerization of ATP into 2',5'-linked oligoadenylate (2-5A), which successively activates RNase L, leading to degradation of viral and cellular RNA (reviewed in Berthoux, 2020; Silverman, 2007). IFITMs mainly interfere with membrane fusion to restrict viral entry. Moreover, recent studies have shown their implication in the regulation of innate and adaptive immune responses (reviewed in Berthoux, 2020; Gómez-Herranz et al., 2023). IFIT proteins block protein synthesis in two different ways. On the one hand, IFIT proteins bind the eIF3 complex and thus inhibit the formation of the preinitiation complex. On the other hand, IFIT proteins bind viral mRNAs that lack the 2'-*O*-methylation in their cap structure and prevent their translation (reviewed in Berthoux, 2020; Franco et al., 2023). TRIM proteins contain a domain with E3 ubiquitin ligase activity and are involved in multiple cellular functions, including antiviral immunity. They exert their antiviral functions by regulating transcription-dependent antiviral responses, e.g. expression of pro-inflammatory cytokines, by modulating cell-intrinsic defense pathways such as autophagy, or by directly targeting viral components for degradation or non-degradative inhibition (reviewed in Koepke et al., 2021). TRIM25 polyubiquitylates RIG-I for increased

downstream signaling (Gack et al., 2007). TRIM65 interacts with TRIF to promote the expression of IFNβ and ISGs via the TLR3 signaling pathway (Shen et al., 2012). TRIM69 mediates NS3 ubiquitination, leading to its proteasomal degradation (Wang et al., 2018).

1.5.1.2 Autophagy

Autophagy is a degradative process responsible for the clearance of cellular waste, and it occurs at a basal level under normal conditions. It targets a wide variety of components, selectively or non-selectively, for lysosomal degradation. There are three major mechanisms of autophagy, namely microautophagy, chaperone-mediated autophagy, and macroautophagy. The latter is the best characterized form of autophagy and involves double-membrane vesicles called autophagosomes. Under stress conditions, such as viral infection, autophagy can be enhanced in order to clear the invading pathogen. The selective autophagy that specifically targets intracellular microorganisms, such as entire viral particles, to autophagosomes for degradation is called xenophagy. Moreover, the process of autophagy targeting newly synthesized viral components is called virophagy (reviewed in Chiramel and Best, 2018; Choi et al., 2018; Mao et al., 2019).

The autophagy pathway can be divided into multiple phases, namely induction and nucleation, elongation, closure and maturation, fusion, and degradation (reviewed in Chiramel and Best, 2018; Ke, 2018; Mao et al., 2019; Parzych and Klionsky, 2014). The autophagy induction complex forms in cells under any conditions. In the absence of stress, however, mTORC1 binds the complex and inactivates it. Under stress conditions, mTORC1 dissociates from the complex, leading to its dephosphorylation and translocation to the autophagy initiation site, thus activating autophagy. Then, the class III PI3K complex comprising BECN1 is recruited to the site of autophagosome formation to generate phosphatidylinositol-3-phosphate, which is the major lipid involved in autophagy. It also participates in the nucleation of the phagophore, which is the primary double-membrane sequestering compartment. The activity of the PI3K complex is mostly regulated through proteins that interact with BECN1. Membrane expansion of the phagophore relies on two ubiquitin-like (UBL) conjugation systems. Eventually, the membrane of the expanding phagophore bends to fully surround its cargo and fuses to form a spherical double-membrane

autophagosome. Finally, the outer membrane of the autophagosome fuses with the lysosomal membrane to form an autolysosome, and its cargo is degraded by acidic proteases (reviewed in Chiramel and Best, 2018; Ke, 2018; Parzych and Klionsky, 2014).

There are multiple ways in which autophagy is activated upon viral infection to degrade viral components or viral particles. Toll-like receptors (TLRs) detect viral molecular patterns, such as ssRNA and dsRNA, leading to MYD88 or TRIF binding to BECN1, thus disrupting its association with the inhibitory BCL2 and activating autophagy. Interferon-induced PKR also binds to BECN1 within the PI3K complex to initiate autophagosome formation (reviewed in Choi et al., 2018). In addition, PKR-mediated phosphorylation of eIF2α triggers autophagy (reviewed in Choi et al., 2018; Flint et al., 2015). Two other interferon-induced kinases, namely JAK1 and TYK2, activate the PI3K-AKT-mTOR pathway via phosphorylation of IRS1 and IRS2. AKT phosphorylates the FOXO3 transcription factor, thus inducing the transcription of autophagy-related genes (reviewed in Choi et al., 2018).

Reticulophagy consists in the autophagic degradation of the ER. Although it does not degrade viruses or their components, it restricts Flavivirus replication, given that the formation of viral replication compartments involves the ER membrane (reviewed in Lee et al., 2021).

1.5.1.3 Unfolded protein response

Flaviviruses cause ER stress via remodelling of the ER membrane to form compartments for viral replication and maturation, and accumulation of viral proteins in these compartments prior to virion assembly (Su et al., 2002; reviewed in Blázquez et al., 2014). To cope with this stress and survive, host cells activate the unfolded protein response (UPR). The UPR aims to reduce the number of misfolded proteins by promoting protein folding or degradation, or by inhibiting mRNA translation to ensure tight coupling of protein synthesis and folding (reviewed in Harding et al., 2002). The URP includes three pathways, namely the IRE1 pathway, the PERK pathway, and the ATF6 pathway. IRE1, PERK and ATF6 are transmembrane proteins with their N-terminal stress sensing domain located in the ER lumen and their C-terminal effector domains located in the cytoplasm. Under normal conditions, the

N-termini of these three proteins are bound by BiP, which maintains them in an inactive state. However, upon ER stress, BiP is sequestered by misfolded proteins, leading to the activation of IRE1, PERK and ATF6 (reviewed in Blázquez et al., 2014; Perera et al., 2017).

Activated IRE1 homodimerizes and autophosphorylates, resulting in the activation of its RNase domain. On the one hand, the RNase domain degrades several mRNAs in a process termed regulated IRE1-dependent decay (RIDD). On the other hand, the RNase domain removes a section of the XBP1 mRNA, resulting in the production of functional XBP1. This transcription factor activates the expression of ER-associated degradation (ERAD)-associated genes. These genes encode proteins which promote protein folding or contribute to the degradation of misfolded proteins (reviewed in Perera et al., 2017).

Like IRE1, activated PERK homodimerizes and autophosphorylates, leading to the activation of its kinase domain. The kinase domain then phosphorylates eIF2α, thus globally inhibiting translation to match protein synthesis to the ER protein folding capacity and to prevent further accumulation of misfolded proteins in the ER. Moreover, phosphorylated eIF2α induces the translation of ATF4, a transcription factor involved in the expression of ER chaperones (reviewed in Harding et al., 2002; Perera et al., 2017).

Upon dissociation from BiP, ATF6 is cleaved to generate its active form called ATF6p50. This transcription factor translocates to the nucleus and induces the expression of ER chaperones and genes involved in the ERAD pathway (reviewed in Perera et al., 2017).

Activation of the UPR upon ER stress may also lead to activation of autophagy and/or apoptosis (reviewed in Perera et al., 2017). As previously mentioned in section 1.5.1.2, PKR-mediated phosphorylation of eIF2α triggers autophagy (reviewed in Choi et al., 2018; Flint et al., 2015). Therefore, PERK-mediated phosphorylation of eIF2α during UPR signaling may also activate autophagy. In fact, the activation of the PERK pathway has been shown to be linked to autophagy turnover during DENV infection (Datan et al., 2016). Regarding the interplay between UPR and apoptosis, activated IRE1 has been shown to bind TRAF2 and

ASK1, thus inducing JNK-mediated apoptosis. Moreover, ATF4 activates CHOP and GADD34, which also results in apoptosis (reviewed in Perera et al., 2017).

1.5.1.4 Translation arrest and formation of stress granules

Environmental stresses, including viral infections, trigger translation arrest and stress granule formation to conserve energy for processes involved in the restoration of homeostasis, as well as to prevent synthesis of viral proteins. Translation initiation can be thwarted via two different mechanisms. On the one hand, stress conditions inhibit the kinase subunit of mTORC1, preventing it from phosphorylating eIF4E-binding proteins (4EBPs). When hypophosphorylated, 4EBPs bind eIF4E and block its association with eIF4G which is required to form the eIF4F complex. Without eIF4F, the 43S preinitiation complex (PIC) cannot be recruited to the 5' UTR of the mRNA to form the 48S initiation complex, and translation initiation cannot occur. On the other hand, different stress conditions activate one of four kinases that phosphorylate the eIF2α subunit of eIF2 (i.e. HRI, GCN2, PKR and PERK). Viral dsRNA activates PKR, which then phosphorylates eIF2α. Phosphorylated eIF2α stably binds to eIF2B, thus preventing it from converting eIF2-GDP to eIF2-GTP. Without eIF2-GTP, the eIF2-GTP/Met-tRNA$_i$ ternary complex cannot be formed, and translation (re)initiation is inhibited (reviewed in Li and Wang, 2023; McCormick and Khaperskyy, 2017).

Blocked translation initiation results in untranslated mRNPs which aggregate to form stress granules (SGs). Stress granules have been shown to contain seven main components, namely polysome-free mRNAs, translation initiation factors, RNA-binding proteins (RBPs) that regulate translation and protect RNA stability, mRNA metabolism-related proteins, signaling proteins, expression products of ISGs, and regulatory proteins involved in SG formation. SGs are dynamic structures which can exchange components with the cytoplasm or be completely disassembled into translating mRNPs. They can also be degraded by autophagy (reviewed in Li and Wang, 2023; McCormick and Khaperskyy, 2017; Protter and Parker, 2016).

In addition to accumulating untranslated mRNPs of cellular and viral origin, stress granules recruit numerous antiviral proteins, including RIG-I, MDA5, PKR, OAS, and RNase L. This increases their local concentration and places them in close proximity to viral RNAs, thus stimulating their activation and enhancing the innate antiviral response. Viral proteins have also been shown to accumulate in stress granules, resulting in inhibition of viral replication via sequestration of essential components. Finally, SGs also recruit signaling proteins, such as TRAF2, leading to suppression of pro-apoptotic signaling (reviewed in Li and Wang, 2023; McCormick and Khaperskyy, 2017; Protter and Parker, 2016).

1.5.1.5 Apoptosis

Apoptosis is a type of programmed cell death that removes senescent, damaged, or infected cells. Two main signaling pathways, namely the intrinsic and extrinsic pathways, can lead to apoptosis (reviewed in Elmore, 2007; Okamoto et al., 2017; Pan et al., 2021). Each pathway is activated by specific triggering signals, and both signaling cascades lead to caspase 3 activation and the same execution pathway resulting in DNA fragmentation, degradation and cross-linking of proteins, formation of apoptotic bodies, expression of cell surface markers, and ultimately uptake by phagocytic cells. The extrinsic pathway is activated by ligand binding to death receptors. Cytoplasmic adaptor proteins are recruited, a death-inducing signaling complex (DISC) is formed, and pro-caspase 8 is activated. Caspase 8 then activates caspase 3 and the execution pathway to induce apoptosis. In contrast, the intrinsic pathway is activated by non-receptor-mediated stimuli, such as the absence of growth factors or cytokines, or the presence of radiation, hypoxia, or viral infections. These stimuli cause changes in the inner mitochondrial membrane via the Bcl-2 family of proteins. These mitochondrial changes result in release of pro-apoptotic proteins, such as cytochrome c, DIABLO/Smac, and HtrA2/Omi, from the intermembrane space into the cytosol. On the one hand, cytochrome c interacts with APAF1 and pro-caspase 9 to form an apoptosome. Clustering of pro-caspase 9 leads to its activation, and caspase 9 then activates the executing caspase 8. On the other hand, DIABLO/Smac and HtrA2/Omi suppress the action of IAPs (inhibitors of apoptosis proteins) to promote apoptosis (reviewed in Elmore, 2007; Pan et al., 2021).

The mitochondria-mediated apoptosis pathway is connected with the IRE1, PERK, and ATF6 pathways of the UPR, so that long-term activation of UPR can trigger apoptosis. IRE1 activation initiates a signaling cascade resulting in phosphorylation of JNK, which then activates pro-apoptotic genes such as Bak to induce apoptosis. Moreover, functional XBP1 activates caspase 3 and caspase 9 to promote apoptosis. PERK activation leads to translation of ATF4, which induces expression of CHOP. The latter suppresses the expression of anti-apoptotic genes Bcl-2 and Bcl-X_L, thus activating apoptosis. Finally, cleaved ATF6 can also upregulate CHOP to induce apoptosis (reviewed in Pan et al., 2021; Perera et al., 2017).

1.5.2 Viral suppression of or escape from antiviral response

As described in the previous sections, host cells activate several mechanisms to defend themselves against invading viruses. In turn, viruses have evolved strategies to escape or suppress the antiviral response.

1.5.2.1 Suppression of the interferon response

Since the interferon system is a crucial part of the antiviral defense response, Flaviviruses have evolved multiple strategies to suppress this pathway. These strategies include inhibition of signal transduction to prevent synthesis of IFNs and inhibition of the JAK-STAT signaling cascade to prevent expression of ISGs (Figure 15). IFN-inhibitory activity has been shown for most non-structural proteins as well as sfRNA (reviewed in Chen et al., 2017; Cumberworth et al., 2017; Lee et al., 2021; Slonchak and Khromykh, 2018). In order to inhibit the synthesis of type I IFNs, NS3 prevents translocation of RIG-I and MDA5 to the mitochondria for the activation of MAVS. Moreover, NS4A binds MAVS to further block its activation. Further downstream, several non-structural proteins interact with TBK1 to prevent it from phosphorylating transcription factors (IRFs). Finally, some non-structural proteins interact with IRFs to inhibit their activity as transcription factor for type I IFNs. In order to inhibit IFN signaling and the expression of ISGs, several non-structural proteins induce the degradation of JAK1 and/or STAT2, or inhibit phosphorylation of STAT1/STAT2 (reviewed in Chen et al., 2017; Lee et al., 2021).

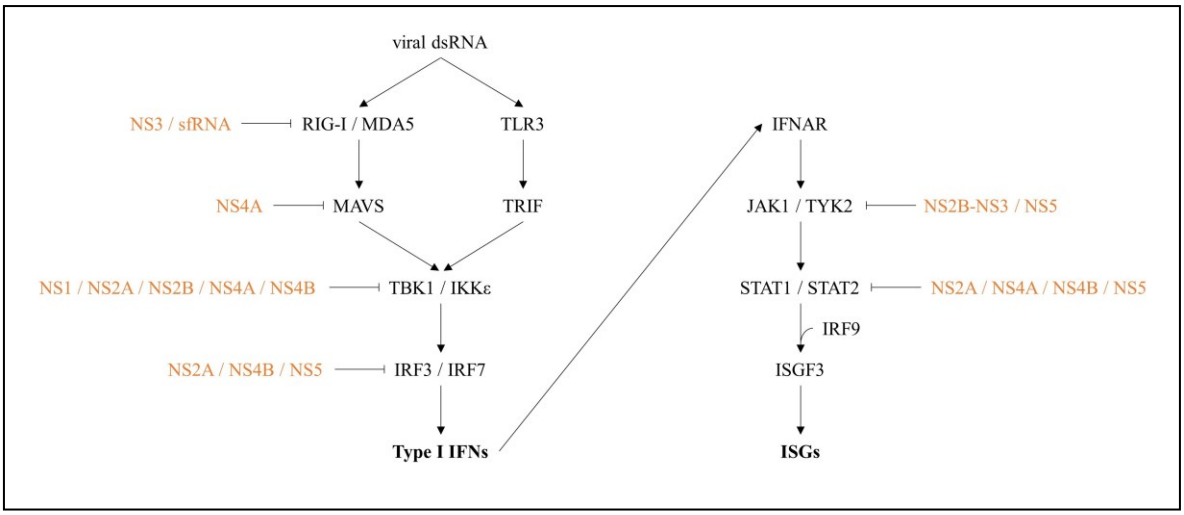

Figure 15. Flavivirus-induced suppression of the interferon response. Figure of the IFN synthesis and signaling pathways adapted from (Haller et al., 2006) with information on inhibitory proteins from (Chen et al., 2017; Lee et al., 2021).

1.5.2.2 Inhibition of autophagy

As described in section 1.5.1.2, autophagy is an intrinsic cellular defense mechanism against viruses. Unsurprisingly, Flaviviruses have evolved strategies to interfere with autophagy. In fact, DENV, ZIKV, and WNV NS2B-NS3 proteases have been shown to cleave FAM134B to block reticulophagy, thus allowing these viruses to utilize the ER membrane for the formation of replication organelles and as a source of the lipid envelopes of nascent virions (Lennemann and Coyne, 2017).

1.5.2.3 Subversion of the unfolded protein response

As described in section 1.5.1.3, the unfolded protein response (UPR) promotes cellular stress reduction and survival. It has also been intimately linked to innate immunity. While host cells induce the UPR to restrict viral infections, viruses subvert the UPR to sustain the infection (reviewed in Chan, 2014). In fact, ZIKV has been shown to interfere with the UPR by downregulating expression of the chaperone GRP78/BiP (Turpin et al., 2020), and DENV has been shown to suppress PERK-mediated eIF2α phosphorylation early during infection (Peña and Harris, 2011).

1.5.2.4 Antagonization of stress granules

As described in section 1.5.1.4, translation is inhibited and stress granules (SGs) are formed in response to viral infections to prevent synthesis of viral proteins, as well as to conserve energy for processes involved in the restoration of cellular homeostasis (reviewed in Li and Wang, 2023; McCormick and Khaperskyy, 2017). However, viruses have evolved strategies to prevent stress granule formation by sequestering core SG proteins (reviewed in Guan et al., 2023; Lee et al., 2021; Li and Wang, 2023). More specifically, WNV and DENV minus-strand 3' terminal stem loop binds and relocates TIA-1 and TIAR (Emara and Brinton, 2007), whereas ZIKV genomic RNA binds G3BP1 to inhibit SG assembly (Hou et al., 2017). The JEV and ZIKV capsid proteins have been shown to form complexes with Caprin-1 and G3BP1 to prevent SG formation (Hou et al., 2017; Katoh et al., 2013). Moreover, ZIKV and DENV impair phosphorylation of eIF2α (Amorim et al., 2017; Roth et al., 2017). Finally, JEV and DENV NS4B recruit the NPL4-VCP complex, which is involved in SG clearance, to facilitate the synthesis of viral proteins required for viral genome replication (Arakawa et al., 2022).

1.5.2.5 Inhibition of apoptosis

As described in section 1.5.1.5, apoptosis is a type of programmed cell death that removes senescent, damaged, or infected cells. Indeed, Flavivirus infections as well as the expression of several individual Flavivirus proteins have been shown to induce apoptosis. Accordingly, Flaviviruses have evolved multiple anti-apoptotic mechanisms to promote cell survival for longer virus progeny production (reviewed in Okamoto et al., 2017; Pan et al., 2021). The capsid protein of several Flaviviruses has been associated with an increase in PI3K-dependently phosphorylated AKT, possibly due to sequestering PP-1 phosphatase and preventing it from dephosphorylating AKT (Airo et al., 2018; Lee et al., 2005; Urbanowski and Hobman, 2013). Moreover, DENV has been shown to increase expression of CAML, which alters caspase 3 activation to subvert apoptosis (Li et al., 2012). Finally, DENV also blocks IRE1-mediated activation of apoptosis (reviewed in Perera et al., 2017).

1.5.3 Viral hijacking of cellular processes

As previously mentioned, viruses rely on several host cell functions for their replication. Therefore, they hijack cellular processes and use them for their benefit.

1.5.3.1 Hijacking of the translation machinery

Like any virus, Flaviviruses are completely dependent on the host cell translation machinery for the synthesis of viral proteins. As most cellular mRNAs, Flavivirus RNA harbors a methylated cap structure at its 5' end to enable canonical cap-dependent translation initiation (reviewed in Shivaprasad and Sarnow, 2021). Moreover, the cellular translation machinery can also be recruited to Flavivirus RNA via a cap-independent mechanism (Berzal-Herranz et al., 2022; Edgil et al., 2006; Song et al., 2019; Wang et al., 2020).

1.5.3.2 Hijacking of stress granule proteins

In addition to sequestering stress granule (SG) proteins to prevent SG formation, Flaviviruses hijack these proteins to promote their replication. A pro-viral role for several SG proteins has been demonstrated. For example, knockdown of TIAR has been shown to result in less efficient WNV growth, suggesting a functional role for TIAR in WNV replication (Li et al., 2002). Knockdown of DDX6 was associated with a reduction of DENV RNA levels and DENV focus forming units, suggesting a role for DDX6 in the production and/or release of viral particles (Ward et al., 2011). Knockdown of G3BP1, TIAR and Caprin-1 has been observed to result in a significant reduction in ZIKV titers, indicating that these proteins are important for ZIKV replication (Hou et al., 2017). G3BP1 depletion has also been associated with a decrease in viral protein and viral genomic RNA, whereas overexpression has been shown to increase viral RNA and viral titers, which further indicates that G3BP1 facilitates ZIKV replication (Bonenfant et al., 2019).

1.5.3.3 Hijacking of autophagy

In addition to being an intrinsic cellular defense mechanism against viruses, autophagy is also exploited by Flaviviruses to promote their replication (Figure 16). Autophagy-related double-membrane structures can serve as a platform for viral replication complexes, increase the local concentration of essential intermediates, and shield viral RNAs from detection and degradation by the host cell (reviewed in Choi et al., 2018).

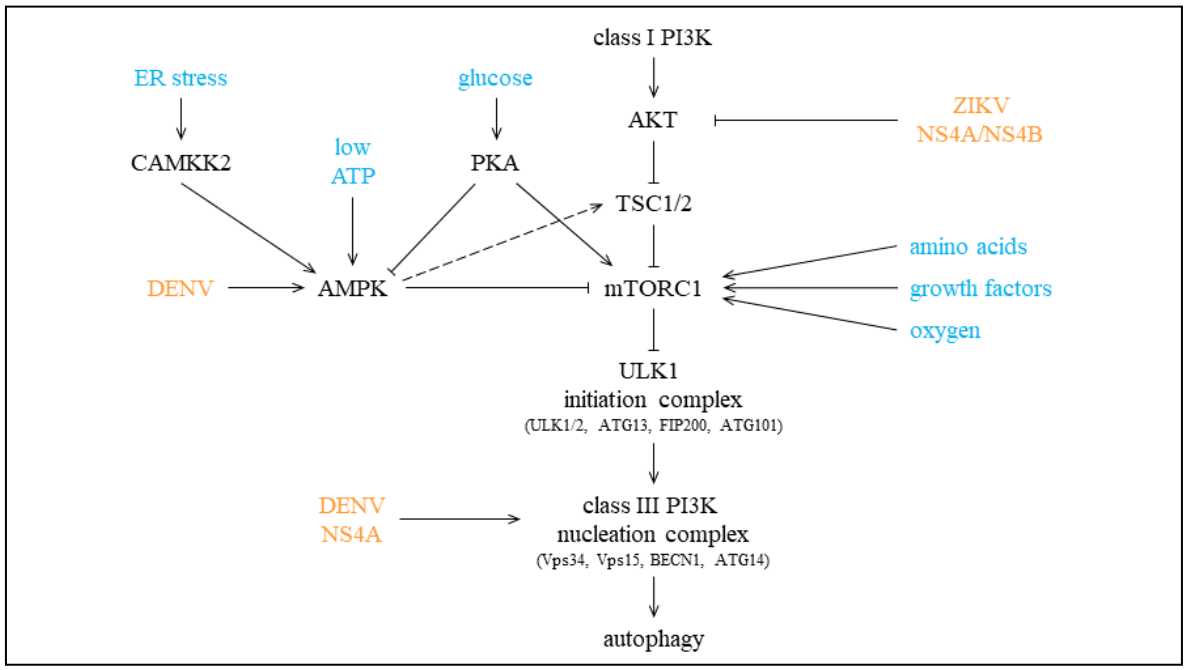

Figure 16. Viral activation of autophagy. Autophagy initiation pathways are displayed. Environmental stimuli are shown in blue, and viruses or viral proteins are shown in orange. Figure adapted from (Choi et al., 2018; Ke, 2018; Mao et al., 2019; Parzych and Klionsky, 2014).

DENV relies on autophagy for the formation of membranous structures essential for viral replication, as well as for the generation of ATP and free fatty acids from the degradation of lipid droplets. DENV NS4A activates autophagy in a PI3K-dependent manner. In addition, DENV has been shown to activate AMPK, leading to the suppression of mTORC1 and the activation of lipophagy (reviewed in Ke, 2018; Mao et al., 2019). JEV-induced autophagy plays a role in the JEV entry process, rather than providing membranes for the formation of viral replication compartments. JEV C, prM and NS3 proteins have been shown to induce autophagy (reviewed in Ke, 2018). In the case of ZIKV, NS4A and NS4B

have been shown to inhibit AKT, thus suppressing mTORC1 and activating autophagy (reviewed in Choi et al., 2018; Mao et al., 2019).

1.5.3.4 Hijacking of the UPR

In addition to being induced by the host cell to restrict viral replication, the UPR has also been found to be activated by Flaviviruses for their benefit. JEV has been reported to initiate the regulated IRE1-dependent decay (RIDD) pathway, leading to the degradation of host transcripts but not JEV RNA. Moreover, JEV titers were found to be reduced upon inhibition of IRE1 RNase activity, which further suggests a pro-viral role for IRE1 (Bhattacharyya et al., 2014). Furthermore, ZIKV has been shown to activate ATF6, resulting in an increased expression of the chaperone BIP, which contributes to ZIKV replication (Tan et al., 2018).

1.5.3.5 Hijacking of other cellular processes and structures

Flaviviruses also alter cellular metabolic pathways to increase the synthesis of macromolecules needed for viral replication and virion assembly, as well as to promote an energetically favorable state. More specifically, they increase glycolysis to produce ATP via the TCA cycle, and they stimulate fatty acid biosynthesis to alter the composition of the ER membrane (reviewed in Jordan and Randall, 2016; Thaker et al., 2019). As described in section 1.3.3, Flavivirus replication occurs in association with the ER membrane. In fact, Flaviviruses remodel the ER membrane to form replication compartments for efficient viral replication (Heaton et al., 2010; Welsch et al., 2009; reviewed in Miller and Krijnse-Locker, 2008). Finally, DENV has been shown to induce apoptosis by activating NF-κB to increase viral spread via phagocytic myeloid cells (reviewed in Rahman and McFadden, 2011).

1.5.4 Viral influence on host cell gene expression

As previously described in section 1.4.2, gene expression is a complex process which can be influenced at multiple stages, including transcription, pre-mRNA processing, translation, and mRNA decay (reviewed in Alberts et al., 2002; Karp, 2010; Watson et al., 2012). Transcript abundance depends on both its rate of synthesis and its rate of degradation

(reviewed in Heck and Wilusz, 2018). Subgenomic Flavivirus RNA (sfRNA) has been shown to impair cellular mRNA turnover by strongly inhibiting the 5'-to-3' exonuclease XRN1, leading to increased stability of short-lived transcripts and an apparent upregulation of gene expression (Michalski et al., 2019; Moon et al., 2012). Moreover, sfRNA interacts with two more decay factors as well as proteins involved in other RNA-related biological processes including splicing, editing, and translation. Sequestration of these proteins by sfRNA leads to dysregulation of host cell gene expression.

1.5.4.1 Transcriptome of Flavivirus-infected cells

High throughput techniques, such as microarray and next generation RNA sequencing (RNA-Seq), have allowed for the large-scale analysis of cellular transcriptomes and comparison of gene expression levels in different experimental conditions, including viral infections. Table 3 shows a selection of previous studies comparing gene expression between Flavivirus-infected and mock-infected cells. These studies have identified up to several thousand genes whose expression levels are modulated in the presence of Flaviviruses. Gene ontology enrichment analyses have shown that the affected genes are involved in many cellular processes, with the most commonly and most significantly enriched pathways including immune response, antiviral response, inflammatory response, and type I interferon signaling (Banerjee et al., 2017; Bonenfant et al., 2020; Ekkapongpisit et al., 2007; Fernandez et al., 2022; Gupta et al., 2010; Horibata et al., 2021; Liew and Chow, 2004; O'Neal et al., 2019; Qian et al., 2013; Sessions et al., 2013; Sotcheff et al., 2022; Tang et al., 2016; Warke et al., 2003; Yang et al., 2011; Zanini et al., 2018).

A few studies have investigated changes in alternative splicing (AS) of host mRNAs in Flavivirus-infected cells via RNA-Seq, and several hundred genes were found to be alternatively spliced compared to mock-infected cells (Bonenfant et al., 2020; De Maio et al., 2016; Sessions et al., 2013). Since AS may affect the function of the protein encoded by the mRNA, as well as the transcript's localization, efficiency of translation, and stability, missplicing of some identified genes has been hypothesized to promote or limit viral infection (Bonenfant et al., 2020). Furthermore, mechanistic studies indicate that the observed changes

Table 3. Previous studies comparing the transcriptomes of Flavivirus-infected and mock-infected cells.

Authors	Method	Virus	Cells	MOI	Time	Fold-change cutoff	Number of differentially expressed genes
Warke et al., 2003	Microarray	DENV	HUVECs	1	48h	4	269 up, 126 down
Liew and Chow, 2004	DD-RT-PCR	DENV	ECV304	1	1/3/5/7d	n/a	78 (46 up, 32 down)
Ekkapongpisit et al., 2007	cDNA-AFLP	DENV	HepG2	5	3d	n/a	27
Gupta et al., 2010	Microarray	JEV	N2A	5	36h	n/a	80
Yang et al., 2011	Microarray	JEV	mice inoculated with $5x10^6$ PFU		spleen: 3d brain: 6d	n/a	spleen: 437 brain: 1119
Qian et al., 2013	RNA-Seq	WNV	primary human macro-phages	1	24h	4	732
Sessions et al., 2013	RNA-Seq	DENV	HuH7	20	20h	n/a	wild-type: 2859 (1818 up, 1041 down) attenuated: 9047 (4610 up, 4437 down)
Clarke et al., 2014	Microarray	JEV and WNV	Mice inoculated intracerebrally with 40/100 PFU		5-6d	2	JEV: 1116 (614 up, 502 down) WNV: 757 (582 up, 174 down)
Tang et al., 2016	RNA-Seq	ZIKV	hNPCs	<0.1	56h	n/a	6864 (3443 up, 3421 down)
Banerjee et al., 2017	RNA-Seq	DENV	PBMCs	variable (cells isolated from patients)		2	376
Zanini et al., 2018	scRNA-Seq	DENV	PBMCs	variable (cells isolated from patients)			
O'Neal et al., 2019	scRNA-Seq	WNV	L929	1	24h		
Bonenfant et al., 2020	RNA-Seq	ZIKV and DENV	SH-SY5Y	5	24h	n/a	$ZIKV^{PR}$: 1464 (703 up, 651 down) $ZIKV^{MR}$: 243 DENV: 182
Horibata et al., 2021	RNA-Seq	ZIKV	HEK293	1	48h	2	659
Fernandez et al., 2022	RNA-Seq	ZIKV	MDMs	5	24h	2	1067
Sotcheff et al., 2022	PAC-Seq	ZIKV	JEG3	3	16h	1.5	126 (98 up, 28 down)

in AS are, at least partially, due to NS5 interacting with components of the U5 snRNP of the spliceosome, which negatively affects the efficiency of pre-mRNA splicing (De Maio et al., 2016).

1.5.4.1.1 Virus-induced modulation of (alternative) splicing in antiviral response-related cellular transcripts

JEV and DENV have been shown to trigger splicing of XBP1 (Yu et al., 2006). As previously mentioned, splicing of XBP1 is usually mediated by IRE1 in response to ER stress and triggers the unfolded protein response (UPR) (reviewed in Perera et al., 2017). In Flavivirus-infected cells, viral glycoproteins (E, NS1) and ER-anchored small hydrophobic proteins (NS2A, NS2B, 2K-NS4B) were shown to induce XBP1 splicing. The activation of the UPR alleviates virus-induced ER stress and cytotoxicity to prevent apoptosis, thus ensuring viral survival (Yu et al., 2006).

DENV and ZIKV have been shown to change SAT1 splicing patterns (Pozzi et al., 2020). Normally, exon 4 is removed from the SAT1 pre-mRNA to give rise to a functional SAT1 protein that plays an antiviral role by depleting cellular polyamines required for viral replication. However, during DENV infection, an increased inclusion of exon 4 in SAT1 mRNA has been observed. The inclusion of exon 4 leads to the occurrence of a premature stop codon, and therefore the degradation of SAT1 mRNA. This changed alternative splicing pattern of SAT1 pre-mRNA is due to the DENV NS5-triggered proteasomal degradation of RBM10, a splicing factor that targets SAT1 and promotes exon skipping (Pozzi et al., 2020).

1.5.4.2 Proteome of Flavivirus-infected cells

The first comprehensive studies comparing the expression of multiple proteins between virus-infected and mock-infected cells used two-dimensional differential gel electrophoresis (2D DIGE), excision of spots of interest and protein identification by mass spectrometry. They identified up to 127 differentially expressed proteins. Many of these proteins were found to be involved in apoptosis, transcription/translation, stress response and cytoskeleton network (Dhingra et al., 2005; Pastorino et al., 2009; Pattanakitsakul et al., 2007).

Quantitative proteomics methods based on stable isotope labeling by amino acids in cell culture (SILAC) have replaced 2D gel-based methods given their higher resolution and sensitivity. They have allowed for the identification of up to two hundred differentially expressed proteins with functions in antiviral defense response, immune response, interferon

signaling, and lipid metabolism (Chiu et al., 2014; Wichit et al., 2019; Zhang et al., 2013). Table 4 shows a summary of previous studies comparing protein expression between Flavivirus-infected and mock-infected cells.

Table 4. Previous studies comparing the proteomes of Flavivirus-infected and mock-infected cells.

Authors	Method	Virus	Cells	MOI	Time	Fold-change cutoff	Number of differentially expressed proteins
Dhingra et al., 2005	2D DIGE	WNV	rat neuron	5	5 days	n/a	55 (38 up, 17 down)
Pattanakitsakul et al., 2007	2D PAGE	DENV	HepG2	1	24h	n/a	17 (10 up, 7 down)
Pastorino et al., 2009	2D DIGE	WNV	Vero	1	24h	2	127 (68 up, 59 down)
Zhang et al., 2013	SILAC	JEV	HeLa	10	48h	1.5	nuclear: 63 cytoplasmic: 99
Chiu et al., 2014	SILAC	DENV	A549	5	28h	2/1.5	cytoplasmic: 69/211 (12/28 up, 57/183 down) nuclear: 57/207 (13/82 up, 44/125 down)
Wichit et al., 2019	SILAC	ZIKV	HFF1	8	48h	n/a	16 (15 up, 1 down)

Two of the afore-mentioned proteomics studies (Pattanakitsakul et al., 2007; Zhang et al., 2013) compared their sets of differentially expressed proteins to differentially expressed transcripts in JEV/DENV-infected cells reported in other studies. Zhang et al. found that only 5 of their 158 differentially expressed proteins had been reported to have altered mRNA levels, whereas Pattanakitsakul et al. found no overlap of their differentially expressed proteins and altered transcripts. The authors suggest that these discrepancies might be explained by different experimental conditions, such as different virus strains, host cells, duration of infection and MOI (Pattanakitsakul et al., 2007; Zhang et al., 2013). Alternatively, inconsistencies in mRNA levels and protein levels might be due to post-transcriptional regulation of protein synthesis, or differences in mRNA and protein stability (reviewed in Nie et al., 2007).

Although transcriptomic and proteomic profiling studies have already been performed on Flavivirus-infected cells, very few have been done with cells of the nervous system despite many Flaviviruses being neurotropic. Moreover, past studies have focused on either the

transcriptome or the proteome of Flavivirus-infected cells, but no matched transcriptomic and proteomic data from identical experimental conditions is available, thus preventing comparison of changes in mRNA and protein levels.

1.6 Rationale and hypothesis

As described in the previous sections, Flaviviruses include important human pathogens that constitute a significant burden on health care systems worldwide. Vaccines to prevent these infections are available for some of these viruses only. Moreover, despite being generally efficient and safe, not everyone is able to benefit from immunization due to contraindications for certain populations and/or limited access in remote areas. In addition, current treatment options for symptomatic Flavivirus infections are very limited and rely on rest as well as supportive care to relieve symptoms. Given that decades-long research efforts to develop specific antiviral drugs have not yet resulted in the approval of an inhibitory compound to treat these infections, we hypothesized that new strategies will be needed for the discovery and/or design of successful antiviral therapies. First off, however, new potential targets will need to be identified.

1.6.1 Goals

The overall goal of my work during my graduate studies was to explore Flavivirus interactions, including interactions between viral components as well as Flavivirus-host interactions, to uncover new potential drug targets.

Goal #1

Investigate interactions between three Flaviviruses, namely Kunjin virus, Zika virus, and yellow fever virus, and their host cells (U87 cell line) after 24h of infection.

A - Identify changes in host cell gene expression levels as well as alternative splicing during Flavivirus infections using RNA-Seq.

B - Identify changes in host cell protein expression during Flavivirus infections using SILAC/MS.

C - Compare the identified changes in each infection.

Goal #2

Characterize the interaction between the WNV NS3 and NS5 proteins for the purpose of identifying hotspots in the protein-protein interaction which could be targeted for the development of antiviral therapeutics.

A - Develop a model for the NS3:NS5 interaction during positive-strand RNA synthesis based on information available in the literature, such as the individual protein structures, enzymatic activities, and locations of catalytic sites and RNA binding regions. Using this model, predict which residues of NS3 and NS5 may mediate this potential interaction.

B - Determine the importance of these residues for viral replication through site-directed mutagenesis in a WNV replicon. More precisely, transfect BHK17 cells with the wild-type and mutant replicons, and measure luciferase activity which is proportional to viral replication.

C - If some mutations are associated with a significant loss of interaction, determine whether this is caused by a loss of interaction between NS3 and NS5.

2 ARTICLE 1: KUNJIN VIRUS, ZIKA VIRUS AND YELLOW FEVER VIRUS INFECTIONS HAVE DISTINCT EFFECTS ON THE CODING TRANSCRIPTOME AND PROTEOME OF BRAIN-DERIVED U87 CELLS

Authors: Carolin Brand, Gabrielle Deschamps-Francoeur, Kristen M. Bullard-Feibelman, Michelle S. Scott, Brian J. Geiss, Martin Bisaillon

Status: Published in Viruses on June 23, 2023, https://doi.org/10.3390/v15071419

Preface: I designed the project with Brian Geiss and Martin Bisaillon. I performed approximately half of the wet lab experiments, I analyzed the RNA-Seq data as well as the MS data, and I created the figures. I wrote most of the article under the supervision and with the participation of Brian Geiss and Martin Bisaillon. I also wrote the response to the reviewers.

Summary : Flaviviruses include important human pathogens, such as ZIKV and YFV. As any other virus, they rely heavily on host cells for replication, and therefore interact with host cells in many ways. On the one hand, they dysregulate cellular processes to promote viral replication. On the other hand, host cells defend themselves against the invading pathogen by activating multiple signaling pathways. In the present study, the complex interplay between Flaviviruses and their host cells was investigated using RNA sequencing as well as SILAC/MS. The coding transcriptomes and proteomes of cells infected with three different Flaviviruses, namely KUNV, ZIKV and YFV, was compared to those of mock-infected cells. Several hundred genes and proteins were found to be differentially expressed, and alternative splicing of hundreds of cellular transcripts was also found to be modulated. Among these genes/proteins, several would be interesting candidates to study further for their roles in viral infections and their potential to be targeted to suppress viral replication.

Kunjin Virus, Zika Virus, and Yellow Fever Virus Infections Have Distinct Effects on the Coding Transcriptome and Proteome of Brain-Derived U87 Cells

Carolin Brand[1], Gabrielle Deschamps-Francoeur[1], Kristen M. Bullard-Feibelman[2], Michelle S. Scott[1], Brian J. Geiss[2] and Martin Bisaillon[1,*]

[1] Département de Biochimie et de Génomique Fonctionnelle, Faculté de Médecine et des Sciences de la Santé, Université de Sherbrooke, 3201 rue Jean-Mignault, Sherbrooke, QC J1E 4K8, Canada; carolin.brand@usherbrooke.ca (C.B.); gabrielle.deschamps-francoeur@usherbrooke.ca (G.D.-F.); michelle.scott@usherbrooke.ca (M.S.S.)

[2] Department of Microbiology, Immunology, and Pathology, School of Biomedical Engineering, Colorado State University, 1682 Campus Delivery, Fort Collins, CO 80523, USA; feibelman.k@gmail.com (K.M.B.-F.); brian.geiss@colostate.edu (B.J.G.)

[*] Correspondence: martin.bisaillon@usherbrooke.ca

Abstract

As obligate intracellular parasites, viruses rely heavily on host cells for replication, and therefore dysregulate several cellular processes for their benefit. In return, host cells activate multiple signaling pathways to limit viral replication and eradicate viruses. The present study explores the complex interplay between viruses and host cells through next generation RNA sequencing as well as mass spectrometry (SILAC). Both the coding transcriptome and the proteome of human brain-derived U87 cells infected with Kunjin virus, Zika virus, or Yellow Fever virus were compared to the transcriptome and the proteome of mock-infected cells. Changes in the abundance of several hundred mRNAs and proteins were found in each infection. Moreover, the alternative splicing of hundreds of mRNAs was found to be modulated upon viral infection. Interestingly, a significant disconnect between the changes in the transcriptome and those in the proteome of infected cells was observed. These findings provide a global view of the coding transcriptome and the proteome of Flavivirus-infected cells, leading to a better comprehension of Flavivirus–host interactions.

Keywords

flavivirus; Kunjin virus; Zika virus; yellow fever virus; virus–host interaction; transcriptomics; alternative splicing; proteomics; RNA-Seq; SILAC

Introduction

Viruses are obligate intracellular parasites that are dependent on host cells for replication. During infection, viruses modulate several cellular processes for their benefit. In response, host cells activate multiple signaling pathways to restrict viral replication and eliminate the pathogen. Innate immune sensors, also called pattern recognition receptors (PRRs), recognize pathogen-associated molecular patterns (PAMPs), such as viral nucleic acids and proteins, and activate signaling cascades to induce antiviral and proinflammatory genes, including interferons. Interferons then promote the expression of interferon-stimulated genes (ISGs), the protein products of which have antiviral effector functions [1]. One example of an interferon-induced gene is protein kinase R (PKR). PKR is activated upon interaction with viral double-stranded RNA, phosphorylates eIF2, and thus blocks the translation of both viral and host mRNAs [2] by sequestering stalled translation preinitiation complexes in stress granules.

Flaviviruses are mosquito-borne viruses with an 11 kb, positive sense, single-stranded RNA genome [3]. They are globally distributed, putting more than half of the world's population at risk for infection. Although most Flavivirus infections are asymptomatic and the most common clinical manifestation is a flu-like illness, Flaviviruses can cause a wide variety of severe diseases, such as encephalitis, hemorrhagic fever, or jaundice in a small percentage of cases. Members of the Flavivirus genus include the important human pathogens Yellow Fever virus (YFV), Zika virus (ZIKV), West Nile virus (WNV), Dengue virus (DENV), and Japanese Encephalitis virus (JEV) [4,5]. When transmitted by a mosquito vector, Flaviviruses infect human skin cells, such as skin dendritic cells. These cells then migrate to lymphoid organs, from where the virus can be disseminated throughout the body including the central nervous system where they can cause life-threatening encephalitis [6].

Upon infection, Flaviviruses dysregulate a multitude of cellular processes for their benefit. For example, DENV has been shown to increase fatty acid biosynthesis by recruiting fatty acid synthase (FASN) to the sites of viral replication and stimulating FASN activity [7]. This contributes to the alteration of the lipid profile of DENV-infected cells, affecting membrane properties and promoting the formation of viral replication compartments [8]. Flaviviruses also counteract measures taken by the host cell to limit viral replication. For instance, they have been shown to inhibit interferon signaling [1] as well as the formation of stress granules [9,10] to evade the antiviral response and overcome the translational block of viral RNA, respectively. Moreover, recent studies have shown that Flaviviruses alter the host cell's transcriptome by affecting gene expression levels and pre-mRNA splicing [11–15]. For example, DENV has been shown to affect SAT1 splicing patterns. More precisely, an increase in exon 4 inclusion in SAT1 mRNA has been observed in DENV-infected cells, leading to the degradation of SAT1 mRNA, and therefore to a reduction in the amount of the antiviral protein SAT1 [16].

Most of the transcriptomic profiling studies following infection with Flaviviruses have been performed with a single viral species, and experimental conditions between different studies vary greatly, preventing the comparison of changes induced in the host cell transcriptome by these closely related viruses. Here, to gain insight into the range of molecular effects Flavivirus infections bring about in host cells, we investigate the changes in the coding transcriptome and the proteome of host cells upon infection with three different Flaviviruses (Kunjin, Zika, and Yellow Fever) using next-generation RNA sequencing and Stable Isotope Labeling by Amino acids in Cell culture (SILAC), respectively.

Materials and Methods

Viruses

Kunjin virus (strain FLSDX, GenBank AY274504.1), Zika virus (strain PRVABC59, GenBank, KU501215.1), Yellow Fever virus (strain 17D, GenBank X03700.1), and Sindbis virus (strain TE302J, NCBI reference sequence NC_001547.1) were used for viral infections. To generate viral stocks, VeroE6 cells were grown in DMEM (Wisent Bioproducts, St-Jean-

Baptiste, QC, Canada, 319-015-CL) supplemented with 10% FBS (Wisent 081-110) and 50 mM HEPES (Wisent 330-050-EL) to 50% confluency. Viruses were added to the cells for 72 h, infected media were collected, clarified by centrifugation at 15,000 rpm, and frozen at -80 °C. Viral titers were determined using focus-forming assays (KUNV, YFV, ZIKV) or plaque assay titrations (SINV) on VeroE6 cells. VeroE6 cells seeded on 12-well tissue culture plates (250,000 cells per well) were infected with serial dilutions of virus samples for 1 h at 37 °C, and then an agarose nutrient overlay was added (1.5 mL per well; 50% *v*/*v* mix of 2X DMEM (Wisent 319-205-CL) supplemented with 5% FBS and 0.6% agarose). Cells were maintained at 37 °C for 3 days, and on day 3, cells were fixed by adding 1 mL of 10% formaldehyde (Fisher Scientific, Waltham, MA, USA, BP531-500) for 30 min. For the plaque assay (SINV), fixed cells were treated with 1% crystal violet in 20% ethanol for 15 min. The stain was washed off with water, viral plaques were counted, and viral titers were determined as plaque forming units (PFU)/mL. For the focus-forming assay (Flaviviruses), fixed cells were washed with PBS prior to incubation with monoclonal anti-flavivirus group antigen (clone D1-4G2-4-15) antibody at 500 ng/mL in PBS/0.3% Tween 20/1 mg/mL BSA for 16 h at 4 °C. Cells were washed with PBS/0.5% Tween 20 (PBS-T), incubated with anti-mouse HRP antibody (NEB, Ipswitch, MA, USA, 7076), diluted 1:5000 in PBS/0.3% Tween 20/1 mg/mL BSA for 2 h at room temperature, washed with PBS-T, and treated with 3,30,5,50-tetramethylbenzidine (TMB, Sigma-Aldrich, St. Louis, MO, USA, 613548) for 30 min. Spots were counted and viral titers determined as focus-forming units (FFU)/mL.

Cell Culture and Infections for RNA Sequencing

U87 cells were grown in complete Dulbecco's modified Eagle's Medium (cDMEM) containing 10% fetal bovine serum (Atlas Biologicals, Fort Collins, CO, USA), and L-glutamine, and cells were incubated at 37 °C in humidified incubators supplemented with 5% CO_2. To perform infections, 50% confluent U87 cells in T150 flasks were either infected at a multiplicity of infection (MOI) of 5 or treated with cell-conditioned media (n = 3 for each virus and control). Then, 24 h post-infection, cells were harvested and homogenized using QIAshredder (Qiagen, Hilden, Germany).

Next Generation RNA Sequencing

RNA was isolated using the RNeasy kit (Qiagen) following the manufacturer's recommended protocols. RNA was stabilized for storage using an RNA transport kit (OMEGA bio-tek, Norcross, GA, USA, R0527). PolyA-RNA was purified from 5 µg total RNA using NEB magnetic mRNA Isolation Kit (NEB, Ipswitch, MA, USA, #S1550S) and eluted into a final volume of 25 µL. Sequencing libraries were prepared using 9 µL of isolated mRNA and ScriptSeq RNA-Seq Library Preparation Kit (Epicentre Biotechnologies, Madison, WI, USA, SSV21124). Paired-end 100 bp sequencing was performed on a HiSeq 4000 system (Illumina, San Diego, CA, USA) at McGill University and Génome Québec Innovation Centre, obtaining between 34 and 72 million reads per sample.

Building of the Reference Genome for RNA Sequencing Analysis

The human genome as well as an annotation file (GRCh38, release 89) were obtained from Ensembl. The viral genome sequences were obtained from NCBI (AY274504.1 for Kunjin virus, KU501215.1 for Zika virus, X03700.1 for Yellow Fever virus, NC_001547.1 for Sindbis virus). A reference genome containing the human genome as well as the viral genomes was generated with STAR 2.5.1b [17] and the parameter --sjdbOverhang 99.

Differential Gene Expression Analysis

Reads were trimmed using Trimmomatic 0.32 [18] to remove adapter sequences as well as nucleotides with low quality scores (TRAILING: 30). The quality of output reads was verified using FastQC 0.11.5. Reads were aligned to the reference genome (hg38 + viral genomes) using STAR 2.5.1b [17] with default parameters except for --outFilterMismatchNmax 5. The numbers of raw reads and aligned reads are given for each sample in Supplementary Figure S2. Aligned reads were then assigned to genes and quantified using Rsubread. FeatureCounts 1.20.6 with options isGTFAnnotationFile = TRUE, countChimericFragments = FALSE, largestOverlap = TRUE, isPairedEnd = TRUE, useMetaFeatures = TRUE, requireBothEndsMapped = TRUE, strandSpecific = 1, minOverlap = 10, autosort = TRUE. Differential gene expression analysis was performed with DESeq2 [19] using default parameters.

Differential Alternative Splicing Analysis

As required for downstream analysis, all reads were trimmed to the same length using Trimmomatic 0.32 [18] before being aligned to the reference genome using STAR 2.5.1b [17]. Alternative splicing analysis was performed using rMATS 3.2.5 [20] with the options -len 93 -a 3 -t paired -analysis U. ΔPSI (percent spliced in) values for each alternative splicing event were calculated by subtracting the PSI value in infected cells from the PSI value in non-infected cells. Therefore, a positive ΔPSI value indicates an increase in the short form upon infection, whereas a negative ΔPSI value indicates an increase in the long form upon infection.

RT-qPCR

Twenty-one genes for which their expression was significantly altered upon viral infection, as determined by RNA sequencing, were selected for RT-qPCR validation: ATOH8, BMPER, CSF2, CXCL8, DDIT3, DGAT2, ENG, ERN1, HBEGF, HERPUD1, IFIT2, IGFL3, IL6, IL7R, INSIG1, MSC, PLAU, RSAD2, TGOLN2, TNFRSF11B, and VAV2. This selection represents genes associated with a varying range of fold-change values, some of which are positive (overexpressed upon infection), and some of which are negative (repressed upon infection). Some of the selected genes are overexpressed or repressed in multiple infections, whereas others are associated with significant fold-change values in one infection only. Reverse transcription reactions were performed on 2.2 µg of total RNA using Transcriptor reverse transcriptase, random hexamers, dNTPs (Roche Diagnostics, Rotkreuz, Switzerland), and 10U RNaseOUT (Invitrogen, Waltham, MA, USA, #10777019), according to the manufacturer's protocol in a total volume of 20 µL. All gene-specific primers (IDT) were resuspended individually to 20–100 µM in TE buffer (IDT) and then diluted as forward/reverse primer pairs in nuclease-free water (IDT) to a final concentration of 1 µM. Quantitative PCR was performed with 5 µL iTaq Universal SYBR Green Supermix (Bio-Rad Laboratories, Hercules, CA, USA), 2 µL primer pair solution, and 3 µL (10 ng) cDNA in a total volume of 10 µL on a CFX-96 thermocycler (Bio-Rad). After an initial denaturation at 95 °C for 3 min, 50 three-step cycles (denaturation at 95 °C for 15 s, annealing at 60 °C for 30 s, and elongation at 72 °C for 30 s) were executed. For each primer

pair, a negative control reaction without a template was performed. Relative expression levels were calculated using the qBASE framework [21].

ASPCR (Alternative Splicing Analysis by End-Point RT-PCR)

Six alternative splicing events that were significantly altered upon viral infection, as determined by RNA sequencing, were selected for ASPCR validation. Primers were designed to anneal on both sides of the alternative splicing event to be analyzed, thus allowing the amplification of both isoforms in the same reaction. RNA integrity was assessed with an Agilent 2100 Bioanalyzer (Agilent Technologies, Santa Clara, CA, USA). Reverse transcription was performed on 1.1 µg total RNA with Transcriptor reverse transcriptase, random hexamers, dNTPs (Roche Diagnostics, Rotkreuz, Switzerland), and 10 units of RNAse-OUT (Invitrogen, #10777019) following the manufacturer's protocol in a total volume of 10 µL. All forward and reverse primers were individually resuspended to 20–100 µM in Tris-EDTA buffer (IDT) and diluted as a primer pair in RNase DNase-free water (IDT) to a final concentration of 1.2 µM. End-point PCR reactions were carried out on 10 ng cDNA in a 10 µL final volume containing 0.2 mmol/L of each dNTP, 0.6 mol/L of each primer, and 0.2 units of TransStart FastPfu Fly DNA Polymerase (TransGen Biotech, Beijing, China). An initial incubation of 2 min at 95 °C was followed by 35 cycles of denaturation at 95 °C for 20 s, annealing at 55 °C for 20 s, and elongation at 72 °C for 60 s. The amplification was completed by a 5 min incubation at 72 °C. PCR reactions were carried out on thermocyclers C1000 Touch Thermal cycler (Bio-Rad Laboratories, Hercules, CA, USA), and the amplified products were analyzed by automated chip-based microcapillary electrophoresis on Labchip GX Touch HT instruments (Perkin Elmer, Waltham, MA, USA). Amplicon sizing and relative quantitation was performed by the manufacturer's software.

Cell Culture and Infections for SILAC

U87 cells were grown in SILAC DMEM Flex Media (Life Technologies, Carlsbad, CA, USA, A2493901) supplemented with Glutamax, 50 mM HEPES (pH 7.5), glucose, 10% dialyzed fetal bovine serum, as well as light/medium/heavy L-arginine (R0/R6/R10) and L-lysine (K0/K4/K8). Cells were incubated at 37 °C in humidified incubators supplemented

with 5% CO_2. Cells were passaged by scraping in a cell dissociation buffer (Thermo Fisher Scientific 13151014) instead of using trypsin to maintain isotope-specific labeling. To perform infections, 50% confluent U87 cells in T150 flasks were either infected at a multiplicity of infection (MOI) of 3 or treated with cell-conditioned media (n = 3 for each virus and control). Then, 24 h post-infection, cells were scraped from the flask, pelleted, and resuspended in 1 ml lysis buffer (50 mM Tris-Base pH 7.4, 1 mM EDTA, 150 mM NaCl, 1% NP40, 0.25% sodium deoxycholic acid, 1 tablet of cOmplete Protease Inhibitor Cocktail (Roche 05892791001) per 50 mL).

Viruses used for the SILAC experiment were grown as described above, but in cell culture media containing medium/heavy L-arginine (R6/R10) and L-lysine (K4/K8).

Gel Electrophoresis, in-Gel Digestion, and Extraction of Peptides

The protein concentration of each cell lysate was determined using a BCA assay (Pierce, Waltham, MA, USA, 23223), and equal amounts of light, medium, and heavy lysates were mixed (15 µg of each sample for L:M:H mix, and 25 µg of each sample for L:M mix, final volume of approximately 40 µL for each mix). Samples were reduced by adding 0.5 µL of 1M dithiothreitol (DTT) and 8 µL of 5x Laemmli buffer, followed by an incubation at 95 °C for 2 min. Proteins were alkylated by adding 2.5 µL of 1M iodoacetamide and incubating at room temperature in the dark for 30 min prior to separation by one-dimensional SDS-PAGE (4–12% Bis-Tris Novex mini-gel, Life Technologies, Carlsbad, CA, USA) and visualization by Coomassie Blue staining (Simply Blue Safe Stain, Life Technologies). Following extensive washes in water, each lane of the gel was cut into five slices, and each slice was cut into small pieces with a clean scalpel. To de-stain the gel bands, they were washed four times for 15 min in a shaker. The first wash was with water (Fluka Analytical, Buchs, Switzerland, 39253), and for the second wash, an equal volume of acetonitrile (CH_3CN, Fluka Analytical 34967) was added. For the third wash, the supernatant was removed before adding 20 mM ammonium bicarbonate (NH_4HCO_3), and for the fourth wash, the supernatant was discarded and a 50% v/v mix of 20 mM NH_4HCO_3 and 100% CH_3CN was added to the gel bands. To dehydrate the gel band pieces, the supernatant from the last wash was removed and 150 µL acetonitrile was added, followed by incubation at room

temperature in a shaker for 5 min twice. Finally, the pieces were dried in a speed vacuum centrifuge at 60 °C for 15 min.

Proteins were digested by adding 75 µL of 12.5 ng/mL trypsin (Promega, Madison, WI, USA, V5280) in 20 mM NH_4HCO_3 at 30 °C for 16 h. For the extraction of peptides from the gel band pieces, an equal volume of CH_3CN was added, followed by a 30 min incubation at 30 °C, and the supernatant was transferred to a LoBind tube (Eppendorf, Hamburg, Germany). To further extract peptides, the gel band pieces were incubated at room temperature on a shaker with 75 µL of 1% formic acid (FA, Fisher Scientific, Waltham, MA, USA, A11750) for 20 min (twice), and with 150 µL CH_3CN for 10 min (three times). All supernatants were pooled in the same LoBind tube. The solvent was removed by lyophilization in a speed vacuum centrifuge at 60 °C for 5 h, and the tryptic peptides were resuspended in 30 µL of 0.1% trifluoroacetic acid (TFA, Sigma Aldrich, St. Louis, MO, USA, T6508) and cleaned up using a ZipTip (Millipore, Burlington, MA, USA, ZTC18S960). The resin was wetted with 100% acetonitrile and equilibrated with 0.1% TFA before the peptides were aspirated. The peptides were then washed with 0.1% TFA and eluted with 1% FA/50% acetonitrile. The clean peptides were dried in a speed vacuum centrifuge at 60 °C for 75 min before being resuspended in 25 µL of 1% formic acid.

LC-MS/MS

A Dionex Ultimate 3000 nanoHPLC system was used to separate 2 µg of trypsin-digested peptides. The sample was loaded onto a Trap column (Acclaim PepMap 100 C18 column (0.3 mm id 5 mm, Dionex Corporation, Sunnyvale, CA, USA)) with a constant flow of 4 µL/min. Peptides were eluted with a linear gradient of 5–35% solvent B (90% acetonitrile with 0.1% formic acid) onto an analytical column (PepMap C18 nano column (75 mm 50 cm, Dionex Corporation) over 4 h with a constant flow of 200 nL/min. An EasySpray source was set to 40 °C and a spray voltage of 2.0 kV was used to connect the nanoHPLC system to an OrbiTrap QExactive mass spectrometer (Thermo Fisher Scientific, Waltham, MA, USA). Full scan MS survey spectra (m/z 350–1600) were acquired in profile mode at a resolution of 70,000 after the accumulation of 1,000,000 ions. The ten most intense peptide ions from the preview scan were selected for fragmentation by collision induced

dissociation (CID) with a normalized energy of 35% and a resolution of 17,500 after the accumulation of 50,000 ions, with a filling time of 250 ms and 60 ms for the full scans and the MS/MS scans, respectively. The screening of the precursor ion charge state was enabled, and all unassigned charge states as well as single, 7, and 8 charged species were rejected. A dynamic exclusion list was allowed for a maximum of 500 entries, with a relative mass window of 10 ppm and a retention time of 60 s. The lock mass option was enabled for survey scanning to improve mass accuracy. Data were acquired using the Xcalibur software version 4.3.73.11 (Thermo Fisher Scientific, Waltham, MA, USA).

Peptide Quantification and Differential Protein Expression Analysis

Peptide identification and quantification were performed using the MaxQuant software package version 1.6.14, with the protein database from Uniprot (Homo sapiens, 16 July 2013, 88,354 entries). The evidence.txt output file was used for differential protein expression analysis with the Proteus R package 0.2.15 (default parameters).

Venn Diagrams

Venn diagrams were created using InteractiVenn [22] and/or BioVenn [23]. The statistical significance of the overlaps was calculated using a Fisher's Exact Test available at https://www.langsrud.com/fisher.htm (accessed on 10 May 2022).

Correlation Coefficients

Nonparametric Spearman correlation matrices were computed using GraphPad Prism with default parameters.

Gene Ontology Enrichment Analysis

Gene ontology (GO) enrichment analysis was performed using the Database for Annotation, Visualization, and Integrated Discovery (DAVID) 6.8 [24]. The background for the enrichment analysis included all genes detected in the experimental condition (i.e., all genes in the DESeq2 or rMATS output files), whereas the gene list included only genes that

were significantly different between infected and control cells, regarding gene expression levels or alternative splicing. In the Functional Annotation Tool, GOTERM_BP_DIRECT in the section “Gene Ontology” was chosen. Obtained *p* values were subjected to Bonferroni correction.

Western Blot

Two of the most downregulated proteins in Flavivirus infections, as determined in the SILAC experiment, were selected for validation by Western blot: HMGA1 and MRPS27. In total, 1 µg (HMGA1) and 10 µg (MRPS27) of total protein extract were separated by one-dimensional SDS-PAGE at 180 V for approximately 1 h before being transferred to a PVDF blotting membrane (GE 10600023) at 100 V for 1 h 15 min. After blocking in 2.5% non-fat milk in PBS for 1 h, the membranes were incubated with a 1:3000 dilution of primary antibody (anti-HMGA1: Abcam ab129153; anti-MRPS27: Abcam ab153940) for 6 h at room temperature, washed three times in TBS-T for 5 min, incubated with a 1:6000 dilution of anti-rabbit HRP secondary antibody (Abcam, Cambridge, UK, ab205718), washed twice in TBS-T and once in PBS for 5 min. Finally, ECL substrate (Bio-Rad Laboratories, Hercules, CA, USA, 1705061) was used to visualize the target proteins. The membranes were stripped by boiling in PBS for 1 min, blocked again, and incubated with anti-actin primary antibody (Sigma-Aldrich, St. Louis, MO, USA, A5441) for 1 h at RT followed by an incubation with anti-mouse HRP secondary antibody (NEB 7076) for 1 h at RT.

Comparison of Proteome and Transcriptome Results

The UniProt identifiers of all proteins detected in the mass spectrometry analysis were mapped to the corresponding ensemble gene IDs using the UniProt Retrieve/ID mapping tool available at https://www.uniprot.org/id-mapping/ (accessed on 27 April 2022) with the following parameters: from database UniProtKB AC/ID to database Ensembl. Changes in gene/protein expression upon viral infections were compared using the UniProt/Ensembl identifiers and DESeq2/Proteus output data. The Splicify pipeline [25] was used for differential splice variant analysis in the transcriptome and proteome.

Results

Global Profiling of the Cellular Coding Transcriptome during Flavivirus Infections

In this study, we investigated the changes in the coding transcriptome as well as in the proteome of virus-infected cells compared to non-infected cells, especially regarding differential gene expression and differential alternative splicing. We chose to include three closely-related Flaviviruses that cause distinct pathologies, as well as a fourth (+)ssRNA arbovirus from a different family (Sindbis virus, Alphavirus genus, Togaviridae family) to distinguish Flavivirus-specific effects on host cells from effects that are instead due to viral infection in general. Sindbis virus was chosen specifically since it is a positive-ssRNA mosquito-borne virus which can cause encephalitis, similar to some Flaviviruses. Given that two of the above-mentioned Flaviviruses are neurotropic, we chose to work with U87 cells, which were isolated from human gliomas, and are widely used [26]. U87 cells were infected at an MOI of 5 for 24 h with either KUNV, ZIKV, YFV, SINV, or treated with cell-conditioned media. PolyA-RNAs were purified prior to cDNA library construction and 100 nt paired-end RNA-Sequencing (Figure 1A). Viral infections were confirmed by ddPCR (Figure S1). At least 34 million reads were obtained for each sample (Figure S2). Reads were processed with Trimmomatic before being aligned to the reference genome (hg38 and viral genomes) using STAR. Rsubread.featureCounts was used to quantify reads for each gene prior to differential gene expression analysis using DESeq2, and rMATS was used for differential alternative splicing analysis (Figure 1B,C). Approximately 30,000 genes and 70,000 alternative splicing events (ASEs) were detected for each condition. The gene lists obtained from DESeq2 were filtered to retain only genes that were detected in triplicate in both experimental conditions (infected and non-infected cells), with an abundance of more than one transcript per million (TPM) in at least one experimental condition, with an absolute log2 (fold-change) greater than 1, and p and q values below 0.05. The ASE lists obtained from rMATS were filtered to retain only events that were detected in triplicate in both the infected and non-infected cells, with an absolute ΔPSI greater than 0.1 (or 10%), and p and FDR values below 0.05 (Figure 2). After applying these filters, several hundred genes were found to be significantly differentially expressed between virus-infected and mock-infected cells: 274 for KUNV, 463 for ZIKV, 520 for YFV, and 33 for SINV (Tables S1–S4).

Moreover, several hundred ASEs were found to be significantly modulated during viral infections: 603 for KUNV, 720 for ZIKV, 930 for YFV, and 665 for SINV (Tables S5–S8).

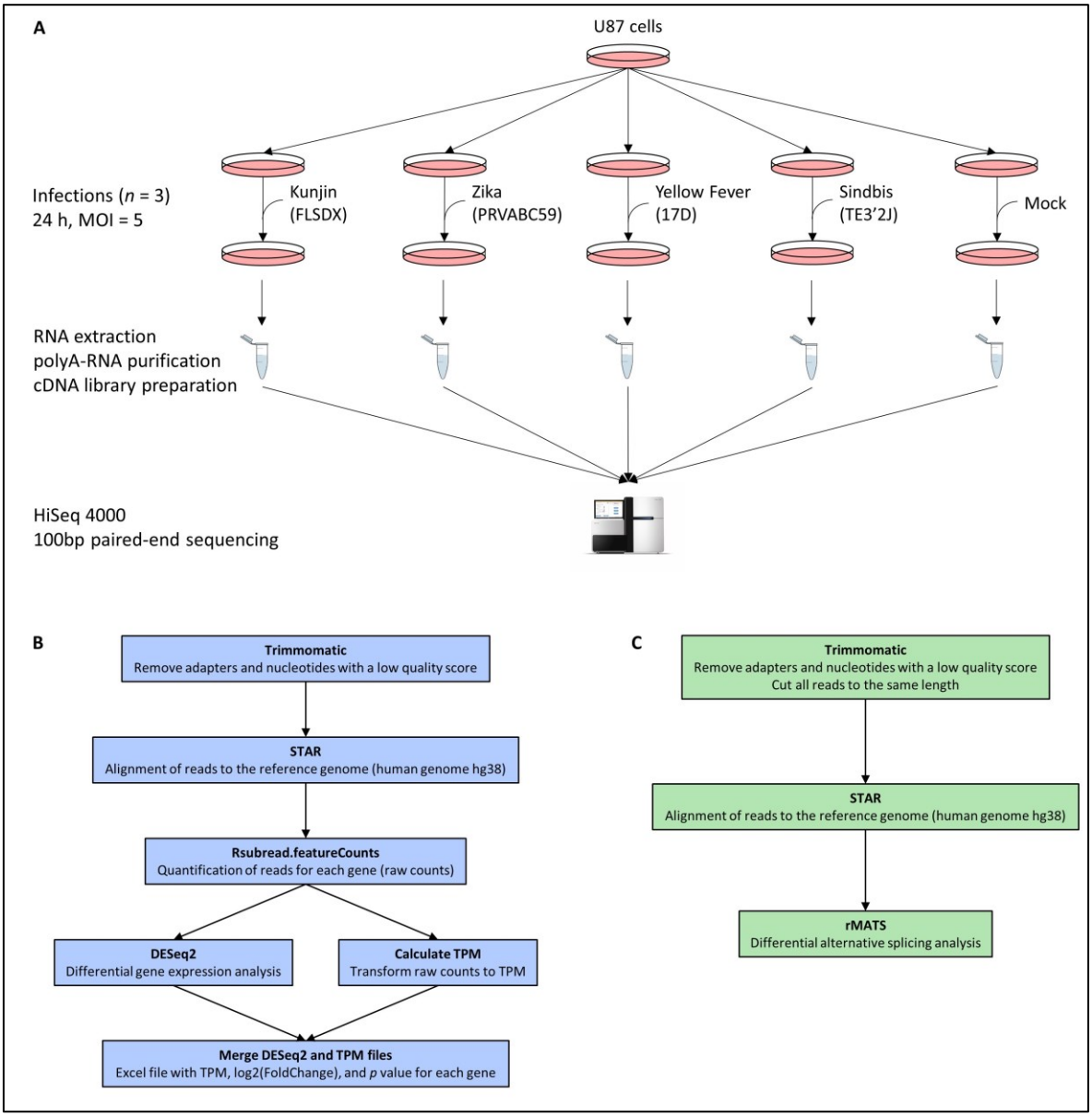

Figure 1. Experimental workflow. (A) The 50% confluent U87 cells were infected with either of the four viruses, or treated with cell-conditioned media, in biological triplicate. Then, 24 h post-infection, cells were harvested and RNA was isolated. PolyA-RNA was purified and used for the construction of cDNA libraries. Paired-end 100 bp sequencing was performed on a HiSeq 4000 system. (B,C) Data obtained from 100 bp paired-end RNA sequencing were analyzed for differential gene expression (B) and differential alternative splicing (C).

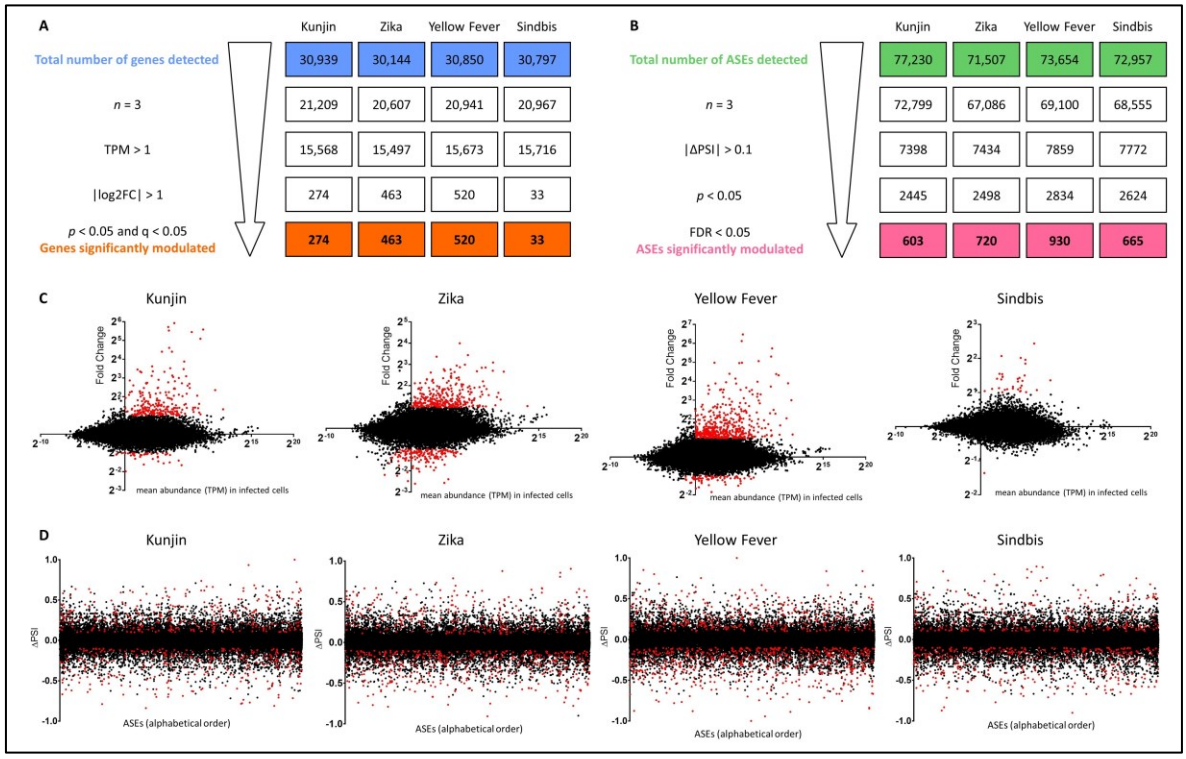

Figure 2. RNA-Seq data filtering. (A) Following differential gene expression analysis with DESeq2, the gene lists were filtered to retain only genes that were detected in triplicate in both experimental conditions (infected and non-infected cells), with an average abundance of more than 1 transcript per million (TPM) in at least one experimental condition, with an absolute log2 (fold-change) greater than 1, and p and q values below 0.05. (B) Following differential alternative splicing analysis with rMATS, the alternative splicing event (ASE) lists were filtered to retain only ASEs that were detected in triplicate in both the infected and non-infected cells, with an absolute ΔPSI greater than 0.1 (or 10%), and p and FDR values below 0.05. (C) The MA plots show fold changes between infected and non-infected cells (y axis) as well as gene abundance in infected cells (x axis) for each gene that was detected. Genes retained as being significantly up- or downregulated are displayed in red. (D) ΔPSI values for all detected alternative splicing events are displayed on the graphs, and ASEs that were significantly modulated upon infection are shown in red.

Validation of RNA-Seq Data

To validate the results obtained from RNA-Seq with a second approach, RT-qPCR was performed on 21 genes, the expression levels of which were found to be altered upon infection, as well as six ASEs that were dysregulated during infection (Figure 3, Table S9). Fold-changes as well as ΔPSI values obtained from both methods were correlated with R^2 values of 0.84 ($p < 0.0001$) and 0.29 ($p = 0.0193$), respectively. This suggests that the results

obtained from RNA-Seq are reliable, attaching significance to the subsequent analyses of the RNA-Seq results.

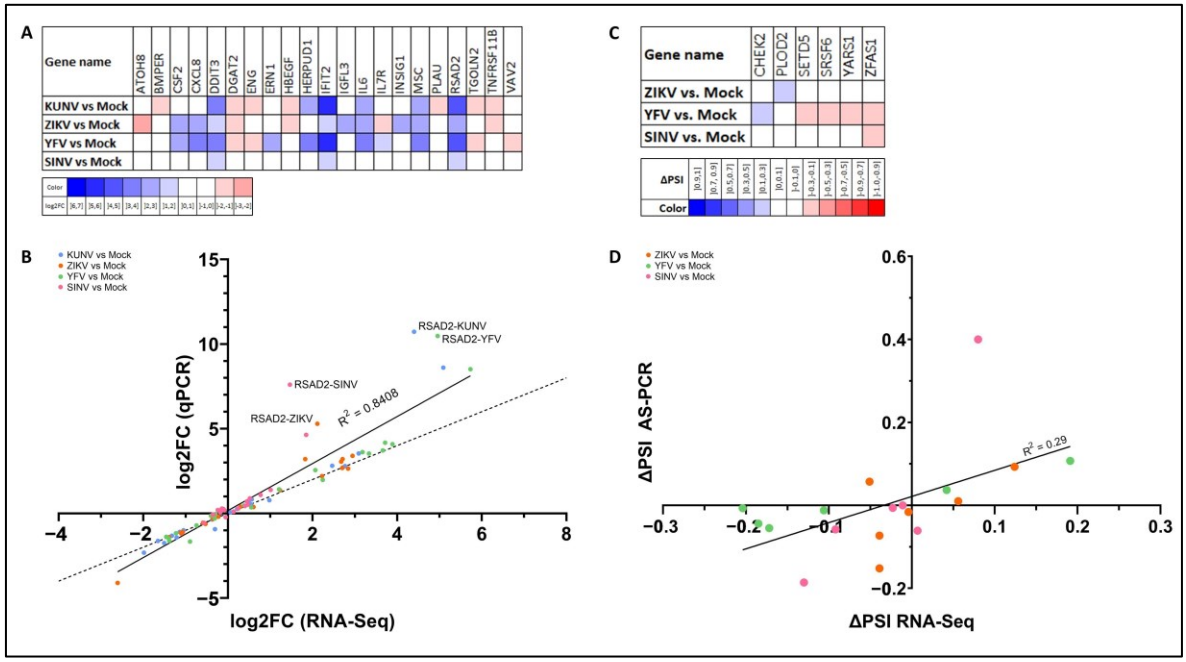

Figure 3. Validation of RNA-Seq data. (A) Overall, 21 genes were chosen for RT-qPCR validation of the RNA-Seq results. Their fold-changes in each infection compared to mock-infected cells are color-coded, with blue being upregulated, red being downregulated, and white meaning no significant change, according to the RNA-Seq data. (B) Fold-changes obtained from qPCR are plotted against fold-changes obtained from RNA-Seq. Both datasets correlate well (linear regression $R^2 = 0.84$). Each dot represents one gene in one infection compared to control cells (blue: KUNV vs. Mock, orange: ZIKV vs. Mock, green: YFV vs. Mock, pink: SINV vs. Mock). The solid line is the linear regression, whereas the dashed line is the identity line (y = x). (C) Six alternative splicing events (ASEs) were chosen for the AS-PCR validation of the RNA-Seq results. Their ΔPSI values in each infection compared to mock-infected cells are color-coded, with blue favoring the short form in infected cells, red favoring the long form in infected cells, and white meaning no significant change, according to the RNA-Seq data. (D) ΔPSI values obtained from AS-PCR are plotted against ΔPSI values obtained from RNA-Seq. Each dot represents one ASE in one infection compared to control cells (orange: ZIKV vs. Mock, green: YFV vs. Mock, pink: SINV vs. Mock), and the solid line is the linear regression.

Alterations to Gene Expression Levels upon Viral Infection

We found that most cellular genes for which expression levels were modulated upon viral infections were overexpressed (Figure 4A). However, it should be noted that ZIKV repressed a higher proportion of differentially expressed genes (155/463 = 33%) than KUNV

and YFV (40/274 = 15% and 69/520 = 13%, respectively). Considering that SINV only minimally affected host cell gene expression levels, it was not included in further analyses of the alterations to gene expression levels upon viral infection.

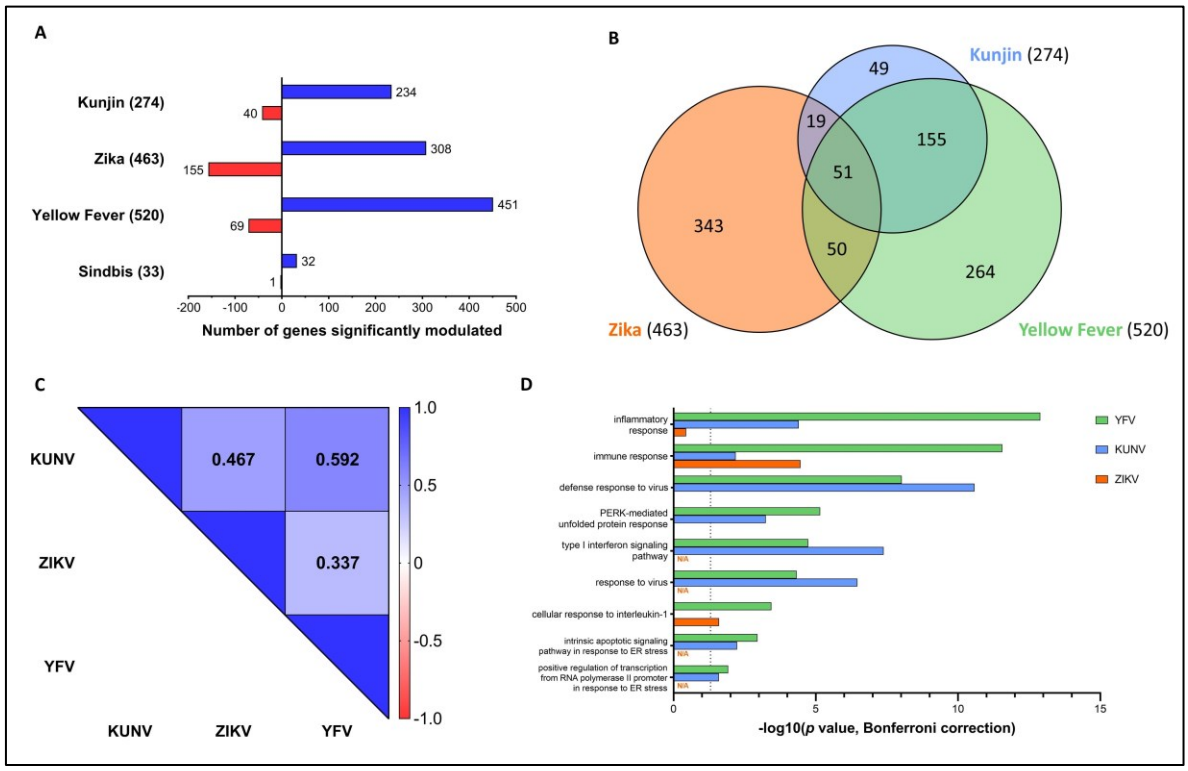

Figure 4. Genes with significant fold-changes upon viral infection. (A) The numbers of upregulated (blue) and downregulated (red) genes in each infection are shown. (B) The area-proportional Venn diagram shows overlaps in the sets of genes for which expression levels were significantly altered upon viral infection. (C) Genes that were detected in all experimental conditions and all replicates were used to calculate Spearman correlation coefficients. (D) Gene ontology enrichment analysis was performed, and GO terms that were significantly enriched (p value with Bonferroni correction < 0.05, represented by the dashed line) in at least two Flavivirus infections are shown. "N/A" indicates that no data was available.

We next compared the genes with significant changes in each infection (Figure 4B) and found considerable overlaps between the three infections. Fisher's Exact Tests yielded p values of 3.49×10^{-54} for KUNV/ZIKV, 1.32×10^{-65} for ZIKV/YFV, and 4.15×10^{-288} for KUNV/YFV. Interestingly, there is a greater overlap between the sets of genes for which expression levels were influenced by KUNV and YFV than between those influenced by KUNV and ZIKV or YFV and ZIKV, although KUNV and YFV genomes are

phylogenetically more distant from each other than from ZIKV (Figure S3). Moreover, the majority (225/274 = 82%) of genes that were affected by KUNV were also dysregulated in at least one of the other infections, whereas most alterations in host gene expression levels upon infection with ZIKV (343/463 = 74%) and YFV (264/520 = 51%) were unique to those infections.

To confirm a higher correlation between changes to host gene expression levels induced by KUNV and YFV than by KUNV/ZIKV and YFV/ZIKV, Spearman correlation coefficients based on fold-change values of all genes detected in all experimental conditions (all three infections as well as mock-infected cells) were calculated (Figure 4C). The Spearman correlation coefficient for gene expression levels in KUNV/YFV-infected cells was 0.592 ($p < 0.0001$) compared to 0.467 ($p < 0.0001$) and 0.337 ($p < 0.0001$) for gene expression levels in KUNV/ZIKV- and YFV/ZIKV-infected cells, respectively. Scatter plots of fold-change values for all genes detected in all biological replicates in each experimental condition are shown in Figure S4. This suggests a higher similarity in the polyA-mRNA profile of cells infected with KUNV and YFV compared to cells infected with ZIKV.

Gene ontology enrichment analysis was performed on the genes for which expression levels were affected in each of the three Flavivirus infections, and the nine GO terms that were significantly enriched in at least two infections are shown in Figure 4D. Only the GO term ‘immune response’ was enriched in all three Flavivirus infections, whereas seven GO terms were enriched in both KUNV and YFV infections, and one GO term was enriched in ZIKV and YFV infections. This again indicates a higher similarity in the effects on the host cell by KUNV and YFV compared to ZIKV. Moreover, we compared the genes involved in the immune response that were affected in each infection (16 for KUNV, 25 for ZIKV and 35 for YFV), and found that only four genes were dysregulated in all three infections (Figure S5).

Interestingly, we found 17 genes associated with the GO term ‘nervous system development’ (DCLK1, FGF2, INHBA, CXCL1, DOK5, TPP1, ENC1, BDNF, CRIM1, MYLIP, JAG1, NRG1, NDP, PCDH18, FOS, DLX5, ATOH8) to be differentially expressed

upon infection with ZIKV, although this GO term was not significantly enriched (Bonferroni-corrected $p = 0.36$). Only 4 of these 17 genes were found to be differentially expressed upon infection with YFV, and none of them were associated with altered gene expression levels in KUNV-infected cells (Table S10). This correlates with the fact that ZIKV is the only Flavivirus known to affect brain development and cause microcephaly [27], and it would be interesting to study the role of these genes and their expression levels in this regard.

Modulations Regarding Alternative Splicing Events (ASEs) during Viral Infection

One pre-mRNA can contain many splice sites that may be differentially regulated during viral infection [28]. We therefore investigated the number of significantly altered ASEs per gene in virus-infected cells compared to mock-infected cells. In more than 80% of the genes in which AS was modulated upon infection, only one ASE was altered, and very few genes were subject to the dysregulation of more than three ASEs (Figure 5A). We also analyzed the nature of the ASEs which were modulated upon infection and found an underrepresentation of skipped exons and an overrepresentation of retained introns among the ASEs dysregulated in viral infections compared to all ASEs analyzed (Figure 5B).

When comparing the ASEs dysregulated in each infection, there are significant overlaps between ASEs changed in the three Flavivirus infections, with Exact Fisher's Test p values of 1.65×10^{-87}, 9.25×10^{-92} and 3.64×10^{-166} for KUNV/ZIKV, ZIKV/YFV, and KUNV/YFV, respectively (Figure 5C). Nevertheless, more than half of the ASEs that were significantly modulated by each virus (353/603 = 59% for KUNV, 515/720 = 72% for ZIKV, 656/930 = 71% for YFV) were found to be unique to that particular infection. Spearman correlation coefficients based on ΔPSI values of all ASEs detected in all experimental conditions (all infections as well as mock-infected cells) were calculated and are shown in Figure 5D. Interestingly, correlation coefficients obtained when comparing Flavivirus infections with each other and Flavivirus infections with the SINV infection are very similar. Taken together, these results suggest that there are many more dysregulated ASEs common to infections than one would expect randomly, indicating that viruses have rather similar effects on alternative splicing. However, infections with closely related viruses do not share

significantly more altered ASEs than infections with viruses that have a greater phylogenetic distance.

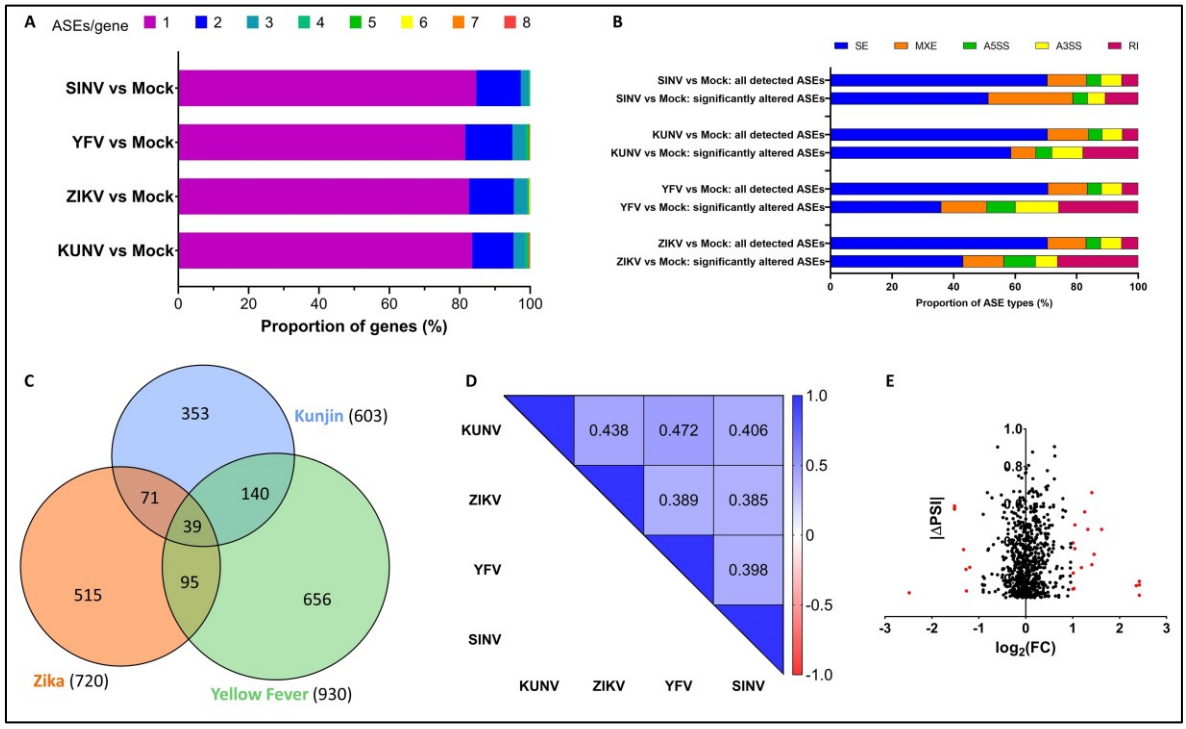

Figure 5. ASEs modulated during viral infection. (A) For all genes that had at least one ASE significantly altered upon viral infection, the number of ASEs per gene is shown. (B) The proportions of the different types of ASEs (SE: skipped exon, MXE: mutually exclusive exons, A5SS: alternative 5' splice site, A3SS: alternative 3' splice site, RI: retained intron) among all events analyzed as well as events that were significantly changed upon viral infections are shown. (C) The area-proportional Venn diagram shows overlaps in the sets of ASEs that were significantly altered during viral infections. (D) ASEs that were detected in all experimental conditions and all replicates were used to calculate Spearman correlation coefficients. (E) The fold-change values for all genes that had at least one ASE significantly altered upon ZIKV infection are shown. Each dot represents one significantly modulated ASE, and red dots represent events on genes that are also overexpressed or repressed.

Gene ontology enrichment analysis was performed with the genes that were subject to modulations in alternative splicing. However, no biological process was significantly enriched. Nonetheless, we found several significantly modulated ASEs that might be interesting to characterize further in future studies. For example, regarding genes involved in the immune response, an increase in the retention of intron 12 in the STAT2 pre-mRNA as well as an increase in the retention of intron 7 in the IRF7 pre-mRNA were observed in ZIKV and YFV infections (ΔPSI of −0.111/−0.165 and −0.336/−0.598, respectively). In both cases,

the intron retention leads to the occurrence of a premature termination codon in the mRNA (Figure S7).

Finally, we compared the genes in which expression levels were altered, and the genes in which alternative splicing was affected upon viral infection. We found that only very few genes that were subjected to the dysregulation of one or more ASEs were also overexpressed or repressed (Figures 5E and S6). Only one gene, PNLIPRP3, showed dysregulated expression levels (overexpression) as well as dysregulated alternative splicing in all three Flavivirus infections (the same three ASEs in KUNV and ZIKV infection, but only one of the three ASEs in YFV infection). Moreover, the protein–protein interaction network and functional enrichment analysis with STRING revealed, among other things, an enrichment for genes involved in the ER unfolded protein response, among the genes in which expression levels, as well as alternative splicing, were significantly modulated upon infection with KUNV and YFV (FDR of 0.0025 and 0.0100, respectively). However, no biological process was enriched in the case of ZIKV infection (Figure S6).

Changes in the Host Proteome upon Flavivirus Infections

Given the considerable number of changes observed in the coding transcriptome of the host cells, both in terms of gene expression and alternative splicing, we wondered if they affected only the RNA level, or if they were translated into modifications in the host cell proteome. We used SILAC to detect differences in protein abundance among infected and non-infected cells. Briefly, U87 cells were cultured in the presence of light, medium or heavy L-arginine (R0/R6/R10), and L-Lysine (K0/K4/K8) before being treated with cell-conditioned media (R0K0) or infected with either ZIKV (R6K4), YFV (R6K4), or SINV (R10K8). Equal amounts of total protein from light, medium, and heavy lysates were mixed, proteins were digested using trypsin, and peptides were analyzed using mass spectrometry. MaxQuant (Max Planck Institute of Biochemistry, Martinsried, Germany) was used to identify and quantify peptides, and differential protein expression analysis was performed with Proteus. Approximately 3500 proteins were detected for each condition. The protein lists obtained from Proteus were filtered to retain only proteins that were detected in at least two replicates, with an absolute log2 (fold-change) greater than 1, and an adjusted *p* value

below 0.05 (Figure 6A). After applying these filters, several hundred proteins were found to be significantly differentially expressed between virus-infected and mock-infected cells: 711 for ZIKV, 712 for YFV, and 560 for SINV (Tables S11–S13). We found that most proteins were repressed upon viral infection (Figure 6B). Only a few dozen proteins were overexpressed in infected cells, including viral proteins.

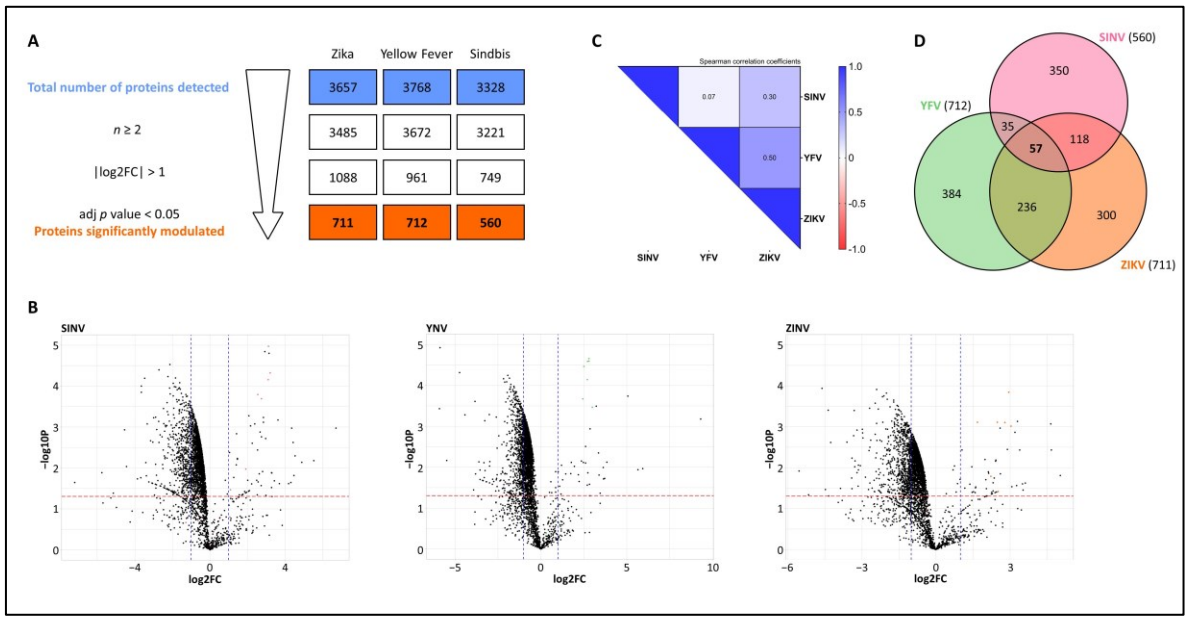

Figure 6. Host cell proteome upon viral infections. (A) Following differential protein expression analysis with Proteus, the protein lists were filtered to retain only proteins that were detected in at least two replicates, with an absolute log2 (fold-change) greater than 1, and an adjusted *p* value below 0.05. (B) Volcano plots show fold changes in protein expression. Black dots represent host proteins, whereas orange/green/pink dots represent viral (ZIKV/YFV/SINV) proteins. (C) Log2FC values of proteins that were detected in at least two infections were used to calculate Spearman correlation coefficients. (D) The area-proportional Venn diagram shows overlaps in the sets of proteins for which expression levels were significantly altered during viral infections.

Fold-change values of all proteins detected in at least two infections were used to calculate Spearman correlation coefficients (Figure 6C). The proteomes of cells infected with ZIKV and YFV were more alike than cells infected with SINV, with correlation coefficients of 0.50 for ZIKV/YFV ($p = 3.86 \times 10^{-169}$), 0.30 for ZIKV/SINV ($p = 5.24 \times 10^{-62}$), and 0.007 for YFV/SINV ($p = 0.0004$). The scatter plots of fold-change values for all proteins detected in at least two infections are shown in Figure S8. Moreover, the lists of proteins significantly differentially expressed in each infection were compared (Figure 6D), and overlaps were

found to be significant (p values of 1.29×10^{-23} for ZIKV/YFV, 1.04×10^{-4} for ZIKV/SINV, and 3.19×10^{-13} for YFV/SINV). A greater overlap between differentially expressed proteins in Flavivirus infections was observed compared to the infection with SINV, and 57 proteins were found to be affected in all three infections. All 57 proteins that were common to the three infections were repressed upon infection, and Reactome overrepresentation analysis revealed an enrichment for pathways involved in the cellular response to stimuli (stress), (infectious) disease, the metabolism of RNA, metabolism of proteins, developmental biology, and extracellular matrix organization (Figure 7).

Figure 7. Functions of the 57 proteins repressed in all three infections. (A) Reactome overrepresentation analysis results. (B) The top 20 enriched pathways and their associated -log10 (FDR) are shown. (C) Western blot analysis confirms the downregulation of HMGA1 (involved in the regulation of gene transcription) and MRPS27 (involved in protein synthesis) in infected cells.

Validation of SILAC Data

We next selected two of the most downregulated proteins in Flavivirus infections (previously identified in the SILAC experiment), HMGA1 and MRPS27, for validation by Western blot. HMGA1 is associated with the cellular response to stimuli as well as disease, whereas MRPS27 plays a role in the metabolism of proteins. As shown in Figure 7C, Western blot analysis shows a downregulation of both proteins in infected cells, which correlates with the changes in protein expression found through mass spectrometry analysis.

Comparison of Proteome and Transcriptome Results

As previously mentioned, the majority of genes in which expression was affected in the viral infections were overexpressed (Figure 4A), whereas most proteins with significant changes in expression upon infection were downregulated (Figure 6B). To further investigate any correlation or disconnect in alterations in gene/protein expression in infected cells, we looked at the top 20 overexpressed and repressed proteins in each infection and their corresponding mRNAs. As shown in Figure 8, the expression levels of these mRNAs are minimally affected. It is noteworthy that for several proteins, no data are available regarding their mRNAs. For a more global comparison of proteome and transcriptome results, we examined all genes/proteins for which data were available in both the RNA-Seq and SILAC experiments. Figure S9 shows scatter plots of fold-changes in protein and RNA expression. Taken together, these results suggest the absence of correlation between mRNA and protein expression levels following viral infections.

We also investigated whether the changes in alternative splicing observed in the RNA-Seq experiment had an impact on protein isoforms. The proteogenomic pipeline Splicify [25] was applied to our RNA-Seq and mass spectrometry data to identify differentially expressed splice variants. Despite many significant changes in alternative splicing observed in the RNA-Seq data described above, no significantly differentially expressed peptides corresponding to these alternative splicing events were found. This further suggests a disconnect between the transcriptome and the proteome of virus-infected cells.

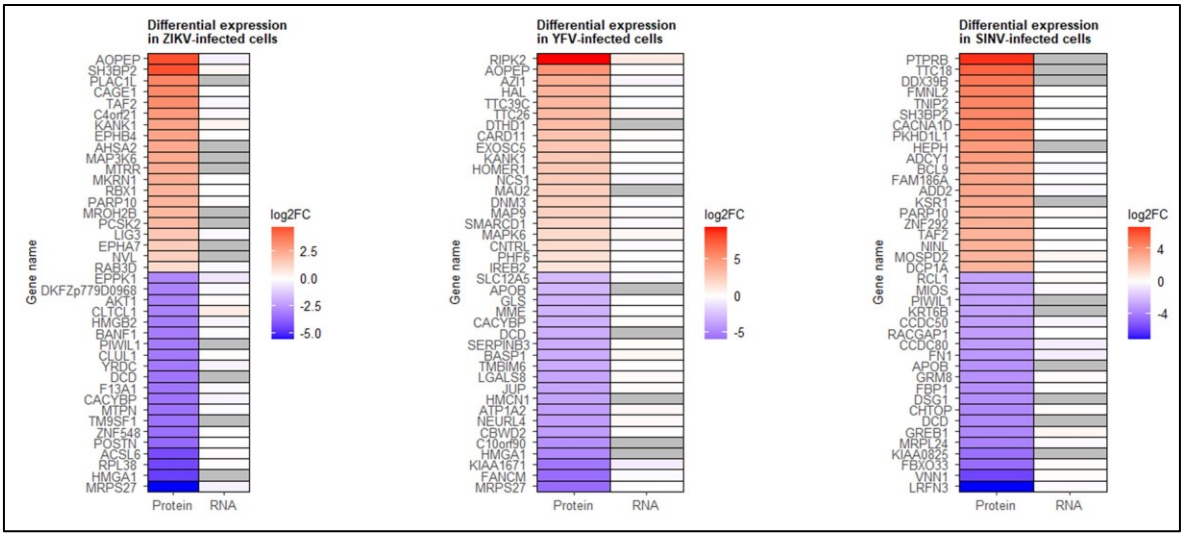

Figure 8. Comparison of proteome and transcriptome results. The top 20 overexpressed and repressed proteins in each infection, along with the fold-change values of their mRNAs, are shown. Red represents positive fold-change values (overexpression in infected cells), blue represents negative fold-change values (repression in infected cells), and gray represents missing data. Only host proteins were included in this analysis, and viral proteins were excluded.

Discussion

In the present study, we report the effects of three Flaviviruses, namely KUNV, ZIKV, and YFV, on gene expression levels and alternative splicing in U87 cells. Previous RNA-Seq studies mostly focused on a single viral species, sometimes comparing different strains of the same species, and most of them examined either gene expression levels or alternative splicing [11–15]. Here, we present our findings regarding the modulations of gene expression levels as well as alternative splicing upon infection with three different Flavivirus species under the same experimental conditions, allowing for comparisons between KUNV, ZIKV, and YFV, and their effects on the coding transcriptome of their host cells. Moreover, we examined the proteome of cells infected with these viruses to determine whether modulations in the coding transcriptome observed via RNA-Seq translated into alterations in the proteome.

Upon infection with KUNV, ZIKV, and YFV, we observed 274, 463, and 520 genes to be differentially expressed compared to non-infected cells. These numbers are lower compared to the number of genes/transcripts that have been identified in other RNA-Seq studies with Flavivirus-infected cells [12,15], possibly due to different experimental

conditions and/or bioinformatic tools used. Moreover, we identified only 33 genes to be differentially expressed upon infection with SINV. Given that SINV replicates faster and is more cytopathic than Flaviviruses [29], it might kill cells faster and not allow for many significant changes in gene expression levels. In the three Flavivirus infections, most of the differentially expressed genes were found to be overexpressed. This could be due to the cell activating the expression of genes that produce proteins with antiviral functions [1]. It could also be an apparent upregulation as a result of increased mRNA stability. In fact, subgenomic flavivirus RNA (sfRNA), which is derived from the 3' UTR of the viral genome, has been shown to sequester and inactivate the exonuclease XRN1, thus increasing the stability of cellular mRNAs [30,31].

Gene ontology enrichment analysis revealed 17 genes associated with the GO term 'nervous system development', the expression of which was dysregulated upon infection with ZIKV. These genes include BDNF and NRG1, which are involved in neuronal survival and growth [32,33] and are both repressed in ZIKV-infected cells. More specifically, NRG1 has been shown to be expressed in the early stages of brain development [33], and it would be interesting to investigate the effect of its repression with respect to ZIKV-induced microcephaly [34]. In addition, since decreased levels of BDNF have been observed in several neurodegenerative diseases [32], and ZIKV is potentially associated with the development and/or progression of neurodegenerative diseases [35], it would be interesting to study the role of BDNF repression in this context. Two other attractive candidates for further studies are the genes DLX5 and ATOH8, which are also repressed in ZIKV-infected cells. DLX5 has been shown to be involved in the development of the olfactory system [36], and ZIKV has recently been associated with olfactory disorders in mice [37] as well as reduced olfactory function in patients with ZIKV-induced Guillain-Barré syndrome [38]. ATOH8 is involved in the developing nervous system as well as the inner ear [39], and ZIKV has been observed to cause hearing loss [40]. Further studies on the roles of the downregulation of these genes may shed more light on ZIKV pathogenesis.

In addition to altered gene expression levels, RNA-Seq revealed modulations in several hundred alternative splicing events upon viral infection: 603 for KUNV, 720 for

ZIKV, 930 for YFV, and 665 for SINV. In contrast to what was observed for gene expression levels, changes in alternative splicing induced by the three Flaviviruses and by SINV are of the same order of magnitude. Moreover, when comparing the effects of the different viruses on host cell alternative splicing, no greater similarity among Flavivirus infections compared to the infection with SINV was observed. This suggests that alterations in cellular alternative splicing are caused by viral infections in general, rather than being Flavivirus-specific.

To shed light on the mechanism behind the alterations in alternative splicing, we further investigated 212 known splicing factors. None of their mRNAs were found to be differentially expressed upon infection (Table S14). Therefore, the observed changes in host cell alternative splicing are most likely not due to an up- or downregulation of splicing factors. Interestingly, we found several alternative splicing events on the mRNAs of splicing factors to be significantly modulated upon viral infection (Table S15). These modulations could lead to the degradation of the mRNA or the translation of different isoforms of these splicing factors, and further studies are needed to examine the functional consequences of these alterations in alternative splicing.

Upon the identification of several hundred modulations in host cell gene expression levels and alternative splicing events via RNA sequencing, we wondered if these changes in the transcriptome could result in changes at the protein level. We analyzed the proteome of virus-infected cells for alterations in protein abundance and isoforms using SILAC. The differential expression of several hundred proteins (711 for ZIKV, 712 for YFV, and 560 for SINV) was observed, and the majority of these proteins were found to be repressed upon infection. This is somewhat surprising, given that the RNA-Seq revealed that most genes that were affected by the viruses were upregulated. However, many viruses are known to induce a translation shutoff of cellular genes to promote the translation of viral proteins [29,41,42], which could explain our observations. Moreover, the analysis of our data with the proteogenomic pipeline Splicify [25] did not identify any significant differential splice variants within the proteome of infected cells. Further studies are needed to better understand the impact of transcriptomic modulations, which occur upon infection, on the functions of the host cell.

The observation that most differentially expressed transcripts were upregulated whereas most differentially expressed proteins were downregulated in infected cells, in addition to the detection of several hundred differentially regulated ASEs in the transcriptome but no matching differential splice variants in the proteome, suggests a disconnect between the transcriptome and the proteome in Flavivirus-infected cells. We therefore analyzed the fold-changes of the differentially expressed proteins and the fold-changes of the corresponding mRNAs and found no significant correlation. One possible reason for the disconnect between mRNA regulation and protein expression could be that the viruses use the mRNAs themselves to control viral or host cell activities, as is the case with sfRNA, rather than dysregulating mRNA levels to affect protein abundance. The lack of correlation between mRNA and protein levels could also be due to post-transcriptional and post-translational regulation. For example, the stability of mRNAs could be increased due to the sequestration of XRN1 by sfRNA, whereas the half-life of the corresponding protein is unaffected [30,31]. Alternatively, proteins may be ubiquitinated and degraded [43] while mRNA levels are unchanged. A third option would be the repression of translation and sequestering of mRNAs in stress granules [44], leading to low protein abundance despite high amounts of mRNAs. Overall, our findings are in agreement with previous studies on DENV- and JEV-infected cells that have reported little or no overlap between differentially expressed transcripts and protein levels [45,46].

In this study, we report a global view of the coding transcriptome and the proteome of virus-infected cells compared to non-infected cells, but little is known about the mechanisms behind the modulations that are observed for mRNA and protein abundance as well as mRNA alternative splicing. These alterations could be brought about directly by the virus, initiated by the host cell as a defense mechanism, or be connected to the antiviral response. On the one hand, the viruses could induce these changes for their benefit, for example, to promote viral replication or to inhibit the immune response. In fact, DENV NS5 has been shown to interact with the spliceosome and modulate the splicing of cellular transcripts [47]. Moreover, DENV NS5 has been reported to trigger the degradation of the splicing factor RBM10, leading to the alternative splicing of the SAT1 pre-mRNA. This prompts the degradation of the transcript and a decrease in the functional SAT1 protein with

antiviral activity [16]. On the other hand, the host cell could induce these changes to fight the infection and limit viral replication. For example, upon the detection of viral components, the host cell produces interferons and induces the expression of many interferon-stimulated genes, which play a role in the antiviral response [1]. Most likely, the observed modulations are a combination of virus-induced and host-cell-induced alterations, and further studies will be needed to elucidate the role of each of them, as well as the mechanisms behind them.

Supplementary Materials: The following supporting information can be downloaded at https://www.mdpi.com/article/10.3390/v15071419/s1. Figure S1. Quantification of viral RNA. Abundance of viral RNAs in total RNA extracts from infected cells was measured using droplet digital PCR (ddPCR). To correct for differences in the amounts of input cDNA, four housekeeping genes (B2M, MRPL19, PUM1, YWHAZ) were quantified, and copies/µL of viral cDNA were divided by copies/µL of housekeeping genes. Figure S2. RNA-Seq data. PolyA-enriched cDNA libraries from infected (Kunjin, Zika, Yellow Fever, Sindbis) and non-infected (control) cells were subjected to 100 bp paired-end sequencing using the Illumina HiSeq4000 system. At least 34 million reads were obtained for each sample. At least 83% of the reads were uniquely mapped to the reference genome. Figure S3. Flavivirus phylogenetic tree. The polyprotein sequences of the three Flaviviruses used in this study were aligned using SeaView5/Clustal Omega, and a phylogenetic tree was constructed based on this alignment using SeaView5/PhyML. Figure S4. Correlations in changes to gene expression levels and alternative splicing upon viral infection. (A) Fold-change values (log2) for all genes detected in every experimental condition are shown. (B) ΔPSI values for all ASEs detected in every experimental condition are shown. Figure S5. Gene ontology enrichment analysis results for the term ‘immune response’. The GO term ‘immune response’ was found to be significantly enriched among the genes in which expression levels were altered following all three Flavivirus infections. Here, the genes involved in the immune response that are affected in each infection are shown. Figure S6. Expression levels of genes with one or more dysregulated ASEs upon infection. (A) The absolute ΔPSI values as well as fold-change values for all genes with at least one dysregulated ASE are shown. Each dot represents one significantly modulated ASE, and red dots represent events on genes that are also significantly overexpressed or repressed. (B) The area-proportional Venn diagram

shows overlaps in the sets of genes for which expression levels as well as alternative splicing were significantly altered upon each viral infection. (C) An analysis of the genes that showed dysregulated expression levels as well as alternative splicing was performed with STRING. One of the most significantly enriched biological processes in KUNV and YFV infections was 'GO:0030968 endoplasmic reticulum unfolded protein response' (FDR = 0.0025 and 0.0100, respectively), and the proteins involved in these processes are highlighted with black circles. No biological process was significantly enriched among the genes dysregulated in the ZIKV infections. Figure S7. Intron retention in genes involved in the immune response. (A) Increased retention of intron 12 in the STAT2 mRNA in infected cells is shown. (B) Increased retention of intron 7 in the IRF7 mRNA is shown. Figure S8. Correlations in changes to protein expression levels upon viral infection. Scatter plots of fold-change values for all proteins detected in at least two infections are shown. Figure S9. Comparison of transcriptome and proteome results. (A) Scatter plots of fold-change values for all proteins and their mRNAs detected in each viral infection are shown. (B) Spearman correlation coefficients of RNA and protein fold-changes in each infection, along with their *p* values, are displayed. Table S1. Changes in gene expression levels upon infection with Kunjin virus. Overall, 274 genes were found to be differentially expressed between KUNV-infected and mock-infected U87 cells. Table S2. Changes in gene expression levels upon infection with Zika virus. In total, 463 genes were found to be differentially expressed between ZIKV-infected and mock-infected U87 cells. Table S3. Changes in gene expression levels upon infection with Yellow Fever virus. In total, 520 genes were found to be differentially expressed between YFV-infected and mock-infected U87 cells. Table S4. Changes in gene expression levels upon infection with Sindbis virus. In total, 33 genes were found to be differentially expressed between SINV-infected and mock-infected U87 cells. Table S5. Changes in alternative splicing upon infection with Kunjin virus. In total, 603 alternative splicing events were found to be significantly different between KUNV-infected and mock-infected U87 cells. Overall, there were (A) 61 alternative 3' splice sites; (B) 32 alternative 5' splice sites; (C) 48 mutually exclusive exons; (D) 108 retained introns; (E) 354 skipped exons. Table S6. Changes in alternative splicing upon infection with Zika virus. In total, 720 alternative splicing events were found to be significantly different between ZIKV-infected and mock-infected U87 cells: (A) 43 alternative 3' splice sites; (B) 62 alternative 5' splice

sites; (C) 80 mutually exclusive exons; (D) 158 retained introns; (E) 377 skipped exons. Table S7. Changes in alternative splicing upon infection with Yellow Fever virus. In total, 930 alternative splicing events were found to be significantly different between YFV-infected and mock-infected U87 cells: (A) 85 alternative 3' splice sites; (B) 56 alternative 5' splice sites; (C) 89 mutually exclusive exons; (D) 156 retained introns; (E) 544 skipped exons. Table S8. Changes in alternative splicing upon infection with Sindbis virus. In total, 665 alternative splicing events were found to be significantly different between SINV-infected and mock-infected U87 cells: (A) 38 alternative 3' splice sites; (B) 32 alternative 5' splice sites; (C) 183 mutually exclusive exons; (D) 71 retained introns; (E) 341 skipped exons. Table S9. Validation of changes in gene expression levels. In total, 21 genes were chosen for qRT-PCR validation of the RNA-Seq results. Table S10. Expression levels of genes associated with the GO term 'nervous system development'. Genes significantly overexpressed are shown in blue, and genes significantly repressed are shown in red. Table S11. Changes in protein expression levels upon infection with Zika virus. In total, 711 proteins were found to be differentially expressed between ZIKV-infected and mock-infected U87 cells. Table S12. Changes in protein expression levels upon infection with Yellow Fever virus. In total, 712 proteins were found to be differentially expressed between YFV-infected and mock-infected U87 cells. Table S13. Changes in protein expression levels upon infection with Sindbis virus. In total, 560 proteins were found to be differentially expressed between SINV-infected and mock-infected U87 cells. Table S14. Gene expression levels of known splicing factors. No known splicing factor was found to be significantly differentially expressed upon infection with KUNV, ZIKV, YFV, or SINV. Table S15. Alternative splicing of known splicing factors. Several alternative splicing events on mRNAs encoding known splicing factors were found to be significantly altered upon infection with KUNV, ZIKV, YFV, or SINV.

Author Contributions: Conceptualization, C.B., B.J.G. and M.B.; methodology, C.B., G.D.-F. and K.M.B.-F.; formal analysis, C.B.; investigation, C.B.; resources, B.J.G. and M.B.; data curation, C.B.; writing—original draft preparation, C.B.; writing—review and editing, C.B., G.D.-F., K.M.B.-F., M.S.S., B.J.G. and M.B.; visualization, C.B.; supervision,

M.S.S., B.J.G. and M.B.; project administration, B.J.G. and M.B.; funding acquisition, B.J.G. and M.B. All authors have read and agreed to the published version of the manuscript.

Funding: This work was supported by National Institutes of Health grant R01 AI132668 to B.J.G. and Natural Sciences and Engineering Research Council of Canada grant RGPIN-2022-04026 to M.B.; C.B. held a Vanier Canada Graduate Scholarship.

Institutional Review Board Statement: Not applicable.

Informed Consent Statement: Not applicable.

Data Availability Statement: RNA-Seq data have been deposited with the Gene Expression Omnibus (GEO) [48] under accession number GSE232504. Mass spectrometry proteomics data have been deposited to the ProteomeXchange Consortium [49] via the proteomics identification database (PRIDE) partner repository [50] with the dataset identifier PXD042208.

Acknowledgments: The authors would like to thank Vincent Boivin for help with bioinformatics analysis at the beginning of the project, the RNomics platform at Université de Sherbrooke (Mathieu Durand, Elvy Lapointe, Philippe Thibault, Danny Bergeron) for sequencing library preparation as well as RT-qPCR and ASPCR validations, and the proteomics platform (Dominique Lévesque, Jennifer Raisch) as well as Marie Brunet at Université de Sherbrooke for help with the MS analysis.

Conflicts of Interest: The authors declare no conflict of interest.

References

1. Gack, M.U.; Diamond, M.S. Innate immune escape by Dengue and West Nile viruses. Curr. Opin. Virol. 2016, 20, 119–128. [CrossRef]

2. García, M.A.; Meurs, E.F.; Esteban, M. The dsRNA protein kinase PKR: Virus and cell control. Biochimie 2007, 89, 799–811. [CrossRef] [PubMed]

3. Lindenbach, B.D.; Thiel, H.-J.; Rice, C.M. Flaviviridae: The Viruses and Their Replication. In Fields Virology; Knipe, D.M., Howley, P.M., Eds.; Lippincott-Raven Publishers: Philadelphia, PA, USA, 2007; pp. 1101–1152.

4. Pierson, T.C.; Diamond, M.S. The continued threat of emerging flaviviruses. Nat. Microbiol. 2020, 5, 796–812. [CrossRef] [PubMed]

5. Daep, C.A.; Muñoz-Jordán, J.L.; Eugenin, E.A. Flaviviruses, an expanding threat in public health: Focus on dengue,West Nile, and Japanese encephalitis virus. J. Neurovirol. 2014, 20, 539–560. [CrossRef] [PubMed]

6. Laureti, M.; Narayanan, D.; Rodriguez-Andres, J.; Fazakerley, J.K.; Kedzierski, L. Flavivirus Receptors: Diversity, Identity, and Cell Entry. Front. Immunol. 2018, 9, 2180. [CrossRef]

7. Heaton, N.S.; Perera, R.; Berger, K.L.; Khadka, S.; LaCount, D.J.; Kuhn, R.J.; Randall, G. Dengue virus nonstructural protein 3 redistributes fatty acid synthase to sites of viral replication and increases cellular fatty acid synthesis. Proc. Natl. Acad. Sci. USA 2010, 107, 17345–17350. [CrossRef]

8. Perera, R.; Riley, C.; Isaac, G.; Hopf-Jannasch, A.S.; Moore, R.J.; Weitz, K.W.; Pasa-Tolic, L.; Metz, T.O.; Adamec, J.; Kuhn, R.J. Dengue Virus Infection Perturbs Lipid Homeostasis in Infected Mosquito Cells. PLoS Pathog. 2012, 8, e1002584. [CrossRef]

9. Emara, M.M.; Brinton, M.A. Interaction of TIA-1/TIAR withWest Nile and dengue virus products in infected cells interferes with stress granule formation and processing body assembly. Proc. Natl. Acad. Sci. USA 2007, 104, 9041–9046. [CrossRef]

10. Lloyd, R.E. How Do Viruses Interact with Stress-Associated RNA Granules? PLoS Pathog. 2012, 8, e1002741. [CrossRef]

11. Qian, F.; Chung, L.; Zheng, W.; Bruno, V.; Alexander, R.P.; Wang, Z.; Wang, X.; Kurscheid, S.; Zhao, H.; Fikrig, E.; et al. Identification of Genes Critical for Resistance to Infection by West Nile Virus Using RNA-Seq Analysis. Viruses 2013, 5, 1664–1681.e [CrossRef]

12. Sessions, O.M.; Tan, Y.; Goh, K.C.; Liu, Y.; Tan, P.; Rozen, S.; Ooi, E.E. Host Cell Transcriptome Profile during Wild-Type and Attenuated Dengue Virus Infection. PLoS Negl. Trop. Dis. 2013, 7, e2107. [CrossRef]

13. Tang, H.; Hammack, C.; Ogden, S.C.; Wen, Z.; Qian, X.; Li, Y.; Yao, B.; Shin, J.; Zhang, F.; Lee, E.M.; et al. Zika Virus Infects Human Cortical Neural Progenitors and Attenuates Their Growth. Cell Stem Cell 2016, 18, 587–590. [CrossRef] [PubMed]

14. Tiwari, S.K.; Dang, J.; Qin, Y.; Lichinchi, G.; Bansal, V.; Rana, T.M. Zika virus infection reprograms global transcription of host cells to allow sustained infection. Emerg. Microbes Infect. 2017, 6, e24. [CrossRef]

15. Bonenfant, G.; Meng, R.; Shotwell, C.; Badu, P.; Payne, A.F.; Ciota, A.T.; Sammons, M.A.; Berglund, J.A.; Pager, C.T. Asian Zika Virus Isolate Significantly Changes the Transcriptional Profile and Alternative RNA Splicing Events in a Neuroblastoma Cell Line. Viruses 2020, 12, 510. [CrossRef] [PubMed]

16. Pozzi, B.; Bragado, L.; Mammi, P.; Torti, M.F.; Gaioli, N.; Gebhard, L.G.; García Solá, M.E.; Vaz-Drago, R.; Iglesias, N.G.; García, C.C.; et al. Dengue virus targets RBM10 deregulating host cell splicing and innate immune response. Nucleic Acids Res. 2020, 48, 6824–6838. [CrossRef]

17. Dobin, A.; Davis, C.A.; Schlesinger, F.; Drenkow, J.; Zaleski, C.; Jha, S.; Batut, P.; Chaisson, M.; Gingeras, T.R. STAR: Ultrafast universal RNA-seq aligner. Bioinformatics 2013, 29, 15–21. [CrossRef] [PubMed]

18. Bolger, A.M.; Lohse,M.; Usadel, B. Trimmomatic: A flexible trimmer for Illumina sequence data. Bioinformatics 2014, 30, 2114–2120. [CrossRef]

19. Love, M.I.; Huber,W.; Anders, S. Moderated estimation of fold change and dispersion for RNA-seq data with DESeq2. Genome Biol. 2014, 15, 550. [CrossRef]

20. Shen, S.; Park, J.W.; Lu, Z.; Lin, L.; Henry, M.D.; Wu, Y.N.; Zhou, Q.; Xing, Y. rMATS: Robust and flexible detection of differential alternative splicing from replicate RNA-Seq data. Proc. Natl. Acad. Sci. USA 2014, 111, E5593–E5601. [CrossRef]

21. Hellemans, J.; Mortier, G.; De Paepe, A.; Speleman, F.; Vandesompele, J. qBase relative quantification framework and software for management and automated analysis of real-time quantitative PCR data. Genome Biol. 2007, 8, R19. [CrossRef] [PubMed]

22. Heberle, H.; Meirelles, G.V.; da Silva, F.R.; Telles, G.P.; Minghim, R. InteractiVenn: A web-based tool for the analysis of sets through Venn diagrams Henry. BMC Bioinform. 2015, 16, 169. [CrossRef] [PubMed]

23. Hulsen, T.; de Vlieg, J.; Alkema,W. BioVenn—A web application for the comparison and visualization of biological lists using area-proportional Venn diagrams. BMC Genom. 2008, 9, 488. [CrossRef]

24. Huang, D.W.; Sherman, B.T.; Lempicki, R.A. Systematic and integrative analysis of large gene lists using DAVID bioinformatics resources. Nat. Protoc. 2009, 4, 44–57. [CrossRef]

25. Komor, M.A.; Pham, T.V.; Hiemstra, A.C.; Piersma, S.R.; Bolijn, A.S.; Schelfhorst, T.; Delis-van Diemen, P.M.; Tijssen, M.; Sebra, R.P.; Ashby, M.; et al. Identification of Differentially Expressed Splice Variants by the Proteogenomic Pipeline Splicify. Mol. Cell. Proteom. 2017, 16, 1850–1863. [CrossRef] [PubMed]

26. Allen, M.; Bjerke, M.; Edlund, H.; Nelander, S.; Westermark, B. Origin of the U87MG glioma cell line: Good news and bad news. Sci. Transl. Med. 2016, 8, 354re3. [CrossRef] [PubMed]

27. Bhagat, R.; Kaur, G.; Seth, P. Molecular mechanisms of zika virus pathogenesis: An update. Indian J. Med. Res. 2021, 154, 433–445. [CrossRef]

28. Lee, Y.; Rio, D.C. Mechanisms and Regulation of Alternative Pre-mRNA Splicing. Annu. Rev. Biochem. 2015, 84, 291–323. [CrossRef]

29. Akhrymuk, I.; Frolov, I.; Frolova, E.I. Sindbis Virus Infection Causes Cell Death by nsP2-Induced Transcriptional Shutoff or by nsP3-Dependent Translational Shutoff. J. Virol. 2018, 92, e01388-18. [CrossRef]

30. Moon, S.L.; Anderson, J.R.; Kumagai, Y.; Wilusz, C.J.; Akira, S.; Khromykh, A.A.; Wilusz, J. A noncoding RNA produced by arthropod-borne flaviviruses inhibits the cellular exoribonuclease XRN1 and alters host mRNA stability. RNA 2012, 18, 2029–2040. [CrossRef]

31. Michalski, D.; Ontiveros, J.G.; Russo, J.; Charley, P.A.; Anderson, J.R.; Heck, A.M.; Geiss, B.J.; Wilusz, J. Zika virus noncoding sfRNAs sequester multiple host-derived RNA-binding proteins and modulate mRNA decay and splicing during infection. J. Biol. Chem. 2019, 294, 16282–16296. [CrossRef]

32. Bathina, S.; Das, U.N. Brain-derived neurotrophic factor and its clinical implications. Arch. Med. Sci. 2015, 11, 1164–1178. [CrossRef] [PubMed]

33. Liu, Y.; Ford, B.D.; Mann, M.A.; Fischbach, G.D. Neuregulin-1 increases the proliferation of neuronal progenitors from embryonic neural stem cells. Dev. Biol. 2005, 283, 437–445. [CrossRef]

34. Rasmussen, S.A.; Jamieson, D.J.; Honein, M.A.; Petersen, L.R. Zika Virus and Birth Defects—Reviewing the Evidence for Causality. N. Engl. J. Med. 2016, 374, 1981–1987. [CrossRef] [PubMed]

35. Quincozes-Santos, A.; Bobermin, L.D.; Costa, N.L.F.; Thomaz, N.K.; Almeida, R.R.d.S.; Beys-da-Silva, W.O.; Santi, L.; Rosa, R.L.; Capra, D.; Coelho-Aguiar, J.M.; et al. The role of glial cells in Zika virus-induced neurodegeneration. Glia 2023, 71, 1791–1803. [CrossRef]

36. Long, J.E.; Garel, S.; Depew, M.J.; Tobet, S.; Rubenstein, J.L.R. DLX5 Regulates Development of Peripheral and Central Components of the Olfactory System. J. Neurosci. 2003, 23, 568–578. [CrossRef]

37. Zhou, J.; Guan, M.-Y.; Li, R.-T.; Qi, Y.-N.; Yang, G.; Deng, Y.-Q.; Li, X.-F.; Li, L.; Yang, X.; Liu, J.-F.; et al. Zika virus leads to olfactory disorders in mice by targeting olfactory ensheathing cells. eBioMedicine 2023, 89, 104457. [CrossRef] [PubMed]

38. Lazarini, F.; Lannuzel, A.; Cabié, A.; Michel, V.; Madec, Y.; Chaumont, H.; Calmont, I.; Favrat, M.; Montagutelli, X.; Roze, E.; et al. Olfactory outcomes in Zika virus- associated Guillain– Barré syndrome. Eur. J. Neurol. 2022, 29, 2823–2831. [CrossRef] [PubMed]

39. Tang, Q.; Xie, M.-Y.; Zhang, Y.-L.; Xue, R.-Y.; Zhu, X.-H.; Yang, H. Targeted deletion of Atoh8 results in severe hearing loss in mice. Genesis 2021, 59, e23442. [CrossRef]

40. Ficenec, S.C.; Schieffelin, J.S.; Emmett, S.D. A Review of Hearing Loss Associated with Zika, Ebola, and Lassa Fever. Am. J. Trop. Med. Hyg. 2019, 101, 484–490. [CrossRef]

41. Bedard, K.M.; Semler, B.L. Regulation of picornavirus gene expression. Microbes 2004, 6, 702–713. [CrossRef]

42. Clemens, M.J. Translational control in virus-infected cells: Models for cellular stress responses. Semin. Cell Dev. Biol. 2005, 16, 13–20. [CrossRef]

43. Luo, H. Interplay between the virus and the ubiquitin-proteasome system: Molecular mechanism of viral pathogenesis. Curr. Opin. Struct. Biol. 2016, 17, 1–10. [CrossRef] [PubMed]

44. Eiermann, N.; Haneke, K.; Sun, Z.; Stoecklin, G.; Ruggieri, A. Dance with the Devil: Stress Granules and Signaling in Antiviral Responses. Viruses 2020, 12, 984. [CrossRef]
45. Pattanakitsakul, S.; Rungrojcharoenkit, K.; Kanlaya, R.; Sinchaikul, S.; Noisakran, S.; Chen, S.-T.; Malasit, P.; Thongboonkerd, V. Proteomic Analysis of Host Responses in HepG2 Cells during Dengue Virus Infection. J. Proteome Res. 2007, 6, 4592–4600. [CrossRef] [PubMed]
46. Zhang, L.-K.; Chai, F.; Li, H.-Y.; Xiao, G.; Guo, L. Identification of Host Proteins Involved in Japanese Encephalitis Virus Infection by Quantitative Proteomics Analysis. J. Proteome Res. 2013, 12, 2666–2678. [CrossRef]
47. De Maio, F.A.; Risso, G.; Iglesias, N.G.; Shah, P.; Pozzi, B.; Gebhard, L.G.; Mammi, P.; Mancini, E.; Yanovsky, M.J.; Andino, R.; et al. The Dengue Virus NS5 Protein Intrudes in the Cellular Spliceosome and Modulates Splicing. PLoS Pathog. 2016, 12, e1005841. [CrossRef]
48. Edgar, R.; Domrachev, M.; Lash, A.E. Gene Expression Omnibus: NCBI gene expression and hybridization array data repository. Nucleic Acids Res. 2002, 30, 207–210. [CrossRef]
49. Deutsch, E.W.; Bandeira, N.; Perez-Riverol, Y.; Sharma, V.; Carver, J.J.; Mendoza, L.; Kundu, D.J.; Wang, S.; Bandla, C.; Kamatchinathan, S.; et al. The ProteomeXchange consortium at 10 years: 2023 update. Nucleic Acids Res. 2023, 51, D1539–D1548. [CrossRef] [PubMed]
50. Perez-Riverol, Y.; Bai, J.; Bandla, C.; García-Seisdedos, D.; Hewapathirana, S.; Kamatchinathan, S.; Kundu, D.J.; Prakash, A.; Frericks-Zipper, A.; Eisenacher, M.; et al. The PRIDE database resources in 2022: A hub for mass spectrometry-based proteomics evidences. Nucleic Acids Res. 2022, 50, D543–D552. [CrossRef] [PubMed]

3 ARTICLE 2: DECIPHERING THE INTERACTION SURFACE BETWEEN THE WEST NILE VIRUS NS3 AND NS5 PROTEINS

Authors: Carolin Brand, Brian J. Geiss, Martin Bisaillon

Status: Submitted to Journal of General Virology on July 4, 2023 (manuscript number: JGV-D-23-00157)

Preface: I performed all the wet lab experiments, and I analyzed the results. I created the figures, and I wrote the article under the supervision and with the participation of Brian Geiss and Martin Bisaillon.

Summary: West Nile virus (WNV) is the most widespread Flavivirus, and it can lead to severe illness, including encephalitis. Currently, no antiviral drugs are available to treat or prevent WNV infections. Given that protein-protein interactions have emerged as interesting targets for the development of therapeutic compounds, the interaction between the core components of the WNV replicase complex, namely NS3 and NS5, was characterized. Potential interacting residues were identified, and seven residues on the surface of the NS3 protein were found to be critical for viral replication. They were found to be clustered in two 'hotspots' which could be new targets for future anti-flaviviral drug development.

Deciphering the interaction surface between the West Nile virus NS3 and NS5 proteins

Author names

Carolin Brand (ORCID ID: 0009-0009-4048-746X)[1], Brian J Geiss (ORCID ID: 0000-0001-8180-5772)[2,3], Martin Bisaillon (ORCID ID: 0000-0001-7822-0933)[1]

Affiliation(s)

[1] Département de Biochimie et de Génomique Fonctionnelle, Université de Sherbrooke, Sherbrooke, QC, Canada

[2] Department of Microbiology, Immunology, and Pathology, Colorado State University, Fort Collins, CO, USA

[3] School of Biomedical Engineering, Colorado State University, Fort Collins, CO, USA

Corresponding author and email address

Martin Bisaillon, martin.bisaillon@usherbrooke.ca

Keywords

West Nile virus, NS3, NS5, protein-protein interaction

Repositories

Not applicable.

Abstract

West Nile virus (WNV) is the most prevalent mosquito-borne disease and the leading cause of viral encephalitis in the continental United States. It belongs to the Flavivirus family which includes other important human pathogens such as dengue virus (DENV), Japanese encephalitis virus (JEV), and Zika viruses (ZIKV). Despite several decades of research, no specific antiviral drugs are available to treat Flavivirus infections. The present study

characterizes the interaction between the WNV NS3 and NS5 proteins for the purpose of identifying hotspots in the protein-protein interaction which could be targeted for the development of antiviral therapeutics. We previously developed an interaction model *in silico* based on data available in the literature. Here, potential interacting residues on NS3 and NS5 were mutated in a WNV replicon, and seven mutations in the NS3 protein were found to drastically reduce viral replication. In addition to being well conserved among mosquito-borne Flaviviruses, these residues are located on the protein's surface in two clusters which might be interesting new targets for future drug development.

Impact statement

West Nile virus (WNV) is present on all continents except Antarctica, making it the most widespread Flavivirus [1,2]. Although approximately 80% of infections are asymptomatic, and most symptomatic cases are associated with a flu-like illness, WNV can lead to severe illness including neurological symptoms in less than 1% of infections. Currently, no specific antiviral drug is available, and treatment consists of supportive care to relieve symptoms [3]. Protein-protein interactions have emerged as an interesting target for the development of therapeutic compounds [4,5]. We previously developed a model for the interaction between WNV NS3 and NS5 proteins [6]. Here, we identified residues in a potential interaction interface, and we evaluated the importance of these residues for viral replication. We identify two 'hotspots' on the surface of the WNV NS3 protein that are crucial for efficient viral replication, possibly by mediating the interaction between NS3 and NS5, which could be new targets for the development of anti-flaviviral drugs.

Data summary

The authors confirm all supporting data, code and protocols have been provided within the article or through supplementary data files.

Introduction

West Nile virus (WNV) is a member of the genus Flavivirus (family Flaviviridae) and has a positive-sense, single-stranded RNA genome of approximately 11kb. The genome is

capped at the 5’ end but not polyadenylated at the 3’ end, and it contains a single open reading frame. It is translated into a viral polyprotein which is subsequently processed into ten proteins, namely the structural proteins C, prM, and E, as well as the non-structural proteins NS1, NS2A, NS2B, NS3, NS4A, NS4B, and NS5 [7,8]. Among the viral proteins, only two exhibit enzymatic functions. NS3 possesses a protease domain and a helicase domain. Its protease activity is involved in polyprotein processing [9]. The helicase domain unwinds the double-stranded RNA replication intermediate [10]. This domain also harbors nucleoside triphosphatase (NTPase) [11] and RNA triphosphatase (RTPase) [12] activities, which are responsible for ATP hydrolysis to drive helicase activity and removal of the γ-phosphate from the newly synthesized viral RNA to form a diphosphorylated RNA during the synthesis of the 5’ cap structure, respectively. The NS5 protein also possesses two domains, namely a capping enzyme domain and an RNA-dependent RNA polymerase (RdRp) domain. The capping enzyme domain exhibits guanylyltransferase (GTase) activity which transfers a GMP to the 5’ end of nascent viral RNA [13], and methyltransferase (MTase) activity which methylates the N7 position of the guanine as well as the 2’-O position of the first nucleotide’s ribose to complete the 5’ cap structure [14]. The RdRp domain replicates the viral RNA genome [15]. The two viral enzymes NS3 and NS5 have been shown to interact directly [16–18], and they have been proposed to constitute the main components of the viral replicase complex [19].

Previous efforts to develop antiviral drugs against Flaviviruses have mainly focused on inhibiting NS3 or NS5, since they have been well characterized and their enzymatic activities are essential for viral replication. Most potential antiviral compounds that have been identified inhibit enzymatic activity either directly by binding the catalytic site, or they induce a conformational change in the protein by binding an allosteric site [3]. Only three of these compounds, all nucleoside analog inhibitors of the NS5 RdRp, have reached the clinical stage of drug development [20–22].

An alternative strategy for drug development is the targeting of essential protein-protein interactions. This approach has been studied in various contexts, and protein-protein interactions appear to be promising targets for the development of therapeutics against

multiple diseases [4,5]. Regarding the development of specific anti-flaviviral therapeutics, several protein-protein interactions have been proposed and studied as potential drug targets, namely the interaction of NS3 with its essential cofactors NS2B [23,24] and NS4B [25,26], as well as the NS3:NS5 interaction. Mutations that abolish the NS3:NS5 interaction have been shown to inhibit DENV replication [17,18]. Within the last year, two independent groups have reported small molecules that disrupt the NS3:NS5 interaction via binding to NS5, leading to strong antiviral activity against DENV, ZIKV and WNV [27,28].

We have previously developed and presented an interaction model for WNV NS3 and NS5 during positive strand RNA synthesis [6]. In this model, NS3 and NS5 interact via their helicase and RdRp domain, respectively, and their RNA-binding tunnels are aligned. The dsRNA replication intermediate passes through the helical gate of the NS3 helicase domain, resulting in its separation into two individual strands. The 5' end of the positive strand gets capped by the NS5 capping enzyme domain. The 3' end of the negative strand is guided through the RNA-binding tunnel of the NS3 helicase domain and is fed into the NS5 RdRp domain, where it serves as template for the synthesis of a new positive strand of viral RNA [6].

Here, we identified residues in a potential interaction interface between WNV NS3 and NS5 based on the previously described model [6]. Site-directed mutagenesis of a WNV replicon [29] was used to determine the importance of these identified residues for viral replication. Seven residues on the NS3 protein were found to be essential for viral replication and to be clustered in two 'hotspots' on the protein surface, suggesting a potential protein interaction surface on NS3.

Materials and methods

Interaction model

A model of the WNV NS3:NS5 interaction during positive strand RNA synthesis was developed and described previously [6].

WNV replicon and site-directed mutagenesis

A WNV replicon (strain WN 956 D117 3B) [29] was used to study viral replication levels of mutants based on the NS3:NS5 interaction model. A replication-defective WNV replicon, containing a NS5 D668V mutation [30], was used as a negative control. Amino acids that were identified as possibly mediating the NS3:NS5 interaction were substituted with alanine residues in the WNV replicon using QuikChange mutagenesis (Agilent) as previously described [31].

Luciferase assay

BHK17 cells were grown at 37°C and 5% CO2 in DMEM (Wisent, 319-015-CL) supplemented with 10% FBS (Wisent, 080-150) and 1mM sodium pyruvate (Wisent, 600-110-EL). 24h prior to transfection, cells were seeded into 12-well plates at a concentration of 50,000 cells per well. They were then transfected with 250 ng of the replicon expression plasmid using 0.5µl Lipofectamine 2000 transfection reagent (Invitrogen, 11668019) in opti-MEM (Gibco, 31958070). The luciferase activity was determined 48h post-transfection by mixing 10µl of cell lysate (total amount of lysate for each well: 200µl) with 50µl of luciferase assay substrate (Promega, E4550) and measuring emitted light with a GloMax 20/20 Luminometer (Promega). Data was collected from at least three independent experiments, each containing technical triplicates. Luciferase activity from the wild-type replicon was fixed at 100%, and luciferase activity from each mutant was expressed relative to the wild-type. A one-sample t-test with a hypothetical value of 100 was performed for each mutant. Mutants with a p-value below 0.05, 0.005, 0.001 and 0.0001 were labelled with 1 star, 2 stars, 3 stars and 4 stars, respectively.

Conservation of amino acids among Flaviviruses

NS3 and NS5 protein sequences of the WNV replicon were aligned with the corresponding sequences of closely related Flaviviruses, namely JEV (AY303791.1), ZIKV (KU321639.1), DENV1 (KJ189367.1), DENV2 (AY037116.1), DENV3 (AY662691), DENV4 (KF955510.1), and YFV (AF094612.1), using PRALINE multiple sequence alignment with default parameters (available at

https://www.ibi.vu.nl/programs/pralinewww/). Conservation scoring was also performed by PRALINE, with 0 being the least conserved alignment position and 10 being the most conserved alignment position.

Co-immunoprecipitation and western blot

HEK293T cells were grown at 37°C and 5% CO2 in DMEM (Wisent, 319-015-CL) supplemented with 10% FBS (Wisent, 080-150). 24h prior to transfection, cells were seeded into 6cm dishes at a concentration of 1,000,000 cells per dish. 2.5µg of pcDNA3.1+ NS3 and 2.5µg of pcDNA3.1+ NS5 were mixed with 30µl PEI (Sigma-Aldrich, 408727) in opti-MEM (Gibco, 31958070), incubated for 15min at room temperature, and added to the cells. 48h post transfection, cells were harvested using trypsin, pelleted, and stored at -80°C.

Cells were lysed by adding 300µl lysis buffer (50mM Tris-HCl pH 7.5, 150mM NaCl, 0.1% NP-40) with cOmplete protease inhibitor (Roche, 11873580001, 1 tablet per 50ml) for 10min at room temperature, followed by 2 x 5sec sonication at 15% amplitude (Branson Digital Sonifier). Total protein concentration of the cell lysate was determined using a Bradford assay (Thermo Scientific, 23200). For samples treated with RNase A, 300µg of total proteins were incubated with 5µg RNase A (Biotech, RB0473) for 10min at room temperature. Prior to co-IP, 20µl of anti-DYKDDDDK(Flag) Affinity Gel (Bimake, B23101) were conditioned with 1ml lysis buffer with protease inhibitor and centrifuged at 2500rpm for 5min at 4°C. Once the supernatant was removed, cell lysate (300µg of total proteins) and 1ml lysis buffer with protease inhibitor were added to the beads and incubated for 4h at 4°C on a rotating mixer. Samples were then centrifuged at 2500rpm for 5min at 4°C, washed with 1ml lysis buffer without protease inhibitor, and centrifuged at 2500rpm for 5min at 4°C. The wash step was repeated four times. Finally, bound proteins were eluted using 40µl loading buffer (200mM Tris-HCl pH 6.8, 40% glycerol, 4% SDS, 1.47M β-mercaptoethanol, bromophenol blue).

20µl of eluate were separated using one-dimensional SDS-PAGE at 180V for approximately 1h before being transferred to a PVDF blotting membrane (GE, 10600023) at 100V for 1h15min. After blocking in 5% non-fat milk in PBS for 1h at room temperature,

the membranes were incubated with a 1:5000 dilution of primary antibody (NS3-myc: Myc Tag Polyclonal Antibody, Invitrogen, PA1-981; NS5-Flag: Monoclonal Anti-Flag M2 Antibody, Sigma, F1804) in 2.5% non-fat milk/PBS for 4h at room temperature, washed three times in TBS-T for 5min, incubated with a 1:10,000 dilution of anti-mouse/rabbit HRP secondary antibody (NS3-myc: Goat Anti-Rabbit IgG H&L (HRP), Abcam, ab205718; NS5-Flag: Anti-mouse IgG HRP-linked Antibody, NEB, 7076) for 1h at room temperature, washed twice in TBS-T and once in PBS for 5min. Finally, ECL substrate (Biorad, 1705061) was used to visualize the target proteins.

Results

Site-directed mutagenesis of residues predicted to mediate the NS3:NS5 interaction

In this study, we identified residues which might be involved in the WNV NS3:NS5 interaction based on our previously developed interaction model [6]. In this model, NS3 and NS5 interact via their helicase and RdRp domains, respectively (Figure 1). Residues on the surface of each protein, pointing towards the inter-protein space, were hypothesized to mediate the potential NS3:NS5 interaction. To evaluate the importance of these residues, site-directed mutagenesis was performed in a WNV replicon, and replication levels of mutants was compared to the wild-type (Figure 2). Some mutations had little or no effect, and some even increased viral replication. Interestingly, several alanine substitutions were found to reduce viral replication below 5% of the wild-type (WT) replicon, namely NS3 K186A, NS3 R216A, NS3 R218A, NS3 G254A, NS3 E523A, NS3 R525A, NS3 R257A, NS5 N48A, and NS5 G317A, suggesting that residues at these positions are critical for efficient viral replication. Next, we investigated whether these residues are conserved among related Flaviviruses (Figure 3). Only two of these nine residues have a conservation score below 9 (PRALINE conservation score, 0 being least conserved and 10 being most conserved) when comparing WNV, Zika virus (ZIKV), Japanese encephalitis virus (JEV), Yellow Fever virus (YFV), and all four serotypes of Dengue virus (DENV), which further suggests an important role for these residues.

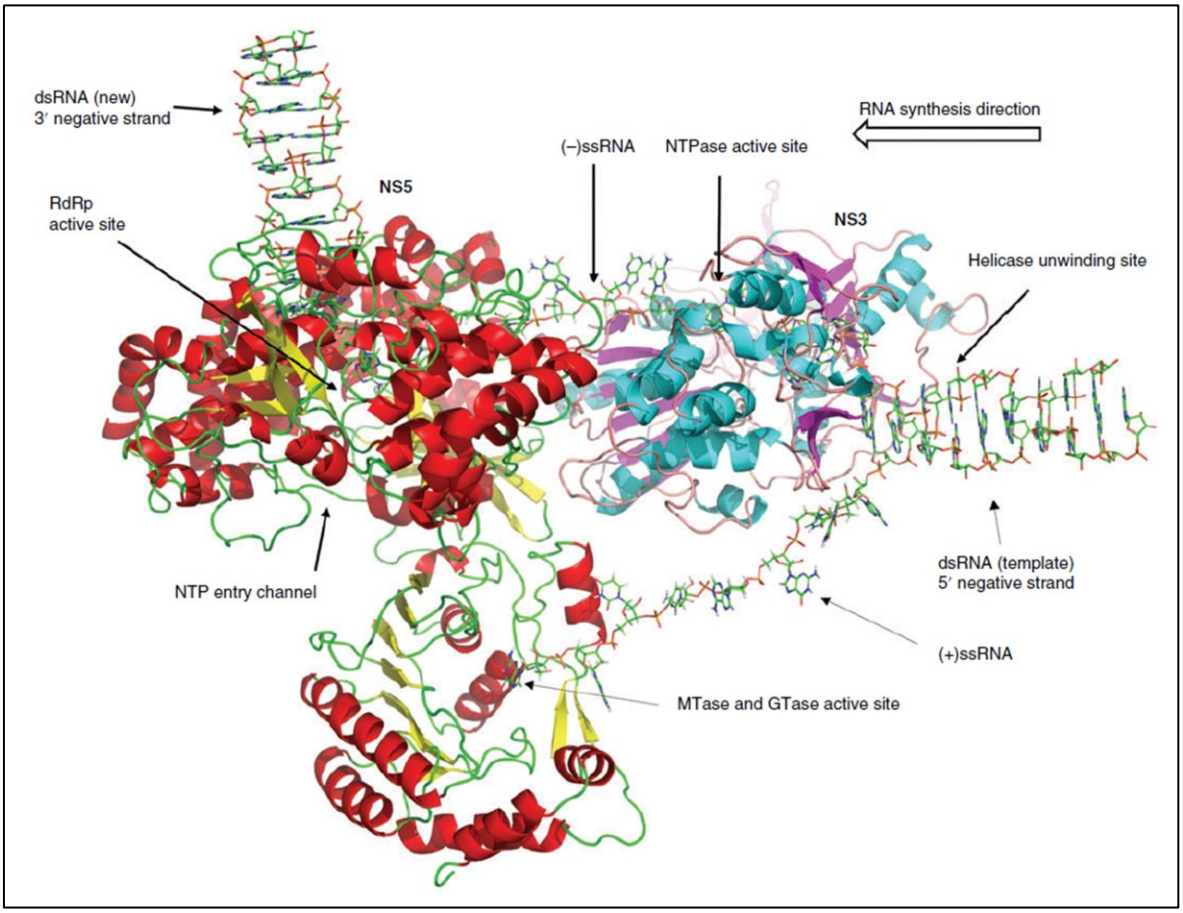

Figure 1. WNV NS3:NS5 interaction model. In the interaction model [6], the incoming dsRNA is unwound by the NS3 helicase. The 5' end of the positive strand gets capped by the NS5 capping enzyme domain. The 3' end of the negative strand is guided through the RNA-binding tunnel of the NS3 helicase domain and is fed into the NS5 RdRp domain, where it serves as template for the synthesis of a new positive strand of viral RNA.

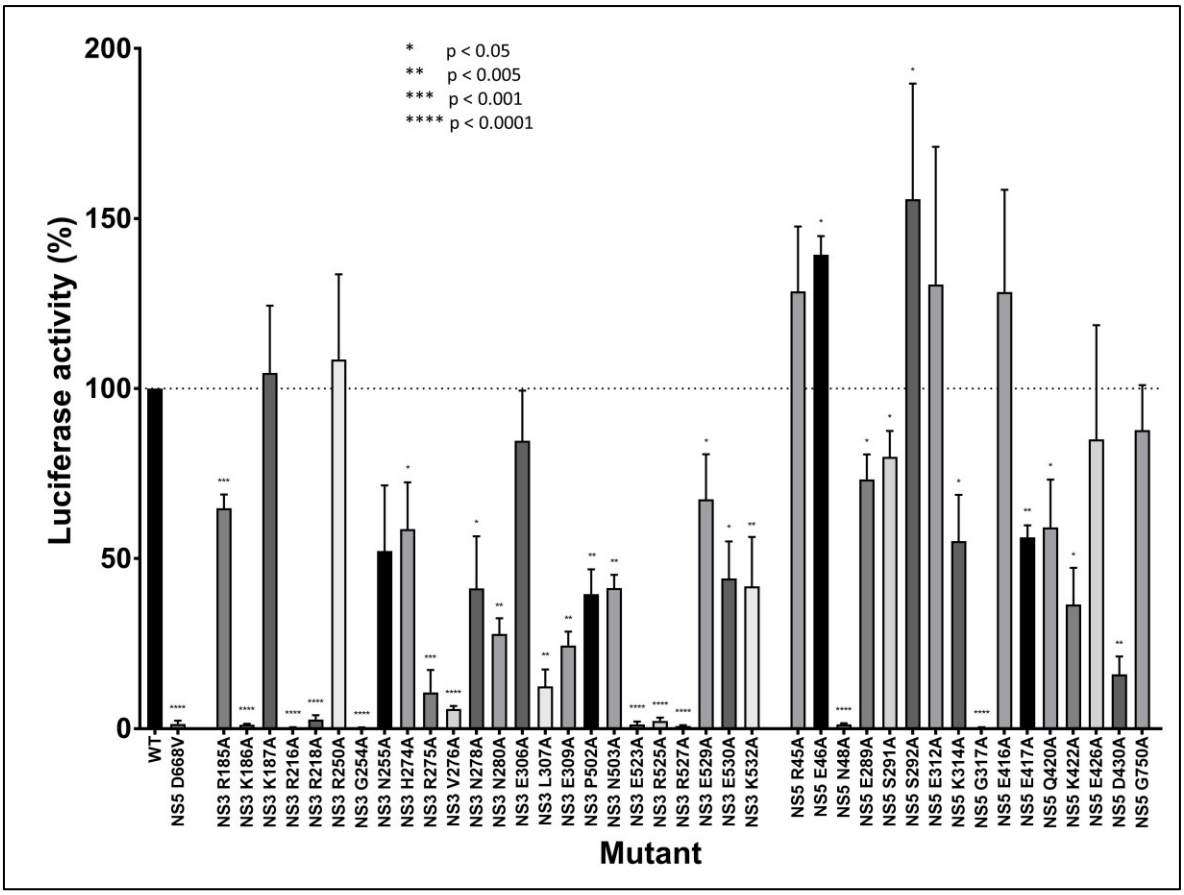

Figure 2. Viral replication levels after alanine substitutions in a WNV replicon. Amino acids in a potential interaction interface between WNV NS3 and NS5 according to the interaction model were replaced by alanine residues in a WNV replicon encoding a luciferase gene. Levels of viral replication were evaluated by measuring luciferase activity in at least three independent experiments, each containing technical triplicates. Luciferase activity from the wild-type replicon was fixed at 100%, and luciferase activity from each mutant was expressed relative to the wild-type. A one-sample t-test with a hypothetical value of 100 was performed for each mutant. Mutants with a p-value below 0.05, 0.005, 0.001 and 0.0001 were labelled with 1 star, 2 stars, 3 stars and 4 stars, respectively. The following mutations reduced viral replication below 5% of the WT replicon: NS3 K186A, NS3 R216A, NS3 R218A, NS3 G254A, NS3 E523A, NS3 R525A, NS3 R257A, NS5 N48A, and NS5 G317A.

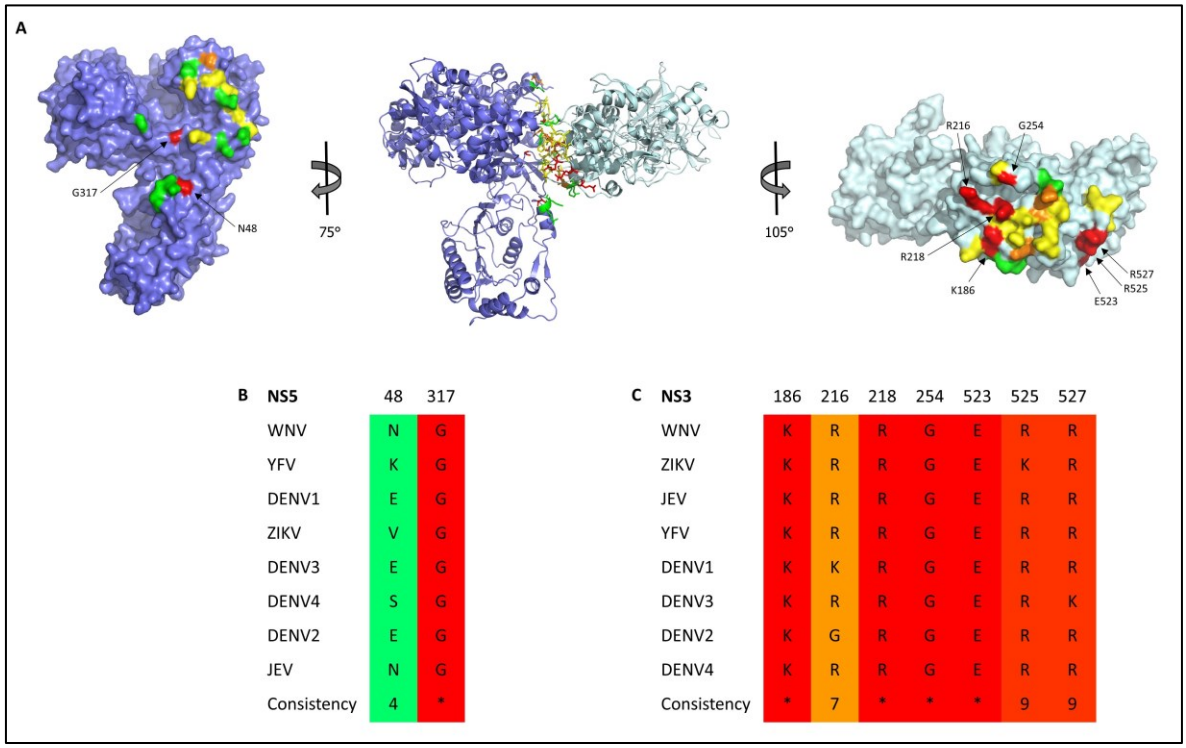

Figure 3. Amino acids whose substitution with alanine reduce replication levels below 5% of the wild-type replicon. (A) The position of amino acids at the potential NS3:NS5 interaction surface chosen for site-directed mutagenesis are shown on the NS3:NS5 interaction model as well as on the individual proteins (left and right). Residues are colored according to the effect of alanine substitution on viral replication (>80% of WT is green, 20-80% of WT is yellow, 5-20% of WT is orange, and <5% of WT is red). (B and C) Conservation of the highlighted amino acids among mosquito-borne Flaviviruses was analyzed by PRALINE.

Co-immunoprecipitation of mutant NS3 with wild-type NS5

Finally, we examined whether the observed loss of viral replication is due to a loss of interaction between NS3 and NS5 by co-immunoprecipitation of mutant NS3 proteins with wild-type NS5 (Figure 4). Co-immunoprecipitation was observed for all mutants, with and without RNase treatment. RNase treatment was used to rule out indirect interaction via RNA, since both proteins are known to bind RNA. No drastic loss of interaction between the two proteins was observed, although the mutations R186A and E523A on NS3 had a modest negative effect on the interaction with NS5. At first sight, these results may suggest that the observed reduction in viral replication is not caused by an impaired NS3:NS5 interaction. However, it is very likely that multiple pairs of interactions are present between NS3 and NS5, and breaking one pair would be expected to reduce interaction affinity but not

completely ablate the interaction. Alternatively, these results might suggest that the formation of the NS3:NS5 complex is mediated by different pairs of interacting residues during different stages of viral replication. The previously described mutations may prevent NS3 and NS5 from interacting in a specific way at one step of viral replication, resulting in loss of viral replication, but other ways of interacting during other phases of viral replication may be unaffected, leading to sustained interaction and co-immunoprecipitation in vitro.

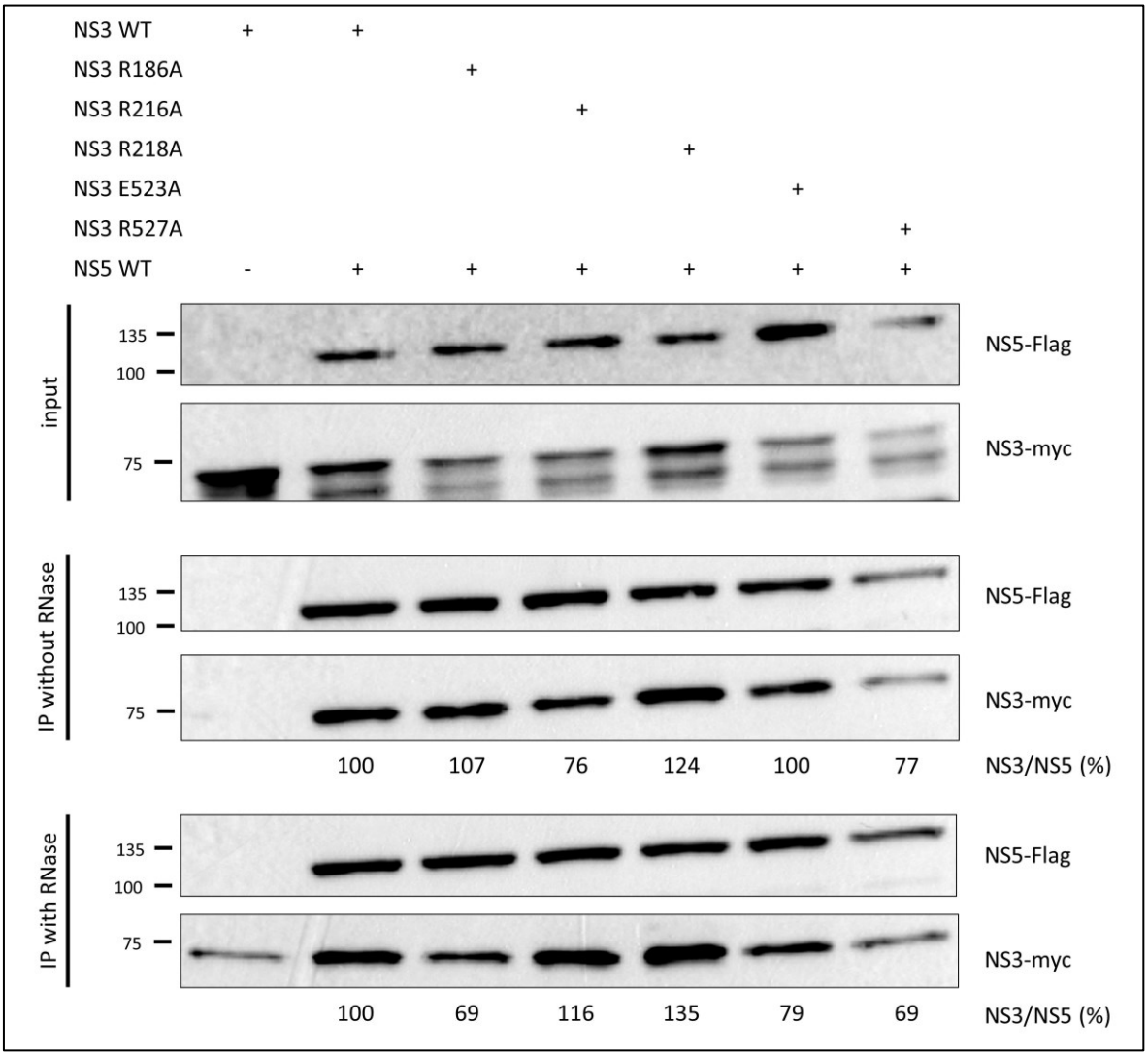

Figure 4. Co-immunoprecipitation of NS3 mutants with wild-type NS5. Cells were co-transfected with WT Flag-tagged NS5 and either WT or mutant myc-tagged NS3. NS5 was immunoprecipitated, and co-precipitated NS3 was revealed by western blotting.

Discussion

In the present study, we built on our previously published interaction model of WNV NS3 and NS5 during positive strand RNA synthesis [6] by identifying residues in a potential interaction interface. These residues were then substituted with alanine in a WNV replicon, and the effect of these mutations on viral replication were evaluated. Nine substitutions were found to reduce viral replication below 5% of the wild-type replicon, suggesting that these residues are essential for efficient viral replication. Moreover, when aligning protein sequences from several pathogenic mosquito-borne Flaviviruses, we discovered that seven of these nine residues are highly conserved among WNV, ZIKV, JEV, YFV and DENV, which further highlights their importance. Five of these alanine substitutions on NS3 were investigated for their ability to directly interact with wild-type NS5, and only two of them showed a limited loss of interaction. This suggests that single point mutations may not be sufficient to disrupt the NS3:NS5 interaction. Alternatively, they may not be involved in the NS3:NS5 interaction, but rather have some other function (e.g. structure, allostery).

Previous studies on DENV NS3 and NS5 have identified one residue of each protein, namely NS3 N570 [18] and NS5 K330 [17], to be involved in the NS3:NS5 interaction. The corresponding residues were mutated in our WNV replicon, and viral replication of the mutants was evaluated (Figure S1A). Reduction of viral replication below 5% of the wild-type replicon was observed for the NS5 K332A mutant (WNV numbering). However, the NS3 N571A (WNV numbering) substitution had no significant effect on viral replication. This may suggest that, despite both residues being well conserved among mosquito-borne Flaviviruses (Figure S1B), only the role of NS5 K332, but not that of NS3 N571, in the NS3:NS5 interaction is conserved among Flaviviruses.

Here, we identify two ‘hotspots’ on the surface of the WNV NS3 protein that are crucial for efficient viral replication, possibly by mediating the interaction between NS3 and NS5, which could be alternative targets for the development of anti-flaviviral drugs. To better identify NS3:NS5 interactions and confirm that the two ‘hotspots’ on NS3 identified here mediate the interaction with NS5, cross-link mass spectrometry could be used. Alternatively, cryoEM could be used to better understand how the NS3:NS5 complex is assembled.

Figures and tables

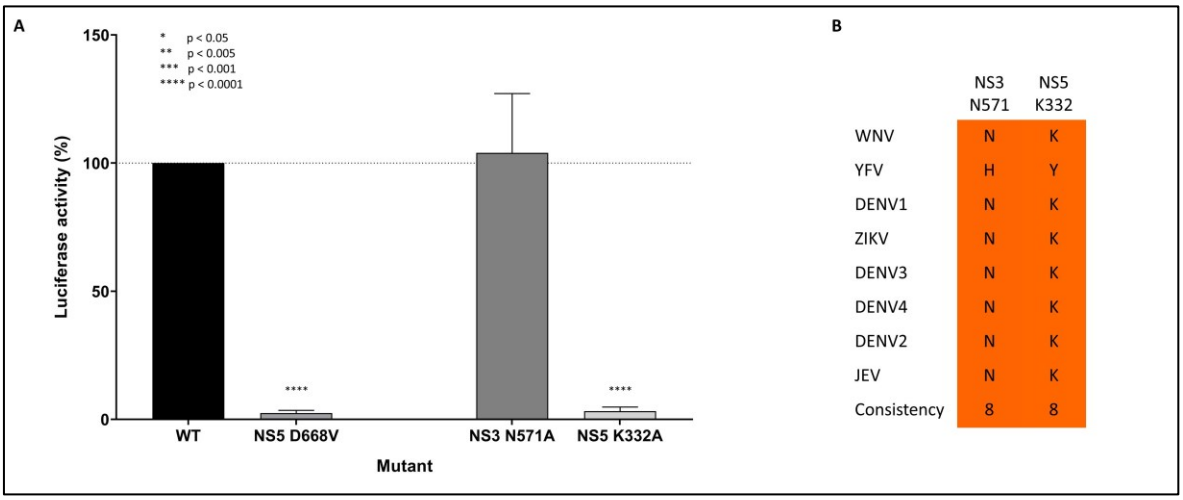

Figure S1. Viral replication levels after alanine substitutions of residues previously shown to be involved in the DENV NS3-NS5 interaction. DENV NS3 N570 and DENV NS5 K330 have been demonstrated to be critical for the DENV NS3-NS5 interaction [17,18]. (A) The corresponding residues in the WNV replicon were substituted by alanine, and levels of viral replication were evaluated by measuring luciferase activity in four independent experiments, each containing technical triplicates. (B) Conservation of amino acids (WNV numbering) among mosquito-borne Flaviviruses was analyzed by PRALINE.

Author statements

Author contributions

Conceptualization: C.B., B.J.G., M.B.

Data Curation: C.B.

Formal Analysis: C.B.

Funding Acquisition: B.J.G., M.B.

Investigation: C.B.

Methodology: C.B.

Project Administration: B.J.G., M.B.

Resources: B.J.G., M.B.

Software: Not applicable.

Supervision: B.J.G., M.B.

Validation: C.B.

Visualization: C.B.

Writing - Original Draft: C.B.
Writing - Review & Editing: C.B., B.J.G., M.B.

Conflicts of interest

The author(s) declare that there are no conflicts of interest.

Funding information

This work was supported by a Vanier Canada Graduate Scholarship to C.B., a grant from the National Institutes of Health (R01AI132668) to B.J.G., and a grant from the Natural Sciences and Engineering Research Council of Canada (RGPIN-2022-04026) to M.B.

Ethical approval

Not applicable.

Consent for publication

Not applicable.

Acknowledgements

Not applicable.

References

1. Kramer, L.D.; Ciota, A.T.; Kilpatrick, A.M. Introduction, Spread, and Establishment of West Nile Virus in the Americas. J. Med. Entomol. 2019, 56, 1448–1455, doi:10.1093/jme/tjz151.
2. Hayes, E.B.; Komar, N.; Nasci, R.S.; Montgomery, S.P.; O'Leary, D.R.; Campbell, G.L. Epidemiology and Transmission Dynamics of West Nile Virus Disease. Emerg. Infect. Dis. 2005, 11, 1167–1173, doi:10.3201/eid1108.050289a.

3. Qian, X.; Qi, Z. Mosquito-Borne Flaviviruses and Current Therapeutic Advances. Viruses 2022, 14, 1226, doi:10.3390/v14061226.

4. Celegato, M.; Messa, L.; Goracci, L.; Mercorelli, B.; Bertagnin, C.; Spyrakis, F.; Suarez, I.; Cousido-Siah, A.; Travé, G.; Banks, L.; et al. A novel small-molecule inhibitor of the human papillomavirus E6-p53 interaction that reactivates p53 function and blocks cancer cells growth. Cancer Lett. 2020, 470, 115–125, doi:10.1016/j.canlet.2019.10.046.

5. Marcello, A.; Loregian, A.; Cross, A.; Marsden, H.; Hirst, T.R.; Palù, G. Specific inhibition of herpes virus replication by receptor-mediated entry of an antiviral peptide linked to Escherichia coli enterotoxin B subunit. Proc. Natl. Acad. Sci. U. S. A. 1994, 91, 8994–8998, doi:10.1073/pnas.91.19.8994.

6. Brand, C.; Bisaillon, M.; Geiss, B.J. Organization of the Flavivirus RNA replicase complex. Wiley Interdiscip. Rev. RNA 2017, e1437, doi:10.1002/wrna.1437.

7. Chambers, T.J.; Hahn, C.S.; Galler, R.; Rice, C.M. Flavivirurs Genome Organization, Expression and Replication. Annu. Rev. Microbiol. 1990, 44, 649–688, doi:10.1146/annurev.mi.44.100190.003245.

8. Lindenbach, B.D.; Thiel, H.-J.; Rice, C.M. Flaviviridae: The Viruses and Their Replication. In Fields Virology; Knipe, D.M., Howley, P.M., Eds.; Lippincott-Raven Publishers, 2007; pp. 1101–1152.

9. Wengler, G.; Czaya, G.; Färber, P.M.; Hegemann, J.H. In vitro synthesis of West Nile virus proteins indicates that the amino-terminal segment of the NS3 protein contains the active centre of the protease which cleaves the viral polyprotein after multiple basic amino acids. J. Gen. Virol. 1991, 72, 851–858, doi:10.1099/0022-1317-72-4-851.

10. Du Pont, K.E.; Sexton, N.R.; McCullagh, M.; Ebel, G.D.; Geiss, B.J. A Hyperactive Kunjin Virus NS3 Helicase Mutant Demonstrates Increased Dissemination and Mortality in Mosquitoes. J. Virol. 2020, 94, e01021-20, doi:10.1128/JVI.01021-20.

11. Wengler, G.; Wengler, G. The Carboxy-Terminal Part of the NS 3 Protein of the West Nile Flavivirus Can Be Isolated as a Soluble Protein after Proteolytic Cleavage and Represents an RNA-stimulated NTPase. Virology 1991, 184, 707–715, doi:10.1016/0042-6822(91)90440-M.

12. Wengler, G.; Wengler, G. The NS 3 Nonstructural Protein of Flaviviruses Contains an RNA Triphosphatase Activity. Virology 1993, 197, 265–273.

13. Issur, M.; Geiss, B.J.; Bougie, I.; Picard-Jean, F.; Despins, S.; Mayette, J.; Hobdey, S.E.; Bisaillon, M. The flavivirus NS5 protein is a true RNA guanylyltransferase that catalyzes a two-step reaction to form the RNA cap structure. RNA 2009, 15, 2340–2350, doi:10.1261/rna.1609709.

14. Ray, D.; Shah, A.; Tilgner, M.; Guo, Y.; Zhao, Y.; Dong, H.; Deas, T.S.; Zhou, Y.; Li, H.; Shi, P.-Y. West Nile Virus 5'-Cap Structure Is Formed by Sequential Guanine N-7 and Ribose 2'-O Methylations by Nonstructural Protein 5. J. Virol. 2006, 80, 8362–8370, doi:10.1128/JVI.00814-06.

15. Guyatt, K.J.; Westaway, E.G.; Khromykh, A.A. Expression and purification of enzymatically active recombinant RNA-dependent RNA polymerase (NS5) of the flavivirus Kunjin. J. Virol. Methods 2001, 92, 37–44, doi:10.1016/S0166-0934(00)00270-6.

16. Kapoor, M.; Zhang, L.; Ramachandra, M.; Kusukawa, J.; Ebner, K.E.; Padmanabhan, R. Association between NS3 and NS5 Proteins of Dengue Virus Type 2 in the Putative RNA Replicase Is Linked to Differential Phosphorylation of NS5. J. Biol. Chem. 1995, 270, 19100–19106.

17. Zou, G.; Chen, Y.-L.; Dong, H.; Lim, C.C.; Yap, L.J.; Yau, Y.H.; Geifman Shochat, S.; Lescar, J.; Shi, P.-Y. Functional Analysis of Two Cavities in Flavivirus NS5 Polymerase. J. Biol. Chem. 2011, 286, 14362–14372, doi:10.1074/jbc.M110.214189.

18. Tay, M.Y.F.; Saw, W.G.; Zhao, Y.; Chan, K.W.K.; Singh, D.; Chong, Y.; Forwood, J.K.; Ooi, E.E.; Grüber, G.; Lescar, J.; et al. The C-terminal 50 Amino Acid Residues of Dengue NS3 Protein Are Important for NS3-NS5 Interaction and Viral Replication. J. Biol. Chem. 2015, 290, 2379–2394, doi:10.1074/jbc.M114.607341.

19. van den Elsen, K.; Quek, J.P.; Luo, D. Molecular Insights into the Flavivirus Replication Complex. Viruses 2021, 13, 956, doi:10.3390/v13060956.

20. ClinicalTrials.gov A Study of Balapiravir in Patients With Dengue Virus Infection. Available online: https://clinicaltrials.gov/ct2/show/NCT01096576 (accessed on May 22, 2023).

21. ClinicalTrials.gov A Phase 1 Study to Evaluate the Safety, Tolerability and Pharmacokinetics of BCX4430. Available online: https://clinicaltrials.gov/ct2/show/NCT02319772 (accessed on May 22, 2023).

22. ClinicalTrials.gov Study of AT-752 in Healthy Subjects. Available online: https://clinicaltrials.gov/ct2/show/NCT04722627 (accessed on May 22, 2023).
23. Li, Z.; Brecher, M.; Deng, Y.-Q.; Zhang, J.; Sakamuru, S.; Liu, B.; Huang, R.; Koetzner, C.A.; Allen, C.A.; Jones, S.A.; et al. Existing drugs as broad-spectrum and potent inhibitors for Zika virus by targeting NS2B-NS3 interaction. Cell Res. 2017, 27, 1046–1064, doi:10.1038/cr.2017.88.
24. Yao, Y.; Huo, T.; Lin, Y.-L.; Nie, S.; Wu, F.; Hua, Y.; Wu, J.; Kneubehl, A.R.; Vogt, M.B.; Rico-Hesse, R.; et al. Discovery, X-ray Crystallography and Antiviral Activity of Allosteric Inhibitors of Flavivirus NS2B-NS3 Protease. J. Am. Chem. Soc. 2019, 141, 6832–6836, doi:10.1021/jacs.9b02505.
25. Kaptein, S.J.F.; Goethals, O.; Kiemel, D.; Marchand, A.; Kesteleyn, B.; Bonfanti, J.-F.; Bardiot, D.; Stoops, B.; Jonckers, T.H.M.; Dallmeier, K.; et al. A pan-serotype dengue virus inhibitor targeting the NS3–NS4B interaction. Nature 2021, 598, 504–509, doi:10.1038/s41586-021-03990-6.
26. Goethals, O.; Kaptein, S.J.F.; Kesteleyn, B.; Bonfanti, J.-F.; Van Wesenbeeck, L.; Bardiot, D.; Verschoor, E.J.; Verstrepen, B.E.; Fagrouch, Z.; Putnak, J.R.; et al. Blocking NS3–NS4B interaction inhibits dengue virus in non-human primates. Nature 2023, 615, 678–686,
doi:10.1038/s41586-023-05790-6.
27. Yang, S.N.Y.; Maher, B.; Wang, C.; Wagstaff, K.M.; Fraser, J.E.; Jans, D.A. High Throughput Screening Targeting the Dengue NS3-NS5 Interface Identifies Antivirals against Dengue, Zika and West Nile Viruses. Cells 2022, 11, 730, doi:10.3390/cells11040730.
28. Celegato, M.; Sturlese, M.; Vasconcelos Costa, V.; Trevisan, M.; Lallo Dias, A.S.; Souza Passos, I.B.; Queiroz-Junior, C.M.; Messa, L.; Favaro, A.; Moro, S.; et al. Small-Molecule Inhibitor of Flaviviral NS3-NS5 Interaction with Broad-Spectrum Activity and Efficacy In Vivo. MBio 2023, 14, e0309722, doi:10.1128/mbio.03097-22.
29. Pierson, T.C.; Sánchez, M.D.; Puffer, B.A.; Ahmed, A.A.; Geiss, B.J.; Valentine, L.E.; Altamura, L.A.; Diamond, M.S.; Doms, R.W. A rapid and quantitative assay for measuring antibody-mediated neutralization of West Nile virus infection. Virology 2006, 346, 53–65, doi:10.1016/j.virol.2005.10.030.

30. Gullberg, R.C.; Steel, J.J.; Moon, S.L.; Soltani, E.; Geiss, B.J. Oxidative stress influences positive strand RNA virus genome synthesis and capping. Virology 2015, 475, 219–229, doi:10.1016/j.virol.2014.10.037.
31. Du Pont, K.E.; Davidson, R.B.; McCullagh, M.; Geiss, B.J. Motif V regulates energy transduction between the flavivirus NS3 ATPase and RNA-binding cleft. J. Biol. Chem. 2020, 295, 1551–1564, doi:10.1074/jbc.RA119.011922.

4 DISCUSSION

4.1 Summary of the work presented in this thesis

The work presented in this thesis explores Flavivirus interactions with the overall goal to uncover new potential targets for the development of antiviral compounds. More specifically, Flavivirus-host interactions were investigated using RNA-Seq and SILAC/MS to identify changes in host cell gene expression and alternative splicing as well as changes in host cell protein expression, respectively, during infections with Kunjin virus, Zika virus, and Yellow Fever virus. Furthermore, the interaction between West Nile virus NS3 and NS5 proteins was characterized to identify residues that potentially mediate this protein-protein interaction.

4.1.1 Summary of the Flavivirus-host interactions project

RNA-Seq analysis of polyA-RNAs isolated from Flavivirus-infected cells revealed modulations in expression levels of several hundred genes compared to mock-infected cells, many of which are involved in the antiviral response. Moreover, approximately 600-900 alterations in alternative splicing of host mRNAs were identified, but no GO term was significantly enriched among the genes whose alternative splicing was affected. SILAC/MS analysis determined approximately 550-700 proteins to be differentially expressed between Flavivirus-infected and mock-infected cells, with significant enrichments for pathways related to protein metabolism. Identified changes in each infection were compared, and 51 genes, 39 ASEs and 57 proteins were found to be affected in all three infections. Moreover, mRNA levels and protein levels were compared and were found to not correlate significantly, suggesting a disconnect between the transcriptome and the proteome. Further studies will be needed to characterize the roles of these genes and proteins in the context of viral infections, and to determine how they could potentially be targeted to treat Flavivirus infections (Brand et al., 2023a).

4.1.2 Summary of the WNV NS3:NS5 interaction project

A model of the WNV NS3:NS5 interaction during positive strand RNA synthesis was developed based on data available in the literature, including crystal structures and the positions of RNA-binding regions and catalytic active sites (Brand et al., 2017). This model was used to identify residues in the potential NS3:NS5 interaction interface, and the importance of these residues for viral replication was determined through site-directed mutagenesis of a WNV replicon. Seven mutations on the NS3 protein were found to highly suppress viral replication, and two of them also had a moderate impact on NS3:NS5 interaction in a co-immunoprecipitation experiment, suggesting that these residues potentially mediate interaction with NS5. Further studies will be needed to confirm whether the two surface regions of NS3 in which these seven residues are clustered could be promising targets for the development of antiviral compounds (Brand et al., 2023b).

4.2 Strengths and limitations of the projects presented in this thesis

4.2.1 Strengths and limitations of the Flavivirus-host interactions project

There are several strengths in the design of this project. We used high-throughput techniques to generate a large amount of data which can be analyzed in various ways to answer different questions. In fact, the work presented here was intended to be the starting point for multiple projects, as will be described in section 4.4.1. Moreover, we used the same experimental conditions for all infections, thus allowing for comparisons between the different infections to determine similarities and differences in virus-host interactions for the three Flaviviruses.

There are also a few caveats to this project. We used bulk RNA sequencing instead of single cell RNA sequencing, which means that we may have missed genes that are highly up- or downregulated in only a small fraction of the cell population (O'Neal et al., 2019). Moreover, we used whole cell extracts in the SILAC/MS analysis, and we may have missed proteins that are differentially regulated in different cell fractions (Zhang et al., 2013), or proteins that are relocated during infection (Chiu et al., 2014).

4.2.2 Strengths and limitations of the WNV NS3:NS5 interaction project

The WNV NS3:NS5 interaction model has multiple strengths. It is based on a large body of literature including structures, enzymatic functions of the proteins, and critical steps in the viral RNA replication process. The substrate entry channels for both proteins are approximately on the same side, thus facilitating substrate access to the replicase complex which is most likely membrane-associated within the replication organelle (Brand et al., 2017). Another positive aspect of this project is the possibility to test the model using site-directed mutagenesis of a WNV replicon or *in vitro* assays with the two individual proteins.

Caveats of the NS3:NS5 interaction model include the fact that it does not address how it would be anchored to the membrane of the replication compartment. Moreover, the model assumes a 1:1 stoichiometry, although other ratios may be possible. For example, recent cryoEM studies have shown that major replication proteins from other (+)ssRNA viruses form oligomeric pore-like structures at the neck of the replication organelles (reviewed in Kumar and Altan-Bonnet, 2021). As described in section 1.3.4.3.1 and 1.3.4.3.2, there is evidence that both proteins may undergo conformational changes, and the structures used in our model may not be in the proper confirmation for positive strand RNA synthesis (Brand et al., 2017). Finally, the data generated during this project confirm that some of the residues that were hypothesized to mediate the NS3:NS5 interaction are critical for viral replication, but it has not been clearly established that the observed loss of replication is due to a loss of interaction between the two viral proteins.

4.3 Impact of the results presented in this thesis

4.3.1 Impact of the Flavivirus-host interactions project

Most previous studies investigating the host cell transcriptome or proteome during Flavivirus infections have focused on one specific Flavivirus, mostly DENV or ZIKV, in various cell types (for more details, see Table 3 on p. 57). Only three studies have compared the impact of either two different strains (DENV wild-type vs. attenuated) or two different Flavivirus species (JEV vs. WNV, and DENV vs. ZIKV) (Bonenfant et al., 2020; Clarke et al., 2014; Sessions et al., 2013). Comparisons between transcriptomic and proteomic

dysregulations have been limited so far, and they have been made using datasets that were generated by different groups and under different experimental conditions (Pattanakitsakul et al., 2007; Zhang et al., 2013). Our study is the first to use high throughput techniques to compare the coding transcriptome as well as the proteome of host cells during infection with three different Flaviviruses (Brand et al., 2023a). Given the large amount of data generated, the results from this study may give rise to multiple follow-up research projects, such as further investigation of dysregulated host genes/proteins to better understand viral pathogenesis, or to determine their potential as drug targets to restrict Flavivirus replication (see section 4.4.1).

Transcriptome profiling has been realized for many types of viral infections. For example, one such study on reovirus-infected L929 cells reported several hundred modulations in alternative splicing (Boudreault et al., 2016). Follow-up studies revealed that one viral protein interacts with core components of the U5 snRNP of the spliceosome (Boudreault et al., 2022a), which led to the discovery of novel roles for these components in cell survival, apoptosis, necroptosis, and interferon induction (Boudreault et al., 2022b). Similarly, the Flavivirus-host interactions project presented in this thesis may be the first step in a series of investigations that ultimately reveal novel roles for cellular proteins, whether it be in viral replication and pathogenesis or in the cellular antiviral response.

Given the recent COVID-19 pandemic, SARS-CoV-2 has been extensively studied, and RNA-Sequencing of infected cells has been performed to explore differential gene expression and alternative splicing patterns (Blanco-Melo et al., 2020; Fredericks et al., 2022; Haslbauer et al., 2023; Jain et al., 2020; Mehta et al., 2023). Similar to what we observed in Flavivirus infections, it was reported that the majority of dysregulated genes in SARS-CoV-2-infected cells were upregulated compared to control cells (Blanco-Melo et al., 2020; Haslbauer et al., 2023; Jain et al., 2020). However, when comparing patients that succumbed to the disease to those that recovered, gene expression was found to be mostly downregulated in patients that died (Fredericks et al., 2022; Mehta et al., 2023). Moreover, modulations in alternative splicing have also been observed in SARS-CoV-2-infected cells, and similar to our findings in Flavivirus-infected cells, only a small number of genes showed significant

changes in expression levels as well as alternative splicing (Fredericks et al., 2022). Finally, gene expression profiles in SARS-CoV-2-infected cells were found to vary depending on disease severity and might therefore act as predictors for patient outcome (Fredericks et al., 2022; Jain et al., 2020). Given that Flavivirus infections are also associated with extremely heterogenous clinical outcomes, it might be interesting to perform RNA-Sequencing on cells from patients with varying severity of disease to determine if gene expression and/or alternative splicing profiles are characteristic for mild and severe disease and could thus be used for prognostic purposes and adaptation of treatment.

4.3.2 Impact of the WNV NS3:NS5 interaction project

Protein-protein interactions have previously been shown to be promising targets for the development of therapeutics against multiple diseases (Celegato et al., 2020; Marcello et al., 1994). Moreover, mutations that abolish the DENV NS3:NS5 interaction have been associated with the inhibition of DENV replication (Tay et al., 2015; Zou et al., 2011), and recently, small molecules that disrupt the NS3:NS5 interaction have been shown to possess strong antiviral activity against DENV, ZIKV and WNV (Celegato et al., 2023; Yang et al., 2022). The molecules reported in both studies target the NS5 protein. Our study reveals two surface regions on the NS3 protein that are crucial for efficient viral replication, possibly by mediating the interaction between NS3 and NS5, which could be new targets for the development of anti-flaviviral drugs (Brand et al., 2023b).

4.4 Future work arising from the data presented in this thesis

4.4.1 Future work arising from the Flavivirus-host interactions project

There are multiple avenues to continue this project. On the one hand, it would be interesting to investigate by which mechanism(s) gene and protein expression as well as alternative splicing are dysregulated in infected cells. On the other hand, it would be compelling to pick a few candidate genes/proteins among those identified to be affected and characterize their roles in the context of viral infections to better understand viral pathogenesis and to determine whether they could be potential drug targets to treat Flavivirus infections.

4.4.1.1 Investigation of the mechanism(s) by which gene/protein expression and alternative splicing are dysregulated

Regarding the mechanism(s) that result in dysregulation of gene/protein expression and alternative splicing, there are a few hypotheses. Viruses could directly induce these alterations for their benefit. Alternatively, host cells may initiate these changes as part of their defense response. Finally, the observed modulations may be a side effect of the perturbed cellular homeostasis and the establishment of an antiviral state.

To investigate whether soluble cytokines and chemokines produced as part of the antiviral response trigger modulations in gene and protein expression or alternative splicing, a bystander experiment could be used (Boudreault et al., 2022a). Briefly, cells are seeded on a semi-permeable membrane and infected before being placed on top of a second layer of uninfected cells. Soluble factors produced and secreted by the infected cells can diffuse through the semi-permeable membrane and stimulate the interferon response in the uninfected cells. Both cell populations can then be analyzed for transcriptomic and proteomic changes to determine whether soluble molecules involved in the antiviral response are sufficient to trigger changes in gene/protein expression or alternative splicing.

To determine whether the observed dysregulations in the coding transcriptome and proteome are directly caused by Flaviviruses, it would be interesting to express one viral protein at a time and compare the effects with those of the infections. NS5 would be a good candidate protein to start with, since DENV NS5 has been shown to contain two nuclear localization signals and localize in the nucleus throughout infection (Brooks et al., 2002; Tay et al., 2013). Moreover, DENV NS5 has been reported to interact with components of the U5 snRNP and interferes with splicing (De Maio et al., 2016).

4.4.1.2 Better understanding of viral pathogenesis

Our RNA-Seq experiment revealed 17 genes associated with the GO term ‘nervous system development’ to be dysregulated in ZIKV-infected cells. Only 4 of these 17 genes were affected in YFV-infected cells, and the expression of none of them was altered in cells infected with KUNV. Given that ZIKV is the only Flavivirus that has been shown to affect

brain development and cause microcephaly (reviewed in Bhagat et al., 2021), it would be interesting to further investigate the role of these genes in ZIKV pathogenesis. For example, NRG1 has been reported to be expressed in the early stages of brain development (Liu et al., 2005), and we observed that this gene was significantly repressed during ZIKV infection (Brand et al., 2023a). Therefore, NRG1 would be an attractive candidate for further investigation regarding the mechanism by which ZIKV causes microcephaly.

4.4.1.3 Investigation of candidate genes/proteins as potential drug targets

Identifying and understanding virus-host interactions has been proposed to allow to establish novel strategies to treat or prevent infections (Pastorino et al., 2009; Zhang et al., 2013). For example, drugs affecting stress granule assembly and dynamics have been shown to possess antiviral activity (reviewed in Guan et al., 2023). Our RNA-Seq and SILAC/MS data reveal many genes and proteins whose expression levels are dysregulated during Flavivirus infections, and which may be further investigated as potential drug targets. For example, RIMS1 protein levels are significantly upregulated during YFV infection. This protein is known to regulate synaptic vesicle exocytosis (NCBI, 2023; Persoon et al., 2019). Given that nascent Flavivirus virions exit host cells via exocytosis, it might be interesting to investigate the role of RIMS1 in exocytosis of newly assembled virions, and whether inhibiting its activity would inhibit the release of virus particles from infected cells and therefore limit viral spread.

Previous studies have shown that viruses target alternative splicing and influence isoform ratios for their benefit (Álvarez et al., 2011; Verma et al., 2010). For example, Epstein-Barr virus decreases the STAT1α/STAT1β ratio. Since STAT1β lacks the transactivation domain and acts as a dominant-negative repressor of STAT1α, this change in alternative splicing inhibits IFNγ signaling (Verma et al., 2010; Verma and Swaminathan, 2008). Another example is poliovirus which increases skipping of exon 6 of the Fas transcript. Fas is an apoptosis receptor which is membrane-bound in the presence of exon 6. When this exon is absent, however, Fas is soluble, resulting in inhibition of Fas signaling. Therefore, poliovirus-induced modulation of Fas splicing inhibits apoptosis (Álvarez et al., 2011). Our RNA-Seq data revealed increased intron retention in two transcripts of genes

involved in interferon signaling, more specifically intron 7 of IRF7 and intron 12 of the STAT2. Both intron retention events are predicted to result in a premature stop codon in the transcript which would lead to either nonsense mediated decay of the mRNA or the synthesis of truncated proteins (Svidritskiy et al., 2018; reviewed in Kurosaki and Maquat, 2016). If the mRNAs are degraded, less IRF7 and STAT2 proteins may be produced and interferon signaling may be suppressed. If the transcripts are not degraded and truncated proteins are synthesized, they would lack their phosphorylation sites, and may not be active, resulting in inhibition of interferon signaling (reviewed in Ning et al., 2011; Steen and Gamero, 2013). In the event that the described modulations in alternative splicing contribute to the suppression of the interferon pathway, it would be interesting to investigate whether it would be possible to reverse these virus-induced changes in alternative splicing using targeted oligonucleotides enhancers of splicing (Brosseau et al., 2014) to help re-establish proper interferon signaling and thereby limit viral replication.

4.4.2 Future work arising from the WNV NS3:NS5 interaction project

As stated in section 4.1.2, further characterization of the NS3:NS5 interaction will be needed before this protein-protein interaction can be targeted for the development of potential antiviral compounds.

4.4.2.1 Further development of the NS3:NS5 interaction model

The current WNV NS3:NS5 interaction model is the result of manual docking of the two individual protein structures which represent static snapshots in time and may not represent physiologically relevant structures. This model could be used as a starting point for long timescale molecular dynamics (MD) simulations to determine dynamic interactions between the two proteins. In fact, we started to perform MD simulations of up to 220 ns in which the two proteins were observed to rotate approximately 20° with regard to each other (Brand, 2017). However, this is a very short timescale, and the MD simulations would need to be performed for several tens of microseconds. Structures of the NS3:NS5 complex could be exported at different time points during these simulations to identify additional residues that might mediate the interaction between the two proteins.

4.4.2.2 Confirmation of NS3:NS5 interaction suppression

To continue the NS3:NS5 interaction project, with or without MD simulations, it would be important to confirm that the observed loss of viral replication for the seven NS3 mutants is indeed due to a loss of interaction between the two proteins. Our co-IP data show that only two NS3 mutations, namely R186A and E523A, have a negative effect on NS3:NS5 interaction, which is not nearly as drastic as the effect on viral replication (Brand et al., 2023b). It may be possible that multiple pairs of interactions are present between NS3 and NS5, and breaking only one pair is not sufficient to completely interrupt the interaction. Therefore, it would be interesting to generate double or triple mutants of NS3 and determine their interaction with NS5, compared to the wild-type NS3. Moreover, we identified seven mutants of NS3 and two mutants of NS5 that critically suppressed viral replication, but only five of the NS3 mutants were included in the co-IP experiment (due to technical difficulties in producing the other constructs). It would be interesting to include NS3 G254A, NS3 R525A, NS5 N48A and NS5 G317A in the interaction assay.

Given that the co-IP experiment was performed using whole cell extracts, it is possible that other cellular components contributed to the NS3:NS5 interaction. It might be interesting to consider another technique that measures the direct protein-protein interaction. In fact, we initially intended to use isothermal titration calorimetry (ITC) to measure the interaction between purified NS3 and NS5. During ITC, one protein is in the sample cell, and small amounts of the second protein are injected using a syringe. Upon interaction between the two proteins, heat is generated or absorbed, and the energy needed to keep the sample cell and the reference cell at the same temperature is measured and used to determine the binding constant (K_D) (reviewed in Pierce et al., 1999). I had cloned both genes into bacterial expression vectors and optimized recombinant protein expression and purification (Figure 1). However, for the ITC experiment to be successful, the concentration of the protein in the syringe needs to be approximately ten times higher than the concentration of the protein in the sample cell. When I tried to concentrate the purified recombinant proteins, both NS3 and NS5 precipitated, and ITC was no longer an option. An alternative technique to measure protein-protein interactions, which requires less concentrated proteins, is surface plasmon resonance (SPR). In this method, one protein is immobilized on a sensor surface, and the

other protein is injected over this surface. Binding of the injected protein to the immobilized protein changes the refractive index which is measured to determine the binding affinity of the two proteins (reviewed in Douzi, 2017). When I tried to use SPR to quantify the NS3:NS5 interaction, I noticed that even relatively low concentrations of proteins had a tendency to aggregate and block the tubing, thus putting an end to the SPR experiment. However, it might be interesting to revisit the experimental design and try to optimize protein concentrations and buffer composition to avoid protein aggregation, since SPR is a quantitative, high-throughput method which is commonly used to study protein-protein interactions (reviewed in Kyo et al., 2009). Therefore, it could be used to investigate the interaction between one wild-type protein and many mutants, or the interaction between NS3 or NS5 and a large number of potential protein-protein interaction (PPI) inhibitors (see section 4.4.2.3).

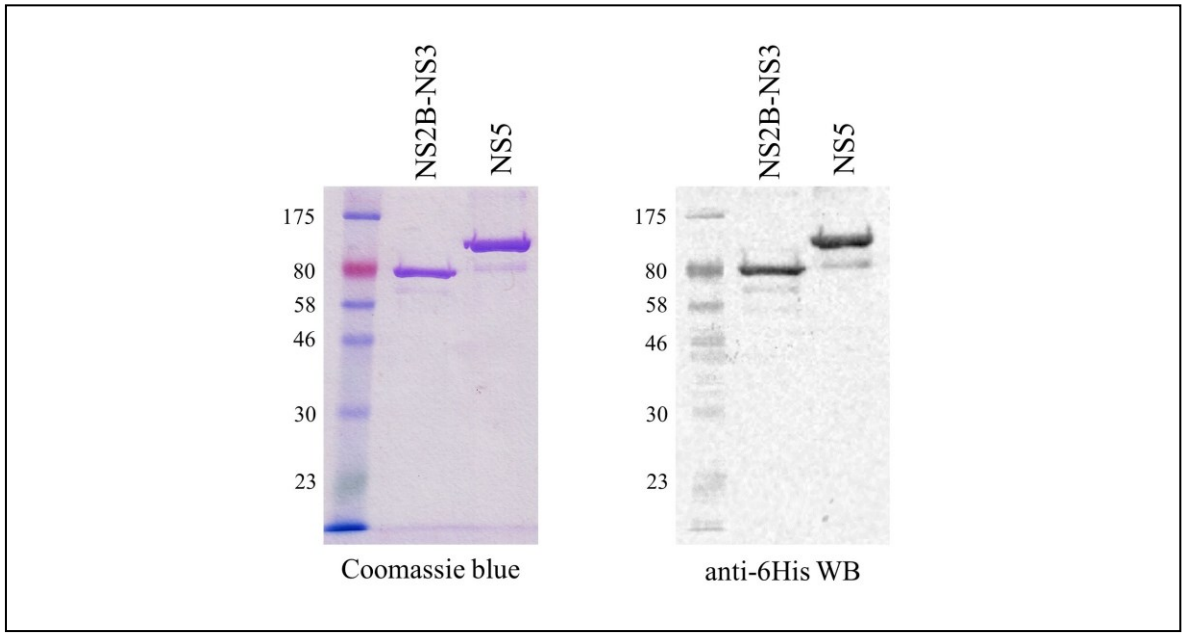

Figure 1. Expression and purification of recombinant WNV NS3 and NS5. WNV NS3 and NS5 were cloned into the pET21b and pET28a expression vectors and expressed in BL21(DE3) cells and Rosetta2(DE3)pLysS cells, respectively. Bacterial lysates were applied to a HisTrap column, followed by a HiLoad 16/60 Superdex 200pg column on a FPLC system. Purified proteins were analyzed by SDS-PAGE followed by Coomassie blue staining as well as western blotting (WB). Figure adapted from (Brand, 2017).

4.4.2.3 Determine if the NS3:NS5 interaction is conserved among Flaviviruses

Once the WNV NS3:NS5 interaction is well characterized and residues that mediate the interaction have been clearly identified, it would be interesting to investigate whether these residues are conserved among Flaviviruses. If so, targeting these residues may not only be promising for the development of compounds that inhibit WNV infection, but also for antiviral therapeutics for other Flavivirus infections.

4.4.2.4 Screening for potential NS3:NS5 interaction inhibitors

Ultimately, the goal of characterizing the NS3:NS5 interaction is to target this interaction for the development of potential antiviral compounds. Once a specific surface region on either protein is determined to mediate the interaction between NS3 and NS5, a high throughput virtual screening can be performed to identify small molecules that bind this region (Celegato et al., 2023; Yang et al., 2022). Binding of promising candidate molecules can be confirmed using an in vitro assay such as SPR, as described in section 4.4.2.2. Finally, antiviral activity of candidate molecules can be investigated in cell-based assays and eventually animal models.

5 CONCLUSION

In conclusion, the work presented in this thesis explored Flavivirus interactions in the search of new potential drug targets. First, I investigated Flavivirus-host interactions using RNA-Seq and SILAC/MS to identify changes in gene/protein expression and alternative splicing during Flavivirus infections. I found several host genes and proteins that would be interesting candidates to study further for their roles in viral infections and their potential to be targeted to suppress viral replication. Second, I examined the interaction between the WNV NS3 and NS5 proteins. I identified seven residues on the surface of the NS3 protein that are critical for viral replication, possibly by mediating the interaction with NS5. These residues are clustered in two 'hotspots' which could be new potential targets for the development of anti-flaviviral drugs.

6 ACKNOWLEDGEMENTS

First, I would like to thank the evaluation committee for accepting to read my thesis and providing valuable feedback on my work.

I am grateful to my research directors Prof. Martin Bisaillon at UdeS and Prof. Brian Geiss at CSU for their trust, guidance, encouragements, and patience. Thank you for allowing me to take charge of my two research projects, while providing support in times of difficulty and for all the big decisions.

I would also like to express my appreciation to the members of my mentoring committee, Prof. Xavier Roucou and Prof. Lee-Hwa Tai, for their support and valuable advice over the years. Thanks should also go to the funding agencies for supporting our work in the form of grants (Natural Sciences and Engineering Research Council of Canada, National Institutes of Health) and scholarships (Faculté de Médecine et des Sciences de la Santé de l'Université de Sherbrooke, Fonds de Recherche du Québec Nature et technologies, Vanier Canada Graduate Scholarships).

I am thankful to past and present members of the Bisaillon lab team for many enriching discussions and their support during my graduate studies, especially interns Marie-Joëlle Doré and Kasandra Blais who contributed to the NS3:NS5 project for several months. I am immensely appreciative to fellow PhD students Gabrielle Deschamps-Francoeur and Vincent Boivin as well as Prof. Michelle Scott for their tremendous help with the bioinformatic analysis of our RNA-Seq data.

I would like to acknowledge our many collaborators for their contribution to various aspects of our research projects: Kristen Bullard-Feibelman at CSU for the initial round of viral infections; Mathieu Durand, Elvy Lapointe, Philippe Thibeault and Danny Bergeron at the RNomics platform at UdeS for RNA sequencing library preparation and validation of RNA-Seq results via qRT-PCR and AS-PCR; Dominique Lévesque from the proteomics

platform, as well as Jennifer Raisch and Marie Brunet at UdeS for their help with the analysis of our mass spectrometry data.

Finally, I would like to express my gratitude to my family and friends who have always been there for me, both to celebrate successes and stand by me during more difficult times. Thank you to my parents Peter and Elisabeth who have always encouraged me to pursue my interest in science. Special thanks to my partner Philippe as well as our children Felix and Annabelle for believing in me, motivating me, and brightening my day-to-day life.

7 LIST OF REFERENCES

Ackermann, M., Padmanabhan, R., 2001. De Novo Synthesis of RNA by the Dengue Virus RNA-dependent RNA polymerase Exhibits Temperature Dependence at the Initiation but Not Elongation Phase. J. Biol. Chem. 276(43):39926–39937. PMID: 11546770. DOI: 10.1074/jbc.M104248200

Adams, M.J., Lefkowitz, E.J., King, A.M.Q., Carstens, E.B., 2013. Recently agreed changes to the International Code of Virus Classification and Nomenclature. Arch. Virol. 158(12):2633–2639. PMID: 23836393. DOI: 10.1007/s00705-013-1749-9

Airo, A.M., Urbanowski, M.D., Lopez-Orozco, J., You, J.H., Skene-Arnold, T.D., Holmes, C., Yamshchikov, V., Malik-Soni, N., Frappier, L., Hobman, T.C., 2018. Expression of flavivirus capsids enhance the cellular environment for viral replication by activating Akt-signalling pathways. Virology 516:147–157. PMID: 29358114. DOI: 10.1016/j.virol.2018.01.009

Alberts, B., Johnson, A., Lewis, J., Raff, M., Roberts, K., Walter, P., 2002. An Overview of Gene Control. In: Molecular Biology of the Cell. Garland Science, New York.

Aleshin, A.E., Shiryaev, S.A., Strongin, A.Y., Liddington, R.C., 2007. Structural evidence for regulation and specificity of flaviviral proteases and evolution of the Flaviviridae fold. Protein Sci. 16(5):795–806. PMID: 17400917. DOI: 10.1110/ps.072753207

Álvarez, E., Castelló, A., Carrasco, L., Izquierdo, J.M., 2011. Alternative splicing, a new target to block cellular gene expression by poliovirus 2A protease. Biochem. Biophys. Res. Commun. 414(1):142–147. PMID: 21945619. DOI: 10.1016/j.bbrc.2011.09.040

Amorim, R., Temzi, A., Griffin, B.D., Mouland, A.J., 2017. Zika virus inhibits eIF2α-dependent stress granule assembly. PLoS Negl. Trop. Dis. 11(7):e0005775. PMID: 28715409. DOI: 10.1371/journal.pntd.0005775

Arakawa, M., Tabata, K., Ishida, K., Kobayashi, M., Arai, A., Ishikawa, T., Suzuki, R., Takeuchi, H., Tripathi, L.P., Mizuguchi, K., Morita, E., 2022. Flavivirus recruits the valosin-containing protein-NPL4 complex to induce stress granule disassembly for efficient viral genome replication. J. Biol. Chem. 298(3):101597. PMID: 35063505. DOI: 10.1016/j.jbc.2022.101597

Ashour, J., Laurent-Rolle, M., Shi, P.-Y., García-Sastre, A., 2009. NS5 of Dengue Virus Mediates STAT2 Binding and Degradation. J. Virol. 83(11):5408–5418. PMID: 19279106. DOI: 10.1128/JVI.02188-08

Assenberg, R., Mastrangelo, E., Walter, T.S., Verma, A., Milani, M., Owens, R.J., Stuart, D.I., Grimes, J.M., Mancini, E.J., 2009. Crystal Structure of a Novel Conformational State of the Flavivirus NS3 protein: Implications for Polyprotein Processing and Viral Replication. J. Virol. 83(24):12895–12906. PMID: 19793813. DOI: 10.1128/JVI.00942-09

Baltimore, D., 1971. Expression of Animal Virus Genomes. Bacteriol. Rev. 35(3):235–241. PMID: 4329869. DOI: 10.1128/br.35.3.235-241.1971

Banerjee, A., Shukla, S., Pandey, A.D., Goswami, S., Bandyopadhyay, B., Ramachandran, V., Das, S., Malhotra, A., Agarwal, A., Adhikari, S., Rahman, M., Chatterjee, S., Bhattacharya, N., Basu, N., Pandey, P., Sood, V., Vrati, S., 2017. RNA-Seq analysis of peripheral blood mononuclear cells reveals unique transcriptional signatures associated with disease progression in dengue patients. Transl. Res. 186:62-78.e9. PMID: 28683259. DOI: 10.1016/j.trsl.2017.06.007

Baralle, F.E., Giudice, J., 2017. Alternative splicing as a regulator of development and tissue identity. Nat. Rev. Mol. Cell Biol. 18(7):437–451. PMID: 28488700. DOI: 10.1038/nrm.2017.27

Bartelma, G., Padmanabhan, R., 2002. Expression, Purification, and Characterization of the RNA 5'-triphosphatase activity of Dengue Virus Type 2 Nonstructural Protein 3. Virology 299(1):122–132. PMID: 12167347. DOI: 10.1006/viro.2002.1504

Baylor College of Medecine, 2022. Introduction to Infectious Diseases [WWW Document]. URL https://www.bcm.edu/departments/molecular-virology-and-microbiology/emerging-infections-and-biodefense/introduction-to-infectious-diseases (accessed 2022-04-04).

Bazan, J.F., Fletterick, R.J., 1989. Detection of a Trypsin-like Serine Protease Domain in Flaviviruses and Pestiviruses. Virology 171(2):637–639. PMID: 2548336. DOI: 10.1016/0042-6822(89)90639-9

Benarroch, D., Selisko, B., Locatelli, G.A., Maga, G., Romette, J.-L., Canard, B., 2004. The RNA helicase, nucleotide 5'-triphosphatase, and RNA 5'-triphosphatase activities of

Dengue virus protein NS3 are Mg2+-dependent and require a functional Walker B motif in the helicase catalytic core. Virology 328(2):208–218. PMID: 15464841. DOI: 10.1016/j.virol.2004.07.004

Benzaghou, I., Bougie, I., Picard-Jean, F., Bisaillon, M., 2006. Energetics of RNA binding by the West Nile virus RNA triphosphatase. FEBS Lett. 580(3):867–877. PMID: 16413541. DOI: 10.1016/j.febslet.2006.01.006

Berthoux, L., 2020. The Restrictome of Flaviviruses. Virol. Sin. 35(4):363–377. PMID: 32152893. DOI: 10.1007/s12250-020-00208-3

Berzal-Herranz, A., Berzal-Herranz, B., Ramos-Lorente, S.E., Romero-López, C., 2022. The Genomic 3′ UTR of Flaviviruses Is a Translation Initiation Enhancer. Int. J. Mol. Sci. 23(15):8604. PMID: 35955738. DOI: 10.3390/ijms23158604

Bhagat, R., Kaur, G., Seth, P., 2021. Molecular mechanisms of zika virus pathogenesis: An update. Indian J. Med. Res. 154(3):433–445. PMID: 35345069. DOI: 10.4103/ijmr.IJMR_169_20

Bhattacharyya, S., Sen, U., Vrati, S., 2014. Regulated IRE1-dependent decay pathway is activated during Japanese encephalitis virus-induced unfolded protein response and benefits viral replication. J. Gen. Virol. 95(Pt 1):71–79. PMID: 24114795. DOI: 10.1099/vir.0.057265-0

Bista, M.B., Banerjee, M.K., Shin, S.H., Tandan, J.B., Kim, M.H., Sohn, Y.M., Ohrr, H.C., Tang, J.L., Halstead, S.B., 2001. Efficacy of single-dose SA 14-14-2 vaccine against Japanese encephalitis: a case control study. Lancet 358(9284):791–795. PMID: 11564484. DOI: 10.1016/s0140-6736(01)05967-0

Blanco-Melo, D., Nilsson-Payant, B.E., Liu, W.-C., Uhl, S., Hoagland, D., Møller, R., Jordan, T.X., Oishi, K., Panis, M., Sachs, D., Wang, T.T., Schwartz, R.E., Lim, J.K., Albrecht, R.A., TenOever, B.R., 2020. Imbalanced Host Response to SARS-CoV-2 Drives Development of COVID-19. Cell 181(5):1036-1045.e9. PMID: 32416070. DOI: 10.1016/j.cell.2020.04.026

Blázquez, A.-B., Escribano-Romero, E., Merino-Ramos, T., Saiz, J.-C., Martín-Acebes, M.A., 2014. Stress responses in flavivirus-infected cells: activation of unfolded protein response and autophagy. Front. Microbiol. 5:266. PMID: 24917859. DOI: 10.3389/fmicb.2014.00266

Blohm, G.M., Lednicky, J.A., Márquez, M., White, S.K., Loeb, J.C., Pacheco, C.A., Nolan, D.J., Paisie, T., Salemi, M., Rodríguez-Morales, A.J., Glenn Morris, J.J., Pulliam, J.R.C., Paniz-Mondolfi, A.E., 2018. Evidence for Mother-to-Child Transmission of Zika Virus Through Breast Milk. Clin. Infect. Dis. 66(7):1120–1121. PMID: 29300859. DOI: 10.1093/cid/cix968

Bonenfant, G., Meng, R., Shotwell, C., Badu, P., Payne, A.F., Ciota, A.T., Sammons, M.A., Berglund, J.A., Pager, C.T., 2020. Asian Zika Virus Isolate Significantly Changes the Transcriptional Profile and Alternative RNA Splicing Events in a Neuroblastoma Cell Line. Viruses 12(5):510. PMID: 32380717. DOI: 10.3390/v12050510

Bonenfant, G., Williams, N., Netzband, R., Schwarz, M.C., Evans, M.J., Pager, C.T., 2019. Zika Virus Subverts Stress Granules To Promote and Restrict Viral Gene Expression. J. Virol. 93(12):e00520-19. PMID: 30944179. DOI: 10.1128/JVI.00520-19

Boudreault, S., Durand, M., Martineau, C.-A., Perreault, J.-P., Lemay, G., Bisaillon, M., 2022a. Reovirus μ2 protein modulates host cell alternative splicing by reducing protein levels of U5 snRNP core components. Nucleic Acids Res. 50(9):5263–5281. PMID: 35489070. DOI: 10.1093/nar/gkac272

Boudreault, S., Lemay, G., Bisaillon, M., 2022b. U5 snRNP Core Proteins Are Key Components of the Defense Response against Viral Infection through Their Roles in Programmed Cell Death and Interferon Induction. Viruses 14(12):2710. PMID: 36560714. DOI: 10.3390/v14122710

Boudreault, S., Martenon-Brodeur, C., Caron, M., Garant, J.-M., Tremblay, M.-P., S. Armero, V.E., Durand, M., Lapointe, E., Thibault, P., Tremblay-Létourneau, M., Perreault, J.-P., Scott, M.S., Lemay, G., Bisaillon, M., 2016. Global Profiling of the Cellular Alternative RNA Splicing Landscape during Virus-Host Interactions. PLoS One 11(9):e0161914. PMID: 27598998. DOI: 10.1371/journal.pone.0161914

Brand, C., 2017. In-depth characterization of the NS3:NS5 interaction within the West Nile virus replicase complex during positive strand RNA synthesis. Université de Sherbrooke. Thesis available at: http://savoirs.usherbrooke.ca/handle/11143/10487

Brand, C., Bisaillon, M., Geiss, B.J., 2017. Organization of the Flavivirus RNA replicase complex. Wiley Interdiscip. Rev. RNA 8(6):e1437. PMID: 28815931. DOI: 10.1002/wrna.1437

Brand, C., Deschamps-Francoeur, G., Bullard-Feibelman, K.M., Scott, M.S., Geiss, B.J., Bisaillon, M., 2023a. Kunjin Virus, Zika Virus, and Yellow Fever Virus Infections Have Distinct Effects on the Coding Transcriptome and Proteome of Brain-Derived U87 Cells. Viruses 15(7):1419. PMID: 37515107. DOI: 10.3390/v15071419

Brand, C., Geiss, B.J., Bisaillon, M., 2023b. Deciphering the interaction surface between the West Nile virus NS3 and NS5 proteins. Submitt. to J. Gen. Virol.

Brito Querido, J., Sokabe, M., Kraatz, S., Gordiyenko, Y., Skehel, J.M., Fraser, C.S., Ramakrishnan, V., 2020. Structure of a human 48S translational initiation complex. Science 369r(6508):1220–1227. PMID: 32883864. DOI: 10.1126/science.aba4904

Brooks, A.J., Johansson, M., John, A. V., Xu, Y., Jans, D.A., Vasudevan, S.G., 2002. The Interdomain Region of Dengue NS5 Protein That Binds to the Viral Helicase NS3 Contains Independently Functional Importin β1 and Importin α/β-Recognized Nuclear Localization Signals. J. Biol. Chem. 277(39):36399–36407. PMID: 12105224. DOI: 10.1074/jbc.M204977200

Brosseau, J.-P., Lucier, J.-F., Lamarche, A.-A., Shkreta, L., Gendron, D., Lapointe, E., Thibault, P., Paquet, É., Perreault, J.-P., Abou Elela, S., Chabot, B., 2014. Redirecting splicing with bifunctional oligonucleotides. Nucleic Acids Res. 42(6):e40. PMID: 24375754. DOI: 10.1093/nar/gkt1287

Buccitelli, C., Selbach, M., 2020. mRNAs, proteins and the emerging principles of gene expression control. Nat. Rev. Genet. 21(10):630–644. PMID: 32709985. DOI: 10.1038/s41576-020-0258-4

Bullard, K.M., Gullberg, R.C., Soltani, E., Steel, J.J., Geiss, B.J., Keenan, S.M., 2015. Murine Efficacy and Pharmacokinetic Evaluation of the Flaviviral NS5 Capping Enzyme 2-Thioxothiazolidin-4-One Inhibitor BG-323. PLoS One 10(6):e0130083. PMID: 26075394. DOI: 10.1371/journal.pone.0130083

Burrell, C.J., Howard, C.R., Murphy, F.A., 2017. Flaviviruses. In: Fenner and White's Medical Virology. pp. 493–518. DOI: https://doi.org/10.1016/B978-0-12-375156-0.00036-9

Bussetta, C., Choi, K.H., 2012. Dengue Virus Nonstructural Protein 5 Adopts Multiple Conformations in Solution. Biochemistry 51(30):5921–5931. PMID: 22757685. DOI: 10.1021/bi300406n

Calisher, C.H., Karabatsos, N., Dalrymple, J.M., Shope, R.E., Porterfield, J.S., Westaway, E.G., Brandt, W.E., 1989. Antigenic relationships between flaviviruses as determined by cross-neutralization tests with polyclonal antisera. J. Gen. Virol. 70(1):37–43. PMID: 2543738. DOI: 10.1099/0022-1317-70-1-37

Campbell, N.A., Reece, J.B., 2007. Biologie, 3e ed. Éditions du Renouveau Pédagogique Inc.

Celegato, M., Messa, L., Goracci, L., Mercorelli, B., Bertagnin, C., Spyrakis, F., Suarez, I., Cousido-Siah, A., Travé, G., Banks, L., Cruciani, G., Palù, G., Loregian, A., 2020. A novel small-molecule inhibitor of the human papillomavirus E6-p53 interaction that reactivates p53 function and blocks cancer cells growth. Cancer Lett. 470:115–125. PMID: 31693922. DOI: 10.1016/j.canlet.2019.10.046

Celegato, M., Sturlese, M., Vasconcelos Costa, V., Trevisan, M., Lallo Dias, A.S., Souza Passos, I.B., Queiroz-Junior, C.M., Messa, L., Favaro, A., Moro, S., Teixeira, M.M., Loregian, A., Mercorelli, B., 2023. Small-Molecule Inhibitor of Flaviviral NS3-NS5 Interaction with Broad-Spectrum Activity and Efficacy In Vivo. MBio 14(1):e0309722. PMID: 36622141. DOI: 10.1128/mbio.03097-22

Centers for Disease Control and Prevention, 2022a. Zoonotic Diseases [WWW Document]. URL https://www.cdc.gov/onehealth/basics/zoonotic-diseases.html (accessed 2022-04-05).

Centers for Disease Control and Prevention, 2022b. Transmission of Japanese Encephalitis Virus [WWW Document]. URL https://www.cdc.gov/japaneseencephalitis/transmission/index.html (accessed 2023-05-28).

Chambers, T.J., Grakoui, A., Rice, C.M., 1991. Processing of the Yellow Fever Virus Nonstructural Polyprotein: a Catalytically Active NS3 Proteinase Domain and NS2B Are Required for Cleavages at Dibasic Sites. J. Virol. 65(11):6042–6050. PMID: 1833562.

Chambers, T.J., Hahn, C.S., Galler, R., Rice, C.M., 1990a. Flavivirurs Genome Organization, Expression and Replication. Annu. Rev. Microbiol. 44:649–688. PMID: 2174669. DOI: 10.1146/annurev.mi.44.100190.003245

Chambers, T.J., Nestorowicz, A., Amberg, S.M., Rice, C.M., 1993. Mutagenesis of the Yellow Fever Virus NS2B Protein: Effects on Proteolytic Processing, NS2B-NS3

Complex Formation, and Viral Replication. J. Virol. 67(11):6797–6807. PMID: 8411382.

Chambers, T.J., Weir, R.C., Grakoui, A., McCourt, D.W., Bazan, J.F., Fletterick, R.J., Rice, C.M., 1990b. Evidence that the N-terminal domain of nonstructural protein NS3 from yellow fever virus is a serine protease responsible for site-specific cleavages in the viral polyprotein. Proc. Natl. Acad. Sci. U. S. A. 87(22):8898–8902. PMID: 2147282. DOI: 10.1073/pnas.87.22.8898

Chan, S.-W., 2014. The unfolded protein response in virus infections. Front. Microbiol. 5:518. PMID: 25324837. DOI: 10.3389/fmicb.2014.00518

Chatel-Chaix, L., Fischl, W., Scaturro, P., Cortese, M., Kallis, S., Bartenschlager, M., Fischer, B., Bartenschlager, R., 2015. A Combined Genetic-Proteomic Approach Identifies Residues within Dengue Virus NS4B Critical for Interaction with NS3 and Viral Replication. J. Virol. 89(14):7170–7186. PMID: 25926641. DOI: 10.1128/JVI.00867-15

Chen, S., Wu, Z., Wang, M., Cheng, A., 2017. Innate Immune Evasion Mediated by Flaviviridae Non-Structural Proteins. Viruses 9(10):291. PMID: 28991176. DOI: 10.3390/v9100291

Chiramel, A.I., Best, S.M., 2018. Role of autophagy in Zika virus infection and pathogenesis. Virus Res. 254:34–40. PMID: 28899653. DOI: 10.1016/j.virusres.2017.09.006

Chiu, H.-C., Hannemann, H., Heesom, K.J., Matthews, D.A., Davidson, A.D., 2014. High-Throughput Quantitative Proteomic Analysis of Dengue Virus Type 2 Infected A549 Cells. PLoS One 9(3):e93305. PMID: 24671231. DOI: 10.1371/journal.pone.0093305

Choi, K.H., Rossmann, M.G., 2009. RNA-dependent RNA polymerases from Flaviviridae. Curr. Opin. Struct. Biol. 19(6):746–751. PMID: 19914821. DOI: 10.1016/j.sbi.2009.10.015

Choi, Y., Bowman, J.W., Jung, J.U., 2018. Autophagy during viral infection - a double-edged sword. Nat. Rev. Microbiol. 16(6):341–354. PMID: 29556036. DOI: 10.1038/s41579-018-0003-6

Clarke, B.D., Roby, J.A., Slonchak, A., Khromykh, A.A., 2015. Functional non-coding RNAs derived from the flavivirus 3' untranslated region. Virus Res. 206:53–61. PMID: 25660582. DOI: 10.1016/j.virusres.2015.01.026

Clarke, P., Leser, J.S., Bowen, R.A., Tyler, K.L., 2014. Virus-Induced Transcriptional Changes in the Brain Include the Differential Expression of Genes Associated with Interferon, Apoptosis, Interleukin 17 receptor A, and Glutamate Signaling as Well as Flavivirus-Specific Upregulation of tRNA Synthetases. MBio 5(2):e00902-14. PMID: 24618253. DOI: 10.1128/mBio.00902-14

ClinicalTrials.gov, 2016a. A Study of Balapiravir in Patients With Dengue Virus Infection. [WWW Document]. URL https://clinicaltrials.gov/ct2/show/NCT01096576 (accessed 2023-05-22).

ClinicalTrials.gov, 2016b. A Phase 1 Study to Evaluate the Safety, Tolerability and Pharmacokinetics of BCX4430. [WWW Document]. URL https://clinicaltrials.gov/ct2/show/NCT02319772 (accessed 2023-05-22).

ClinicalTrials.gov, 2020. Celgosivir or Modipafant as Treatment for Adult Participants With Uncomplicated Dengue Fever in Singapore [WWW Document]. URL https://clinicaltrials.gov/ct2/show/NCT02569827 (accessed 2023-05-24).

ClinicalTrials.gov, 2022. Study of AT-752 in Healthy Subjects. [WWW Document]. URL https://clinicaltrials.gov/ct2/show/NCT04722627 (accessed 2023-05-22).

ClinicalTrials.gov, 2023. A Study of JNJ-64281802 for the Prevention of Dengue Infection [WWW Document]. URL https://clinicaltrials.gov/ct2/show/NCT05201794 (accessed 2023-05-27).

Collins, N.D., Barrett, A.D.T., 2017. Live Attenuated Yellow Fever 17D Vaccine: A Legacy Vaccine Still Controlling Outbreaks In Modern Day. Curr. Infect. Dis. Rep. 19(3):14. PMID: 28275932. DOI: 10.1007/s11908-017-0566-9

Colpitts, T.M., Conway, M.J., Montgomery, R.R., Fikrig, E., 2012. West Nile Virus: Biology, Transmission, and Human Infection. Clin. Microbiol. Rev. 25(4):635–648. PMID: 23034323. DOI: 10.1128/CMR.00045-12

Cook, S., Holmes, E.C., 2006. A multigene analysis of the phylogenetic relationships among the flaviviruses (Family: Flaviviridae) and the evolution of vector transmission. Arch. Virol. 151(2):309–325. PMID: 16172840. DOI: 10.1007/s00705-005-0626-6

Cramer, P., 2019. Organization and regulation of gene transcription. Nature 573(7772):45–54. PMID: 31462772. DOI: 10.1038/s41586-019-1517-4

Cui, T., Sugrue, R.J., Xu, Q., Lee, A.K.W., Chan, Y.-C., Fu, J., 1998. Recombinant Dengue

Virus Type 1 NS3 Protein Exhibits Specific Viral RNA Binding and NTPase Activity Regulated by the NS5 Protein. Virology 246(2):409–417. PMID: 9657959. DOI: 10.1006/viro.1998.9213

Cumberworth, S.L., Clark, J.J., Kohl, A., Donald, C.L., 2017. Inhibition of type I interferon induction and signalling by mosquito-borne flaviviruses. Cell. Microbiol. 19(5):e12737. PMID: 28273394. DOI: 10.1111/cmi.12737

Daep, C.A., Muñoz-Jordán, J.L., Eugenin, E.A., 2014. Flaviviruses, an expanding threat in public health: focus on dengue, West Nile, and Japanese encephalitis virus. J. Neurovirol. 20(6):539–560. PMID: 25287260. DOI: 10.1007/s13365-014-0285-z

Datan, E., Roy, S., Germain, G., Zali, N., McLean, J., Golshan, G., Harbajan, S., Lockshin, R., Zakeri, Z., 2016. Dengue-induced autophagy, virus replication and protection from cell death require ER stress (PERK) pathway activation. Cell Death Dis. 7(3):e2127. PMID: 26938301. DOI: 10.1038/cddis.2015.409

De Maio, F.A., Risso, G., Iglesias, N.G., Shah, P., Pozzi, B., Gebhard, L.G., Mammi, P., Mancini, E., Yanovsky, M.J., Andino, R., Krogan, N., Srebrow, A., Gamarnik, A. V., 2016. The Dengue Virus NS5 Protein Intrudes in the Cellular Spliceosome and Modulates Splicing. PLoS Pathog. 12(8):e1005841. PMID: 27575636. DOI: 10.1371/journal.ppat.1005841

de Menezes Martins, R., Fernandes Leal, M. da L., Homma, A., 2015. Serious adverse events associated with yellow fever vaccine. Hum. Vaccines Immunother. 11(9):2183–2187. PMID: 26090855. DOI: 10.1080/21645515.2015.1022700

Delgado-Maldonado, T., Moreno-Herrera, A., Pujadas, G., Vázquez-Jiménez, L.K., González-González, A., Rivera, G., 2023. Recent advances in the development of methyltransferase (MTase) inhibitors against (re)emerging arboviruses diseases dengue and Zika. Eur. J. Med. Chem. 252:115290. PMID: 36958266. DOI: 10.1016/j.ejmech.2023.115290

Dever, T.E., Dinman, J.D., Green, R., 2018. Translation Elongation and Recoding in Eukaryotes. Cold Spring Harb. Perspect. Biol. 10(8):a032649. PMID: 29610120. DOI: 10.1101/cshperspect.a032649

Dhingra, V., Li, Q., Allison, A.B., Stallknecht, D.E., Fu, Z.F., 2005. Proteomic Profiling and Neurodegeneration in West-Nile-Virus-Infected Neurons. J. Biomed. Biotechnol.

2005(3):271–279. PMID: 16192685. DOI: 10.1155/JBB.2005.271

Douzi, B., 2017. Protein-Protein Interactions: Surface Plasmon Resonance. In: Walker, J.M. (Ed.), Methods in Molecular Biology. Springer. DOI: 10.1007/978-1-4939-7033-9_21

Du Pont, K.E., Davidson, R.B., McCullagh, M., Geiss, B.J., 2020. Motif V regulates energy transduction between the flavivirus NS3 ATPase and RNA-binding cleft. J. Biol. Chem. 295(6):1551–1564. PMID: 31914411. DOI: 10.1074/jbc.RA119.011922

Eaton, J.D., West, S., 2020. Termination of Transcription by RNA Polymerase II: BOOM! Trends Genet. 36(9):664–675. PMID: 32527618. DOI: 10.1016/j.tig.2020.05.008

Edgil, D., Polacek, C., Harris, E., 2006. Dengue Virus Utilizes a Novel Strategy for Translation Initiation When Cap-Dependent Translation Is Inhibited. J. Virol. 80(6):2976–2986. PMID: 16501107. DOI: 10.1128/JVI.80.6.2976-2986.2006

Egloff, M.-P., Benarroch, D., Selisko, B., Romette, J.-L., Canard, B., 2002. An RNA cap (nucleoside-2'-O-)-methyltransferase in the flavivirus RNA polymerase NS5: crystal structure and functional characterization. EMBO J. 21(11):2757–2768. PMID: 12032088. DOI: 10.1093/emboj/21.11.2757

Egloff, M.-P., Decroly, E., Malet, H., Selisko, B., Benarroch, D., Ferron, F., Canard, B., 2007. Structural and Functional Analysis of Methylation and 5′-RNA Sequence Requirements of Short Capped RNAs by the Methyltransferase Domain of Dengue Virus NS5. J. Mol. Biol. 372(3):723–736. PMID: 17686489. DOI: 10.1016/j.jmb.2007.07.005

Ekkapongpisit, M., Wannatung, T., Susantad, T., Triwitayakorn, K., Smith, D.R., 2007. cDNA-AFLP Analysis of Differential Gene Expression in Human Hepatoma Cells (HepG2) Upon Dengue Virus Infection. J. Med. Virol. 79(5):552–561. PMID: 17387748. DOI: 10.1002/jmv.20806

Ellwanger, J.H., Chies, J.A.B., 2021. Zoonotic spillover: Understanding basic aspects for better prevention. Genet. Mol. Biol. 44(1 Suppl 1):e20200355. PMID: 34096963. DOI: 10.1590/1678-4685-GMB-2020-0355

Elmore, S., 2007. Apoptosis: A Review of Programmed Cell Death. Toxicol. Pathol. 35(4):495–516. PMID: 17562483. DOI: 10.1080/01926230701320337

Emara, M.M., Brinton, M.A., 2007. Interaction of TIA-1/TIAR with West Nile and dengue virus products in infected cells interferes with stress granule formation and processing

body assembly. Proc. Natl. Acad. Sci. U. S. A. 104(21):9041–9046. PMID: 17502609. DOI: 10.1073/pnas.0703348104

Erbel, P., Schiering, N., D'Arcy, A., Renatus, M., Kroemer, M., Lim, S.P., Yin, Z., Keller, T.H., Vasudevan, S.G., Hommel, U., 2006. Structural basis for the activation of flaviviral NS3 proteases from dengue and West Nile virus. Nat. Struct. Mol. Biol. 13(4):372–373. PMID: 16532006. DOI: 10.1038/nsmb1073

European Medicines Agency, 2023. Qdenga [WWW Document]. URL https://www.ema.europa.eu/en/medicines/human/EPAR/qdenga (accessed 2023-05-27).

Evans, J.D., Seeger, C., 2007. Differential Effects of Mutations in NS4B on West Nile Virus Replication and Inhibition of Interferon Signaling. J. Virol. 81(21):11809–11816. PMID: 17715229. DOI: 10.1128/JVI.00791-07

Falgout, B., Pethel, M., Zhang, Y.-M., Lai, C.-J., 1991. Both Nonstructural Proteins NS2B and NS3 Are Required for the Proteolytic Processing of Dengue Virus Nonstructural Proteins. J. Virol. 65(5):2467–2475. PMID: 2016768.

Fernandez, G.J., Ramírez-Mejía, J.M., Urcuqui-Inchima, S., 2022. Transcriptional and post-transcriptional mechanisms that regulate the genetic program in Zika virus-infected macrophages. Int. J. Biochem. Cell Biol. 153:106312. PMID: 36257579. DOI: 10.1016/j.biocel.2022.106312

Filomatori, C. V., Carballeda, J.M., Villordo, S.M., Aguirre, S., Pallarés, H.M., Maestre, A.M., Sánchez-Vargas, I., Blair, C.D., Fabri, C., Morales, M.A., Fernandez-Sesma, A., Gamarnik, A. V., 2017. Dengue virus genomic variation associated with mosquito adaptation defines the pattern of viral non-coding RNAs and fitness in human cells. PLoS Pathog. 13(3):e1006265. PMID: 28264033. DOI: 10.1371/journal.ppat.1006265

Flint, J., Racaniello, V.R., Rall, G.F., Skalka, A.M., 2015. Principles of Virology, 4th ed, Journal of Chemical Information and Modeling. ASM Press, Washington, DC. PMID: 25246403. DOI: 10.1017/CBO9781107415324.004

Franco, J.H., Chattopadhyay, S., Pan, Z.K., 2023. How Different Pathologies Are Affected by IFIT Expression. Viruses 15(2):342. PMID: 36851555. DOI: 10.3390/v15020342

Fredericks, A.M., Jentzsch, M.S., Cioffi, W.G., Cohen, M., Fairbrother, W.G., Gandhi, S.J., Harrington, E.O., Nau, G.J., Reichner, J.S., Ventetuolo, C.E., Levy, M.M., Ayala, A.,

Monaghan, S.F., 2022. Deep RNA sequencing of intensive care unit patients with COVID-19. Sci. Rep. 12(1):15755. PMID: 36130991. DOI: 10.1038/s41598-022-20139-1

Funk, A., Truong, K., Nagasaki, T., Torres, S., Floden, N., Balmori Melian, E., Edmonds, J., Dong, H., Shi, P.-Y., Khromykh, A.A., 2010. RNA Structures Required for Production of Subgenomic Flavivirus RNA. J. Virol. 84(21):11407–11417. PMID: 20719943. DOI: 10.1128/JVI.01159-10

Gack, M.U., Diamond, M.S., 2016. Innate immune escape by Dengue and West Nile viruses. Curr. Opin. Virol. 20:119–128. PMID: 27792906. DOI: 10.1016/j.coviro.2016.09.013

Gack, M.U., Shin, Y.C., Joo, C.-H., Urano, T., Liang, C., Sun, L., Takeuchi, O., Akira, S., Chen, Z., Inoue, S., Jung, J.U., 2007. TRIM25 RING-finger E3 ubiquitin ligase is essential for RIG-I-mediated antiviral activity. Nature 446(7138):916–920. PMID: 17392790. DOI: 10.1038/nature05732

Gaunt, M.W., Sall, A.A., de Lamballerie, X., Falconar, A.K.I., Dzhivanian, T.I., Gould, E.A., 2001. Phylogenetic relationships of flaviviruses correlate with their epidemiology, disease association and biogeography. J. Gen. Virol. 82(Pt 8):1867–1876. PMID: 11457992. DOI: 10.1099/0022-1317-82-8-1867

Gebhard, L.G., Kaufman, S.B., Gamarnik, A. V., 2012. Novel ATP-Independent RNA Annealing Activity of the Dengue Virus NS3 Helicase. PLoS One 7(4):e36244. PMID: 22558403. DOI: 10.1371/journal.pone.0036244

Geiss, B.J., Stahla-Beek, H.J., Hannah, A.M., Gari, H.H., Henderson, B.R., Saeedi, B.J., Keenan, S.M., 2011. A High-Throughput Screening Assay for the Identification of Flavivirus NS5 Capping Enzyme GTP-Binding Inhibitors: Implications for Antiviral Drug Development. J. Biomol. Screen. 16(8):852–861. PMID: 21788392. DOI: 10.1177/1087057111412183

Geiss, B.J., Thompson, A.A., Andrews, A.J., Sons, R.L., Gari, H.H., Keenan, S.M., Peersen, O.B., 2009. Analysis of Flavivirus NS5 Methyltransferase Cap Binding. J. Mol. Biol. 385(5):1643–1654. PMID: 19101564. DOI: 10.1016/j.jmb.2008.11.058

Gibney, E.R., Nolan, C.M., 2010. Epigenetics and gene expression. Heredity (Edinb). 105(1):4–13. PMID: 20461105. DOI: 10.1038/hdy.2010.54

Gillespie, L.K., Hoenen, A., Morgan, G., Mackenzie, J.M., 2010. The Endoplasmic

Reticulum Provides the Membrane Platform for Biogenesis of the Flavivirus Replication Complex. J. Virol. 84(20):10438–10447. PMID: 20686019. DOI: 10.1128/JVI.00986-10

Goethals, O., Kaptein, S.J.F., Kesteleyn, B., Bonfanti, J.-F., Van Wesenbeeck, L., Bardiot, D., Verschoor, E.J., Verstrepen, B.E., Fagrouch, Z., Putnak, J.R., Kiemel, D., Ackaert, O., Straetemans, R., Lachau-Durand, S., Geluykens, P., Crabbe, M., Thys, K., Stoops, B., Lenz, O., Tambuyzer, L., De Meyer, S., Dallmeier, K., McCracken, M.K., Gromowski, G.D., Rutvisuttinunt, W., Jarman, R.G., Karasavvas, N., Touret, F., Querat, G., de Lamballerie, X., Chatel-Chaix, L., Milligan, G.N., Beasley, D.W.C., Bourne, N., Barrett, A.D.T., Marchand, A., Jonckers, T.H.M., Raboisson, P., Simmen, K., Chaltin, P., Bartenschlager, R., Bogers, W.M., Neyts, J., Van Loock, M., 2023. Blocking NS3–NS4B interaction inhibits dengue virus in non-human primates. Nature 615(7953):678–686. PMID: 36922586. DOI: 10.1038/s41586-023-05790-6

Gómez-Herranz, M., Taylor, J., Sloan, R.D., 2023. IFITM proteins : Understanding their diverse roles in viral infection, cancer, and immunity. J. Biol. Chem. 299(1):102741. PMID: 36435199. DOI: 10.1016/j.jbc.2022.102741

Good, S.S., Shannon, A., Lin, K., Moussa, A., Julander, J.G., La Colla, P., Collu, G., Canard, B., Sommadossi, J.-P., 2021. Evaluation of AT-752, a Double Prodrug of a Guanosine Nucleotide Analog with In Vitro and In Vivo Activity against Dengue and Other Flaviviruses. Antimicrob. Agents Chemother. 65(11):e0098821. PMID: 34424050. DOI: 10.1128/AAC.00988-21

Gorbalenya, A.E., Donchenko, A.P., Koonin, E. V., Blinov, V.M., 1989. N-terminal domains of putative helicases of flavi- and pestiviruses may be serine proteases. Nucleic Acids Res. 17(10):3889–97. PMID: 2543956.

Guan, Y., Wang, Y., Fu, X., Bai, G., Li, X., Mao, J., Yan, Y., Hu, L., 2023. Multiple functions of stress granules in viral infection at a glance. Front. Microbiol. 14:1138864. PMID: 36937261. DOI: 10.3389/fmicb.2023.1138864

Guarner, J., Hale, G.L., 2019. Four human diseases with significant public health impact caused by mosquito-borne flaviviruses: West Nile, Zika, dengue and yellow fever. Semin. Diagn. Pathol. 36(3):170–176. PMID: 31006554. DOI: 10.1053/j.semdp.2019.04.009

Gunning, P.W., 2006. Protein Isoforms and Isozymes. Encycl. Life Sci. DOI: 10.1038/npg.els.0005717

Guo, F., Wu, S., Julander, J., Ma, J., Zhang, X., Kulp, J., Cuconati, A., Block, T.M., Du, Y., Guo, J.-T., Chang, J., 2016. A Novel Benzodiazepine Compound Inhibits Yellow Fever Virus Infection by Specifically Targeting NS4B Protein. J. Virol. 90(23):10774–10788. PMID: 27654301. DOI: 10.1128/JVI.01253-16

Gupta, N., Santhosh, S.R., Babu, J.P., Parida, M.M., Rao, P.V.L., 2010. Chemokine profiling of Japanese encephalitis virus-infected mouse neuroblastoma cells by microarray and real-time RT-PCR: Implication in neuropathogenesis. Virus Res. 147(1):107–112. PMID: 19896511. DOI: 10.1016/j.virusres.2009.10.018

Guy, B., Barrere, B., Malinowski, C., Saville, M., Teyssou, R., Lang, J., 2011. From research to phase III: Preclinical, industrial and clinical development of the Sanofi Pasteur tetravalent dengue vaccine. Vaccine 29(42):7229–7241. PMID: 21745521. DOI: 10.1016/j.vaccine.2011.06.094

Guyatt, K.J., Westaway, E.G., Khromykh, A.A., 2001. Expression and purification of enzymatically active recombinant RNA-dependent RNA polymerase (NS5) of the flavivirus Kunjin. J. Virol. Methods 92(1):37–44. PMID: 11164916. DOI: 10.1016/S0166-0934(00)00270-6

Hale, G.L., 2023. Flaviviruses and the Traveler: Around the World and to Your Stage. A Review of West Nile, Yellow Fever, Dengue, and Zika Viruses for the Practicing Pathologist. Mod. Pathol. 36(6):100188. PMID: 37059228. DOI: 10.1016/j.modpat.2023.100188

Haller, O., Kochs, G., Weber, F., 2006. The interferon response circuit: Induction and suppression by pathogenic viruses. Virology 344(1):119–130. PMID: 16364743. DOI: 10.1016/j.virol.2005.09.024

Harding, H.P., Calfon, M., Urano, F., Novoa, I., Ron, D., 2002. Transcriptional and Translational Control in the Mammalian Unfolded Protein Response. Annu. Rev. Cell Dev. Biol. 18:575–599. PMID: 12142265. DOI: 10.1146/annurev.cellbio.18.011402.160624

Haslbauer, J.D., Savic Prince, S., Stalder, A.K., Matter, M.S., Zinner, C.P., Jahn, K., Obermann, E., Hanke, J., Leuzinger, K., Hirsch, H.H., Tzankov, A., 2023. Differential

Gene Expression of SARS-CoV-2 Positive Bronchoalveolar Lavages: A Case Series. Pathobiology. DOI: 10.1159/000532057

Heaton, N.S., Perera, R., Berger, K.L., Khadka, S., LaCount, D.J., Kuhn, R.J., Randall, G., 2010. Dengue virus nonstructural protein 3 redistributes fatty acid synthase to sites of viral replication and increases cellular fatty acid synthesis. Proc. Natl. Acad. Sci. U. S. A. 107(40):17345–17350. PMID: 20855599. DOI: 10.1073/pnas.1010811107

Heck, A.M., Wilusz, J., 2018. The Interplay between the RNA Decay and Translation Machinery in Eukaryotes. Cold Spring Harb. Perspect. Biol. 10(5):a032839. PMID: 29311343. DOI: 10.1101/cshperspect.a032839

Heinz, F.X., Allison, S.L., 2000. Structures and Mechanisms in Flavivirus Fusion. Adv. Virus Res. 55:231–269. PMID: 11050944.

Hellen, C.U.T., 2018. Translation Termination and Ribosome Recycling in Eukaryotes. Cold Spring Harb. Perspect. Biol. 10(10):a032656. PMID: 29735640. DOI: 10.1101/cshperspect.a032656

Henderson, B.R., Saeedi, B.J., Campagnola, G., Geiss, B.J., 2011. Analysis of RNA Binding by the Dengue Virus NS5 RNA Capping Enzyme. PLoS One 6(10):e25795. PMID: 22022449. DOI: 10.1371/journal.pone.0025795

Hindle, E., 1928. A YELLOW FEVER VACCINE. Br. Med. J. 1(3518):976–977. PMID: 20773943. DOI: 10.1136/bmj.1.3518.976

History.com, 2021. Pandemics That Changed History [WWW Document]. URL https://www.history.com/topics/middle-ages/pandemics-timeline (accessed 2022-04-05).

Hiyoshi, A., Miyahara, K., Kato, C., Ohshima, Y., 2011. Does a DNA-less cellular organism exist on Earth? Genes to Cells 16(12):1146–1158. PMID: 22093146. DOI: 10.1111/j.1365-2443.2011.01558.x

Hoenen, A., Liu, W., Kochs, G., Khromykh, A.A., Mackenzie, J.M., 2007. West Nile virus-induced cytoplasmic membrane structures provide partial protection against the interferon-induced antiviral MxA protein. J. Gen. Virol. 88(11):3013–3017. PMID: 17947524. DOI: 10.1099/vir.0.83125-0

Horibata, S., Teramoto, T., Vijayarangan, N., Kuhn, S., Padmanabhan, Raji, Vasudevan, S., Gottesman, M., Padmanabhan, Radhakrishnan, 2021. Host gene expression modulated

by Zika virus infection of human-293 cells. Virology 552:32–42. PMID: 33059318. DOI: 10.1016/j.virol.2020.09.007

Horstick, O., Martinez, E., Guzman, M.G., San Martin, J.L., Ranzinger, S.R., 2015. WHO Dengue Case Classification 2009 and its usefulness in practice: an expert consensus in the Americas. Pathog. Glob. Health 109(1):19–25. PMID: 25630344. DOI: 10.1179/2047773215Y.0000000003

Hou, S., Kumar, A., Xu, Z., Airo, A.M., Stryapunina, I., Wong, C.P., Branton, W., Tchesnokov, E., Götte, M., Power, C., Hobman, T.C., 2017. Zika Virus Hijacks Stress Granule Proteins and Modulates the Host Stress Response. J. Virol. 91(16):e00474-17. PMID: 28592527. DOI: 10.1128/JVI.00474-17

Huang, C.Y.-H., Kinney, R.M., Livengood, J.A., Bolling, B., Arguello, J.J., Luy, B.E., Silengo, S.J., Boroughs, K.L., Stovall, J.L., Kalanidhi, A.P., Brault, A.C., Osorio, J.E., Stinchcomb, D.T., 2013. Genetic and Phenotypic Characterization of Manufacturing Seeds for a Tetravalent Dengue Vaccine (DENVax). PLoS Negl. Trop. Dis. 7(5):e2243. PMID: 23738026. DOI: 10.1371/journal.pntd.0002243

ICTV Executive Committee, 2020. The new scope of virus taxonomy: partitioning the virosphere into 15 hierarchical ranks. Nat. Microbiol. 5(5):668–674. PMID: 32341570. DOI: 10.1038/s41564-020-0709-x

Infectious Diseases Society of America, 2022. Facts about ID [WWW Document]. URL https://www.idsociety.org/public-health/facts-about-id/ (accessed 2022-04-04).

International Committee on Taxonomy of Viruses, 2019. Virus Taxonomy: 2019 Release [WWW Document]. URL https://talk.ictvonline.org/taxonomy/ (accessed 2020-08-06).

Issur, M., Geiss, B.J., Bougie, I., Picard-Jean, F., Despins, S., Mayette, J., Hobdey, S.E., Bisaillon, M., 2009. The flavivirus NS5 protein is a true RNA guanylyltransferase that catalyzes a two-step reaction to form the RNA cap structure. RNA 15(12):2340–2350. PMID: 19850911. DOI: 10.1261/rna.1609709

Ivashkiv, L.B., Donlin, L.T., 2014. Regulation of type I interferon responses. Nat. Rev. Immunol. 14(1):36–49. PMID: 24362405. DOI: 10.1038/nri3581

Jackson, R.J., Hellen, C.U.T., Pestova, T. V., 2010. The mechanism of eukaryotic translation initiation and principles of its regulation. Nat. Rev. Mol. Cell Biol. 11(2):113–127. PMID: 20094052. DOI: 10.1038/nrm2838

Jaenisch, R., Bird, A., 2003. Epigenetic regulation of gene expression: how the genome integrates intrinsic and environmental signals. Nat. Genet. 33 Suppl:245–254. PMID: 12610534. DOI: 10.1038/ng1089

Jain, R., Ramaswamy, S., Harilal, D., Uddin, M., Loney, T., Nowotny, N., Alsuwaidi, H., Varghese, R., Deesi, Z., Alkhajeh, A., Khansaheb, H., Alsheikh-Ali, A., Abou Tayoun, A., 2020. Host transcriptomic profiling of COVID-19 patients with mild, moderate, and severe clinical outcomes. Comput. Struct. Biotechnol. J. 19:153–160. PMID: 33425248. DOI: 10.1016/j.csbj.2020.12.016

Jarus, O., 2021. 20 of the worst epidemics and pandemics in history [WWW Document]. URL https://www.livescience.com/worst-epidemics-and-pandemics-in-history.html (accessed 2022-04-05).

Johansson, M., Brooks, A.J., Jans, D.A., Vasudevan, S.G., 2001. A small region of the dengue virus-encoded RNA-dependent RNA polymerase, NS5, confers interaction with both the nuclear transport receptor importin-β and the viral helicase, NS3. J. Gen. Virol. 82(4):735–745. PMID: 11257177. DOI: 10.1099/0022-1317-82-4-735

Jordan, T.X., Randall, G., 2016. Flavivirus modulation of cellular metabolism. Curr. Opin. Virol. 19:7–10. PMID: 27280383. DOI: 10.1016/j.coviro.2016.05.007

Julander, J.G., Demarest, J.F., Taylor, R., Gowen, B.B., Walling, D.M., Mathis, A., Babu, Y.S., 2021. An update on the progress of galidesivir (BCX4430), a broad-spectrum antiviral. Antiviral Res. 195:105180. PMID: 34551346. DOI: 10.1016/j.antiviral.2021.105180

Kapoor, M., Zhang, L., Ramachandra, M., Kusukawa, J., Ebner, K.E., Padmanabhan, R., 1995. Association between NS3 and NS5 Proteins of Dengue Virus Type 2 in the Putative RNA Replicase Is Linked to Differential Phosphorylation of NS5. J. Biol. Chem. 270(32):19100–19106. PMID: 7642575.

Kaptein, S.J.F., Goethals, O., Kiemel, D., Marchand, A., Kesteleyn, B., Bonfanti, J.-F., Bardiot, D., Stoops, B., Jonckers, T.H.M., Dallmeier, K., Geluykens, P., Thys, K., Crabbe, M., Chatel-Chaix, L., Münster, M., Querat, G., Touret, F., de Lamballerie, X., Raboisson, P., Simmen, K., Chaltin, P., Bartenschlager, R., Van Loock, M., Neyts, J., 2021. A pan-serotype dengue virus inhibitor targeting the NS3–NS4B interaction. Nature 598(7881):504–509. PMID: 34616043. DOI: 10.1038/s41586-021-03990-6

Kariyawasam, R., Lachman, M., Mansuri, S., Chakrabarti, S., Boggild, A.K., 2023. A dengue vaccine whirlwind update. Ther. Adv. Infect. Dis. 10:20499361231167270. PMID: 37114191. DOI: 10.1177/20499361231167274

Karp, G., 2010. Cell and Molecular Biology: Concepts and Experiments, 6th ed. John Wiley & Sons, Inc.

Katoh, H., Okamoto, T., Fukuhara, T., Kambara, H., Morita, E., Mori, Y., Kamitani, W., Matsuura, Y., 2013. Japanese Encephalitis Virus Core Protein Inhibits Stress Granule Formation through an Interaction with Caprin-1 and Facilitates Viral Propagation. J. Virol. 87(1):489–502. PMID: 23097442. DOI: 10.1128/JVI.02186-12

Kaufmann, B., Rossmann, M.G., 2011. Molecular mechanisms involved in the early steps of flavivirus cell entry. Microbes Infect. 13(1):1–9. PMID: 20869460. DOI: 10.1016/j.micinf.2010.09.005

Ke, P.-Y., 2018. The Multifaceted Roles of Autophagy in Flavivirus-Host Interactions. Int. J. Mol. Sci. 19(12):3940. PMID: 30544615. DOI: 10.3390/ijms19123940

Klema, V.J., Padmanabhan, R., Choi, K.H., 2015. Flaviviral Replication Complex: Coordination between RNA Synthesis and 5'-RNA Capping. Viruses 7(8):4640–4656. PMID: 26287232. DOI: 10.3390/v7082837

Koepke, L., Gack, M.U., Sparrer, K.M.J., 2021. The antiviral activities of TRIM proteins. Curr. Opin. Microbiol. 59:50–57. PMID: 32829025. DOI: 10.1016/j.mib.2020.07.005

Kumar, M., Altan-Bonnet, N., 2021. Viral pores are everywhere. Mol. Cell 81(10):2061–2063. PMID: 34019787. DOI: 10.1016/j.molcel.2021.04.025

Kumar, R., Tripathi, P., Rizvi, A., 2009. Effectiveness of One Dose of SA 14-14-2 Vaccine against Japanese Encephalitis. N. Engl. J. Med. 360(14):1465–1466. PMID: 19339732. DOI: 10.1056/NEJMc0808664

Kümmerer, B.M., Rice, C.M., 2002. Mutations in the Yellow Fever Virus Nonstructural Protein NS2A Selectively Block Production of Infectious Particles. J. Virol. 76(10):4773–4784. PMID: 11967294. DOI: 10.1128/JVI.76.10.4773-4784.2002

Kuno, G., Chang, G.-J., Tsuchiya, K.R., Karabatsos, N., Cropp, C.B., 1998. Phylogeny of the Genus Flavivirus. J. Virol. 72(1):73–83. PMID: 9420202.

Kurosaki, T., Maquat, L.E., 2016. Nonsense-mediated mRNA decay in humans at a glance. J. Cell Sci. 129(3):461–467. PMID: 26787741. DOI: 10.1242/jcs.181008

Kwan, T., Thompson, S.R., 2019. Noncanonical Translation Initiation in Eukaryotes. Cold Spring Harb. Perspect. Biol. 11(4):a032672. PMID: 29959190. DOI: 10.1101/cshperspect.a032672

Kyo, M., Ohtsuka, K., Okamoto, E., Inamori, K., 2009. High-Throughput SPR Biosensor. In: Walker, J.M. (Ed.), Methods in Molecular Biology. Springer, pp. 227–234. DOI: 10.1007/978-1-60761-232-2_17

Lai, Z., Zhou, T., Zhou, J., Liu, S., Xu, Y., Gu, J., Yan, G., Chen, X.-G., 2020. Vertical transmission of zika virus in Aedes albopictus. PLoS Negl. Trop. Dis. 14(10):e0008776. PMID: 33057411. DOI: 10.1371/journal.pntd.0008776

Lambert, S.A., Jolma, A., Campitelli, L.F., Das, P.K., Yin, Y., Albu, M., Chen, X., Taipale, J., Hughes, T.R., Weirauch, M.T., 2018. The Human Transcription Factors. Cell 172(4):650–665. PMID: 29425488. DOI: 10.1016/j.cell.2018.01.029

Latanova, A., Starodubova, E., Karpov, V., 2022. Flaviviridae Nonstructural Proteins: The Role in Molecular Mechanisms of Triggering Inflammation. Viruses 14(8):1808. PMID: 36016430. DOI: 10.3390/v14081808

Laurent-Rolle, M., Boer, E.F., Lubick, K.J., Wolfinbarger, J.B., Carmody, A.B., Rockx, B., Liu, W., Ashour, J., Shupert, W.L., Holbrook, M.R., Barrett, A.D., Mason, P.W., Bloom, M.E., García-Sastre, A., Khromykh, A.A., Best, S.M., 2010. The NS5 Protein of the Virulent West Nile Virus NY99 Strain Is a Potent Antagonist of Type I Interferon-Mediated JAK-STAT Signaling. J. Virol. 84(7):3503–3515. PMID: 20106931. DOI: 10.1128/JVI.01161-09

Lee, C.-J., Liao, C.-L., Lin, Y.-L., 2005. Flavivirus Activates Phosphatidylinositol 3-Kinase Signaling To Block Caspase-Dependent Apoptotic Cell Death at the Early Stage of Virus Infection. J. Virol. 79(13):8388–8399. PMID: 15956583. DOI: 10.1128/JVI.79.13.8388-8399.2005

Lee, L.J., Komarasamy, T.V., Adnan, N.A.A., James, W., RMT Balasubramaniam, V., 2021. Hide and Seek: The Interplay Between Zika Virus and the Host Immune Response. Front. Immunol. 12:750365. PMID: 34745123. DOI: 10.3389/fimmu.2021.750365

Lee, Y., Rio, D.C., 2015. Mechanisms and Regulation of Alternative Pre-mRNA Splicing. Annu. Rev. Biochem. 84:291–323. PMID: 25784052. DOI: 10.1146/annurev-biochem-060614-034316

Lennemann, N.J., Coyne, C.B., 2017. Dengue and Zika viruses subvert reticulophagy by NS2B3-mediated cleavage of FAM134B. Autophagy 13(2):322–332. PMID: 28102736. DOI: 10.1080/15548627.2016.1265192

Leung, J.Y., Pijlman, G.P., Kondratieva, N., Hyde, J., Mackenzie, J.M., Khromykh, A.A., 2008. Role of Nonstructural Protein NS2A in Flavivirus Assembly. J. Virol. 82(10):4731–4741. PMID: 18337583. DOI: 10.1128/JVI.00002-08

Li, H., Clum, S., You, S., Ebner, K.E., Padmanabhan, R., 1999. The Serine Protease and RNA-Stimulated Nucleoside Triphosphatase and RNA Helicase Functional Domains of Dengue Virus Type 2 NS3 Converge within a Region of 20 Amino Acids. J. Virol. 73(4):3108–3116. PMID: 10074162.

Li, J., Huang, Rongjie, Liao, W., Chen, Z., Zhang, S., Huang, Renbin, 2012. Dengue virus utilizes calcium modulating cyclophilin-binding ligand to subvert apoptosis. Biochem. Biophys. Res. Commun. 418(4):622–627. PMID: 22281498. DOI: 10.1016/j.bbrc.2012.01.050

Li, K., Phoo, W.W., Luo, D., 2014. Functional interplay among the flavivirus NS3 protease, helicase, and cofactors. Virol. Sin. 29(2):74–85. PMID: 24691778. DOI: 10.1007/s12250-014-3438-6

Li, W., Li, Y., Kedersha, N., Anderson, P., Emara, M., Swiderek, K.M., Moreno, G.T., Brinton, M.A., 2002. Cell Proteins TIA-1 and TIAR Interact with the 3' Stem-Loop of the West Nile Virus Complementary Minus-Strand RNA and Facilitate Virus Replication. J. Virol. 76(23):11989–12000. PMID: 12414941. DOI: 10.1128/JVI.76.23.11989-12000.2002

Li, W., Wang, Y., 2023. Stress granules: potential therapeutic targets for infectious and inflammatory diseases. Front. Immunol. 14:1145346. PMID: 37205103. DOI: 10.3389/fimmu.2023.1145346

Li, Y., Li, Q., Wong, Y.L., Liew, L.S.Y., Kang, C., 2015. Membrane topology of NS2B of dengue virus revealed by NMR spectroscopy. Biochim. Biophys. Acta 1848(10):2244–2252. PMID: 26072288. DOI: 10.1016/j.bbamem.2015.06.010

Li, Z., Brecher, M., Deng, Y.-Q., Zhang, J., Sakamuru, S., Liu, B., Huang, R., Koetzner, C.A., Allen, C.A., Jones, S.A., Chen, H., Zhang, N.-N., Tian, M., Gao, F., Lin, Q., Banavali, N., Zhou, J., Boles, N., Xia, M., Kramer, L.D., Qin, C.-F., Li, H., 2017.

Existing drugs as broad-spectrum and potent inhibitors for Zika virus by targeting NS2B-NS3 interaction. Cell Res. 27(8):1046–1064. PMID: 28685770. DOI: 10.1038/cr.2017.88

Liew, K.J.L., Chow, V.T.K., 2004. Differential Display RT-PCR Analysis of ECV304 Endothelial-Like Cells Infected with Dengue Virus Type 2 Reveals Messenger RNA Expression Profiles of Multiple Human Genes Involved in Known and Novel Roles. J. Med. Virol. 72(4):597–609. PMID: 14981762. DOI: 10.1002/jmv.20034

Lim, S.P., Noble, C.G., Shi, P.-Y., 2015. The dengue virus NS5 protein as a target for drug discovery. Antiviral Res. 119:57–67. PMID: 25912817. DOI: 10.1016/j.antiviral.2015.04.010

Lin, C., Amberg, S.M., Chambers, T.J., Rice, C.M., 1993. Cleavage at a Novel Site in the NS4A Region by the Yellow Fever Virus NS2B-3 Proteinase Is a Prerequisite for Processing at the Downstream 4A/4B Signalase Site. J. Virol. 67(4):2327–35. PMID: 8445732.

Lin, K.-C., Chang, H.-L., Chang, R.-Y., 2004. Accumulation of a 3′-Terminal Genome Fragment in Japanese Encephalitis Virus-Infected Mammalian and Mosquito Cells. J. Virol. 78(10):5133–5138. PMID: 15113895. DOI: 10.1128/jvi.78.10.5133-5138.2004

Lindenbach, B.D., Thiel, H.-J., Rice, C.M., 2007. Flaviviridae: The Viruses and Their Replication. In: Knipe, D.M., Howley, P.M. (Eds.), Fields Virology. Lippincott-Raven Publishers, pp. 1101–1152.

Liu, Q., Fang, L., Wu, C., 2022. Alternative Splicing and Isoforms: From Mechanisms to Diseases. Genes (Basel). 13(3):401. PMID: 35327956. DOI: 10.3390/genes13030401

Liu, W.J., Chen, H.B., Khromykh, A.A., 2003. Molecular and Functional Analyses of Kunjin Virus Infectious cDNA Clones Demonstrate the Essential Roles for NS2A in Virus Assembly and for a Nonconservative residue in NS3 in RNA replication. J. Virol. 77(14):7804–7813. PMID: 12829820. DOI: 10.1128/JVI.77.14.7804-7813.2003

Liu, W.J., Chen, H.B., Wang, X.J., Huang, H., Khromykh, A.A., 2004. Analysis of Adaptive Mutations in Kunjin Virus Replicon RNA Reveals a Novel Role for the Flavivirus Nonstructural Protein NS2A in Inhibition of Beta Interferon Promoter-Driven Transcription. J. Virol. 78(22):12225–12235. PMID: 15507609. DOI: 10.1128/JVI.78.22.12225-12235.2004

Liu, Y., Ford, B.D., Mann, M.A., Fischbach, G.D., 2005. Neuregulin-1 increases the proliferation of neuronal progenitors from embryonic neural stem cells. Dev. Biol. 283(2):437–445. PMID: 15949792. DOI: 10.1016/j.ydbio.2005.04.038

Lobigs, M., 1993. Flavivirus premembrane protein cleavage and spike heterodimer secretion require the function of the viral proteinase NS3. Proc. Natl. Acad. Sci. U. S. A. 90(13):6218–6222. PMID: 8392191.

Lu, G., Gong, P., 2013. Crystal Structure of the Full-Length Japanese Encephalitis Virus NS5 Reveals a Conserved Methyltransferase-Polymerase Interface. PLoS Pathog. 9(8):e1003549. PMID: 23950717. DOI: 10.1371/journal.ppat.1003549

Luo, D., Vasudevan, S.G., Lescar, J., 2015. The flavivirus NS2B-NS3 protease-helicase as a target for antiviral drug development. Antiviral Res. 118:148–158. PMID: 25842996. DOI: 10.1016/j.antiviral.2015.03.014

Luo, D., Wei, N., Doan, D.N., Paradkar, P.N., Chong, Y., Davidson, A.D., Kotaka, M., Lescar, J., Vasudevan, S.G., 2010. Flexibility between the Protease and Helicase Domains of the Dengue Virus NS3 Protein Conferred by the Linker Region and Its Functional Implications. J. Biol. Chem. 285(24):18817–18827. PMID: 20375022. DOI: 10.1074/jbc.M109.090936

Luo, D., Xu, T., Hunke, C., Grüber, G., Vasudevan, S.G., Lescar, J., 2008a. Crystal Structure of the NS3 Protease-Helicase from Dengue Virus. J. Virol. 82(1):173–183. PMID: 17942558. DOI: 10.1128/JVI.01788-07

Luo, D., Xu, T., Watson, R.P., Scherer-Becker, D., Sampath, A., Jahnke, W., Yeong, S.S., Wang, C.H., Lim, S.P., Strongin, A., Vasudevan, S.G., Lescar, J., 2008b. Insights into RNA unwinding and ATP hydrolysis by the flavivirus NS3 protein. EMBO J. 27(23):3209–3219. PMID: 19008861. DOI: 10.1038/emboj.2008.232

Mackenzie, J.M., Jones, M.K., Young, P.R., 1996. Immunolocalization of the Dengue Virus Nonstructural Glycoprotein NS1 Suggests a Role in Viral RNA Replication. Virology 220(1):232–240. PMID: 8659120. DOI: 10.1006/viro.1996.0307

Mackenzie, J.M., Khromykh, A.A., Jones, M.K., Westaway, E.G., 1998. Subcellular Localization and Some Biochemical Properties of the Flavivirus Kunjin Nonstructural Proteins NS2A and NS4A. Virology 245(2):203–215. PMID: 9636360. DOI: 10.1006/viro.1998.9156

Malet, H., Egloff, M.-P., Selisko, B., Butcher, R.E., Wright, P.J., Roberts, M., Gruez, A., Sulzenbacher, G., Vonrhein, C., Bricogne, G., Mackenzie, J.M., Khromykh, A.A., Davidson, A.D., Canard, B., 2007. Crystal Structure of the RNA Polymerase Domain of the West Nile Virus Non-structural Protein 5. J. Biol. Chem. 282(14):10678–10689. PMID: 17287213. DOI: 10.1074/jbc.M607273200

Mao, J., Lin, E., He, L., Yu, J., Tan, P., Zhou, Y., 2019. Autophagy and viral infection. In: Autophagy Regulation of Innate Immunity. Advances in Experimental Medicine and Biology. Springer Singapore, pp. 55–78. PMID: 31728865. DOI: 10.1007/978-981-15-0606-2_5

Marasco, L.E., Kornblihtt, A.R., 2023. The physiology of alternative splicing. Nat. Rev. Mol. Cell Biol. 24(4):242–254. PMID: 36229538. DOI: 10.1038/s41580-022-00545-z

Marcello, A., Loregian, A., Cross, A., Marsden, H., Hirst, T.R., Palù, G., 1994. Specific inhibition of herpes virus replication by receptor-mediated entry of an antiviral peptide linked to Escherichia coli enterotoxin B subunit. Proc. Natl. Acad. Sci. U. S. A. 91(19):8994–8998. PMID: 8090758. DOI: 10.1073/pnas.91.19.8994

Mastrangelo, E., Bolognesi, M., Milani, M., 2012. Flaviviral helicase: Insights into the mechanism of action of a motor protein. Biochem. Biophys. Res. Commun. 417(1):84–87. PMID: 22138238. DOI: 10.1016/j.bbrc.2011.11.060

Mastrangelo, E., Milani, M., Bollati, M., Selisko, B., Peyrane, F., Pandini, V., Sorrentino, G., Canard, B., Konarev, P. V., Svergun, D.I., de Lamballerie, X., Coutard, B., Khromykh, A.A., Bolognesi, M., 2007. Crystal Structure and Activity of Kunjin Virus NS3 Helicase; Protease and Helicase Domain Assembly in the Full Length NS3 Protein. J. Mol. Biol. 372(2):444–455. PMID: 17658551. DOI: 10.1016/j.jmb.2007.06.055

Mayo Clinic, 2022. Dengue fever [WWW Document]. URL https://www.mayoclinic.org/diseases-conditions/dengue-fever/diagnosis-treatment/drc-20353084 (accessed 2023-07-06).

McCormick, C., Khaperskyy, D.A., 2017. Translation inhibition and stress granules in the antiviral immune response. Nat. Rev. Immunol. 17(10):647–660. PMID: 28669985. DOI: 10.1038/nri.2017.63

McNab, F., Mayer-Barber, K., Sher, A., Wack, A., O'Garra, A., 2015. Type I interferons in infectious disease. Nat. Rev. Immunol. 15(2):87–103. PMID: 25614319. DOI:

10.1038/nri3787

Mehta, P., Chattopadhyay, P., Ravi, V., Tarai, B., Budhiraja, S., Pandey, R., 2023. SARS-CoV-2 infection severity and mortality is modulated by repeat-mediated regulation of alternative splicing. Microbiol. Spectr. e0135123. PMID: 37604131. DOI: 10.1128/spectrum.01351-23

Mendoza-Cano, O., Hernandez-Suarez, C.M., Trujillo, X., Diaz-Lopez, H.O., Lugo-Radillo, A., Espinoza-Gomez, F., de la Cruz-Ruiz, M., Sánchez-Piña, R.A., Murillo-Zamora, E., 2017. Cost-Effectiveness of the Strategies to Reduce the Incidence of Dengue in Colima, México. Int. J. Environ. Res. Public Health 14(8):890. PMID: 28786919. DOI: 10.3390/ijerph14080890

Merrick, W.C., Pavitt, G.D., 2018. Protein Synthesis Initiation in Eukaryotic Cells. Cold Spring Harb. Perspect. Biol. 10(12):a033092. PMID: 29735639. DOI: 10.1101/cshperspect.a033092

Mesev, E. V., LeDesma, R.A., Ploss, A., 2019. Decoding type I and III interferon signalling during viral infection. Nat. Microbiol. 4(6):914–924. PMID: 30936491. DOI: 10.1038/s41564-019-0421-x

Michalski, D., Ontiveros, J.G., Russo, J., Charley, P.A., Anderson, J.R., Heck, A.M., Geiss, B.J., Wilusz, J., 2019. Zika virus noncoding sfRNAs sequester multiple host-derived RNA-binding proteins and modulate mRNA decay and splicing during infection. J. Biol. Chem. 294(44):16282–16296. PMID: 31519749. DOI: 10.1074/jbc.RA119.009129

Miller, S., Kastner, S., Krijnse-Locker, J., Bühler, S., Bartenschlager, R., 2007. The Non-structural Protein 4A of Dengue Virus Is an Integral Membrane Protein Inducing Membrane Alterations in a 2K-regulated Manner. J. Biol. Chem. 282(12):8873–8882. PMID: 17276984. DOI: 10.1074/jbc.M609919200

Miller, S., Krijnse-Locker, J., 2008. Modification of intracellular membrane structures for virus replication. Nat. Rev. Microbiol. 6(5):363–374. PMID: 18414501. DOI: 10.1038/nrmicro1890

Miller, S., Sparacio, S., Bartenschlager, R., 2006. Subcellular Localization and Membrane Topology of the Dengue Virus Type 2 Non-structural Protein 4B. J. Biol. Chem. 281(13):8854–8863. PMID: 16436383. DOI: 10.1074/jbc.M512697200

Miorin, L., Romero-Brey, I., Maiuri, P., Hoppe, S., Krijnse-Locker, J., Bartenschlager, R.,

Marcello, A., 2013. Three-Dimensional Architecture of Tick-Borne Encephalitis Virus Replication Sites and Trafficking of the Replicated RNA. J. Virol. 87(11):6469–6481. PMID: 23552408. DOI: 10.1128/JVI.03456-12

Mitsis, T., Efthimiadou, A., Bacopoulou, F., Vlachakis, D., Chrousos, G.P., Eliopoulos, E., 2020. Transcription factors and evolution: An integral part of gene expression (Review). World Acad. Sci. J. 2:3–8. DOI: 10.3892/wasj.2020.32

Monath, T.P., 2001. Yellow fever: an update. Lancet Infect. Dis. 1(1):11–20. PMID: 11871403. DOI: 10.1016/S1473-3099(01)00016-0

Moon, S.L., Anderson, J.R., Kumagai, Y., Wilusz, C.J., Akira, S., Khromykh, A.A., Wilusz, J., 2012. A noncoding RNA produced by arthropod-borne flaviviruses inhibits the cellular exoribonuclease XRN1 and alters host mRNA stability. RNA 18(11):2029–2040. PMID: 23006624. DOI: 10.1261/rna.034330.112

Moquin, S.A., Simon, O., Karuna, R., Lakshminarayana, S.B., Yokokawa, F., Wang, F., Saravanan, C., Zhang, J., Day, C.W., Chan, K., Wang, Q.-Y., Lu, S., Dong, H., Wan, K.F., Lim, S.P., Liu, W., Seh, C.C., Chen, Y.-L., Xu, H., Barkan, D.T., Kounde, C.S., Sim, W.L.S., Wang, G., Yeo, H.-Q., Zou, B., Chan, W.L., Ding, M., Song, J.-G., Li, M., Osborne, C., Blasco, F., Sarko, C., Beer, D., Bonamy, G.M.C., Sasseville, V.G., Shi, P.-Y., Diagana, T.T., Yeung, B.K.S., Gu, F., 2021. NITD-688, a pan-serotype inhibitor of the dengue virus NS4B protein, shows favorable pharmacokinetics and efficacy in preclinical animal models. Sci. Transl. Med. 13(579):eabb2181. PMID: 33536278. DOI: 10.1126/scitranslmed.abb2181

Moreland, N.J., Tay, M.Y.F., Lim, E., Rathore, A.P.S., Lim, A.P.C., Hanson, B.J., Vasudevan, S.G., 2012. Monoclonal antibodies against dengue NS2B and NS3 proteins for the study of protein interactions in the flaviviral replication complex. J. Virol. Methods 179(1):97–103. PMID: 22040846. DOI: 10.1016/j.jviromet.2011.10.006

Mukhopadhyay, S., Kuhn, R.J., Rossmann, M.G., 2005. A structural perspective of the flavivirus life cycle. Nat. Rev. Microbiol. 3(1):13–22. PMID: 15608696. DOI: 10.1038/nrmicro1067

Muller, D.A., Young, P.R., 2013. The flavivirus NS1 protein: Molecular and structural biology, immunology, role in pathogenesis and application as a diagnostic biomarker. Antiviral Res. 98(2):192–208. PMID: 23523765. DOI: 10.1016/j.antiviral.2013.03.008

Muñoz-Jordán, J.L., Laurent-Rolle, M., Ashour, J., Martínez-Sobrido, L., Ashok, M., Lipkin, W.I., García-Sastre, A., 2005. Inhibition of Alpha/Beta Interferon Signaling by the NS4B Protein of Flaviviruses. J. Virol. 79(13):8004–8013. PMID: 15956546. DOI: 10.1128/JVI.79.13.8004-8013.2005

Muñoz-Jordán, J.L., Sánchez-Burgos, G.G., Laurent-Rolle, M., García-Sastre, A., 2003. Inhibition of interferon signaling by dengue virus. Proc. Natl. Acad. Sci. U. S. A. 100(24):14333–14338. PMID: 14612562. DOI: 10.1073/pnas.2335168100

Muylaert, I.R., Chambers, T.J., Galler, R., Rice, C.M., 1996. Mutagenesis of the N-Linked Glycosylation Sites of the Yellow Fever Virus NS1 Protein: Effects on Virus Replication and Mouse Neurovirulence. Virology 222(1):159–168. PMID: 8806496. DOI: 10.1006/viro.1996.0406

NCBI, 2023. RIMS1 regulating synaptic membrane exocytosis 1 [Homo sapiens (human)] [WWW Document]. URL https://www.ncbi.nlm.nih.gov/gene/22999 (accessed 2023-07-04).

Nelms, B.M., Fechter-Leggett, E., Carroll, B.D., Macedo, P., Kluh, S., Reisen, W.K., 2013. Experimental and Natural Vertical Transmission of West Nile Virus by California Culex (Diptera: Culicidae) Mosquitoes. J. Med. Entomol. 50(2):371–378. PMID: 23540126. DOI: 10.1603/me12264

Nemésio, H., Palomares-Jerez, F., Villalaín, J., 2012. NS4A and NS4B proteins from dengue virus: Membranotropic regions. Biochim. Biophys. Acta 1818(11):2818–2830. PMID: 22772157. DOI: 10.1016/j.bbamem.2012.06.022

Nie, L., Wu, G., Culley, D.E., Scholten, J.C.M., Zhang, W., 2007. Integrative Analysis of Transcriptomic and Proteomic Data: Challenges, Solutions and Applications. Crit. Rev. Biotechnol. 27(2):63–75. PMID: 17578703. DOI: 10.1080/07388550701334212

Ning, S., Pagano, J.S., Barber, G.N., 2011. IRF7: activation, regulation, modification and function. Genes Immun. 12(6):399–414. PMID: 21490621. DOI: 10.1038/gene.2011.21

Noble, C.G., Shi, P.-Y., 2012. Structural biology of dengue virus enzymes: Towards rational design of therapeutics. Antiviral Res. 96(2):115–126. PMID: 22995600. DOI: 10.1016/j.antiviral.2012.09.007

Nomaguchi, M., Ackermann, M., Yon, C., You, S., Padmanbhan, R., 2003. De Novo Synthesis of Negative-Strand RNA by Dengue Virus RNA-Dependent RNA

Polymerase In Vitro: Nucleotide, Primer, and Template Parameters. J. Virol. 77(16):8831–8842. PMID: 12885902. DOI: 10.1128/JVI.77.16.8831-8842.2003

Norshidah, H., Vignesh, R., Lai, N.S., 2021. Updates on Dengue Vaccine and Antiviral: Where Are We Heading? Molecules 26(22):6768. PMID: 34833860. DOI: 10.3390/molecules26226768

O'Neal, J.T., Upadhyay, A.A., Wolabaugh, A., Patel, N.B., Bosinger, S.E., Suthar, M.S., 2019. West Nile Virus-Inclusive Single-Cell RNA Sequencing Reveals Heterogeneity in the Type I Interferon Response within Single Cells. J. Virol. 93(6):e01778-18. PMID: 30626670. DOI: 10.1128/JVI.01778-18

Ohrr, H., Tandan, J.B., Sohn, Y.M., Shin, S.H., Pradhan, D.P., Halstead, S.B., 2005. Effect of single dose of SA 14-14-2 vaccine 1 year after immunisation in Nepalese children with Japanese encephalitis: a case-control study. Lancet 366(9494):1375–1378. PMID: 16226615. DOI: 10.1016/S0140-6736(05)67567-8

Okamoto, T., Suzuki, T., Kusakabe, S., Tokunaga, M., Hirano, J., Miyata, Y., Matsuura, Y., 2017. Regulation of Apoptosis during Flavivirus Infection. Viruses 9(9):243. PMID: 28846635. DOI: 10.3390/v9090243

Pan American Health Organization, 2023. Yellow Fever [WWW Document]. URL https://www.paho.org/en/topics/yellow-fever (accessed 2023-08-28).

Pan, Y., Cheng, A., Wang, M., Yin, Z., Jia, R., 2021. The Dual Regulation of Apoptosis by Flavivirus. Front. Microbiol. 12:654494. PMID: 33841381. DOI: 10.3389/fmicb.2021.654494

Parzych, K.R., Klionsky, D.J., 2014. An Overview of Autophagy: Morphology, Mechanism, and Regulation. Antioxidants Redox Signal. 20(3):460–473. PMID: 23725295. DOI: 10.1089/ars.2013.5371

Pastorino, B., Boucomont-Chapeaublanc, E., Peyrefitte, C.N., Belghazi, M., Fusaï, T., Rogier, C., Tolou, H.J., Almeras, L., 2009. Identification of Cellular Proteome Modifications in Response to West Nile Virus Infection. Mol. Cell. Proteomics 8(7):1623–1637. PMID: 19395707. DOI: 10.1074/mcp.M800565-MCP200

Patkar, C.G., Kuhn, R.J., 2008. Yellow Fever Virus NS3 Plays an Essential Role in Virus Assembly Independent of Its Known Enzymatic Functions. J. Virol. 82(7):3342–3352. PMID: 18199634. DOI: 10.1128/JVI.02447-07

Pattanakitsakul, S., Rungrojcharoenkit, K., Kanlaya, R., Sinchaikul, S., Noisakran, S., Chen, S.-T., Malasit, P., Thongboonkerd, V., 2007. Proteomic Analysis of Host Responses in HepG2 Cells during Dengue Virus Infection. J. Proteome Res. 6(12):4592–4600. PMID: 17979228. DOI: 10.1021/pr070366b

Paul, D., Bartenschlager, R., 2013. Architecture and biogenesis of plus-strand RNA virus replication factories. World J. Virol. 2(2):32–48. PMID: 24175228. DOI: 10.5501/wjv.v2.i2.32

Peña, J., Harris, E., 2011. Dengue Virus Modulates the Unfolded Protein Response in a Time-dependent Manner. J. Biol. Chem. 286(16):14226–14236. PMID: 21385877. DOI: 10.1074/jbc.M111.222703

Perera-Lecoin, M., Meertens, L., Carnec, X., Amara, A., 2013. Flavivirus Entry Receptors: An Update. Viruses 6(1):69–88. PMID: 24381034. DOI: 10.3390/v6010069

Perera, N., Miller, J.L., Zitzmann, N., 2017. The role of the unfolded protein response in dengue virus pathogenesis. Cell. Microbiol. 19(5). PMID: 28207988. DOI: 10.1111/cmi.12734

Perera, R., Kuhn, R.J., 2008. Structural proteomics of dengue virus. Curr. Opin. Microbiol. 11(4):369–377. PMID: 18644250. DOI: 10.1016/j.mib.2008.06.004

Persoon, C.M., Hoogstraaten, R.I., Nassal, J.P., van Weering, J.R.T., Kaeser, P.S., Toonen, R.F., Verhage, M., 2019. The RAB3-RIM Pathway Is Essential for the Release of Neuromodulators. Neuron 104(6):1065-1080.e12. PMID: 31679900. DOI: 10.1016/j.neuron.2019.09.015

Pierce, M.M., Raman, C.S., Nall, B.T., 1999. Isothermal Titration Calorimetry of Protein-Protein Interactions. Methods 19(2):213–221. PMID: 10527727. DOI: 10.1006/meth.1999.0852

Pijlman, G.P., Funk, A., Kondratieva, N., Leung, J., Torres, S., van der Aa, L., Liu, W.J., Palmenberg, A.C., Shi, P.-Y., Hall, R.A., Khromykh, A.A., 2008. A Highly Structured, Nuclease-Resistant, Noncoding RNA Produced by Flaviviruses Is Required for Pathogenicity. Cell Host Microbe 4(6):579–591. PMID: 19064258. DOI: 10.1016/j.chom.2008.10.007

Pindel, A., Sadler, A., 2011. The Role of Protein Kinase R in the Interferon Response. J. Interf. Cytokine Res. 31(1):59–70. PMID: 21166592. DOI: 10.1089/jir.2010.0099

Platanias, L.C., 2005. Mechanisms of type-I- and type-II-interferon-mediated signalling. Nat. Rev. Immunol. 5(5):375–386. PMID: 15864272. DOI: 10.1038/nri1604

Pozzi, B., Bragado, L., Mammi, P., Torti, M.F., Gaioli, N., Gebhard, L.G., García Solá, M.E., Vaz-Drago, R., Iglesias, N.G., García, C.C., Gamarnik, A. V., Srebrow, A., 2020. Dengue virus targets RBM10 deregulating host cell splicing and innate immune response. Nucleic Acids Res. 48(12):6824–6838. PMID: 32432721. DOI: 10.1093/nar/gkaa340

Preugschat, F., Yao, C.-W., Strauss, J.H., 1990. In vitro Processing of Dengue Virus Type 2 Nonstructural Proteins NS2A, NS2B, and NS3. J. Virol. 64(9):4364–4374. PMID: 2143543.

Protter, D.S.W., Parker, R., 2016. Principles and Properties of Stress Granules. Trends Cell Biol. 26(9):668–679. PMID: 27289443. DOI: 10.1016/j.tcb.2016.05.004

Proudfoot, N.J., 2016. Transcriptional termination in mammals: Stopping the RNA polymerase II juggernaut. Science 352(6291):aad9926. PMID: 27284201. DOI: 10.1126/science.aad9926

Qian, F., Chung, L., Zheng, W., Bruno, V., Alexander, R.P., Wang, Z., Wang, X., Kurscheid, S., Zhao, H., Fikrig, E., Gerstein, M., Snyder, M., Montgomery, R.R., 2013. Identification of Genes Critical for Resistance to Infection by West Nile Virus Using RNA-Seq Analysis. Viruses 5(7):1664–1681. PMID: 23881275. DOI: 10.3390/v5071664

Qian, X., Qi, Z., 2022. Mosquito-Borne Flaviviruses and Current Therapeutic Advances. Viruses 14(6):1226. PMID: 35746697. DOI: 10.3390/v14061226

Rahman, M.M., McFadden, G., 2011. Modulation of NF-κB signalling by microbial pathogens. Nat. Rev. Microbiol. 9(4):291–306. PMID: 21383764. DOI: 10.1038/nrmicro2539

Ramírez-Clavijo, S., Montoya-Ortíz, G., 2013. Gene expression and regulation. In: Anaya, J.-M., Shoenfeld, Y., Rojas-Villarraga, A., Levy, R.A., Cervera, R. (Eds.), Autoimmunity: From Bench to Bedside. El Rosario University Press, Bogota (Columbia).

Rathore, A.P.S., Paradkar, P.N., Watanabe, S., Tan, K.H., Sung, C., Connolly, J.E., Low, J., Ooi, E.E., Vasudevan, S.G., 2011. Celgosivir treatment misfolds dengue virus NS1

protein, induces cellular pro-survival genes and protects against lethal challenge mouse model. Antiviral Res. 92(3):453–460. PMID: 22020302. DOI: 10.1016/j.antiviral.2011.10.002

Rathore, A.P.S., St. John, A.L., 2020. Cross-Reactive Immunity Among Flaviviruses. Front. Immunol. 11:334. PMID: 32174923. DOI: 10.3389/fimmu.2020.00334

Ray, D., Shah, A., Tilgner, M., Guo, Y., Zhao, Y., Dong, H., Deas, T.S., Zhou, Y., Li, H., Shi, P.-Y., 2006. West Nile Virus 5'-Cap Structure Is Formed by Sequential Guanine N-7 and Ribose 2'-O Methylations by Nonstructural Protein 5. J. Virol. 80(17):8362–8370. PMID: 16912287. DOI: 10.1128/JVI.00814-06

Riva, L., Goellner, S., Biering, S.B., Huang, C.-T., Rubanov, A.N., Haselmann, U., Warnes, C.M., De Jesus, P.D., Martin-Sancho, L., Terskikh, A. V., Harris, E., Pinkerton, A.B., Bartenschlager, R., Chanda, S.K., 2021. The Compound SBI-0090799 Inhibits Zika Virus Infection by Blocking De Novo Formation of the Membranous Replication Compartment. J. Virol. 95(22):e0099621. PMID: 34468177. DOI: 10.1128/JVI.00996-21

Roosendaal, J., Westaway, E.G., Khromykh, A., Mackenzie, J.M., 2006. Regulated Cleavages at the West Nile Virus NS4A-2K-NS4B Junctions Play a Major Role in Rearranging Cytoplasmic Membranes and Golgi Trafficking of the NS4A Protein. J. Virol. 80(9):4623–4632. PMID: 16611922. DOI: 10.1128/JVI.80.9.4623-4632.2006

Rosen, L., 1987. Mechanism of vertical transmission of the dengue virus in mosquitoes. C. R. Acad. Sci. III. 304(13):347–350. PMID: 3105828.

Rosen, L., 1988. Further observations on the mechanism of vertical transmission of flaviviruses by Aedes mosquitoes. Am. J. Trop. Med. Hyg. 39(1):123–126. PMID: 2840833. DOI: 10.4269/ajtmh.1988.39.123

Roth, H., Magg, V., Uch, F., Mutz, P., Klein, P., Haneke, K., Lohmann, V., Bartenschlager, R., Fackler, O.T., Locker, N., Stoecklin, G., Ruggieri, A., 2017. Flavivirus Infection Uncouples Translation Suppression from Cellular Stress Responses. MBio 8(1):e02150-16. PMID: 28074025. DOI: 10.1128/mBio.02150-16

Saeedi, B.J., Geiss, B.J., 2013. Regulation of flavivirus RNA synthesis and capping. Wiley Interdiscip. Rev. RNA 4(6):723–735. PMID: 23929625. DOI: 10.1002/wrna.1191

Sammeth, M., Foissac, S., Guigó, R., 2008. A General Definition and Nomenclature for

Alternative Splicing Events. PLoS Comput. Biol. 4(8):e1000147. PMID: 18688268. DOI: 10.1371/journal.pcbi.1000147

Sampath, A., Padmanabhan, R., 2009. Molecular targets for flavivirus drug discovery. Antiviral Res. 81(1):6–15. PMID: 18796313. DOI: 10.1016/j.antiviral.2008.08.004

Sampath, A., Xu, T., Chao, A., Luo, D., Lescar, J., Vasudevan, S.G., 2006. Structure-Based Mutational Analysis of the NS3 Helicase from Dengue Virus. J. Virol. 80(13):6686–6690. PMID: 16775356. DOI: 10.1128/JVI.02215-05

Samrat, S.K., Xu, J., Li, Z., Zhou, J., Li, H., 2022. Antiviral Agents against Flavivirus Protease: Prospect and Future Direction. Pathogens 11(3):293. PMID: 35335617. DOI: 10.3390/pathogens11030293

Samuel, M.A., Whitby, K., Keller, B.C., Marri, A., Barchet, W., Williams, B.R.G., Silverman, R.H., Gale, M.J., Diamond, M.S., 2006. PKR and RNase L Contribute to Protection against Lethal West Nile Virus Infection by Controlling Early Viral Spread in the Periphery and Replication in Neurons. J. Virol. 80(14):7009–7019. PMID: 16809306. DOI: 10.1128/JVI.00489-06

Schalich, J., Allison, S.L., Stiasny, K., Mandl, C.W., Kunz, C., Heinz, F.X., 1996. Recombinant Subviral Particles from Tick-Borne Encephalitis Virus Are Fusogenic and Provide a Model System for Studying Flavivirus Envelope Glycoprotein Functions. J. Virol. 70(7):4549–4557. PMID: 8676481.

Schlee, M., Hartmann, G., 2016. Discriminating self from non-self in nucleic acid sensing. Nat. Rev. Immunol. 16(9):566–580. PMID: 27455396. DOI: 10.1038/nri.2016.78

Schroder, K., Hertzog, P.J., Ravasi, T., Hume, D.A., 2004. Interferon-γ: an overview of signals, mechanisms and functions. J. Leukoc. Biol. 75(2):163–189. PMID: 14525967. DOI: 10.1189/jlb.0603252

Selisko, B., Dutartre, H., Guillemot, J.-C., Debarnot, C., Benarroch, D., Khromykh, A., Desprès, P., Egloff, M.-P., Canard, B., 2006. Comparative mechanistic studies of de novo RNA synthesis by flavivirus RNA-dependent RNA polymerases. Virology 351(1):145–158. PMID: 16631221. DOI: 10.1016/j.virol.2006.03.026

Selisko, B., Potisopon, S., Agred, R., Priet, S., Varlet, I., Thillier, Y., Sallamand, C., Debart, F., Vasseur, J.-J., Canard, B., 2012. Molecular Basis for Nucleotide Conservation at the Ends of the Dengue Virus Genome. PLoS Pathog. 8(9):e1002912. PMID: 23028313.

DOI: 10.1371/journal.ppat.1002912

Sessions, O.M., Tan, Y., Goh, K.C., Liu, Y., Tan, P., Rozen, S., Ooi, E.E., 2013. Host Cell Transcriptome Profile during Wild-Type and Attenuated Dengue Virus Infection. PLoS Negl. Trop. Dis. 7(3):e2107. PMID: 23516652. DOI: 10.1371/journal.pntd.0002107

Shen, Y., Li, N.L., Wang, J., Liu, B., Lester, S., Li, K., 2012. TRIM56 Is an Essential Component of the TLR3 Antiviral Signaling Pathway. J. Biol. Chem. 287(43):36404–36413. PMID: 22948160. DOI: 10.1074/jbc.M112.397075

Shiryaev, S.A., Chernov, A. V., Aleshin, A.E., Shiryaeva, T.N., Strongin, A.Y., 2009. NS4A regulates the ATPase activity of the NS3 helicase: a novel cofactor role of the non-structural protein NS4A from West Nile virus. J. Gen. Virol. 90(9):2081–2085. PMID: 19474250. DOI: 10.1099/vir.0.012864-0

Shivaprasad, S., Sarnow, P., 2021. The tale of two flaviviruses: subversion of host pathways by RNA shapes in dengue and hepatitis C viral RNA genomes. Curr. Opin. Microbiol. 59:79–85. PMID: 33070015. DOI: 10.1016/j.mib.2020.08.007

Silva, P.A.G.C., Pereira, C.F., Dalebout, T.J., Spaan, W.J.M., Bredenbeek, P.J., 2010. An RNA Pseudoknot Is Required for Production of Yellow Fever Virus Subgenomic RNA by the Host Nuclease XRN1. J. Virol. 84(21):11395–11406. PMID: 20739539. DOI: 10.1128/JVI.01047-10

Silverman, R.H., 2007. Viral Encounters with 2',5'-Oligoadenylate Synthetase and RNase L during the Interferon Antiviral Response. J. Virol. 81(23):12720–12729. PMID: 17804500. DOI: 10.1128/JVI.01471-07

Slonchak, A., Khromykh, A.A., 2018. Subgenomic flaviviral RNAs: What do we know after the first decade of research. Antiviral Res. 159:13–25. PMID: 30217649. DOI: 10.1016/j.antiviral.2018.09.006

Snustad, D.P., Simmons, M.J., 2012. Principles of Genetics, 6th ed. John Wiley & Sons, Inc.

Song, Y., Mugavero, J., Stauft, C.B., Wimmer, E., 2019. Dengue and Zika Virus 5' Untranslated Regions Harbor Internal Ribosomal Entry Site Functions. MBio 10(2):e00459-19. PMID: 30967466. DOI: 10.1128/mBio.00459-19

Soo, K.M., Khalid, B., Ching, S.M., Chee, H.Y., 2016. Meta-analysis of dengue severity during infection by different dengue virus serotypes in primary and secondary infections. PLoS One 11(5):4–14. PMID: 27213782. DOI:

10.1371/journal.pone.0154760

Sotcheff, S.L., Chen, J.Y.C., Elrod, N., Cao, J., Jaworski, E., Kuyumcu-Martinez, M.N., Shi, P.Y., Routh, A.L., 2022. Zika Virus Infection Alters Gene Expression and Poly-Adenylation Patterns in Placental Cells. Pathogens 11(8):1–17. DOI: 10.3390/pathogens11080936

Stahla-Beek, H.J., April, D.G., Saeedi, B.J., Hannah, A.M., Keenan, S.M., Geiss, B.J., 2012. Identification of a Novel Antiviral Inhibitor of the Flavivirus Guanylyltransferase Enzyme. J. Virol. 86(16):8730–8739. PMID: 22674988. DOI: 10.1128/JVI.00384-12

Stanifer, M.L., Pervolaraki, K., Boulant, S., 2019. Differential Regulation of Type I and Type III Interferon Signaling. Int. J. Mol. Sci. 20(6):1445. PMID: 30901970. DOI: 10.3390/ijms20061445

Steen, H.C., Gamero, A.M., 2013. STAT2 phosphorylation and signaling. JAK-STAT 2(4):e25790. PMID: 24416652. DOI: 10.4161/jkst.25790

Stern-Ginossar, N., Thompson, S.R., Mathews, M.B., Mohr, I., 2019. Translational Control in Virus-Infected Cells. Cold Spring Harb. Perspect. Biol. 11(3):a033001. PMID: 29891561. DOI: 10.1101/cshperspect.a033001

Stiasny, K., Fritz, R., Pangerl, K., Heinz, F.X., 2011. Molecular mechanisms of flavivirus membrane fusion. Amino Acids 41(5):1159–1163. PMID: 19882217. DOI: 10.1007/s00726-009-0370-4

Stohlman, S.A., Wisseman, C.L.J., Eylar, O.R., Silverman, D.J., 1975. Dengue Virus-Induced Modifications of Host Cell Membranes. J. Virol. 16(4):1017–1026. PMID: 1165590.

Styer, L.M., Kent, K.A., Albright, R.G., Bennett, C.J., Kramer, L.D., Bernard, K.A., 2007. Mosquitoes Inoculate High Doses of West Nile Virus as They Probe and Feed on Live Hosts. PLoS Pathog. 3(9):1262–1270. PMID: 17941708. DOI: 10.1371/journal.ppat.0030132

Su, H.-L., Liao, C.-L., Lin, Y.-L., 2002. Japanese Encephalitis Virus Infection Initiates Endoplasmic Reticulum Stress and an Unfolded Protein Response. J. Virol. 76(9):4162–4171. PMID: 11932381. DOI: 10.1128/jvi.76.9.4162-4171.2002

Sulakhe, D., D'Souza, M., Wang, S., Balasubramanian, S., Athri, P., Xie, B., Canzar, S., Agam, G., Gilliam, T.C., Maltsev, N., 2019. Exploring the functional impact of

alternative splicing on human protein isoforms using available annotation sources. Brief. Bioinform. 20(5):1754–1768. PMID: 29931155. DOI: 10.1093/bib/bby047

Suthar, M.S., Diamond, M.S., Gale, M.J., 2013. West Nile virus infection and immunity. Nat. Rev. Microbiol. 11(2):115–128. PMID: 23321534. DOI: 10.1038/nrmicro2950

Svidritskiy, E., Demo, G., Korostelev, A.A., 2018. Mechanism of premature translation termination on a sense codon. J. Biol. Chem. 293(32):12472–12479. PMID: 29941456. DOI: 10.1074/jbc.AW118.003232

Takahashi, H., Takahashi, C., Moreland, N.J., Chang, Y.-T., Sawasaki, T., Ryo, A., Vasudevan, S.G., Suzuki, Y., Yamamoto, N., 2012. Establishment of a robust dengue virus NS3-NS5 binding assay for identification of protein-protein interaction inhibitors. Antiviral Res. 96(3):305–314. PMID: 23072882. DOI: 10.1016/j.antiviral.2012.09.023

Takeda, 2022a. Takeda's QDENGA (Dengue Tetravalent Vaccine [Live, Attenuated]) Approved in Indonesia for Use Regardless of Prior Dengue Exposure [WWW Document]. URL https://www.takeda.com/newsroom/newsreleases/2022/takedas-qdenga-dengue-tetravalent-vaccine-live-attenuated-approved-in-indonesia-for-use-regardless-of-prior-dengue-exposure/ (accessed 2023-05-27).

Takeda, 2022b. Takeda's QDENGA (Dengue Tetravalent Vaccine [Live, Attenuated]) Approved for Use in European Union [WWW Document]. URL https://www.takeda.com/newsroom/newsreleases/2022/takedas-qdenga-dengue-tetravalent-vaccine-live-attenuated-approved-for-use-in-european-union/ (accessed 2023-05-27).

Takegami, T., Sakamuro, D., Furukawa, T., 1995. Japanese Encephalitis Virus Nonstructural Protein NS3 Has RNA Binding and ATPase Activities. Virus Genes 9(2):105–112. PMID: 7732656. DOI: 10.1007/BF01702653

Tan, B.-H., Fu, J., Sugrue, R.J., Yap, E.-H., Chan, Y.-C., Tan, Y.H., 1996. Recombinant Dengue Type 1 Virus NS5 Protein Expressed in Escherichia coli Exhibits RNA-Dependent RNA Polymerase Activity. Virology 216(2):317–325. PMID: 8607261. DOI: 10.1006/viro.1996.0067

Tan, Z., Zhang, W., Sun, J., Fu, Z., Ke, X., Zheng, C., Zhang, Y., Li, P., Liu, Y., Hu, Q., Wang, H., Zheng, Z., 2018. ZIKV infection activates the IRE1-XBP1 and ATF6 pathways of unfolded protein response in neural cells. J. Neuroinflammation 15(1):275.

PMID: 30241539. DOI: 10.1186/s12974-018-1311-5

Tang, H., Hammack, C., Ogden, S.C., Wen, Z., Qian, X., Li, Y., Yao, B., Shin, J., Zhang, F., Lee, E.M., Christian, K.M., Didier, R.A., Jin, P., Song, H., Ming, G., 2016. Zika Virus Infects Human Cortical Neural Progenitors and Attenuates Their Growth. Cell Stem Cell 18(5):587–590. PMID: 26952870. DOI: 10.1016/j.stem.2016.02.016

Tatonetti, N.P., Liu, T., Altman, R.B., 2009. Predicting drug side-effects by chemical systems biology. Genome Biol. 10(9):238. PMID: 19723347. DOI: 10.1186/gb-2009-10-9-238

Tay, M.Y.F., Fraser, J.E., Chan, W.K.K., Moreland, N.J., Rathore, A.P., Wang, C., Vasudevan, S.G., Jans, D.A., 2013. Nuclear localization of dengue virus (DENV) 1-4 non-structural protein 5; protection against all 4 DENV serotypes by the inhibitor Ivermectin. Antiviral Res. 99(3):301–306. PMID: 23769930. DOI: 10.1016/j.antiviral.2013.06.002

Tay, M.Y.F., Saw, W.G., Zhao, Y., Chan, K.W.K., Singh, D., Chong, Y., Forwood, J.K., Ooi, E.E., Grüber, G., Lescar, J., Luo, D., Vasudevan, S.G., 2015. The C-terminal 50 Amino Acid Residues of Dengue NS3 Protein Are Important for NS3-NS5 Interaction and Viral Replication. J. Biol. Chem. 290(4):2379–2394. PMID: 25488659. DOI: 10.1074/jbc.M114.607341

Thaker, S.K., Ch'ng, J., Christofk, H.R., 2019. Viral hijacking of cellular metabolism. BMC Biol. 17(1):59. PMID: 31319842. DOI: 10.1186/s12915-019-0678-9

Tortora, G.J., Derrickson, B., 2007. Principes d'anatomie et de physiologie, 2e ed. Éditions du Renouveau Pédagogique Inc.

Tu, Y.-C., Yu, C.-Y., Liang, J.-J., Lin, E., Liao, C.-L., Lin, Y.-L., 2012. Blocking Double-Stranded RNA-Activated Protein Kinase PKR by Japanese Encephalitis Virus Nonstructural Protein 2A. J. Virol. 86(19):10347–10358. PMID: 22787234. DOI: 10.1128/JVI.00525-12

Turpin, J., Frumence, E., Harrabi, W., Haddad, J.G., El Kalamouni, C., Desprès, P., Krejbich-Trotot, P., Viranaïcken, W., 2020. Zika virus subversion of chaperone GRP78/BiP expression in A549 cells during UPR activation. Biochimie 175:99–105. PMID: 32464166. DOI: 10.1016/j.biochi.2020.05.011

Uchil, P.D., Satchidanandam, V., 2003. Architecture of the Flaviviral Replication Complex. Protease, nuclease, and detergents reveal encasement within double-layered membrane

compartments. J. Biol. Chem. 278(27):24388–24398. PMID: 12700232. DOI: 10.1074/jbc.M301717200

Ule, J., Blencowe, B.J., 2019. Alternative Splicing Regulatory Networks: Functions, Mechanisms, and Evolution. Mol. Cell 76(2):329–345. PMID: 31626751. DOI: 10.1016/j.molcel.2019.09.017

Umareddy, I., Chao, A., Sampath, A., Gu, F., Vasudevan, S.G., 2006. Dengue virus NS4B interacts with NS3 and dissociates it from single-stranded RNA. J. Gen. Virol. 87(9):2605–2614. PMID: 16894199. DOI: 10.1099/vir.0.81844-0

Urbanowski, M.D., Hobman, T.C., 2013. The West Nile Virus Capsid Protein Blocks Apoptosis through a Phosphatidylinositol 3-Kinase-Dependent Mechanism. J. Virol. 87(2):872–881. PMID: 23115297. DOI: 10.1128/JVI.02030-12

Utama, A., Shimizu, H., Morikawa, S., Hasebe, F., Morita, K., Igarashi, A., Hatsu, M., Takamizawa, K., Miyamura, T., 2000. Identification and characterization of the RNA helicase activity of Japanese encephalitis virus NS3 protein. FEBS Lett. 465(1):74–78. PMID: 10620709.

Valle, R.P.C., Falgout, B., 1998. Mutagenesis of the NS3 Protease of Dengue Virus Type 2. J. Virol. 72(1):624–632. PMID: 9420267.

van den Elsen, K., Chew, B.L.A., Ho, J.S., Luo, D., 2023. Flavivirus nonstructural proteins and replication complexes as antiviral drug targets. Curr. Opin. Virol. 59:101305. PMID: 36870091. DOI: 10.1016/j.coviro.2023.101305

van den Elsen, K., Quek, J.P., Luo, D., 2021. Molecular Insights into the Flavivirus Replication Complex. Viruses 13(6):956. PMID: 34064113. DOI: 10.3390/v13060956

Van Regenmortel, M.H.V., 2011. Virus Species. In: Tibayrenc, M. (Ed.), Genetics and Evolution of Infectious Diseases. Elsevier. DOI: 10.1016/B978-0-12-384890-1.00001-7

Vasilakis, N., Weaver, S.C., 2016. Flavivirus transmission focusing on Zika. Curr. Opin. Virol. 22:30–35. PMID: 27936448. DOI: 10.1016/j.coviro.2016.11.007

Vasudevan, S.G., Johansson, M., Brooks, A.J., Llewellyn, L.E., Jans, D.A., 2001. Characterisation of inter- and intra-molecular interactions of the dengue virus RNA dependent RNA polymerase as potential drug targets. Farmaco 56(1–2):33–36. PMID: 11347963.

Verma, D., Bais, S., Gaillard, M., Swaminathan, S., 2010. Epstein-Barr Virus SM Protein Utilizes Cellular Splicing Factor SRp20 To Mediate Alternative Splicing. J. Virol. 84(22):11781–11789. PMID: 20810723. DOI: 10.1128/JVI.01359-10

Verma, D., Swaminathan, S., 2008. Epstein-Barr Virus SM Protein Functions as an Alternative Splicing Factor. J. Virol. 82(14):7180–7188. PMID: 18463151. DOI: 10.1128/JVI.00344-08

Wang, C.-C., Huang, Z.-S., Chiang, P.-L., Chen, C.-T., Wu, H.-N., 2009. Analysis of the nucleoside triphosphatase, RNA triphosphatase, and unwinding activities of the helicase domain of dengue virus NS3 protein. FEBS Lett. 583(4):691–696. PMID: 19166847. DOI: 10.1016/j.febslet.2009.01.008

Wang, K., Zou, C., Wang, X., Huang, C., Feng, T., Pan, W., Wu, Q., Wang, P., Dai, J., 2018. Interferon-stimulated TRIM69 interrupts dengue virus replication by ubiquitinating viral nonstructural protein 3. PLoS Pathog. 14(8):e1007287. PMID: 30142214. DOI: 10.1371/journal.ppat.1007287

Wang, T., Merits, A., Wu, Yuanyuan, Wang, M., Jia, R., Zhu, D., Liu, M., Zhao, X., Yang, Q., Wu, Ying, Zhang, S., Liu, Y., Zhang, L., Yu, Y., Pan, L., Chen, S., Cheng, A., 2020. cis -Acting Sequences and Secondary Structures in Untranslated Regions of Duck Tembusu Virus RNA Are Important for Cap-Independent Translation and Viral Proliferation. J. Virol. 94(16):e00906-20. PMID: 32522848. DOI: 10.1128/JVI.00906-20

Ward, A.M., Bidet, K., Yinglin, A., Ler, S.G., Hogue, K., Blackstock, W., Gunaratne, J., Garcia-Blanco, M.A., 2011. Quantitative mass spectrometry of DENV-2 RNA-interacting proteins reveals that the DEAD-box RNA helicase DDX6 binds the DB1 and DB2 3' UTR structures. RNA Biol. 8(6):1173–1186. PMID: 21957497. DOI: 10.4161/rna.8.6.17836

Warke, R. V., Xhaja, K., Martin, K.J., Fournier, M.F., Shaw, S.K., Brizuela, N., de Bosch, N., Lapointe, D., Ennis, F.A., Rothman, A.L., Bosch, I., 2003. Dengue Virus Induces Novel Changes in Gene Expression of Human Umbilical Vein Endothelial Cells. J. Virol. 77(21):11822–11832. PMID: 14557666. DOI: 10.1128/jvi.77.21.11822-11832.2003

Warrener, P., Tamura, J.K., Collett, M.S., 1993. RNA-Stimulated NTPase Activity

Associated with Yellow Fever Virus NS3 Protein Expressed in Bacteria. J. Virol. 67(2):989–996. PMID: 8380474.

Watanabe, S., Chan, K.W.-K., Dow, G., Ooi, E.E., Low, J.G., Vasudevan, S.G., 2016. Optimizing celgosivir therapy in mouse models of dengue virus infection of serotypes 1 and 2: The search for a window for potential therapeutic efficacy. Antiviral Res. 127:10–19. PMID: 26794905. DOI: 10.1016/j.antiviral.2015.12.008

Watson, J., Baker, T., Bell, S., Gann, A., Levine, M., Losick, R., 2012. Biologie moléculaire du gène, 6e ed. Pearson Education France.

Welsch, S., Miller, S., Romero-Brey, I., Merz, A., Bleck, C.K.E., Walther, P., Fuller, S.D., Antony, C., Krijnse-Locker, J., Bartenschlager, R., 2009. Composition and Three-Dimensional Architecture of the Dengue Virus Replication and Assembly Sites. Cell Host Microbe 5(4):365–375. PMID: 19380115. DOI: 10.1016/j.chom.2009.03.007

Wengler, G., Czaya, G., Färber, P.M., Hegemann, J.H., 1991. In vitro synthesis of West Nile virus proteins indicates that the amino-terminal segment of the NS3 protein contains the active centre of the protease which cleaves the viral polyprotein after multiple basic amino acids. J. Gen. Virol. 72(4):851–858. PMID: 1826736. DOI: 10.1099/0022-1317-72-4-851

Wengler, Gerd, Wengler, Gisela, 1991. The Carboxy-Terminal Part of the NS 3 Protein of the West Nile Flavivirus Can Be Isolated as a Soluble Protein after Proteolytic Cleavage and Represents an RNA-stimulated NTPase. Virology 184(2):707–715. PMID: 1716026. DOI: 10.1016/0042-6822(91)90440-M

Wengler, Gerd, Wengler, Gisela, 1993. The NS 3 Nonstructural Protein of Flaviviruses Contains an RNA Triphosphatase Activity. Virology 197(1):265–273. PMID: 8212562. DOI: 10.1006/viro.1993.1587

Wichit, S., Hamel, R., Zanzoni, A., Diop, F., Cribier, A., Talignani, L., Diack, A., Ferraris, P., Liegeois, F., Urbach, S., Ekchariyawat, P., Merits, A., Yssel, H., Benkirane, M., Missé, D., 2019. SAMHD1 Enhances Chikungunya and Zika Virus Replication in Human Skin Fibroblasts. Int. J. Mol. Sci. 20(7):1695. PMID: 30959732. DOI: 10.3390/ijms20071695

Wilder-Smith, A., 2020. Dengue vaccine development: status and future. Bundesgesundheitsblatt, Gesundheitsforschung, Gesundheitsschutz 63(1):40–44.

PMID: 31784763. DOI: 10.1007/s00103-019-03060-3

World Health Organization, 2018. Zika virus Key Facts [WWW Document]. URL https://www.who.int/news-room/fact-sheets/detail/zika-virus (accessed 2022-06-27).

World Health Organization, 2019a. Japanese encephalitis [WWW Document]. URL https://www.who.int/news-room/fact-sheets/detail/japanese-encephalitis (accessed 2022-06-15).

World Health Organization, 2019b. Yellow fever [WWW Document]. URL https://www.who.int/news-room/fact-sheets/detail/yellow-fever (accessed 2022-06-15).

World Health Organization, 2020. Zoonoses [WWW Document]. URL https://www.who.int/news-room/fact-sheets/detail/zoonoses (accessed 2022-04-04).

World Health Organization, 2021. Ebola virus disease [WWW Document]. URL https://www.who.int/news-room/fact-sheets/detail/ebola-virus-disease (accessed 2022-04-05).

World Health Organization, 2022. Dengue and severe dengue [WWW Document]. URL https://www.who.int/news-room/fact-sheets/detail/dengue-and-severe-dengue (accessed 2022-06-15).

Wright, C.J., Smith, C.W.J., Jiggins, C.D., 2022. Alternative splicing as a source of phenotypic diversity. Nat. Rev. Genet. 23(11):697–710. PMID: 35821097. DOI: 10.1038/s41576-022-00514-4

Wu, J., Bera, A.K., Kuhn, R.J., Smith, J.L., 2005. Structure of the Flavivirus Helicase : Implications for Catalytic Activity , Protein Interactions , and Proteolytic Processing. J. Virol. 79(16):10268–10277. PMID: 16051820. DOI: 10.1128/JVI.79.16.10268-10277.2005

Wu, J., Liu, W., Gong, P., 2015. A Structural Overview of RNA-Dependent RNA Polymerases from the Flaviviridae Family. Int. J. Mol. Sci. 16(6):12943–12957. PMID: 26062131. DOI: 10.3390/ijms160612943

Xie, X., Gayen, S., Kang, C., Yuan, Z., Shi, P.-Y., 2013. Membrane Topology and Function of Dengue virus NS2A protein. J. Virol. 87(8):4609–4622. PMID: 23408612. DOI: 10.1128/JVI.02424-12

Xu, T., Sampath, A., Chao, A., Wen, D., Nanao, M., Chene, P., Vasudevan, S.G., Lescar, J.,

2005. Structure of the Dengue Virus Helicase/Nucleoside Triphosphatase Catalytic Domain at a Resolution of 2.4 Å. J. Virol. 79(16):10278–10288. PMID: 16051821. DOI: 10.1128/JVI.79.16.10278-10288.2005

Xu, T., Sampath, A., Chao, A., Wen, D., Nanao, M., Luo, D., Chene, P., Vasudevan, S.G., Lescar, J., 2006. Towards the design of flavivirus helicase/NTPase inhibitors: crystallographic and mutagenesis studies of the dengue virus NS3 helicase catalytic domain. Novartis Found. Symp. 277:87–97. PMID: 17319156. DOI: 10.1002/0470058005.ch7

Xu, Y., Zhou, J., Liu, T., Liu, P., Wu, Y., Lai, Z., Gu, J., Chen, X., 2022. Assessing the risk of spread of Zika virus under current and future climate scenarios. Biosaf. Heal. 4(3):193–204. DOI: 0.1016/j.bsheal.2022.03.012

Yabas, M., Elliott, H., Hoyne, G.F., 2015. The Role of Alternative Splicing in the Control of Immune Homeostasis and Cellular Differentiation. Int. J. Mol. Sci. 17(1):3. PMID: 26703587. DOI: 10.3390/ijms17010003

Yan, N., Chen, Z.J., 2012. Intrinsic antiviral immunity. Nat. Immunol. 13(3):214–222. PMID: 22344284. DOI: 10.1038/ni.2229

Yang, S.N.Y., Maher, B., Wang, C., Wagstaff, K.M., Fraser, J.E., Jans, D.A., 2022. High Throughput Screening Targeting the Dengue NS3-NS5 Interface Identifies Antivirals against Dengue, Zika and West Nile Viruses. Cells 11(4):730. PMID: 35203378. DOI: 10.3390/cells11040730

Yang, Y., Ye, J., Yang, X., Jiang, R., Chen, H., Cao, S., 2011. Japanese encephalitis virus infection induces changes of mRNA profile of mouse spleen and brain. Virol. J. 8:80. PMID: 21345237. DOI: 10.1186/1743-422X-8-80

Yao, Y., Huo, T., Lin, Y.-L., Nie, S., Wu, F., Hua, Y., Wu, J., Kneubehl, A.R., Vogt, M.B., Rico-Hesse, R., Song, Y., 2019. Discovery, X-ray Crystallography and Antiviral Activity of Allosteric Inhibitors of Flavivirus NS2B-NS3 Protease. J. Am. Chem. Soc. 141(17):6832–6836. PMID: 31017399. DOI: 10.1021/jacs.9b02505

Yap, T.L., Xu, T., Chen, Y.-L., Malet, H., Egloff, M.-P., Canard, B., Vasudevan, S.G., Lescar, J., 2007. Crystal Structure of the Dengue Virus RNA-Dependent RNA Polymerase Catalytic Domain at 1.85-Angstrom Resolution. J. Virol. 81(9):4753–4765. PMID: 17301146. DOI: 10.1128/JVI.02283-06

Yon, C., Teramoto, T., Mueller, N., Phelan, J., Ganesh, V.K., Murthy, K.H.M., Padmanabhan, R., 2005. Modulation of the Nucleoside Triphosphatase/RNA Helicase and 5'-RNA Triphosphatase Activities of Dengue Virus Type 2 Nonstructural Protein 3 (NS3) by Interaction with NS5, the RNA-dependent RNA Polymerase. J. Biol. Chem. 280(29):27412–27419. PMID: 15917225. DOI: 10.1074/jbc.M501393200

Yotmanee, P., Rungrotmongkol, T., Wichapong, K., Choi, S.B., Wahab, H.A., Kungwan, N., Hannongbua, S., 2015. Binding specificity of polypeptide substrates in NS2B/NS3pro serine protease of dengue virus type 2: A molecular dynamics Study. J. Mol. Graph. Model. 60:24–33. PMID: 26086900. DOI: 10.1016/j.jmgm.2015.05.008

Yu, C.-Y., Hsu, Y.-W., Liao, C.-L., Lin, Y.-L., 2006. Flavivirus Infection Activates the XBP1 Pathway of the Unfolded Protein Response To Cope with Endoplasmic Reticulum Stress. J. Virol. 80(23):11868–11880. PMID: 16987981. DOI: 10.1128/JVI.00879-06

Yun, S.-I., Lee, Y.-M., 2014. Japanese encephalitis: The virus and vaccines. Hum. Vaccines Immunother. 10(2):263–279. PMID: 24161909. DOI: 10.4161/hv.26902

Zanini, F., Robinson, M.L., Croote, D., Sahoo, M.K., Sanz, A.M., Ortiz-Lasso, E., Albornoz, L.L., Rosso, F., Montoya, J.G., Goo, L., Pinsky, B.A., Quake, S.R., Einav, S., 2018. Virus-inclusive single-cell RNA sequencing reveals the molecular signature of progression to severe dengue. Proc. Natl. Acad. Sci. U. S. A. 115(52):E12363–E12369. PMID: 30530648. DOI: 10.1073/pnas.1813819115

Zhang, L.-K., Chai, F., Li, H.-Y., Xiao, G., Guo, L., 2013. Identification of Host Proteins Involved in Japanese Encephalitis Virus Infection by Quantitative Proteomics Analysis. J. Proteome Res. 12(6):2666–2678. PMID: 23647205. DOI: 10.1021/pr400011k

Zhang, Z., Li, Y., Loh, Y.R., Phoo, W.W., Hung, A.W., Kang, C., Luo, D., 2016. Crystal structure of unlinked NS2B-NS3 protease from Zika virus. Science 354(6319):1597–1600. PMID: 27940580. DOI: 10.1126/science.aai9309

Zhao, Y., Soh, T.S., Zheng, J., Chan, K.W.K., Phoo, W.W., Lee, C.C., Tay, M.Y.F., Swaminathan, K., Cornvik, T.C., Lim, S.P., Shi, P.-Y., Lescar, J., Vasudevan, S.G., Luo, D., 2015. A Crystal Structure of the Dengue Virus NS5 Protein Reveals a Novel Inter-domain Interface Essential for Protein Flexibility and Virus Replication. PLoS Pathog. 11(3):e1004682. PMID: 25775415. DOI: 10.1371/journal.ppat.1004682

Zhou, Y., Ray, D., Zhao, Y., Dong, H., Ren, S., Li, Z., Guo, Y., Bernard, K.A., Shi, P.-Y., Li, H., 2007. Structure and Function of Flavivirus NS5 Methyltransferase. J. Virol. 81(8):3891–3903. PMID: 17267492. DOI: 10.1128/JVI.02704-06

Zou, G., Chen, Y.-L., Dong, H., Lim, C.C., Yap, L.J., Yau, Y.H., Geifman Shochat, S., Lescar, J., Shi, P.-Y., 2011. Functional Analysis of Two Cavities in Flavivirus NS5 Polymerase. J. Biol. Chem. 286(16):14362–14372. PMID: 21349834. DOI: 10.1074/jbc.M110.214189

Zou, G., Puig-Basagoiti, F., Zhang, B., Qing, M., Chen, L., Pankiewicz, K.W., Felczak, K., Yuan, Z., Shi, P.-Y., 2009. A single-amino acid substitution in West Nile virus 2K peptide between NS4A and NS4B confers resistance to lycorine, a flavivirus inhibitor. Virology 384(1):242–252. PMID: 19062063. DOI: 10.1016/j.virol.2008.11.003

Zou, J., Lee, L.T., Wang, Q.Y., Xie, X., Lu, S., Yau, Y.H., Yuan, Z., Geifman Shochat, S., Kang, C., Lescar, J., Shi, P.-Y., 2015. Mapping the Interactions between the NS4B and NS3 Proteins of Dengue Virus. J. Virol. 89(7):3471–3483. PMID: 25589636. DOI: 10.1128/JVI.03454-14

8 APPENDIX

Supplementary Materials of Article 1: Kunjin Virus, Zika Virus and Yellow Fever Virus Infections Have Distinct Effects on the Coding Transcriptome and Proteome of Brain-Derived U87 Cells

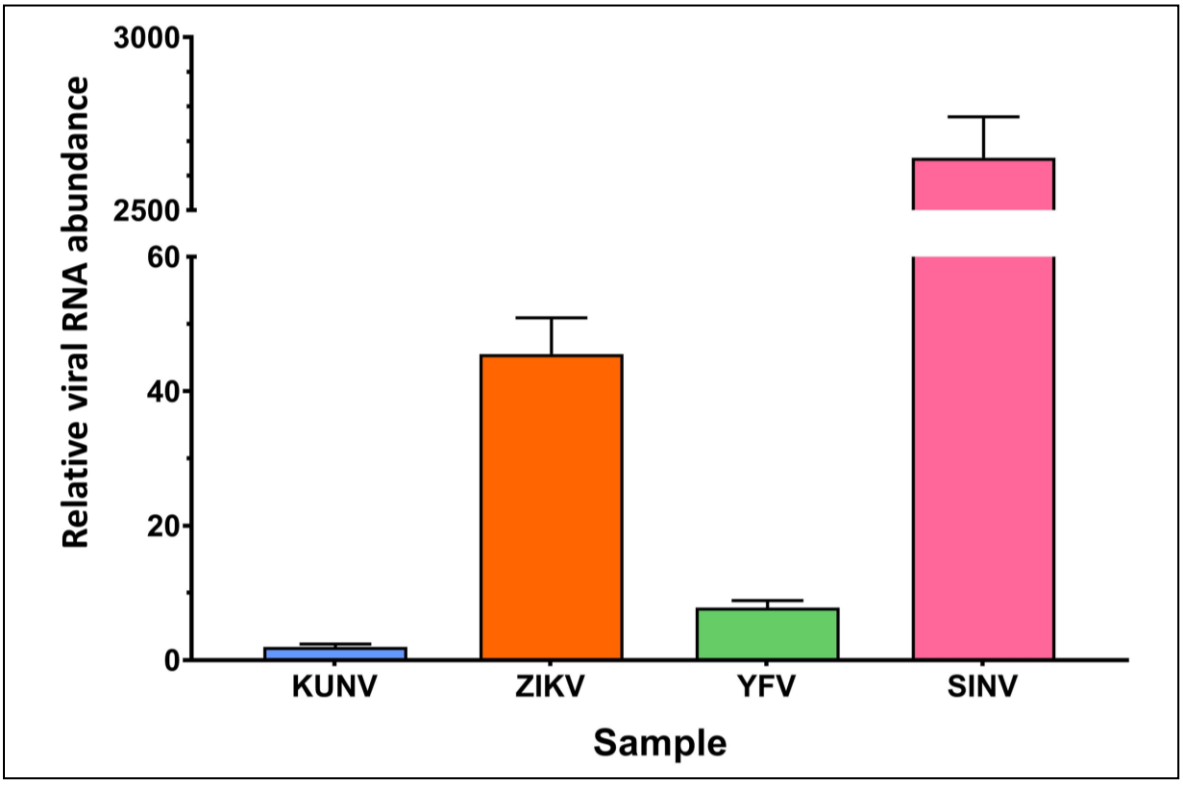

Figure S1. Quantification of viral RNA. Abundance of viral RNAs in total RNA extracts from infected cells was measured using droplet digital PCR (ddPCR). To correct for differences in the amounts of input cDNA, four housekeeping genes (B2M, MRPL19, PUM1, YWHAZ) were quantified, and copies/µL of viral cDNA were divided by copies/µL of housekeeping genes.

Replicate		1	2	3
Control	# raw reads	46,563,828	37,211,645	66,856,469
	# trimmed reads	40,223,825	30,906,590	57,866,094
	# uniquely mapped reads	34,403,883	26,884,686	49,920,215
	% uniquely mapped reads	85.53%	86.99%	86.27%
Kunjin	# raw reads	39,858,770	72,658,971	50,942,153
	# trimmed reads	33,579,831	60,981,291	42,518,357
	# uniquely mapped reads	29,435,085	53,525,237	37,341,451
	% uniquely mapped reads	87.66%	87.77%	87.82%
Zika	# raw reads	46,518,738	38,513,137	35,216,808
	# trimmed reads	39,658,727	33,307,314	29,639,008
	# uniquely mapped reads	35,073,564	29,699,379	26,147,192
	% uniquely mapped reads	88.44%	89.17%	88.22%
Yellow Fever	# raw reads	34,484,039	42,409,310	55,436,160
	# trimmed reads	30,727,508	35,783,488	45,425,791
	# uniquely mapped reads	27,365,936	30,967,899	40,389,149
	% uniquely mapped reads	89.06%	86.54%	88.91%
Sindbis	# raw reads	49,922,652	37,682,694	39,550,651
	# trimmed reads	43,274,016	28,741,054	34,531,210
	# uniquely mapped reads	36,618,079	24,071,706	29,482,609
	% uniquely mapped reads	84.62%	83.75%	85.38%

Figure S2. RNA-Seq data. PolyA-enriched cDNA libraries from infected (Kunjin, Zika, Yellow Fever, Sindbis) and non-infected (control) cells were subjected to 100 bp paired-end sequencing using the Illumina HiSeq4000 system. At least 34 million reads were obtained for each sample. At least 83% of the reads were uniquely mapped to the reference genome.

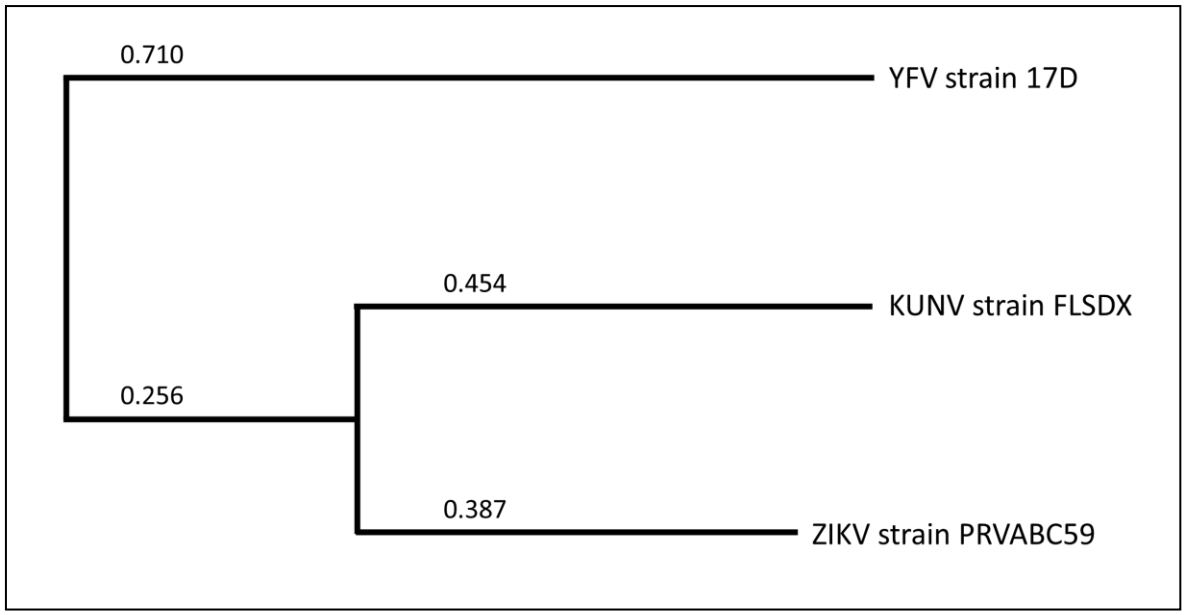

Figure S3. Flavivirus phylogenetic tree. The polyprotein sequences of the three Flaviviruses used in this study were aligned using SeaView5/Clustal Omega, and a phylogenetic tree was constructed based on this alignment using SeaView5/PhyML.

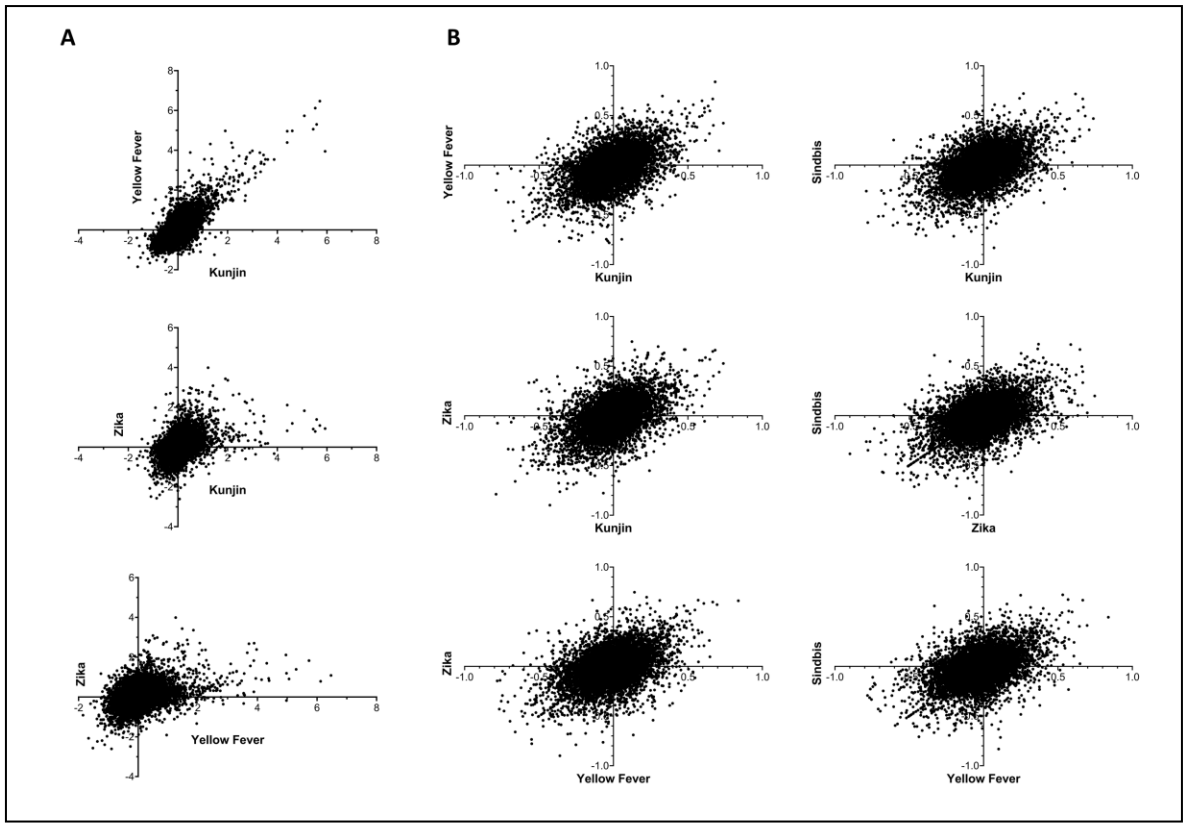

Figure S4. Correlations in changes to gene expression levels and alternative splicing upon viral infection. (A) Fold-change values (log2) for all genes detected in every experimental condition are shown. (B) ΔPSI values for all ASEs detected in every experimental condition are shown.

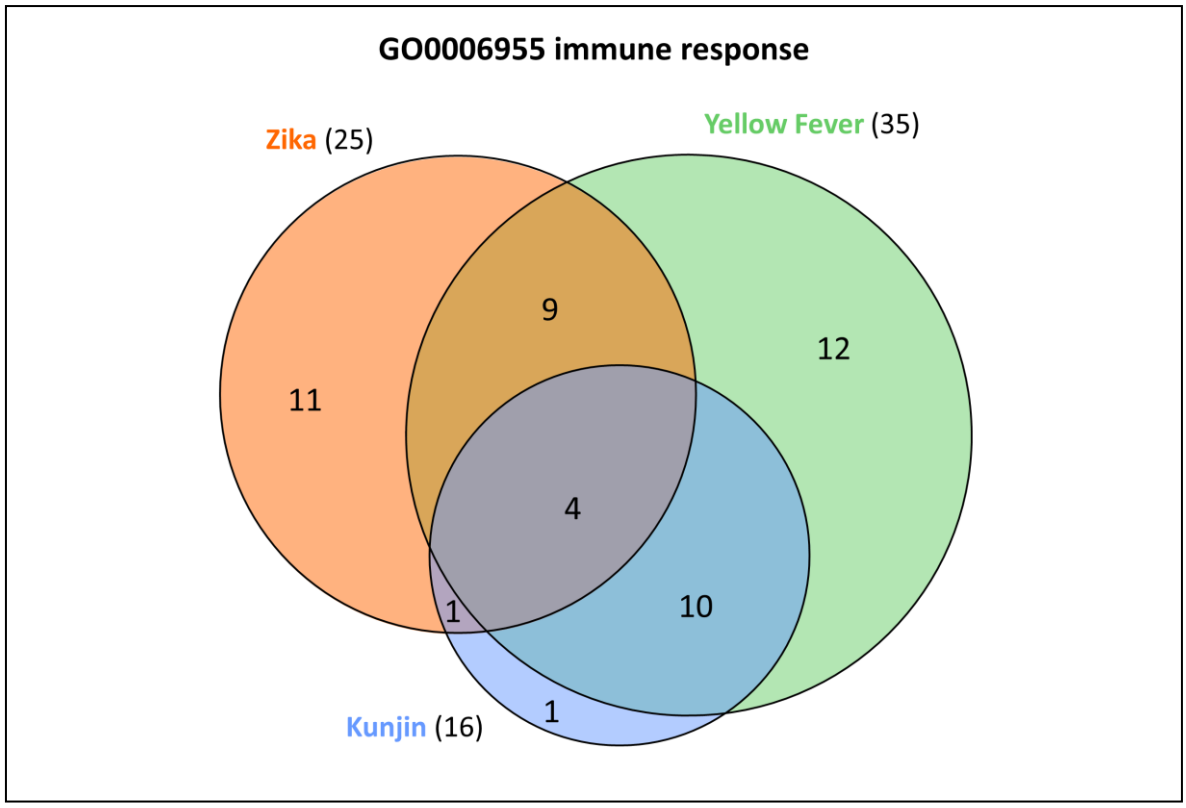

Figure S5. Gene ontology enrichment analysis results for the term 'immune response'. The GO term 'immune response' was found to be significantly enriched among the genes in which expression levels were altered following all three Flavivirus infections. Here, the genes involved in the immune response that are affected in each infection are shown.

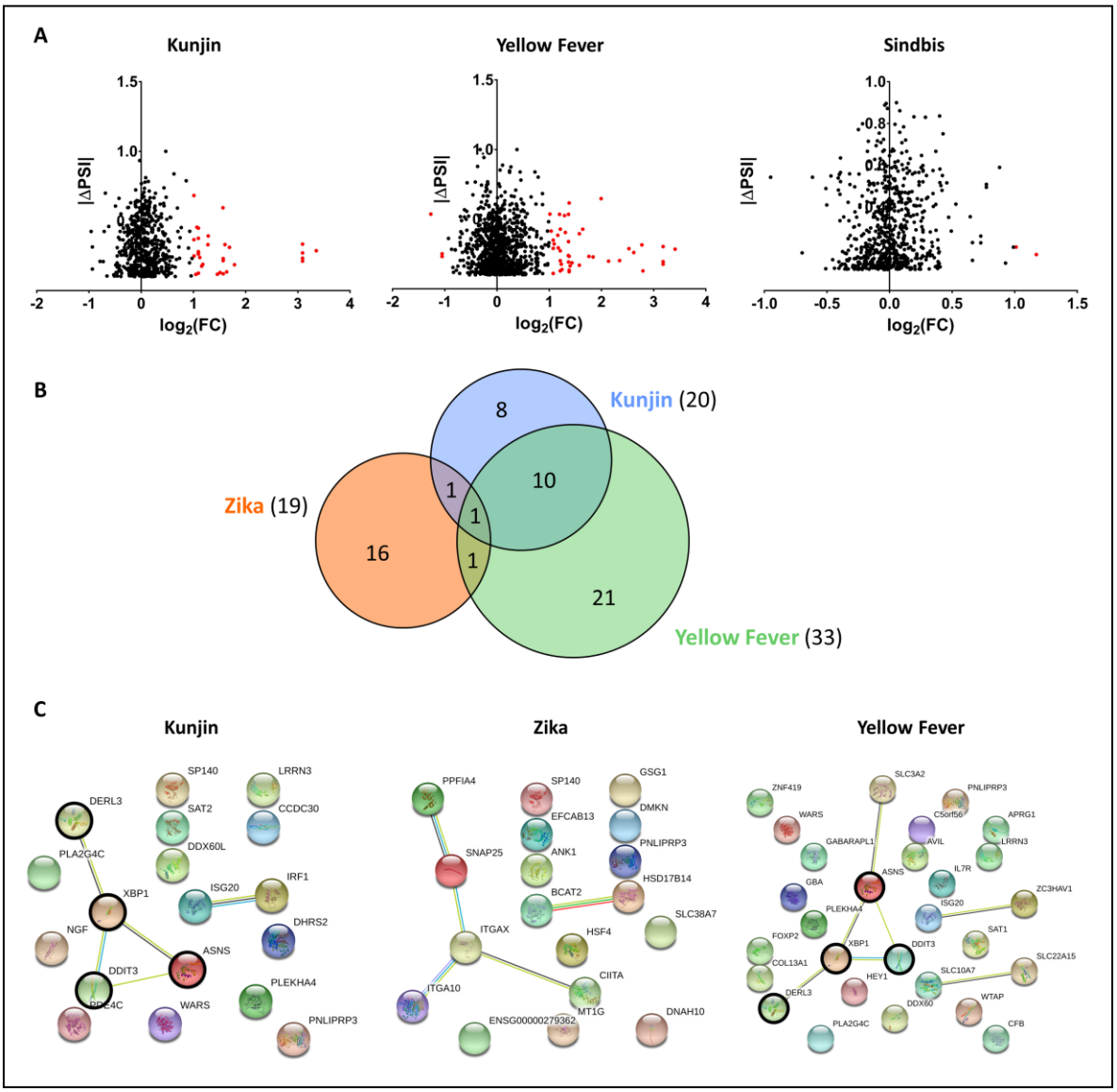

Figure S6. Expression levels of genes with one or more dysregulated ASEs upon infection. (A) The absolute ΔPSI values as well as fold-change values for all genes with at least one dysregulated ASE are shown. Each dot represents one significantly modulated ASE, and red dots represent events on genes that are also significantly overexpressed or repressed. (B) The area-proportional Venn diagram shows overlaps in the sets of genes for which expression levels as well as alternative splicing were significantly altered upon each viral infection. (C) An analysis of the genes that showed dysregulated expression levels as well as alternative splicing was performed with STRING. One of the most significantly enriched biological processes in KUNV and YFV infections was 'GO:0030968 endoplasmic reticulum unfolded protein response' (FDR = 0.0025 and 0.0100, respectively), and the proteins involved in these processes are highlighted with black circles. No biological process was significantly enriched among the genes dysregulated in the ZIKV infections.

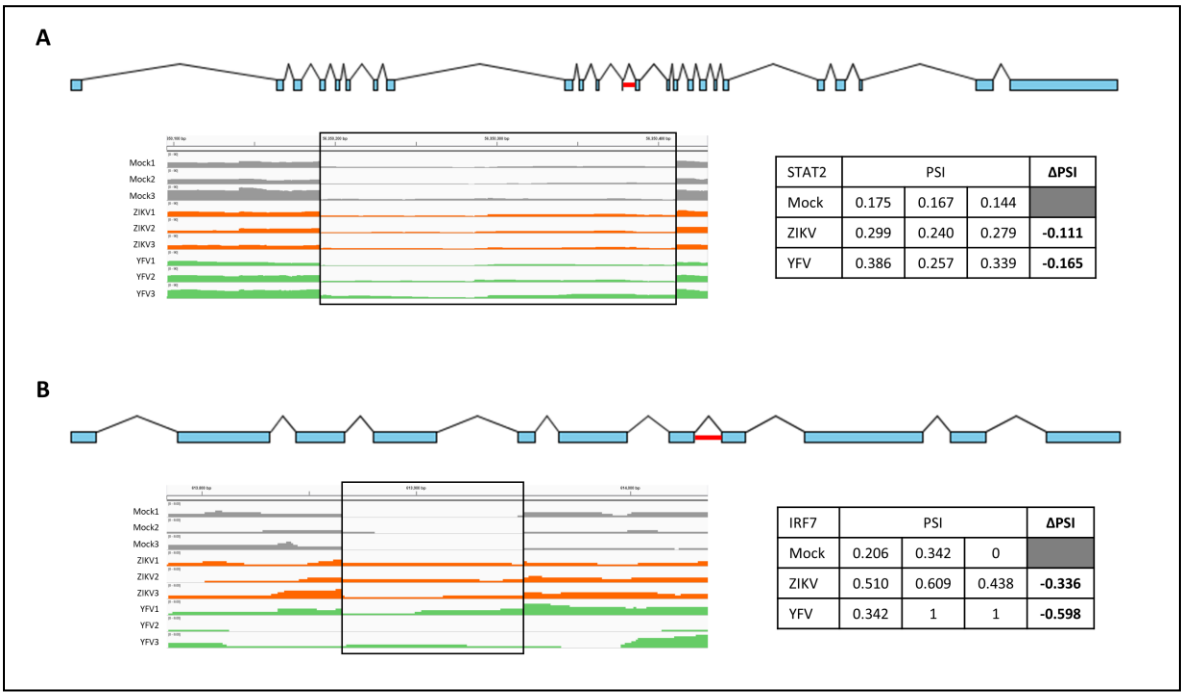

STAT2	PSI			ΔPSI
Mock	0.175	0.167	0.144	
ZIKV	0.299	0.240	0.279	**-0.111**
YFV	0.386	0.257	0.339	**-0.165**

IRF7	PSI			ΔPSI
Mock	0.206	0.342	0	
ZIKV	0.510	0.609	0.438	**-0.336**
YFV	0.342	1	1	**-0.598**

Figure S7. Intron retention in genes involved in the immune response. (A) Increased retention of intron 12 in the STAT2 mRNA in infected cells is shown. (B) Increased retention of intron 7 in the IRF7 mRNA is shown.

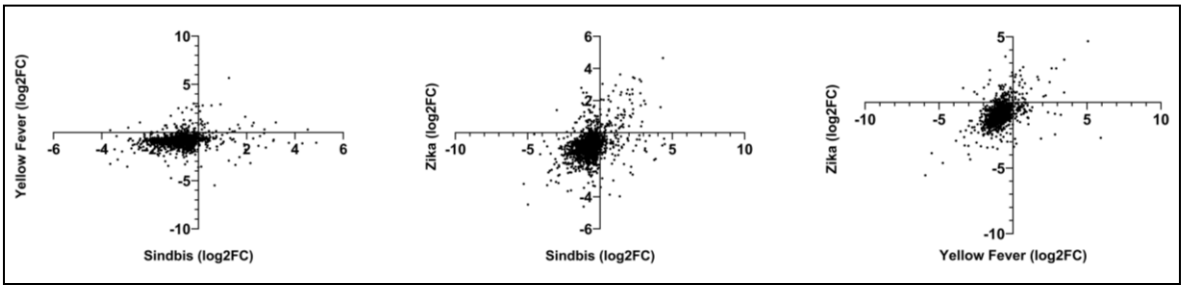

Figure S8. Correlations in changes to protein expression levels upon viral infection. Scatter plots of fold-change values for all proteins detected in at least two infections are shown.

A

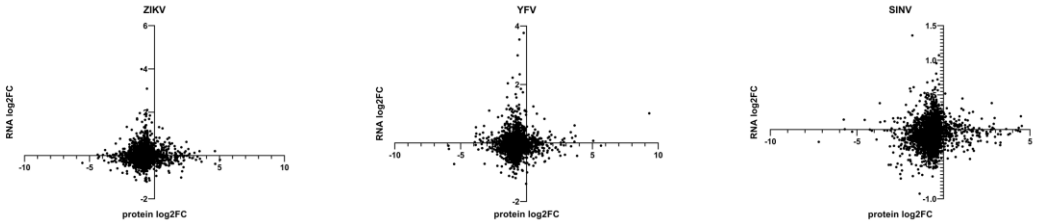

B

	Spearman correlation coefficient	p-value
ZIKV	0.03904	0.0296
YFV	0.03040	0.0830
SINV	0.1112	<0.0001

Figure S9. Comparison of transcriptome and proteome results. (A) Scatter plots of fold-change values for all proteins and their mRNAs detected in each viral infection are shown. (B) Spearman correlation coefficients of RNA and protein fold-changes in each infection, along with their *p* values, are displayed.

Tables S1 - S8, S11 - S13, and S15 are too large to fit in this document; they are available at https://www.mdpi.com/article/10.3390/v15071419/s1

Table S9. Validation of changes in gene expression levels. In total, 21 genes were chosen for qRT-PCR validation of the RNA-Seq results.

Gene	KUNV vs Mock (log2FC)		ZIKV vs Mock (log2FC)		YFV vs Mock (log2FC)		SINV vs Mock (log2FC)	
	RNA-Seq	qPCR	RNA-Seq	qPCR	RNA-Seq	qPCR	RNA-Seq	qPCR
ATOH8	0.065	0.062	-2.605	-4.109	-0.895	-1.668	-0.564	-0.562
BMPER	-1.051	-0.998	-0.588	-0.553	-0.742	-0.715	-0.195	0.112
CSF2	-0.305	-0.935	2.71	3.205	2.066	2.554	0.246	0.287
CXCL8	0.496	0.634	2.704	2.68	3.89	4.086	0.475	0.519
DDIT3	3.09	3.538	1.232	1.367	3.181	3.615	1.011	1.384
DGAT2	-1.984	-2.324	-1.099	-1.195	-1.385	-1.622	-0.08	0.18
ENG	-1.211	-1.425	-0.528	-0.621	-1.457	-1.386	-0.238	0.195
ERN1	0.979	0.776	0.298	0.394	2.242	1.974	0.519	0.884
HBEGF	-1.323	-1.32	-1.068	-1.104	-0.292	-0.039	-0.34	-0.072
HERPUD1	2.715	2.708	0.605	0.373	3.335	3.533	0.136	0.102
IFIT2	5.09	8.604	1.828	3.203	5.732	8.514	1.849	4.632
IGFL3	0.551	0.524	2.945	3.396	0.552	0.358	-0.053	-0.225
IL6	2.464	2.812	2.678	3.05	3.716	4.172	0.447	0.703
IL7R	0.565	0.824	-1.111	-1.15	1.211	1.419	-0.141	0.281
INSIG1	0.22	0.264	2.842	2.644	0.381	0.465	0.403	0.433
MSC	2.768	2.789	2.224	2.195	3.661	3.712	0.773	1.089
PLAU	-1.654	-1.63	-0.585	-0.578	-0.403	-0.139	-0.11	0.257
RSAD2	4.401	10.723	2.113	5.288	4.958	10.472	1.466	7.598
TGOLN2	-1.506	-1.754	-0.223	-0.196	-1.397	-1.482	-0.181	0.057
TNFRSF11B	-1.141	-1.096	-1.388	-1.409	-0.31	-0.302	-0.358	-0.076
VAV2	-0.369	-0.367	-0.356	-0.327	-1.226	-1.176	-0.184	0.128

Table S10. Expression levels of genes associated with the GO term 'nervous system development'. Genes significantly overexpressed are shown in blue, and genes significantly repressed are shown in red.

Gene ID	Gene name	log2FC CvsZ	log2FC CvsYF	log2FC CvsK
ENSG00000133083	DCLK1	1.601	0.509	0.494
ENSG00000138685	FGF2	1.405	1.937	0.902
ENSG00000122641	INHBA	1.404	1.651	0.875
ENSG00000163739	CXCL1	1.215	2.052	-0.246
ENSG00000101134	DOK5	1.19	0.118	0.789
ENSG00000166340	TPP1	1.025	0.357	0.567
ENSG00000171617	ENC1	-1.091	-0.433	-0.79
ENSG00000176697	BDNF	-1.096	-0.051	-0.333
ENSG00000150938	CRIM1	-1.112	-0.391	-0.62
ENSG00000007944	MYLIP	-1.178	-0.026	-0.229
ENSG00000101384	JAG1	-1.255	-0.859	-0.957
ENSG00000157168	NRG1	-1.267	0.813	-0.275
ENSG00000124479	NDP	-1.346	-1.128	-0.954
ENSG00000189184	PCDH18	-1.35	-0.655	-0.301
ENSG00000170345	FOS	-1.437	-0.08	0.286
ENSG00000105880	DLX5	-1.464	-0.779	0.544
ENSG00000168874	ATOH8	-2.605	-0.895	0.065

Table S14. Gene expression levels of known splicing factors. No known splicing factor was found to be significantly differentially expressed upon infection with KUNV, ZIKV, YFV, or SINV.

Gene name	Gene ID	KUNV		ZIKV		YFV		SINV	
		log2FC	p.adj	log2FC	p.adj	log2FC	p.adj	log2FC	p.adj
AAR2	ENSG00000131043	-0.024	0.865	-0.212	0.023	0.013	0.955	0.108	0.331
AQR	ENSG00000021776	0.036	0.704	0.040	0.694	0.016	0.916	-0.027	0.819
BCAS2	ENSG00000116752	0.210	0.006	-0.008	0.946	0.138	0.216	-0.187	0.033
BUD13	ENSG00000137656	-0.323	0.004	-0.059	0.732	-0.075	0.699	-0.119	0.422
BUD31	ENSG00000106245	0.004	0.978	-0.182	0.030	0.086	0.545	-0.045	0.704
C9ORF78	ENSG00000136819	-0.202	0.001	-0.145	0.021	-0.063	0.590	-0.130	0.078
CACTIN	ENSG00000105298	0.060	0.686	-0.082	0.484	0.074	0.697	-0.069	0.603
CCAR1	ENSG00000060339	0.090	0.262	-0.118	0.069	0.029	0.845	-0.011	0.930
CCDC12	ENSG00000160799	0.185	0.066	-0.181	0.120	0.049	0.795	-0.391	0.001
CD2BP2	ENSG00000169217	0.073	0.433	0.134	0.072	0.092	0.452	0.026	0.844
CDC40	ENSG00000168438	-0.004	0.981	-0.203	0.020	-0.024	0.893	-0.085	0.450
CDC5L	ENSG00000096401	-0.079	0.313	0.030	0.758	-0.014	0.928	-0.169	0.015
CDK10	ENSG00000185324	-0.153	0.153	0.194	0.034	-0.040	0.845	0.080	0.540
CELF2	ENSG00000048740	0.233	0.508	0.389	0.257	0.094	0.867	0.218	0.373
CELF3	ENSG00000159409	-0.001	NA	NA	NA	NA	NA	0.002	NA
CHD3	ENSG00000170004	-0.008	0.949	-0.045	0.573	-0.126	0.250	-0.452	0.000
CHERP	ENSG00000085872	-0.285	0.001	0.015	0.899	-0.196	0.115	-0.163	0.081
CRNKL1	ENSG00000101343	0.062	0.606	-0.140	0.166	0.086	0.557	-0.030	0.831
CTNNBL1	ENSG00000132792	-0.028	0.807	-0.011	0.921	-0.091	0.496	-0.235	0.001
CWC15	ENSG00000150316	0.159	0.136	0.017	0.902	0.107	0.460	-0.171	0.121
CWC22	ENSG00000163510	0.381	0.000	-0.205	0.001	0.538	0.000	-0.118	0.153
CWC25	ENSG00000273559	0.299	0.001	0.028	0.834	0.453	0.000	0.034	0.812
CWC27	ENSG00000153015	-0.047	0.631	-0.318	0.000	-0.020	0.894	-0.177	0.023
CXORF56	ENSG00000018610	0.125	0.261	-0.071	0.606	0.105	0.511	0.101	0.424
DAZAP1	ENSG00000071626	-0.121	0.081	0.001	0.993	0.044	0.730	0.003	0.984
DDX23	ENSG00000174243	-0.188	0.020	-0.099	0.179	-0.214	0.065	-0.458	0.000
DDX41	ENSG00000183258	0.225	0.001	0.508	0.000	-0.029	0.849	-0.066	0.493
DDX46	ENSG00000145833	-0.186	0.004	0.014	0.868	-0.200	0.014	-0.210	0.002
DGCR14	ENSG00000100056	0.033	0.838	0.035	0.832	0.071	0.723	0.075	0.616
DHX15	ENSG00000109606	-0.424	0.000	-0.257	0.000	-0.199	0.030	-0.010	0.930
DHX16	ENSG00000204560	-0.064	0.622	-0.040	0.758	-0.032	0.872	-0.324	0.001
DHX35	ENSG00000101452	0.031	0.882	0.103	0.553	0.250	0.124	0.197	0.184
DHX38	ENSG00000140829	0.006	0.961	-0.239	0.000	-0.045	0.760	-0.337	0.000
DHX8	ENSG00000067596	-0.152	0.110	-0.351	0.000	-0.241	0.016	-0.190	0.025
ECM2	ENSG00000106823	0.669	0.005	-0.106	0.814	1.091	0.000	-0.123	0.656
EFTUD2	ENSG00000108883	-0.162	0.011	-0.233	0.000	-0.364	0.000	-0.168	0.004
EIF4A3	ENSG00000141543	-0.215	0.008	-0.183	0.029	-0.266	0.009	0.108	0.273
ELAVL1	ENSG00000066044	-0.255	0.000	-0.038	0.691	-0.169	0.083	0.015	0.902

ELAVL2	ENSG00000107105	-0.807	0.000	-0.431	0.092	-0.402	0.152	0.034	0.907
ELAVL3	ENSG00000196361	0.007	NA	-0.213	NA	0.026	NA	0.000	NA
ELAVL4	ENSG00000162374	NA	NA	NA	NA	NA	NA	NA	NA
ESRP1	ENSG00000104413	0.551	NA	0.238	NA	0.273	NA	0.070	NA
ESRP2	ENSG00000103067	0.135	0.765	0.363	0.383	0.077	0.903	-0.079	NA
FAM32A	ENSG00000105058	-0.027	0.826	-0.303	0.000	-0.070	0.604	-0.063	0.565
FAM50A	ENSG00000071859	0.286	0.000	0.551	0.000	0.104	0.369	-0.138	0.143
FMR1	ENSG00000102081	-0.081	0.359	0.082	0.295	-0.149	0.152	-0.096	0.305
FRA10AC1	ENSG00000148690	0.292	0.000	0.500	0.000	0.443	0.000	0.009	0.951
GPATCH1	ENSG00000076650	0.141	0.210	0.090	0.458	-0.101	0.521	-0.045	0.765
GPKOW	ENSG00000068394	0.174	0.088	-0.098	0.452	-0.279	0.033	-0.219	0.059
HNRNPA0	ENSG00000177733	-0.193	0.002	-0.099	0.144	0.021	0.905	-0.078	0.346
HNRNPA1	ENSG00000135486	-0.246	0.000	-0.197	0.000	-0.078	0.411	-0.102	0.106
HNRNPA1L2	ENSG00000139675	-0.038	0.883	-0.455	0.010	0.218	0.292	0.002	0.994
HNRNPA3	ENSG00000170144	0.056	0.572	-0.045	0.522	0.152	0.141	-0.267	0.000
HNRNPAB	ENSG00000197451	-0.360	0.000	-0.037	0.586	-0.219	0.023	-0.112	0.094
HNRNPC	ENSG00000092199	-0.072	0.255	-0.124	0.009	0.156	0.106	-0.051	0.473
HNRNPD	ENSG00000138668	-0.198	0.000	-0.117	0.010	-0.041	0.748	-0.154	0.007
HNRNPDL	ENSG00000152795	0.026	0.766	-0.086	0.097	0.037	0.749	-0.052	0.484
HNRNPF	ENSG00000169813	-0.397	0.000	0.064	0.267	-0.188	0.028	-0.041	0.631
HNRNPH1	ENSG00000169045	-0.257	0.000	0.015	0.853	0.073	0.502	-0.086	0.187
HNRNPH2	ENSG00000126945	-0.130	0.070	0.156	0.006	-0.035	0.789	-0.201	0.002
HNRNPH3	ENSG00000096746	-0.093	0.165	-0.131	0.013	0.161	0.058	-0.218	0.000
HNRNPK	ENSG00000165119	-0.114	0.041	-0.065	0.194	-0.025	0.835	-0.196	0.001
HNRNPL	ENSG00000104824	0.111	0.117	0.175	0.002	0.213	0.033	0.087	0.264
HnrnpLL	ENSG00000143889	0.084	0.542	-0.123	0.332	-0.170	0.240	0.088	0.503
HNRNPM	ENSG00000099783	-0.167	0.015	-0.069	0.233	-0.086	0.450	-0.232	0.000
HNRNPR	ENSG00000125944	-0.250	0.000	-0.194	0.000	-0.216	0.005	-0.226	0.000
HNRNPU	ENSG00000153187	-0.150	0.007	-0.079	0.108	-0.180	0.027	-0.157	0.010
HNRNPUL1	ENSG00000105323	-0.170	0.006	-0.166	0.001	-0.243	0.026	-0.224	0.000
HNRNPUL2	ENSG00000214753	-0.081	0.363	0.005	0.969	-0.212	0.035	-0.169	0.044
HSPA8	ENSG00000109971	-0.228	0.000	-0.109	0.027	-0.121	0.184	-0.126	0.025
HTATSF1	ENSG00000102241	-0.392	0.000	-0.366	0.000	-0.253	0.004	-0.335	0.000
IK	ENSG00000113141	-0.018	0.879	-0.021	0.811	-0.003	0.987	-0.260	0.000
ISY1	ENSG00000240682	0.074	0.633	0.069	0.667	0.237	0.101	-0.006	0.979
KHDRBS1	ENSG00000121774	-0.251	0.000	-0.170	0.008	-0.158	0.104	-0.104	0.195
KHDRBS2	ENSG00000112232	NA	NA	NA	NA	NA	NA	NA	NA
KHDRBS3	ENSG00000131773	0.119	0.379	0.441	0.000	0.004	0.987	0.024	0.898
KHSRP	ENSG00000088247	0.013	0.919	0.142	0.032	0.031	0.880	-0.028	0.798
LENG1	ENSG00000105617	0.193	0.131	0.065	0.682	-0.298	0.062	-0.394	0.001
LSM2	ENSG00000204392	-0.029	0.914	0.210	0.264	-0.192	0.450	0.114	0.572
LSM3	ENSG00000170860	-0.253	0.000	-0.215	0.003	-0.217	0.066	-0.318	0.000
LSM4	ENSG00000130520	-0.071	0.473	0.078	0.399	-0.043	0.803	0.113	0.225

LSM5	ENSG00000106355	-0.240	0.031	-0.307	0.001	0.120	0.424	-0.006	0.974
LSM6	ENSG00000164167	-0.184	0.133	-0.317	0.004	-0.024	0.919	-0.060	0.704
LSM7	ENSG00000130332	-0.099	0.669	-0.012	0.966	-0.013	0.970	-0.076	0.746
MAGOH	ENSG00000162385	-0.054	0.758	-0.291	0.005	0.245	0.043	-0.113	0.395
MBNL1	ENSG00000152601	-0.103	0.133	-0.529	0.000	0.070	0.571	-0.091	0.228
MFAP1	ENSG00000140259	-0.115	0.164	-0.270	0.000	-0.241	0.017	-0.366	0.000
MSL1	ENSG00000188895	-0.115	0.109	-0.078	0.301	-0.212	0.020	-0.059	0.521
NAA38	ENSG00000183011	0.023	0.889	-0.110	0.393	-0.088	0.653	-0.477	0.000
NOSIP	ENSG00000142546	0.161	0.164	-0.154	0.192	0.010	0.963	-0.006	0.976
NOVA1	ENSG00000139910	0.177	0.184	-0.073	0.696	0.307	0.029	0.087	0.587
NOVA2	ENSG00000104967	-0.197	NA	-0.111	NA	-0.140	NA	-0.022	NA
PABPC1L	ENSG00000101104	0.251	0.016	0.497	0.000	0.407	0.005	0.469	0.000
PCBP1	ENSG00000169564	-0.096	0.122	0.025	0.747	0.010	0.955	-0.063	0.425
PCBP2	ENSG00000197111	-0.074	0.277	0.095	0.096	-0.019	0.893	0.327	0.000
PHF5A	ENSG00000100410	-0.069	0.464	-0.106	0.208	0.152	0.219	-0.061	0.585
PLRG1	ENSG00000171566	-0.007	0.957	-0.272	0.000	0.191	0.064	0.055	0.626
PPIE	ENSG00000084072	0.180	0.101	-0.065	0.652	0.051	0.785	-0.076	0.606
PPIG	ENSG00000138398	0.061	0.463	-0.015	0.877	0.146	0.127	-0.094	0.275
PPIH	ENSG00000171960	-0.237	0.051	-0.077	0.603	-0.094	0.595	-0.034	0.843
PPIL1	ENSG00000137168	0.021	0.920	-0.156	0.296	0.070	0.742	0.093	0.581
PPIL2	ENSG00000100023	-0.034	0.791	0.055	0.596	-0.222	0.029	-0.154	0.100
PPIL3	ENSG00000240344	0.188	0.074	0.109	0.395	0.145	0.310	0.068	0.658
PPIL4	ENSG00000131013	0.343	0.000	0.012	0.914	0.422	0.000	-0.263	0.003
PPWD1	ENSG00000113593	-0.072	0.432	-0.140	0.067	0.128	0.394	-0.125	0.169
PQBP1	ENSG00000102103	0.103	0.340	-0.168	0.077	0.135	0.409	-0.101	0.423
PRCC	ENSG00000143294	-0.083	0.413	-0.197	0.012	0.058	0.750	-0.295	0.000
PRPF18	ENSG00000165630	0.084	0.537	-0.033	0.825	0.036	0.851	-0.266	0.006
PRPF19	ENSG00000110107	-0.212	0.001	0.008	0.936	-0.075	0.608	0.120	0.110
PRPF3	ENSG00000117360	0.421	0.000	0.468	0.000	0.845	0.000	0.098	0.309
PRPF31	ENSG00000105618	0.079	0.394	-0.034	0.711	0.043	0.778	-0.168	0.038
PRPF38A	ENSG00000134748	-0.074	0.392	-0.298	0.000	0.136	0.195	-0.103	0.248
PRPF38B	ENSG00000134186	0.155	0.011	0.173	0.002	0.211	0.021	-0.036	0.724
PRPF39	ENSG00000185246	-0.052	0.729	0.087	0.513	-0.071	0.725	0.005	0.981
PRPF4	ENSG00000136875	-0.252	0.000	-0.118	0.115	-0.143	0.165	0.006	0.965
PRPF40A	ENSG00000196504	-0.043	0.581	-0.077	0.191	-0.095	0.312	-0.063	0.396
PRPF40B	ENSG00000110844	0.196	0.081	0.182	0.098	-0.127	0.451	-0.049	0.772
PRPF4B	ENSG00000112739	-0.192	0.018	0.108	0.169	-0.334	0.001	-0.131	0.116
PRPF6	ENSG00000101161	-0.040	0.705	-0.161	0.006	-0.215	0.037	-0.193	0.007
PRPF8	ENSG00000174231	-0.176	0.005	-0.045	0.511	-0.163	0.071	-0.129	0.053
PRPH2	ENSG00000112619	0.004	NA	-0.028	NA	-0.012	NA	-0.004	NA
PTBP1	ENSG00000011304	0.071	0.353	0.123	0.030	-0.182	0.110	0.104	0.151
PTBP2	ENSG00000117569	0.283	0.068	0.206	0.242	0.451	0.010	0.382	0.006
PUF60	ENSG00000179950	-0.091	0.318	-0.193	0.011	-0.089	0.510	0.019	0.882

QKI	ENSG00000112531	0.029	0.784	-0.197	0.001	0.058	0.671	0.070	0.500
RBFOX2	ENSG00000100320	-0.124	0.035	-0.522	0.000	0.025	0.845	-0.266	0.000
RBM10	ENSG00000182872	0.086	0.362	0.013	0.909	-0.001	0.995	-0.089	0.339
RBM17	ENSG00000134453	-0.083	0.254	0.026	0.760	0.086	0.405	-0.074	0.382
RBM22	ENSG00000086589	0.017	0.882	-0.099	0.194	-0.102	0.363	-0.035	0.744
RBM25	ENSG00000119707	0.045	0.633	-0.053	0.470	-0.101	0.361	0.005	0.968
RBM4	ENSG00000173933	-0.027	0.893	-0.141	0.380	0.002	0.995	0.021	0.920
RBM5	ENSG00000003756	0.312	0.000	-0.026	0.813	0.167	0.133	-0.004	0.977
RBM8A	ENSG00000265241	-0.205	0.001	-0.228	0.000	-0.222	0.029	-0.398	0.000
RBMX	ENSG00000147274	-0.433	0.000	-0.102	0.112	-0.141	0.101	-0.123	0.082
RBMX2	ENSG00000134597	0.136	0.088	-0.015	0.901	0.258	0.013	-0.184	0.039
RBMXL2	ENSG00000170748	0.111	NA	0.136	NA	0.183	NA	0.029	NA
RBPMS2	ENSG00000166831	-0.001	NA	0.281	NA	NA	NA	NA	NA
RNF113A	ENSG00000125352	0.271	0.025	0.242	0.056	0.129	0.524	-0.211	0.137
SAP18	ENSG00000150459	0.101	0.185	-0.040	0.638	0.019	0.918	-0.323	0.000
SART1	ENSG00000175467	-0.008	0.946	0.009	0.915	-0.005	0.981	-0.328	0.000
SF1	ENSG00000168066	-0.238	0.000	0.004	0.967	-0.203	0.021	-0.077	0.412
SF3A1	ENSG00000099995	-0.220	0.004	-0.156	0.017	-0.127	0.324	-0.193	0.007
SF3A2	ENSG00000104897	0.083	0.412	0.225	0.001	0.091	0.441	-0.021	0.885
SF3A3	ENSG00000183431	-0.109	0.086	-0.197	0.000	-0.007	0.963	-0.140	0.027
SF3B1	ENSG00000115524	0.006	0.955	-0.130	0.016	0.026	0.867	-0.038	0.646
SF3B2	ENSG00000087365	0.087	0.226	0.046	0.475	-0.006	0.973	-0.218	0.001
SF3B3	ENSG00000189091	-0.268	0.000	-0.147	0.018	-0.031	0.836	0.013	0.903
SF3B4	ENSG00000143368	-0.314	0.000	-0.137	0.048	-0.033	0.872	-0.065	0.542
SF3B5	ENSG00000169976	0.131	0.353	-0.039	0.843	-0.020	0.941	0.050	0.789
SFPQ	ENSG00000116560	-0.228	0.000	-0.241	0.000	-0.287	0.001	-0.178	0.006
SGPP2	ENSG00000163082	-0.209	NA	-0.162	NA	0.562	0.163	-0.111	NA
SLU7	ENSG00000164609	0.122	0.054	-0.064	0.374	0.205	0.014	-0.139	0.042
SMNDC1	ENSG00000119953	0.099	0.332	0.252	0.001	0.135	0.292	0.141	0.151
SMU1	ENSG00000122692	-0.053	0.607	-0.197	0.003	0.021	0.895	-0.071	0.461
SNIP1	ENSG00000163877	0.247	0.007	0.072	0.583	0.409	0.000	-0.027	0.868
SNRNP200	ENSG00000144028	-0.046	0.599	-0.120	0.066	-0.113	0.309	-0.197	0.005
SNRNP40	ENSG00000060688	-0.027	0.825	-0.072	0.448	-0.100	0.448	0.002	0.986
SNRNP70	ENSG00000104852	-0.191	0.018	0.097	0.197	0.031	0.850	-0.205	0.026
SNRPA	ENSG00000077312	0.087	0.387	-0.036	0.776	0.433	0.000	0.031	0.816
SNRPA1	ENSG00000131876	-0.298	0.000	-0.289	0.000	-0.066	0.629	-0.196	0.014
SNRPB	ENSG00000125835	-0.005	0.974	0.029	0.833	-0.003	0.990	0.011	0.947
SNRPB2	ENSG00000125870	0.230	0.008	0.211	0.012	0.233	0.027	0.063	0.582
SNRPC	ENSG00000124562	0.212	0.009	0.024	0.851	0.201	0.178	-0.076	0.561
SNRPD1	ENSG00000167088	-0.213	0.003	-0.134	0.065	-0.076	0.546	-0.032	0.776
SNRPD2	ENSG00000125743	-0.064	0.561	0.097	0.311	0.010	0.960	-0.167	0.127
SNRPD3	ENSG00000100028	-0.325	0.000	-0.196	0.007	-0.213	0.041	-0.120	0.167
SNRPE	ENSG00000182004	-0.440	0.000	-0.440	0.000	-0.260	0.041	-0.005	0.979

SNRPF	ENSG00000139343	-0.200	0.028	-0.097	0.358	-0.042	0.825	-0.007	0.970
SNRPG	ENSG00000143977	-0.088	0.481	-0.013	0.935	-0.098	0.807	-0.426	0.007
SNU13	ENSG00000100138	-0.171	0.053	-0.123	0.190	0.060	0.707	0.037	0.770
SNW1	ENSG00000100603	0.254	0.000	0.091	0.173	0.188	0.031	-0.178	0.037
SPARCL1	ENSG00000152583	0.068	NA	0.215	NA	0.031	NA	-0.007	NA
SPP2	ENSG00000072080	0.144	NA	NA	NA	NA	NA	0.015	NA
SREK1	ENSG00000153914	0.192	0.004	0.311	0.000	0.262	0.007	0.008	0.950
SRP54	ENSG00000100883	0.155	0.048	-0.115	0.172	0.214	0.034	-0.173	0.042
SRRM1	ENSG00000133226	-0.212	0.013	0.025	0.818	-0.277	0.011	-0.306	0.000
SRRM2	ENSG00000167978	0.002	0.988	-0.034	0.745	0.060	0.659	-0.154	0.101
SRSF1	ENSG00000136450	-0.352	0.000	-0.312	0.000	-0.033	0.815	0.108	0.188
SRSF10	ENSG00000188529	-0.147	0.019	-0.167	0.004	0.119	0.301	0.006	0.959
SRSF12	ENSG00000154548	-0.121	NA	-0.105	NA	0.027	NA	-0.042	NA
SRSF2	ENSG00000161547	-0.520	0.000	-0.054	0.453	-0.514	0.000	0.217	0.001
SRSF3	ENSG00000112081	-0.078	0.366	-0.177	0.004	-0.059	0.624	0.000	0.999
SRSF4	ENSG00000116350	0.164	0.030	0.204	0.001	0.216	0.015	-0.105	0.218
SRSF6	ENSG00000124193	0.166	0.037	0.127	0.098	0.042	0.792	-0.109	0.330
SRSF7	ENSG00000115875	-0.484	0.000	-0.246	0.000	-0.169	0.080	0.088	0.327
SRSF9	ENSG00000111786	-0.027	0.787	0.046	0.588	-0.046	0.740	-0.010	0.930
SUGP1	ENSG00000105705	0.079	0.434	-0.107	0.267	-0.128	0.295	-0.099	0.360
SUN3	ENSG00000164744	0.310	0.374	1.436	0.000	0.272	0.566	-0.051	NA
SYF2	ENSG00000117614	0.267	0.088	0.401	0.002	0.201	0.495	-0.320	0.067
SYNCRIP	ENSG00000135316	-0.238	0.000	-0.210	0.000	-0.235	0.001	-0.093	0.175
TARDBP	ENSG00000120948	-0.363	0.000	-0.248	0.000	-0.139	0.175	-0.093	0.249
TCERG1	ENSG00000113649	-0.154	0.055	0.010	0.931	-0.032	0.832	-0.126	0.126
TFIP11	ENSG00000100109	0.015	0.906	0.042	0.682	0.081	0.520	-0.103	0.269
THRAP3	ENSG00000054118	0.056	0.552	0.066	0.392	-0.063	0.611	-0.238	0.001
TIA1	ENSG00000116001	0.058	0.643	0.014	0.924	0.079	0.646	0.191	0.052
TIAL1	ENSG00000151923	-0.098	0.176	-0.114	0.093	0.034	0.804	-0.010	0.930
TRA2A	ENSG00000164548	0.152	0.024	0.092	0.212	0.372	0.000	0.151	0.044
TRA2B	ENSG00000136527	0.058	0.509	-0.115	0.093	0.210	0.019	0.058	0.504
TXNL4A	ENSG00000141759	-0.031	0.790	-0.024	0.849	0.114	0.336	-0.032	0.805
U2AF1	ENSG00000160201	-0.068	NA	0.029	NA	-0.050	NA	-0.014	NA
U2AF2	ENSG00000063244	-0.062	0.476	0.016	0.856	0.009	0.962	-0.118	0.149
U2SURP	ENSG00000163714	-0.180	0.001	-0.239	0.000	0.004	0.980	-0.079	0.262
USP39	ENSG00000168883	-0.155	0.068	-0.183	0.020	-0.110	0.358	-0.093	0.336
WBP11	ENSG00000084463	-0.124	0.068	-0.182	0.001	-0.073	0.603	-0.182	0.003
WBP4	ENSG00000120688	0.162	0.020	-0.089	0.271	0.268	0.002	-0.164	0.042
WDR83	ENSG00000123154	0.204	0.100	0.208	0.101	0.185	0.310	-0.061	0.730
XAB2	ENSG00000076924	0.076	0.509	0.034	0.809	0.046	0.805	0.134	0.202
YBX1	ENSG00000065978	-0.124	0.123	0.013	0.899	-0.047	0.818	-0.526	0.000
ZMAT2	ENSG00000146007	-0.121	0.083	-0.222	0.000	-0.116	0.350	-0.189	0.016
ZNF830	ENSG00000198783	0.249	0.014	-0.032	0.844	0.194	0.132	-0.153	0.240

ZRANB2	ENSG00000132485	0.235	0.000	-0.458	0.000	0.361	0.000	-0.040	0.637